AD NUMBER

ADB015542

LIMITATION CHANGES

TO:

Approved for public release; distribution is unlimited.

FROM:

Distribution authorized to U.S. Gov't. agencies only; Test and Evaluation; 28 JAN 1976. Other requests shall be referred to Defense Nuclear Agency, Washington, DC 20305.

AUTHORITY

DNA ltr 4 Jan 1983

DNA 3872F

GROUND MOTION ENVIRONMENTS FOR GENERIC SITE CONDITIONS

TRW Systems Group
One Space Park
Redondo Beach, California 90278

31 December 1975

Final Report for Period 28 March 1974—31 December 1975

CONTRACT No. DNA 001-74-C-0249

THIS WORK SPONSORED BY THE DEFENSE NUCLEAR AGENCY
UNDER SUBTASK Y99QAXSC061-27.

Prepared for
Director
DEFENSE NUCLEAR AGENCY
Washington, D. C. 20305

Destroy this report when it is no longer needed. Do not return to sender.

UNCLASSIFIED

SECURITY CLASSIFICATION OF THIS PAGE (When Data Entered)

REPORT DOCUMENTATION PAGE

READ INSTRUCTIONS BEFORE COMPLETING FORM

1. REPORT NUMBER: DNA 3872F	2. GOVT ACCESSION NO.
3. RECIPIENT'S CATALOG NUMBER	
4. TITLE (and Subtitle): GROUND MOTION ENVIRONMENTS FOR GENERIC SITE CONDITIONS	5. TYPE OF REPORT & PERIOD COVERED: Final Report for Period 28 Mar 74—31 Dec 75
6. PERFORMING ORG. REPORT NUMBER: TR-26128-6004-RU-00	
7. AUTHOR(s): Norman Lipner, Donald C. Anderson, Peter K. Dai	8. CONTRACT OR GRANT NUMBER(s): DNA 001-74-C-0249
9. PERFORMING ORGANIZATION NAME AND ADDRESS: TRW Systems Group, One Space Park, Redondo Beach, California 90278	10. PROGRAM ELEMENT, PROJECT, TASK AREA & WORK UNIT NUMBERS: NWED Subtask Y99QAXSC061-27
11. CONTROLLING OFFICE NAME AND ADDRESS: Director, Defense Nuclear Agency, Washington, D.C. 20305	12. REPORT DATE: 31 December 1975
	13. NUMBER OF PAGES: 204 (199 pp.)
14. MONITORING AGENCY NAME & ADDRESS (if different from Controlling Office)	15. SECURITY CLASS (of this report): UNCLASSIFIED
	15a. DECLASSIFICATION/DOWNGRADING SCHEDULE

16. DISTRIBUTION STATEMENT (of this Report)

Distribution limited to U.S. Government agencies only (Test and Evaluation), 28 January 1976. Other requests for this document must be referred to the Director, Defense Nuclear Agency, Washington, D.C. 20305.

17. DISTRIBUTION STATEMENT (of the abstract entered in Block 20, if different from Report)

18. SUPPLEMENTARY NOTES

This work sponsored by the Defense Nuclear Agency under Subtask Y99QAXSC061-27.

19. KEY WORDS (Continue on reverse side if necessary and identify by block number)

Ground Shock
Air Blast
Generic Site Conditions
Nuclear Weapon Effects

20. ABSTRACT (Continue on reverse side if necessary and identify by block number)

The study is a state-of-the-art review for providing methods for predicting air blast and ground shock environments generated by nuclear explosions. Specifically, the report establishes concise ground shock prediction equations which are needed for updating the DNA weapon effects manual EM-1 and for input to the Defense Intelligence Agency (DIA) Vulnerability Analysis System (VAS) computer code. → next page

354 595

DD FORM 1 JAN 73 1473 EDITION OF 1 NOV 65 IS OBSOLETE

UNCLASSIFIED

SECURITY CLASSIFICATION OF THIS PAGE (When Data Entered)

20. ABSTRACT (Continued)

The approach taken was to review the data base, both experimental and analytical, and formulate recommendations and/or simplified equations for prediction of environments and their uncertainties with the concurrence of the technical community. The format and content of the recommendations were reviewed by appropriate DNA contractors and government agencies before reaching their current status. The areas covered are:

(1) Surface and height-of-burst air blast definition;

(2) Ground shock peak motion and stress parameter scaling for both air blast and direct-induced effects for generic site conditions;

(3) Ground shock motion and stress waveforms and shock spectra characteristics.

The recommended nuclear environment prediction methods encompass weapon yields from 20 kT to 50 MT, overpressures from 10 to 5000 psi, depths to 50 ft below the ground surface, and four generic sites (dry soil, wet soil, soft rock, and hard rock) selected as being representative of most sites of interest.

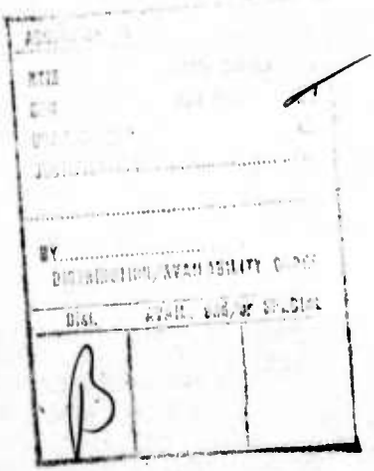

PREFACE

Preparation of this report, "Ground Motion Environments for Generic Site Conditions," was supported by the Defense Nuclear Agency under Contract No. DNA 001-74-C-0249, Project No. NWED Code Y99QAXS Task and Subtask Code C061 Work Unit Code 27 during the period 28 March 1974 through 31 December 1975.

TRW Systems Group is grateful for the many helpful suggestions by Dr. Kent L. Goering, Technical Monitor DNA/SPSS, and by the following weapon effects experts of pertinent Department of Defense agencies and government contractors representing the technical community: Drs. Harold L. Brode and Henry F. Cooper, and Messrs. H. Jerry Carpenter and John G. Lewis, R & D Associates; Drs. Nathan M. Newmark and William J. Hall, University of Illinois; Messrs. Robert J. Port and Jimmie L. Bratton, Air Force Weapons Laboratory; Dr. Melvin L. Baron, Weidlinger Associates; Dr. Paul F. Hadala, Waterways Experiment Station; and Mr. Fred M. Sauer, Physics International Company.

The authors also acknowledge the contributions of Dr. Theodore H. Schiffman in preparation of a portion of the air blast section; Ms. Harriet Mizuno in careful and diligent preparation of the figures; and Ms. Clara Shaw in editing of the manuscript.

Subsequent to their review, this document will be published as a DNA report.

TABLE OF CONTENTS

LIST OF ILLUSTRATIONS

LIST OF ILLUSTRATIONS
(continued)

LIST OF ILLUSTRATIONS
(continued)

LIST OF ILLUSTRATIONS
(continued)

2

LIST OF ILLUSTRATIONS
(continued)

LIST OF TABLES

1.0 INTRODUCTION

This document constitutes the final report on a study conducted for the Defense Nuclear Agency (DNA) under Contract No. DNA 001-74-C-0249. The study was designed to evaluate and summarize the state-of-the-art in nuclear air blast and ground shock phenomenology, and to recommend methods for predicting blast and shock environments for generic sites.

The need for such information for hardened facility design and targeting vulnerability analysis has long been established. This is evidenced by a large volume of published literature such as the nuclear weapon effects reviews of Glasstone, Sauer, Brode, and Newmark (References 1 through 4) covering the time up to the Test Ban Treaty; Brode (References 5 and 6), covering the time to 1969/1970; and, more recently, the new Air Force design manual (Reference 7). From a technology point of view, the Test Ban Treaty forced the nation to develop (1) first principle calculational tools, (2) improved understanding of weapon effects phenomenology, and (3) simulation testing capability for use in providing reliable prediction for the blast and shock environments for surface and above-surface bursts.

By the 1969/1970 period, substantial progress had been made in the areas of dynamic soil and rock mechanical property definition; digital computation of large-scale nonlinear continuum wave propagation problems using the finite difference and finite element techniques; and blast and shock testing with chemical explosives. Progress made in these areas indicated that definition of ground shock phenomena can be achieved for geologies other than those encountered at the Nevada Test Site (NTS) and the Eniwetok Proving Ground (EPG). These sites are the location of U.S. nuclear surface and above-surface burst testing but their geologies do not represent sites where land-based weapon systems were deployed or were being planned. From a system point of view,

1969/1970 was a time when ground shock environments were a key to several programmatic considerations. The hardness assessment of the fully deployed MINUTEMAN force was ongoing, and planning and development for several major land-based hardened systems such as HARD ROCK SILO, MINUTEMAN Upgrade, Shelter-Based MINUTEMAN, SENTINEL/SAFEGUARD/SITE DEFENSE and SANGUINE was in progress.

Ground shock studies conducted since 1969/1970 were typified by (1) calculational activities, such as those of the MINUTEMAN Free-Field Working Group, the SITE DEFENSE Criteria Development Working Group, and the DNA direct-coupling ground shock studies, (2) high explosive phenomenology tests such as PRAIRIE FLAT and DIAL PACK, and the MIDDLE GUST, MIXED COMPANY, and MINE SHAFT SERIES, (3) high explosive tests for simulation of nuclear blast and shock environments (e.g., the HEST air blast simulation), and (4) cratering and related effects studies, such as Cooper's ground motion crater volume scaling investigations and the DNA/AFWL EXPOE program. These studies have furthered understanding of the ground shock phenomenology and have also raised a number of new questions and issues, such as, How can we reconcile observed differences in scaling of ground motion effects between events of different test series? and, What are the technology advancements required to obtain satisfactory continuum code calculation of high explosive test events? While these issues undergo scrutiny in the technical community, planners for new weapon systems and targeteers need state-of-the-art best estimates of blast and shock parameters for certain geologies of interest. It is not only desirable but necessary to periodically evaluate new data and results as they become available and to correlate them with existing information to provide simplified techniques for generating best estimate environment numbers and uncertainty factors. During the course of a study under DNA sponsorship on the application of the FAST (Failure Analysis by Statistical Techniques) computer program to

the survivability evaluation of hardened facilities (Reference 8), it was found that the task of generating a set of blast and shock parameters agreeable to experts in the technical community required a substantial effort.

The present study undertakes to determine ground shock prediction procedures that incorporate results of data analyses generated during the recent years, and to summarize opinions from experts regarding key issues. The procedures can serve as a basis for updating ground motion sections of the DNA weapon effects manual EM-1 and provide ground shock input to the Vulnerability Analysis System (VAS) computer code currently under development by the Defense Intelligence Agency (DIA) for targeting analysis. As the study proceeded, the DIA/VAS requirement became the primary consideration and the study was redirected to provide specific recommendations for blast and shock parameters required for input to the VAS analysis. These recommendations were obtained from the evaluation of test data and analytical results, the correlation of existing technical information, the coordination of latest findings in the technical community, and the integration of results to form a set of prediction techniques for air blast and ground shock effects and corresponding uncertainties.

The recommended environment prediction methods encompass variations of weapon yield (20 kT to 50 MT), burst height (surface to optimum), overpressure level (10 to 5000 psi) or ground range, depth (surface to 50 ft), and site conditions. Four generic sites were selected, in conjunction with DNA and its designated consultants, as being representative of most sites of interest. They can be characterized as dry soil, wet soil, soft rock, and hard rock. Specifically considered are

- Air blast definition for ideal and nonideal surfaces

- Ground shock peak motion and stress parameters (displacements, velocities, accelerations, and stresses) for both air blast and direct-coupling related effects
- Representative ground shock waveforms and corresponding shock spectra

Obtaining the technical community's concurrence with the recommended methods was a goal of the study. As a result, the format and the content of the recommendations have been reviewed by appropriate experts, designated by DNA, before reaching their current status.

Currently there is no complete prediction procedure available to determine ground shock waveforms for this range of conditions without performing large-scale computer code calculations. This report provides the basis for simplified prediction procedures and points out limitations and key issues of the technology. In the attempt to be complete, some estimates of blast and shock parameters are extrapolated from a very minimal data base. However, the report is written in a form that could readily be updated as results of new studies become available.

The next section discusses considerations for obtaining uncertainty predictions. The subsequent two sections describe the development of the air blast and ground shock environment predictions, respectively. The recommended ground shock generic site environments and their corresponding uncertainties are summarized in compact form in the Appendix.

2.0 WEAPON EFFECT UNCERTAINTY CONSIDERATIONS

It is vital to consider weapon effect uncertainties when developing design criteria or performing vulnerability evaluations for hardened systems. Best estimate predictions may indicate that a particular environment parameter is not critical to the system response. However, a large uncertainty in the prediction of that parameter could, for example, cause a design impact if high confidence in meeting hardness design goals is required.

Weapon effect uncertainties are related to the uncertainties in the site properties, in the test and analysis data base, and in the scaling of the data base to other geologies and weapon threat conditions of interest. The uncertainty distribution for a weapon effect parameter defines the probability of that parameter being less (or greater) than any specified value. These distributions are usually assumed to be log-normal (i.e., the logarithms of weapon effect uncertainty variations are distributed normally), a form that evolves from considering the environments to be defined by first- and second-order moments (mean and variance, respectively) of empirical distributions which are more symmetric in log-space than in linear space.

Uncertainty bounds are defined around best estimate values, which have 50% probability of being either too large or too small. In this study, uncertainty "estimates" for environment parameters are given in terms of 2σ K-factors, defined so that there is a 2σ (~95%) probability of the value of the parameter being between K and 1/K times the best estimate prediction. Thus, one might consider that there is "reasonable" confidence that the actual environment will be within the uncertainty bounds.

These estimates are based on the availability and scatter of data and on the confidence in results from calculational studies. Although a detailed analysis of uncertainty factors is beyond the scope of this study these factors can be derived from the uncertainties in the more fundamental material property and analysis uncertainties, as discussed in Reference 8.

3.0 AIR BLAST ENVIRONMENT

In a nuclear explosion, large energies are produced in a short time as a result of the formation of different atomic nuclei accompanied by a net decrease in mass. Two kinds of interaction, fission (involving high atomic number nuclei) and fusion (involving low atomic number nuclei), are present in this process. This sudden liberation of energy causes a considerable increase in temperature and pressure so that everything close to the nuclear device is converted into hot compressed gases, referred to as the "fireball," which expands and initiates a hydrodynamic shock wave. In the air, where strong winds accompany this shock, the environment is referred to as a "blast wave."

Characteristic of the blast wave is a sharp pressure rise (peak overpressure) at the shock front, followed by an interior fall off. Most of the overpressure decay occurs just behind the front. Fireball breakaway time is the time at which the arrival of the shock wave begins to precede the arrival of the fireball. Prior to the fireball breakaway, the interior pressure is roughly one-half the peak overpressure. After breakaway, the free air decay follows spherical divergence laws leading to atmospheric pressure and below at the tail end of the wave.

This study is concerned with the prediction of both air blast static overpressure effects, i.e., loading normal to the ground surface, and dynamic pressure effects. The data base from which the air blast prediction methodology has been formulated is represented by available nuclear data, high explosive data, and calculational results. The quality and quantity of each of these data are discussed in this section as they pertain to the phenomenology described. The section is divided into three subsections, each treating a different surface type, i.e., ideal, precursor (nonideal) planar, and perfectly reflective bermed surface. An ideal surface is one that is planar and perfectly reflective.

3.1 IDEAL SURFACE EFFECTS

Overpressure environments for an air blast over an ideal surface are supplied from three references:

(1) Brode 1-kT free-air standard together with the Brode direct fit HOB interpolation scheme (Reference 6)

(2) Air Force Weapons Laboratory (AFWL) 1-kT free-air standard (Reference 9) together with the Brode HOB interpolation scheme

(3) Results from a series of experiments with 8-lb spherical PBX 9404 charges (Reference 10).

The Brode HOB prediction scheme is based on free-air burst pressure histories, a knowledge of shock behavior in the regular reflection region, and the established correspondence between shock front pressures and shock interior pressures. This scheme prescribes a method for interpolating between 2W (yield) scaling for predicting effects from surface burst air blast and from HOB reflection phenomena. This approximate solution has compared favorably with test data and two-dimensional calculational results.

Developed by Needham as a fit to the results of radiation hydrodynamic and pure hydrodynamic calculations using first and second order differencing methods, the AFWL 1-kT standard provides the blast environment for a free-air detonation at sea level. Calculated were pressure, density, and velocity fields for times ranging from less than 1 msec to over 5 min. "Needham predictions" for HOB are obtained by applying the Brode direct fit methodology to the AFWL 1-kT standard. Currently, AFWL is performing HOB ideal surface first principle calculations.

Small-scale high explosive experiments were conducted by TRW to obtain ideal surface HOB blast effects in the overpressure range of 2000 to 200 psi. These experiments provided blast data for controlled experimental conditions that compared favorably with two-dimensional

hydrodynamic code calculations made by the AFWL and a set of HOB data for an essentially ideal surface.

3.1.1 Static Pressure

Since few experimental air blast data exist above 200 psi for nuclear detonations in the vicinity of the earth surface, it is necessary to rely heavily on analysis and controlled high explosive test data to predict air blast effects for such explosions. In order to determine which, if any, of the Brode or Needham prediction methods discussed best defines the air blast environment, a series of calculations were performed using both methods. The results of these calculations together with available experimental data from Reference 6 are presented in Figures 1 and 2. The figures show peak overpressure and peak impulse HOB data. Comparison of these air blast definitions indicates that the differences are small compared with the scatter of experimental data.

Figure 3 compares the results of each calculational method for determining the overpressure history initial decay time intercept, t_{00}, as a function of peak overpressure. Again the two different methods agree reasonably well. The parameter, t_{00}, is important in calculating the response of structures to air blast loading, particularly for those structures that have a short period of vibration. Since both methods define the air blast environment adequately compared with the scatter of test data, the Brode standard with the Brode HOB interpolation scheme has been suggested for use with the DIA/VAS code because of its immediate availability. Some of the effects of HOB air blast loading on surface flush targets are illustrated in References 11 and 12.

Figures 1 and 2 underscore the uncertainty associated with the prediction of peak overpressures and impulses. The points shown were interpolated from test data to apply to the indicated overpressure and impulse values (Reference 6) and extrapolated to 1 MT. They represent

(a) PEAK OVERPRESSURE vs GROUND RANGE DECAY

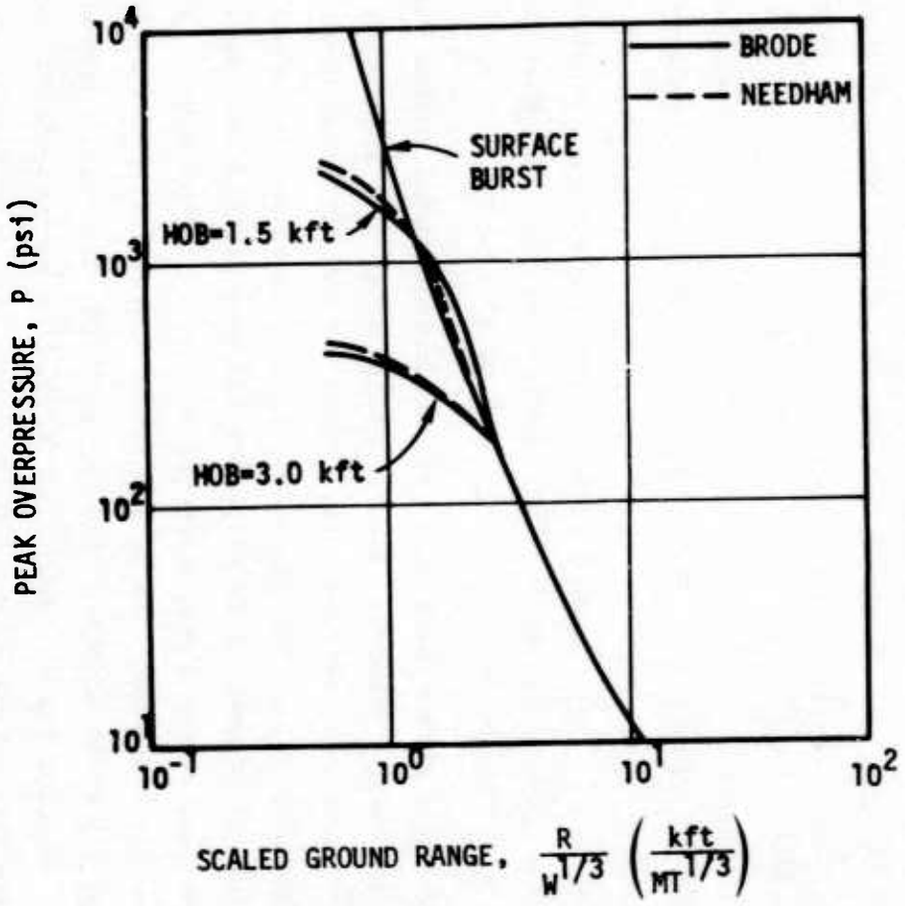

Figure 1. Height-of-Burst Peak Overpressure, Including Brode/Needham Comparison (Continued)

(b) HEIGHT-OF-BURST PEAK OVERPRESSURE, INCLUDING NUCLEAR DATA

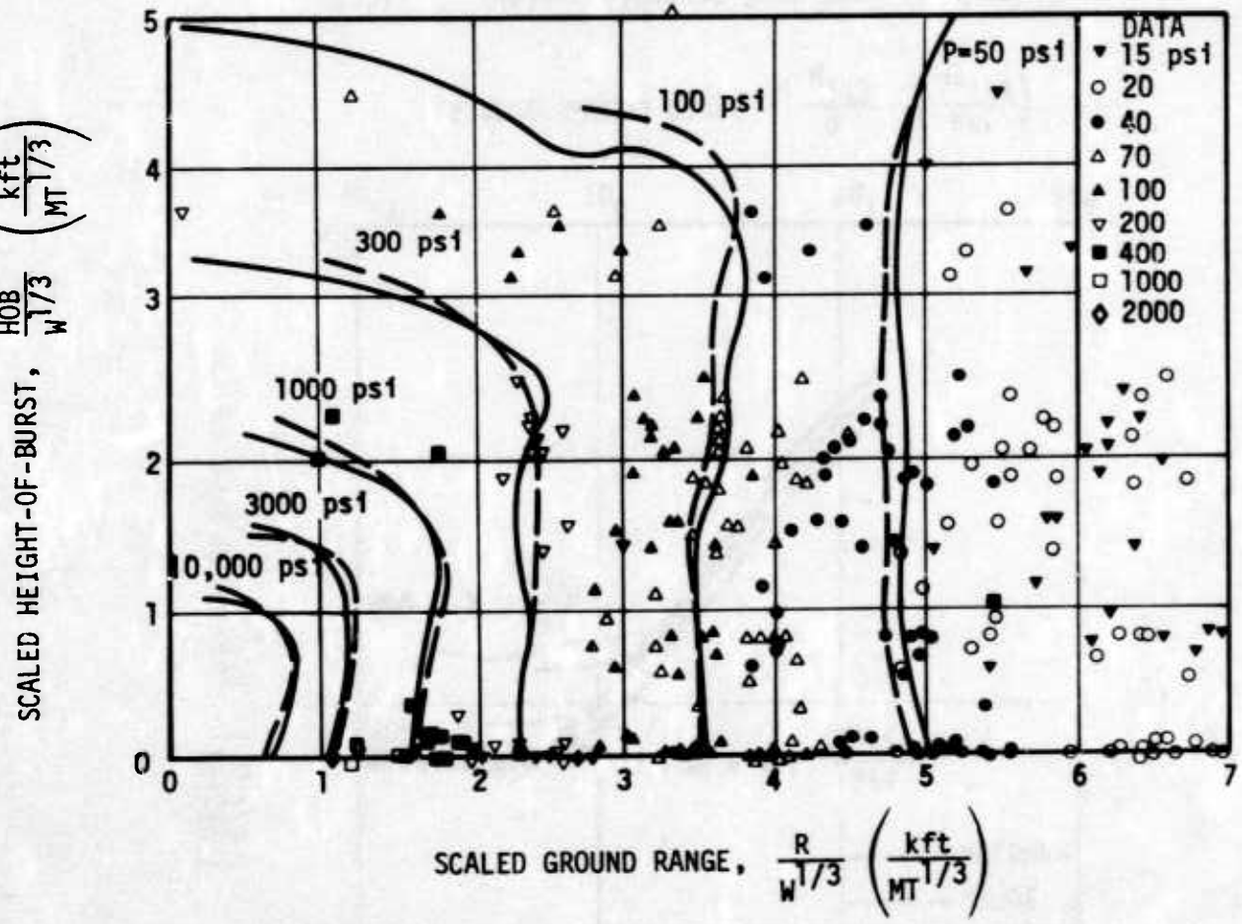

Figure 1. Height-of-Burst Peak Overpressure, Including Brode/Needham Comparison (Concluded)

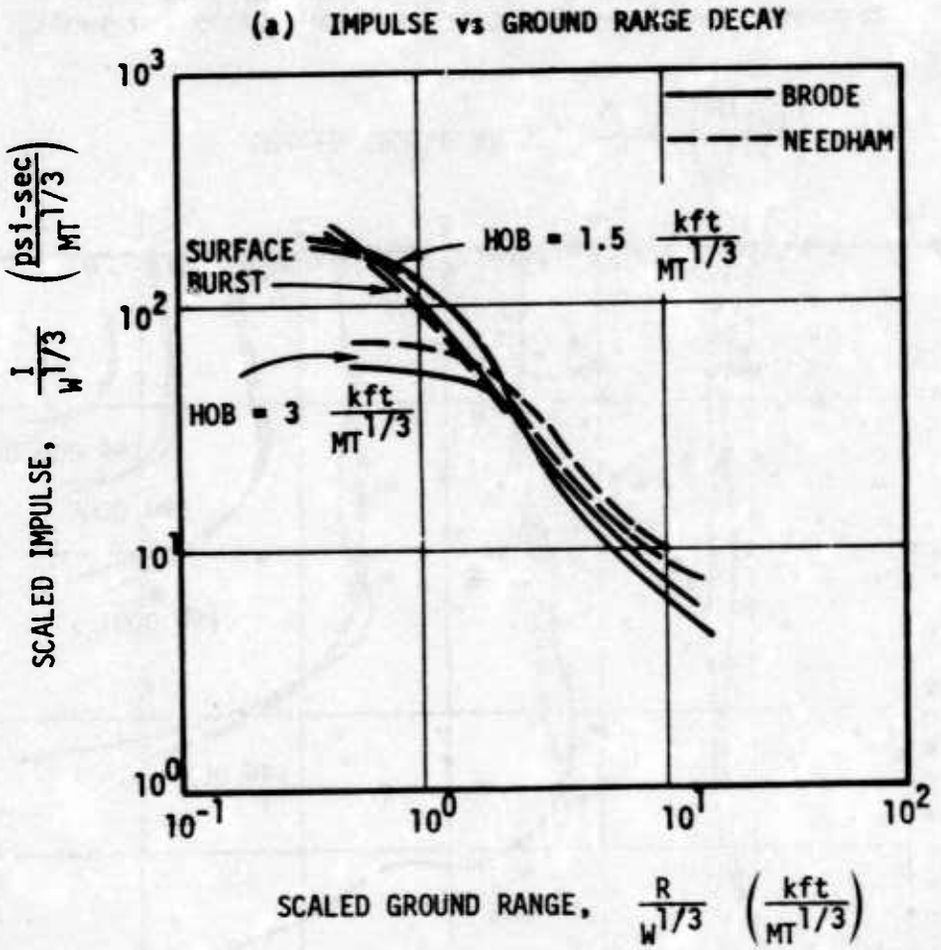

Figure 2. Height-of-Burst Peak Impulse, Including Brode/Needham Comparison (Continued)

(b) HEIGHT-OF-BURST IMPULSE, INCLUDING NUCLEAR DATA

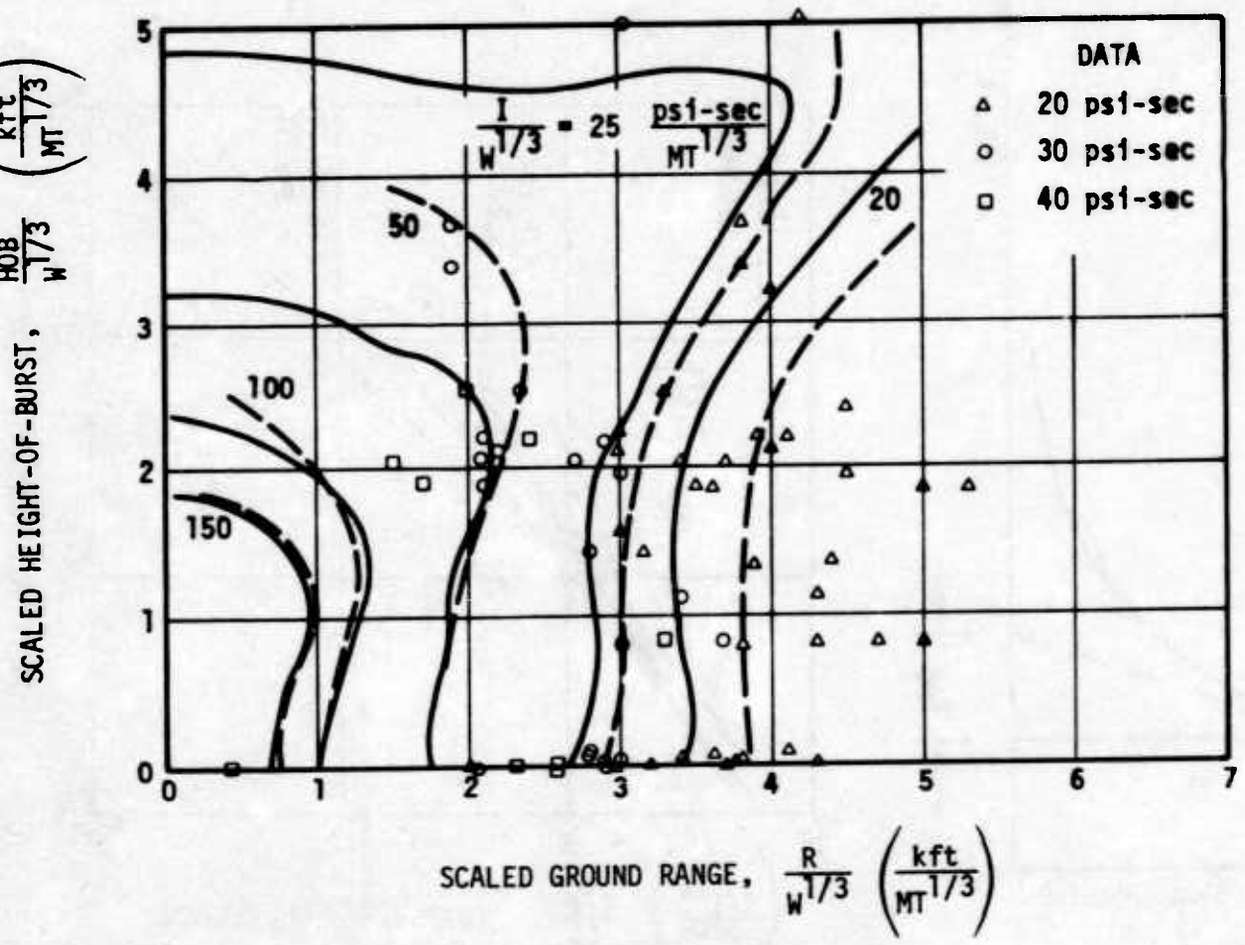

Figure 2. Height-of-Burst Peak Impulse, Including Brode/Needham Comparison (Concluded)

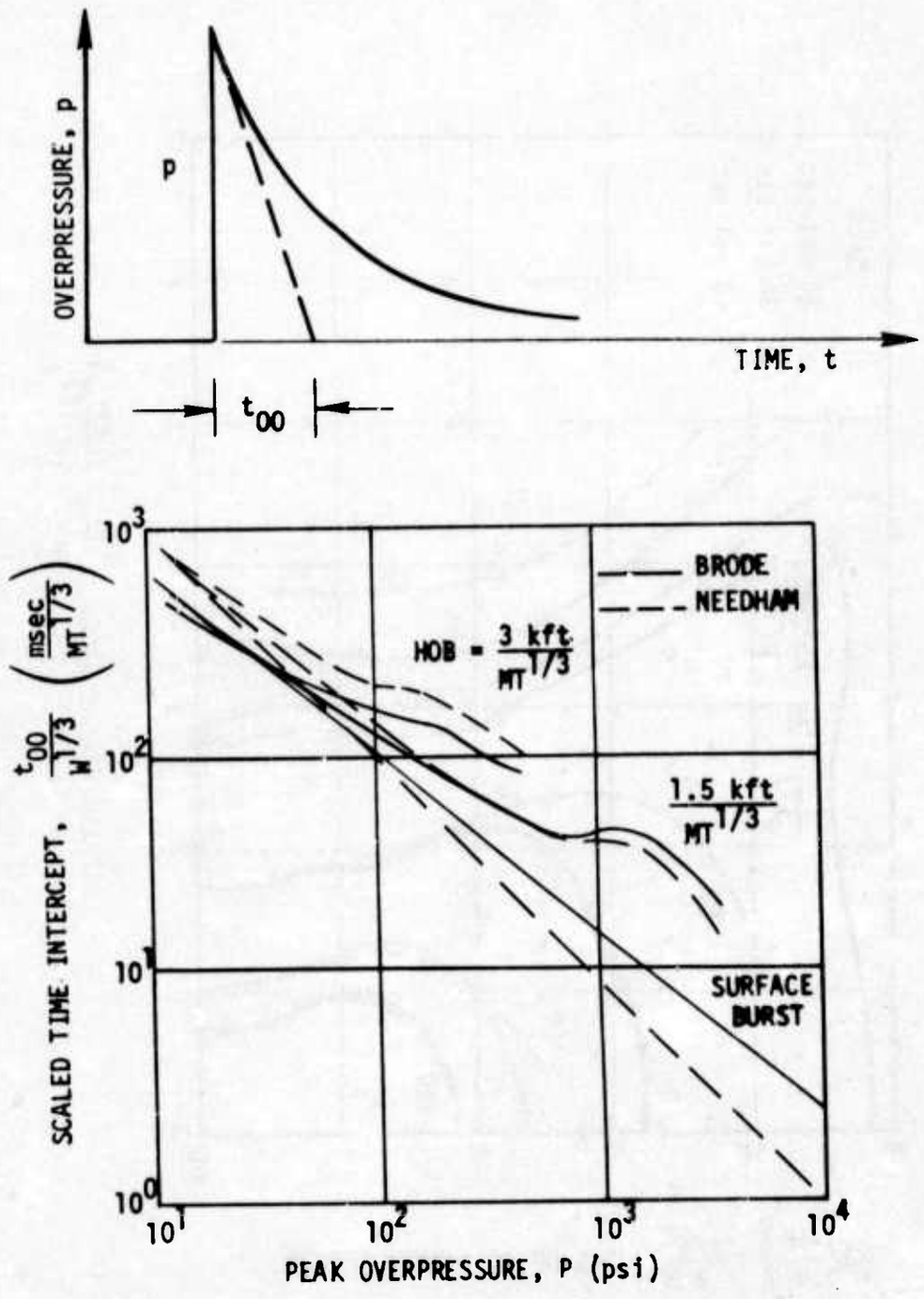

Figure 3. Overpressure Initial Decay Time Intercept

data for real (nonideal) surfaces, which probably explains the tendency for the predicted HOB curves to extend beyond the data scatter. For example, since real surface effects generally tend to reduce the static overpressure environment, ideal surface predictions will probably overestimate the static overpressure effects. As seen from the experimental data spread, the 2σ uncertainty factors are on the order of 2 to 3 depending on range and HOB. For ideal surfaces, the lower bound factor of 2 is a reasonable estimate.

To use small-scale high explosive data for predicting nuclear air blast environments, one must be aware of two basic differences between high explosive and nuclear detonations: the high explosive source efficiency relative to the nuclear source efficiency, and the influence of the high explosive yield to mass ratio compared with that of a nuclear source. Of primary concern is the potential match of the high explosive free-air shock overpressure decay with range to that of a nuclear source, and the high explosive pressure gradient behind the shock front compared with that of a nuclear source.

With regard to efficiency, high explosive sources like TNT, PETN, PBX, etc. are approximately twice as efficient as a nuclear source in generating air blast, except in the extremely close-in region, where differences appear because of the mass to yield ratio differences.

The influence of the yield-to-mass ratio on air blast environment is readily apparent when comparing high explosive and nuclear sources. A nuclear weapon detonated in the atmosphere will release its energy in two forms: approximately half will go into blast and shock and the remainder into thermal and nuclear radiation. A conventional explosive, on the other hand, will convert most of the energy released into blast and shock since the source temperatures are orders of magnitude less than those of a nuclear source.

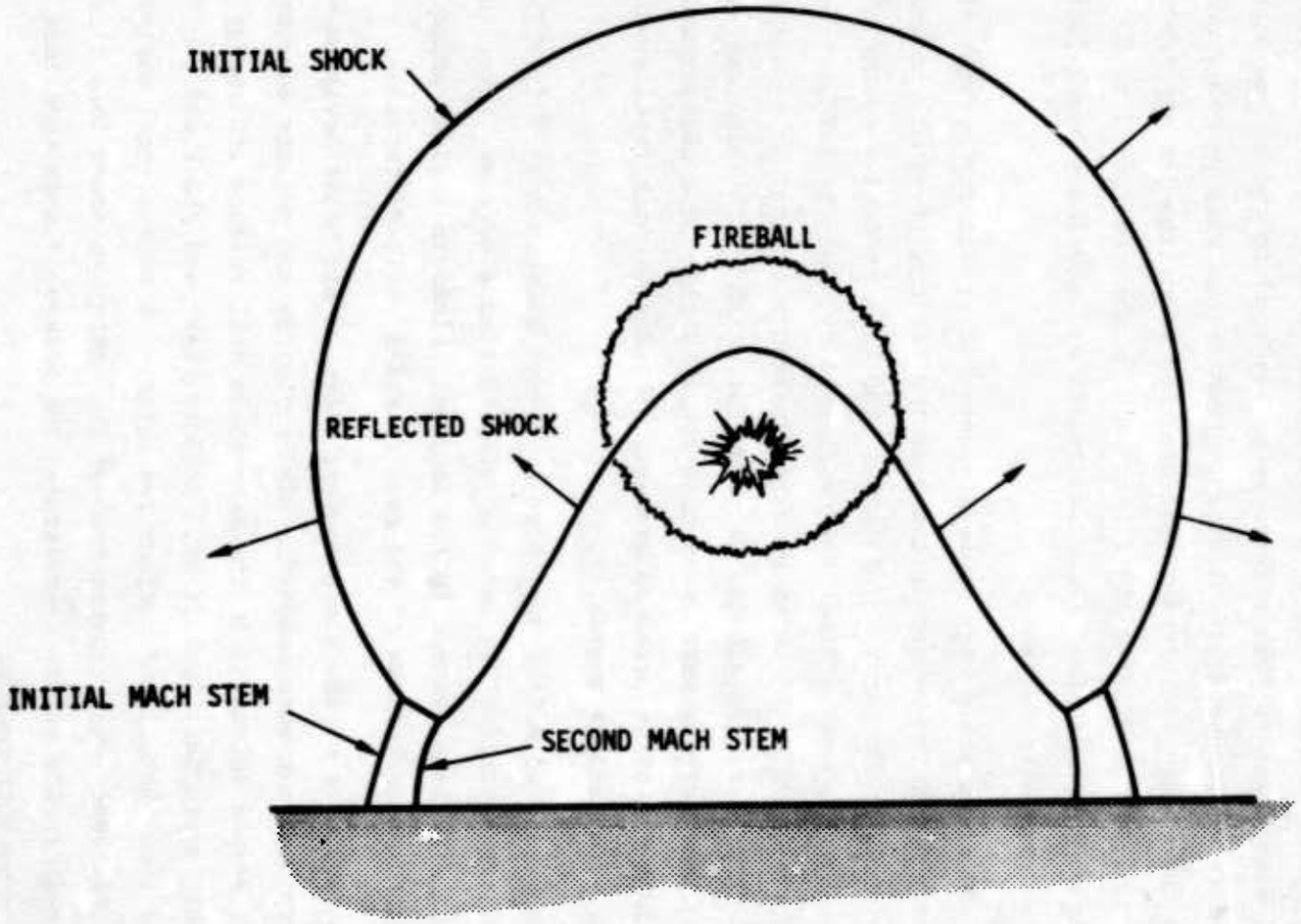

Figure 4. Height-of-Burst Shock Wave Pattern (Reference 13)

From observations of free-air blast data, one concludes (Reference 13) that HOB curves for high explosive can be used to predict nuclear source values provided scaling is restricted to incident pressures below the order of 25 atm, depending on the high explosive source considered. Of particular use for this study are the results from the highly controlled HOB experiments conducted by TRW. The experiments, which were performed with 8-lb spherical PBX 9404 explosives over a well-instrumented nearly ideal surface, revealed the existence of a double-peaked static overpressure waveform. This exists for certain ranges of overpressure, HOB, and ratio of HOB to ground range (Z). The experiment shows that the double-peak phenomenon occurs in the Mach reflection region. These results have also been observed in shock tube experiments (Reference 13) where a flow stagnation phenomenon occurs in the Mach stem region above about 100 psi reflected overpressure which produces a second static pressure "peak" at the surface. The character of the flow encompassing the shock front and this second peak is more complex than the classical concept of a single triple-point connecting the incident shock, the reflected shock, and the Mach shock. As overpressure increases, the flow changes ranging from a mere curl in the slipstream at the surface to a second or even third triple-point formation with additional Mach shocks extending to the surface (Figure 4). Such a phenomenon can be important to blast loading of structures that are protruding above or are flush with the ground surface.

A typical waveform for the double-peak region is shown in Table 1. At the shock front there is an initial peak overpressure, P_1, followed by a decay and a subsequent rise to the second peak, P_2. Depending on Z, the maximum overpressure can occur with either the first or second peak. Shown on Figure 5 are the normalized measured time intervals between peaks plotted against the ratio of ground range to HOB (1/Z) for the 8-lb test data. An approximate fit to the data is given by

TABLE 1. DOUBLE-PEAK PREDICTICN METHODOLOGY

PARAMETER	PREDICTION METHODOLOGY
Maximum Pressure P_1 or P_2	Brode (or Needham) free-air standard and Brode HOB interpolation scheme (Reference 6)
Lower Peak P_1 or P_2	Equation 2 (ratio of P_1/P_2)
Time Spacing Between Peaks Δt	Equation 1, with t_0 (arrival time at ground zero) calculated from Brode (or Needham) free-air standard
Minimum Point Between Peaks	$P_L = 0.6\ P_1$, $t_L = t_2 - 0.3\ \Delta t$
Waveform p(t)	(a) $t_1 < t < t_L$: straight line (b) $t_L < t < t_2$: straight line (c) $t > t_2$: $\overline{P}_B\ (P_2, W, t)$ - Brode (or Needham) HOB overpressure modified to conserve total impulse

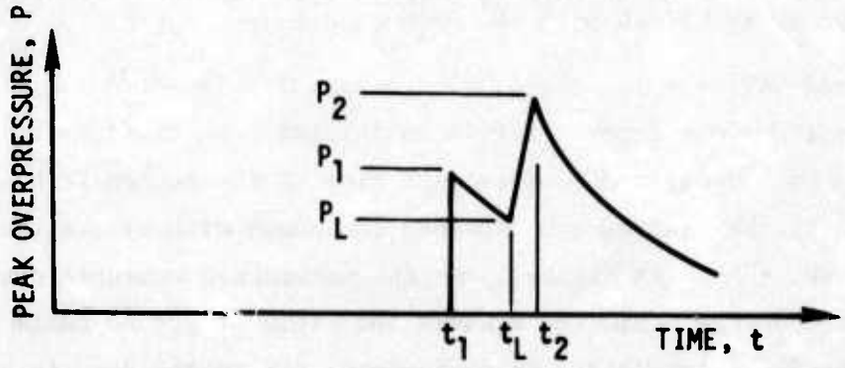

WAVEFORM PARAMETERS

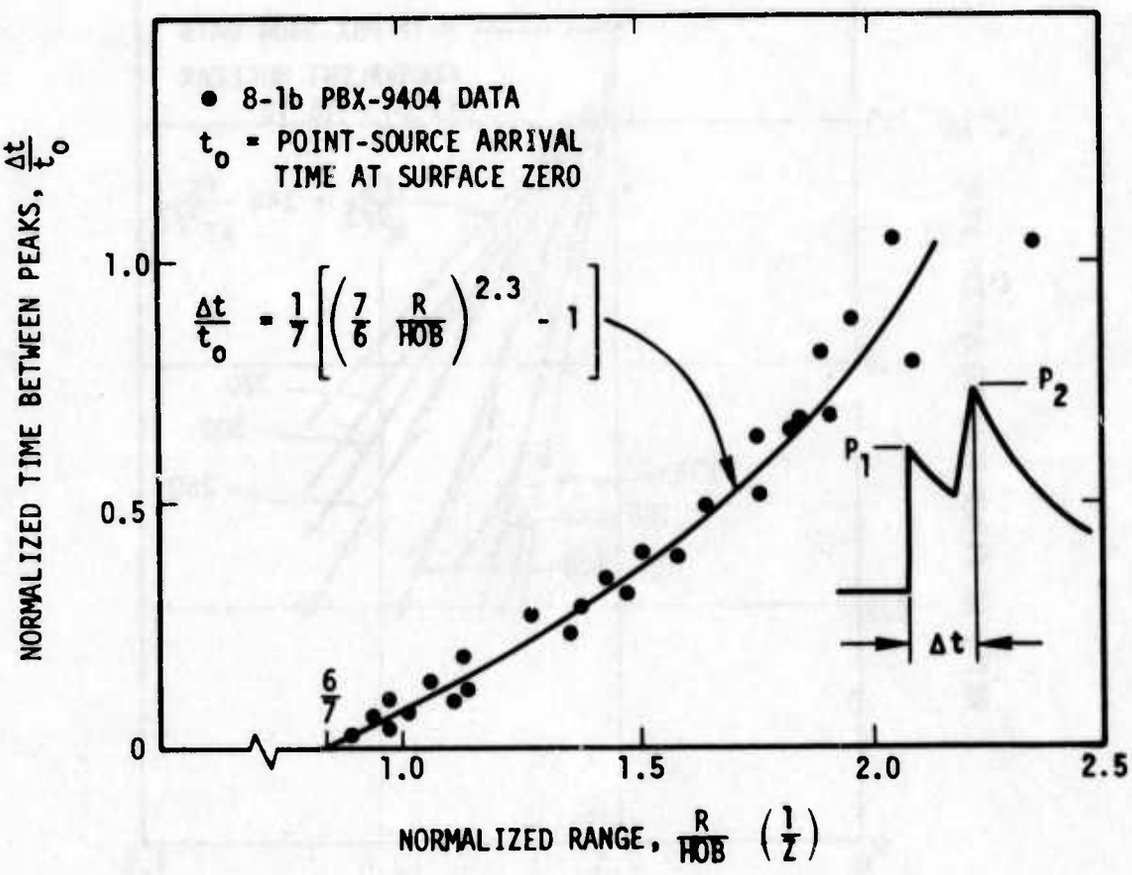

Figure 5. Time Between Peaks for Double-Peak Waveform

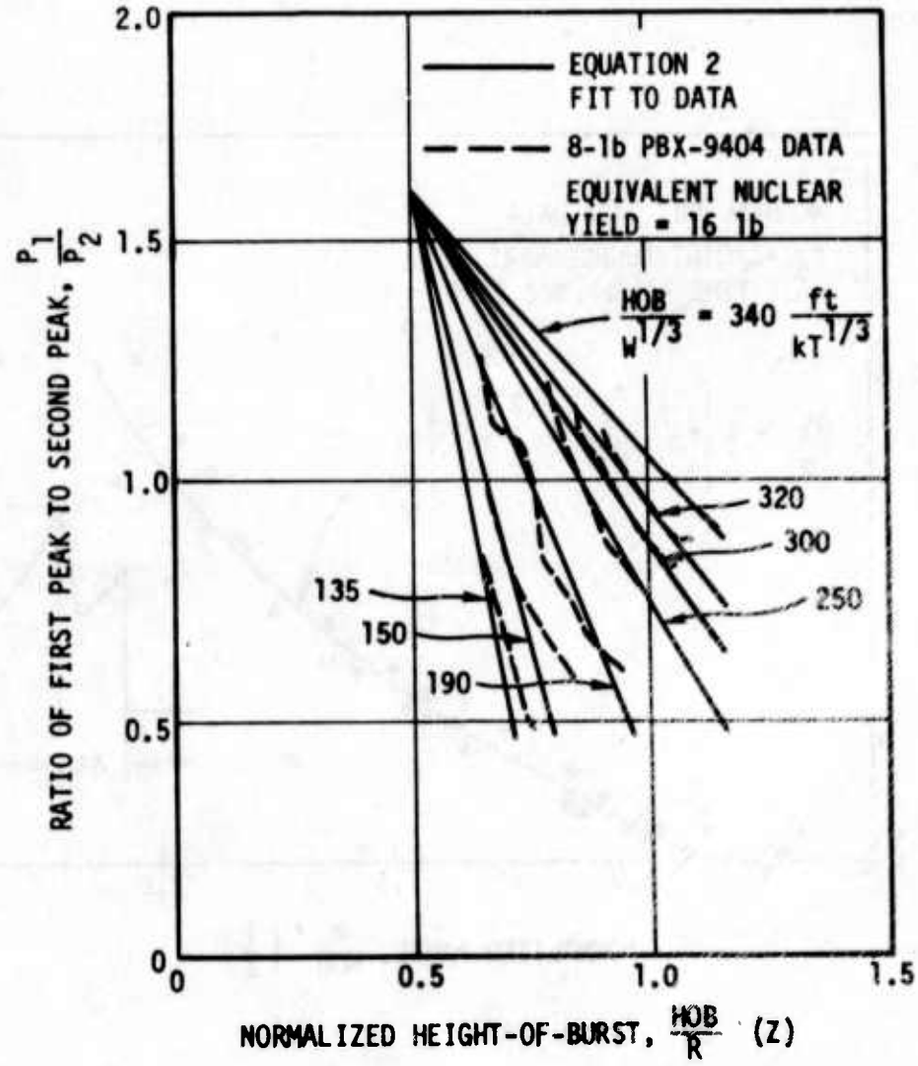

Figure 6. Ratio of Peaks for Double-Peak Waveform

$$\frac{\Delta t}{t_0} = \frac{1}{7}\left[\left(\frac{7}{6Z}\right)^{2.3} - 1\right] \qquad (1)$$

for $Z \leq 7/6$, where t_0 is the shock front arrival time at ground zero for an 8-lb point source detonation at the same HOB. This normalization was used for convenience in scaling the data to nuclear conditions. For Z greater than 7/6 (close-in range), there is only one peak; for very small Z (large range) the second peak is small and occurs much later than the first, at a time when the overpressure has decayed significantly.

Figure 6 shows the ratio of peaks for data from a fixed HOB plotted as a function of Z, thereby forming the family of curves (one for each HOB) shown. An approximate fit to this data was found to be given by

$$\frac{P_1}{P_2} = 1.6 - \frac{2.5 - \left(\dfrac{\text{HOB}/W^{1/3}}{450\ \text{ft}/kT^{1/3}}\right)}{\left(\dfrac{\text{HOB}/W^{1/3}}{450\ \text{ft}/kT^{1/3}}\right) - 0.11}\ \frac{(2Z - 1)}{5} \qquad (2)$$

Here the data show the second peak disappearing as Z goes to 0.5. Figure 7 shows the region (on a HOB-chart format) where the double-peak phenomenon has been observed. Other HOB experiments employing an explosive driver source (Reference 14) have also shown the existence of a double-peak waveform, for cylindrical geometry, in roughly the same overpressure region. Because the HOB high explosive experiments were carefully controlled and showed reproducibility of results, the existence of a double peak for the nuclear case with a nearly ideal surface is acknowledged. To predict the nuclear environment with these data, Equations (1) and (2) are used together with HOB analysis techniques. Table 1 presents the specific methodology for predicting the double-peak waveforms for a given yield and HOB.

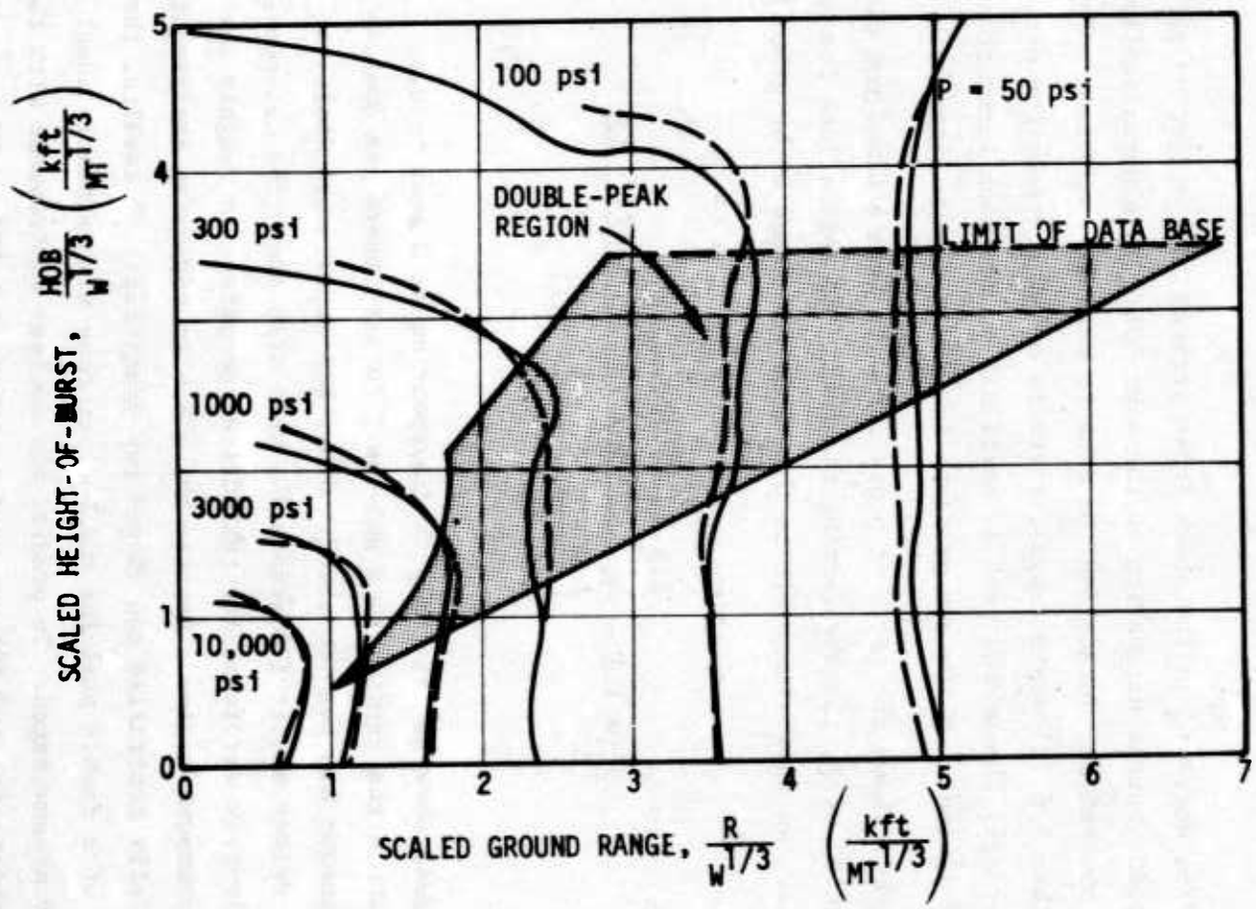

Figure 7. Double-Peak Height-of-Burst Chart

Double-peak overpressure waveforms, for a 1-MT, 1500-ft nuclear HOB are shown in Figure 8 together with the single-peak waveform as predicted using the Brode direct fit methodology. As seen in the figure the double peak begins to appear near 1000 psi overpressure and Z near unity and vanishes in the neighborhood of 100 psi and $Z \approx 0.5$.

3.1.2 Dynamic Pressure

Effects associated with the strong transient winds behind the shock front can sometimes be of primary significance. In particular, some structure geometries are drag-sensitive because they protrude above the ground surface. The drag forces are a function of the structure geometry and the dynamic pressure.

The dynamic pressure, q, results from the air mass flow (wind) behind the shock front and is defined as the local kinetic energy density. As such, its magnitude is proportional to the square of the wind velocity, u, and to the density, ρ, of the air; namely,

$$q = \frac{1}{2} \rho u^2 \tag{3}$$

When the appropriate Rankine-Hugoniot conditions based on mass, energy, and momentum conservation are applied, the peak dynamic pressure, Q, may be calculated as a function of peak overpressure. Figure 9 shows this variation of peak dynamic pressure with peak overpressure for sea level conditions. Also shown on this figure is the positive phase duration, D_u^+, for dynamic pressure resulting from a 1 MT surface burst. The peak dynamic pressure and duration have been taken directly from Reference 5.

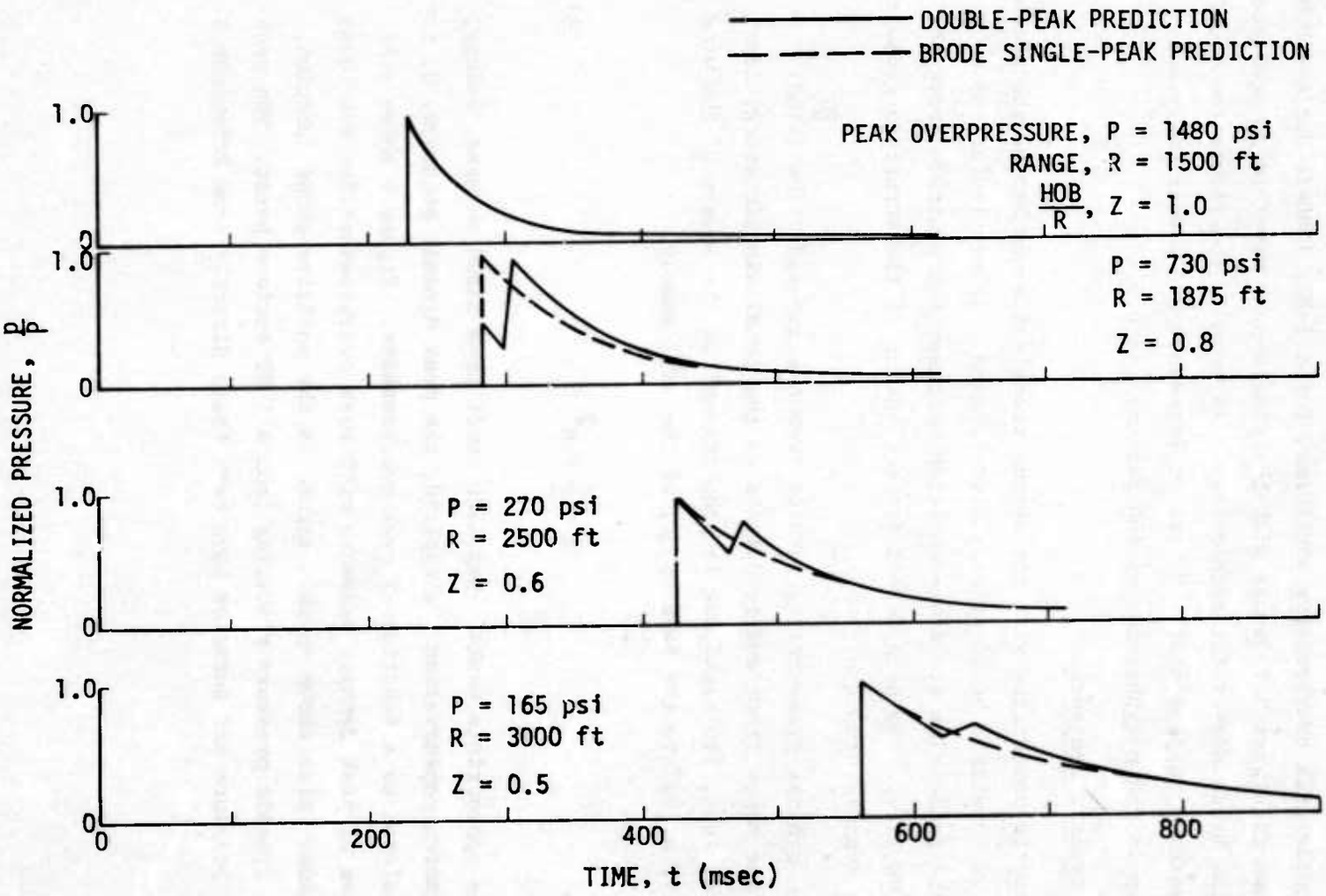

Figure 8. Double-Peak Overpressure Waveforms, 1-MT Yield, 1500-ft HOB

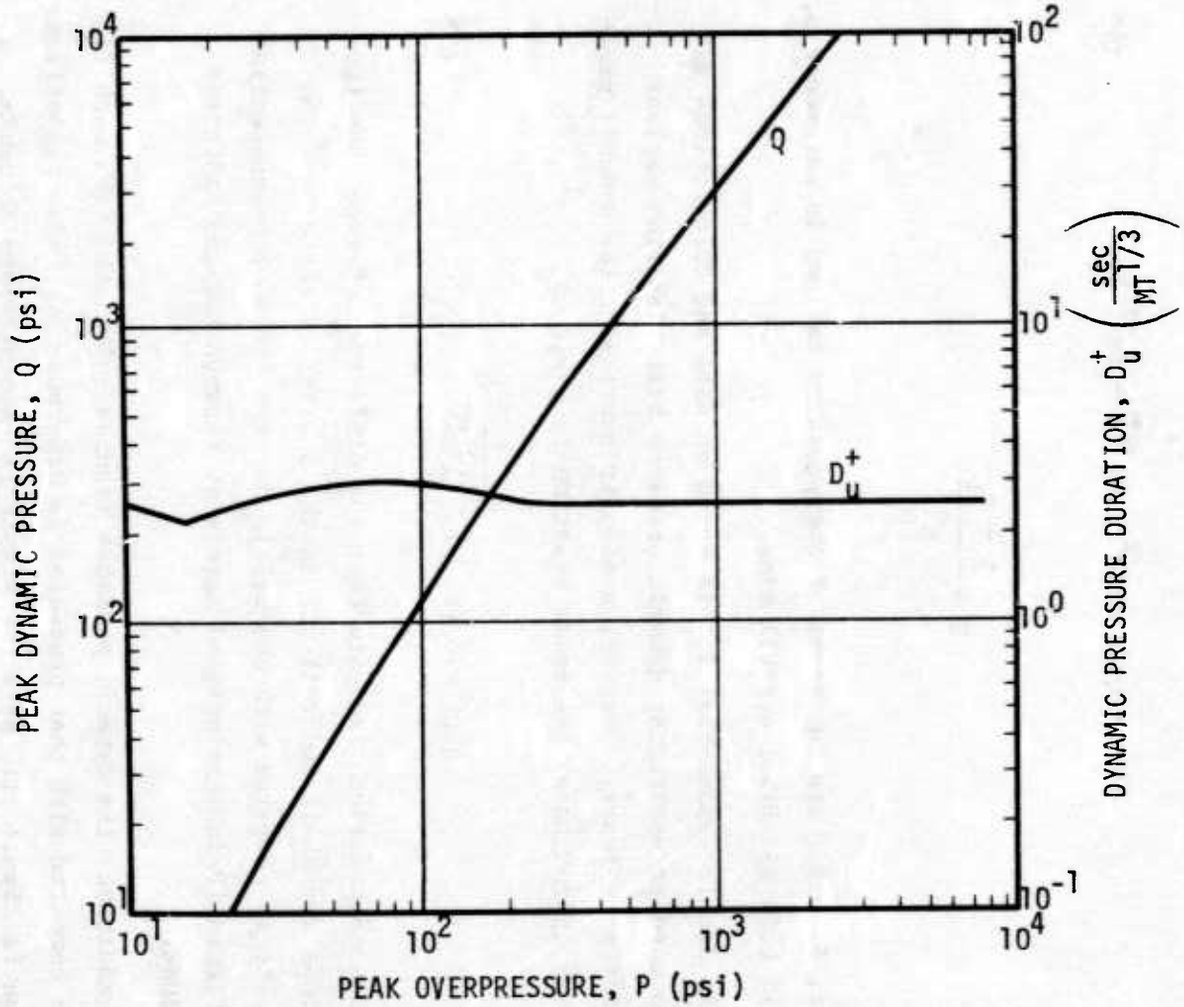

Figure 9. Peak Dynamic Pressure and Dynamic Pressure Duration vs Peak Overpressure (Reference 5)

Reference 5 suggests that the decay of the dynamic pressure with time can be expressed in an exponential form as follows:

$$q(t) = Q\ (1 - T)^2\ \ (de^{-\delta T} + fe^{-\phi T}) \tag{4}$$

where

$$T = \frac{t - t_1}{D_u^+}$$

and d, f, δ, and ϕ are functions of overpressure defined in Reference 5, and t_1 is this air blast arrival time.

This double exponential fit is based on data and calculations and has been used in estimating dynamic pressure histories from nuclear bursts for many years. However, a simpler expression for dynamic pressure which approximates the Brode equation is given by

$$q(t) = Q\ (1 - T)^{3\left(\frac{P}{10\ psi}\right)} \tag{5}$$

Comparison calculations indicate that the differences between the two expressions are small and well within the scatter of the data. The simpler fit is compared with the waveforms from the double-exponential fit in Figure 10 indicating good agreement between the two different expressions.

In addition, the dynamic pressure impulse calculated from each fit has been compared with that presented in Reference 5. These comparisons are given in Figure 11. Here the simple fit appears more accurate. A third comparison considered the initial decay time intercept as a function of peak overpressure. These results are shown in Figure 12. Again the comparison shows excellent agreement. As a result of these comparisons

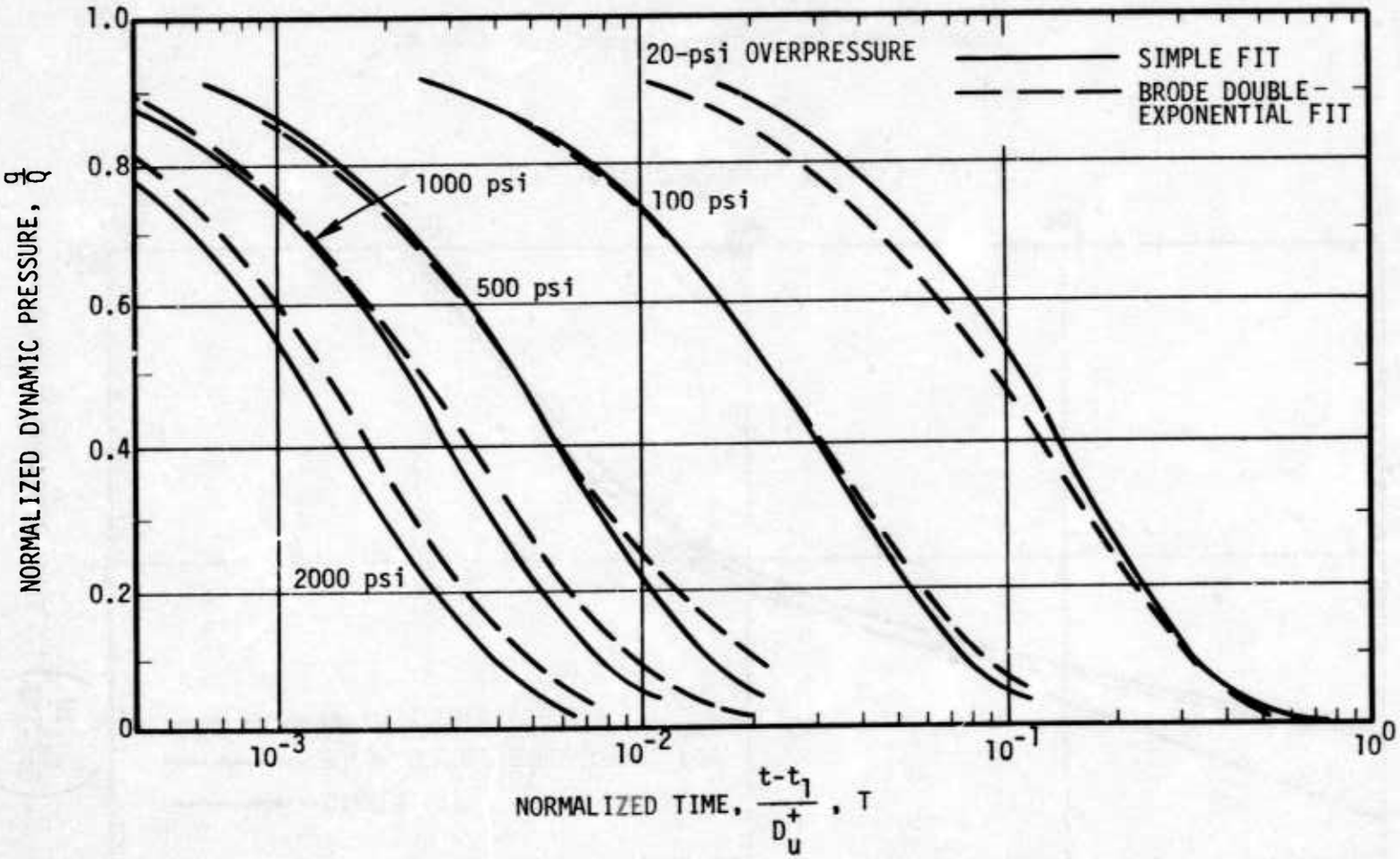

Figure 10. Surface Burst Dynamic Pressure Waveform

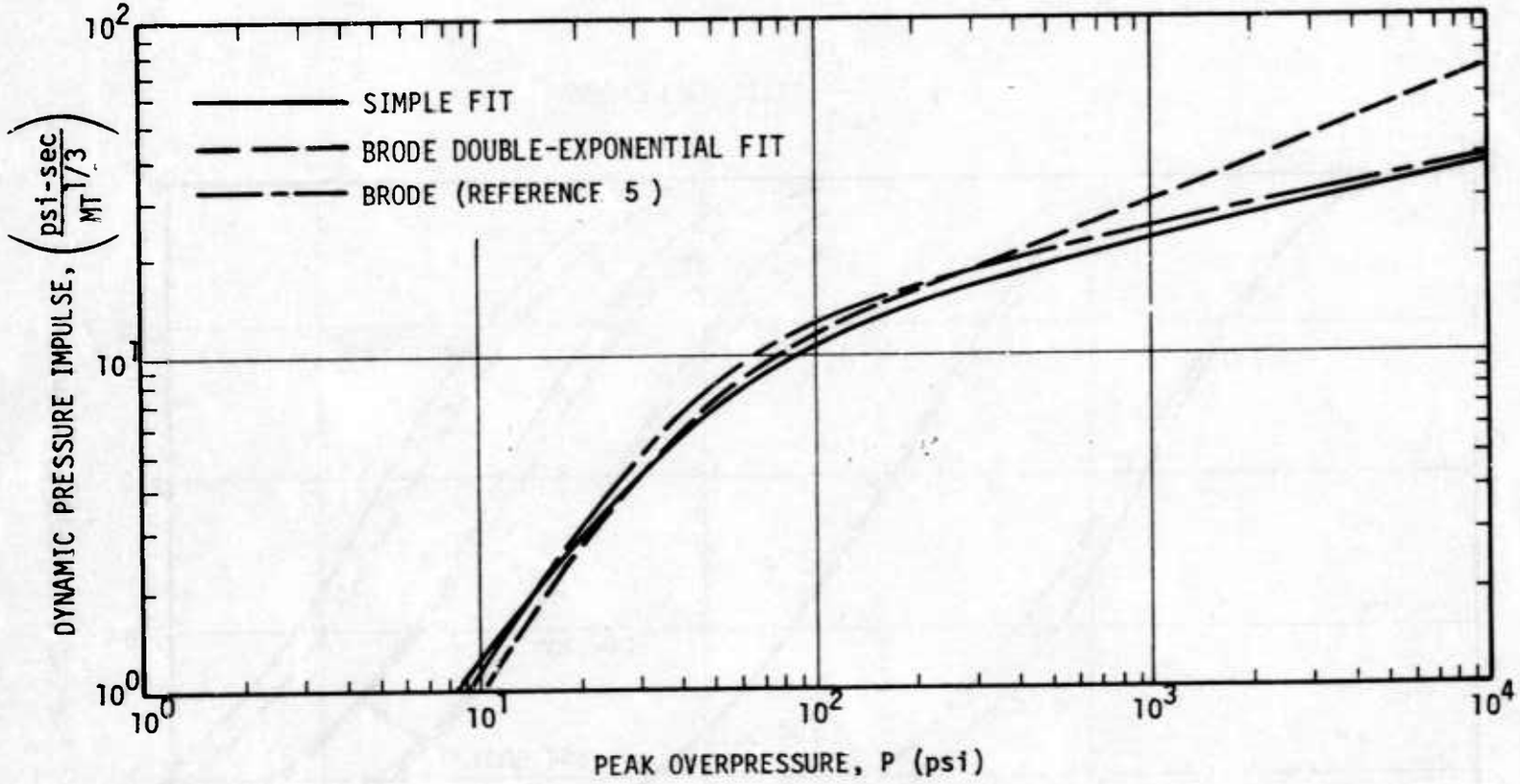

Figure 11. Dynamic Pressure Impulse History

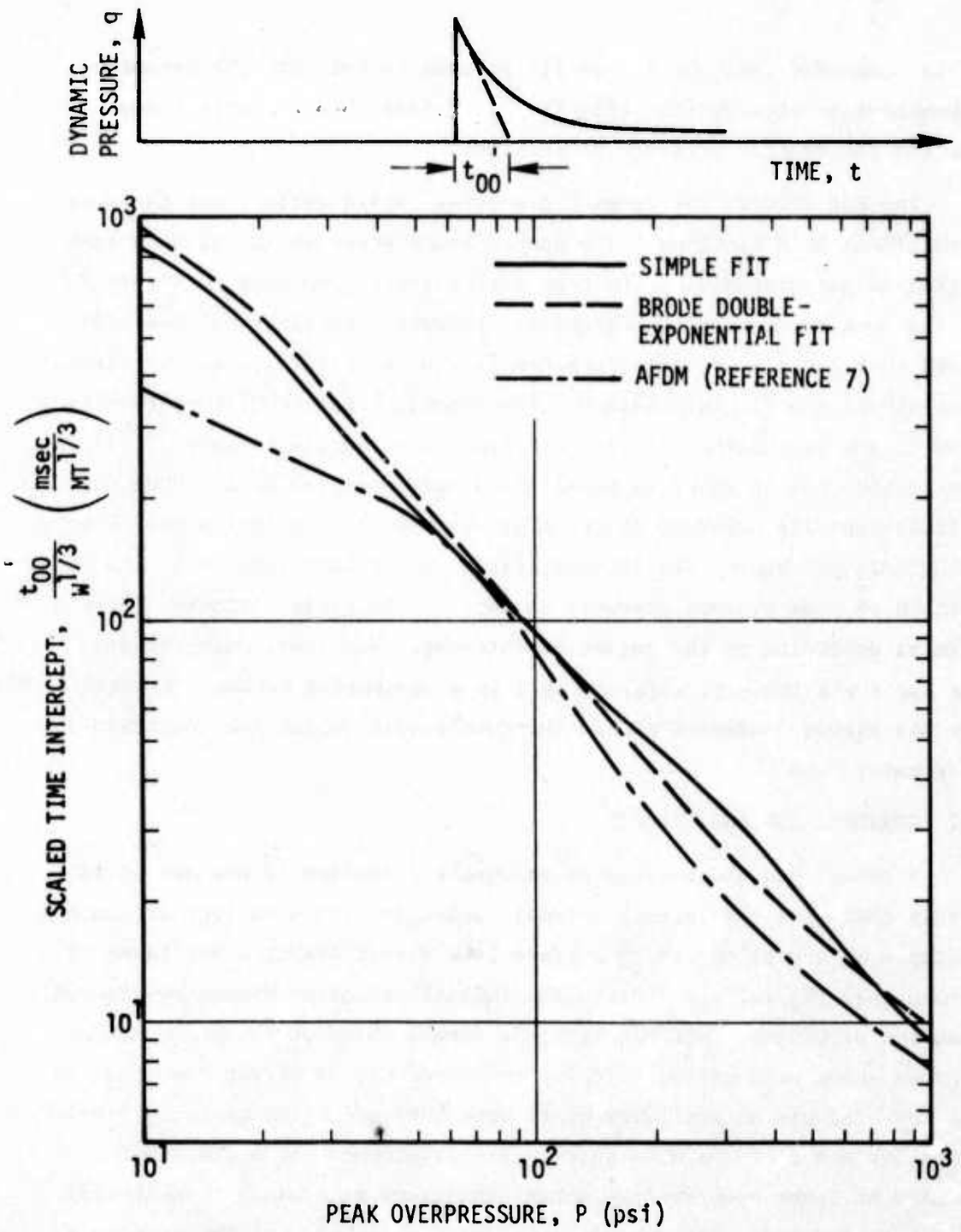

Figure 12. Dynamic Pressure Initial-Decay-Time Intercept

it is suggested that the simple fit be used to estimate the dynamic pressure-time history resulting from a surface burst. Table 2 summarizes the dynamic pressure definitions.

The HOB affects the dynamic pressures considerably since they are directional by definition. The peak dynamic pressure in the Mach stem region is associated with the peak overpressure according to Figure 9. In the double-peak region, Carpenter (private communication) has indicated that the peak dynamic pressure is generally related to the first peak (shock front) overpressure. The dynamic pressure history resulting from an HOB detonation is extremely complex primarily because of slipstream effects and waveform predictions have not been made. Here again calculations are underway at the AFWL which will help define HOB effects on dynamic pressure. The 2σ uncertainty factor associated with the prediction of peak dynamic pressure on ideal surfaces is estimated to be 3 or greater depending on the region of interest. For lower overpressures (10 psi < P < 100 psi) a factor of 3 is a reasonable estimate of uncertainty For the higher pressures and in the double-peak region the uncertainty is greater than 3.

3.2 NONIDEAL SURFACE EFFECTS

Although the exact cause of precursor formation is unknown it is likely that when the intense thermal radiation from a nuclear detonation impinges on a heat absorbing surface like desert playa, a hot layer is formed near the surface. Since the thermal radiation propagates faster than the air blast, this hot layer is formed ahead of the blast wave. Because shock propagation velocity in heated air is higher than that in the unheated air an auxiliary blast wave (the so-called precursor) will propagate ahead of the main shock. The development of a precursor results in lower peak overpressures, increased rise times to peak overpressure, and increased dynamic pressures. A feature of the increased

TABLE 2. DEFINITION OF DYNAMIC PRESSURE HISTORY

PARAMETER	DEFINITION
Q	Peak Dynamic Pressure (see Figure 9)
D_u^+	Positive Phase Duration (see Figure 9)
t, t_1	Time, Initial Arrival Time
d, f, δ, ϕ	Parameters used for computing Brode dynamic pressure history q(t) (see Reference 5)
T	Dimensionless Time $\frac{t - t_1}{D_u^+}$
q(t)	Dynamic pressure history (a) Brode double exponential fit: $Q\,(1 - T)^2\ (de^{-\delta T} + fe^{-\phi T})$ (b) Simple Fit: $Q\,(1 - T)^{3(\frac{P}{10\ psi})}$

dynamic pressures is the greater air densities caused by dust from thermal radiation effects and blast wave scouring.

Because the formation of a precursor is attributed to the presence of a hot thermal layer preceding the air blast, it is not to be expected for large HOB or for nondusty heat-reflecting surfaces such as snow, ice, or water. Instead, it is most likely to occur over

heat-absorbing materials such as dry soil. In the low overpressure region ($P < 10$ psi) a precursor air blast will have "shocked-up" and show a more classical waveform.

The significance of the precursor is dramatically illustrated by superimposing the Brode HOB ideal surface pressure-time prediction on the experimental precursor data from PRISCILLA. Figure 13 shows three such overpressure records. The precursor precedes the arrival of the predicted waveform for the ideal surface case. In addition, the peak overpressure associated with the precursor waveform is generally lower than the corresponding peak for the ideal surface case. The impulses associated with each pressure history are approximately equal.

The data base for nonideal surface effects on air blast is small. A few overpressure histories were recorded on the PRISCILLA shot and records are available from the TEAPOT, UPSHOT KNOTHOLE (U/K), and TUMBLER test series, but again the data are scarce for the higher overpressure regions. Currently, the data base is being increased by the development of calculational tools and investigations into the feasibility of conducting simulation experiments. Specifically, the AFWL is performing first principle computer code calculations for describing the PRISCILLA air blast environment to validate a precursor prediction capability. However, the thermal initial conditions are a key uncertainty in these calculations.

All this activity is current and consequently the only technique now available for predicting precursor phenomena is that which was initially reported in DASA 1460 and incorporated in the Air Force design manual (Reference 7). Figure 14, reproduced from these references, shows several characteristic waveforms which are used to describe precursor effects. The figure uses a HOB-chart format to illustrate the waveforms one might expect in the precursor zone. For those combinations of HOB and ground range falling outside of the shaded area, precursors are not expected to occur.

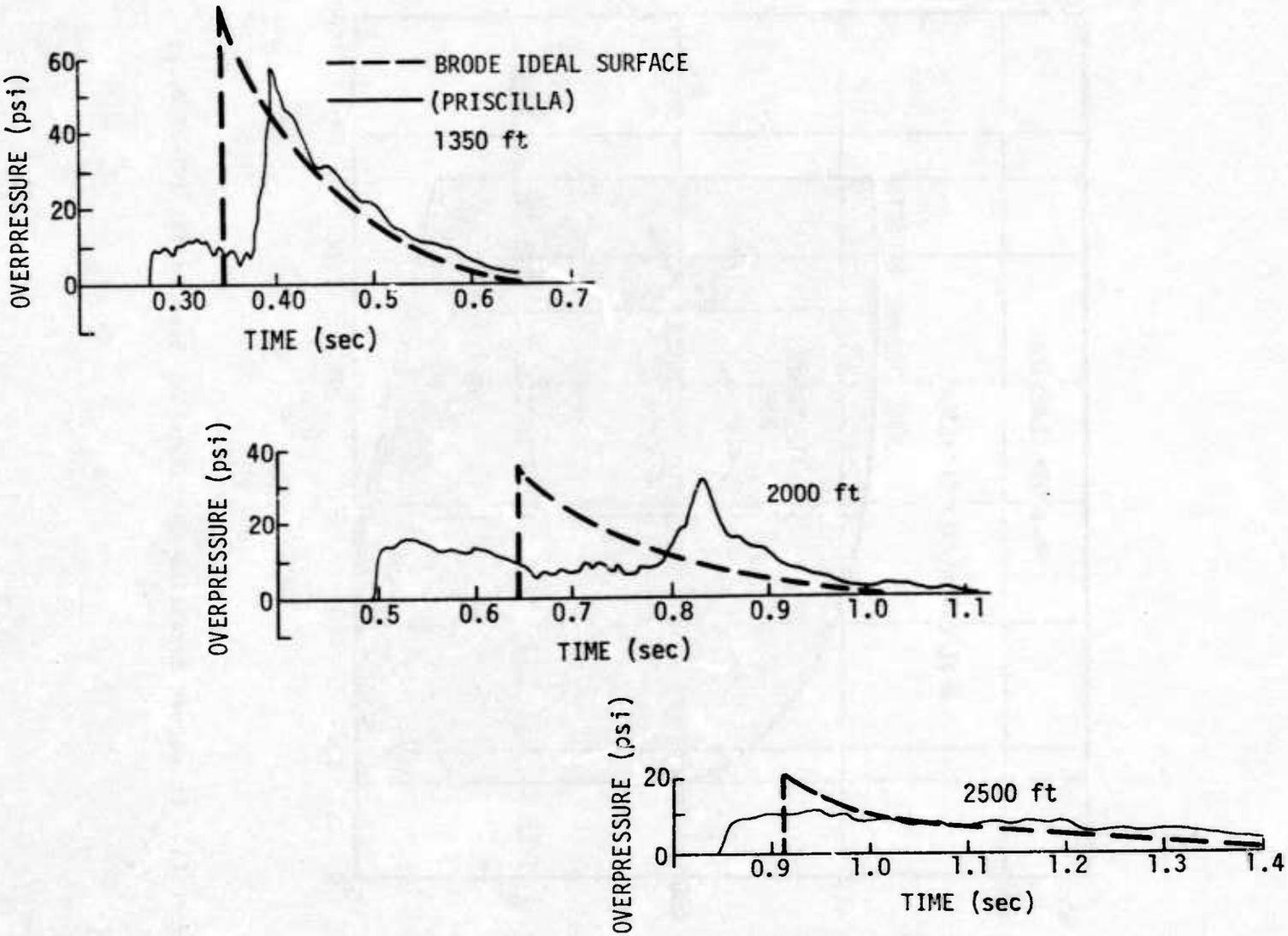

Figure 13. PRISCILLA Overpressure Waveforms

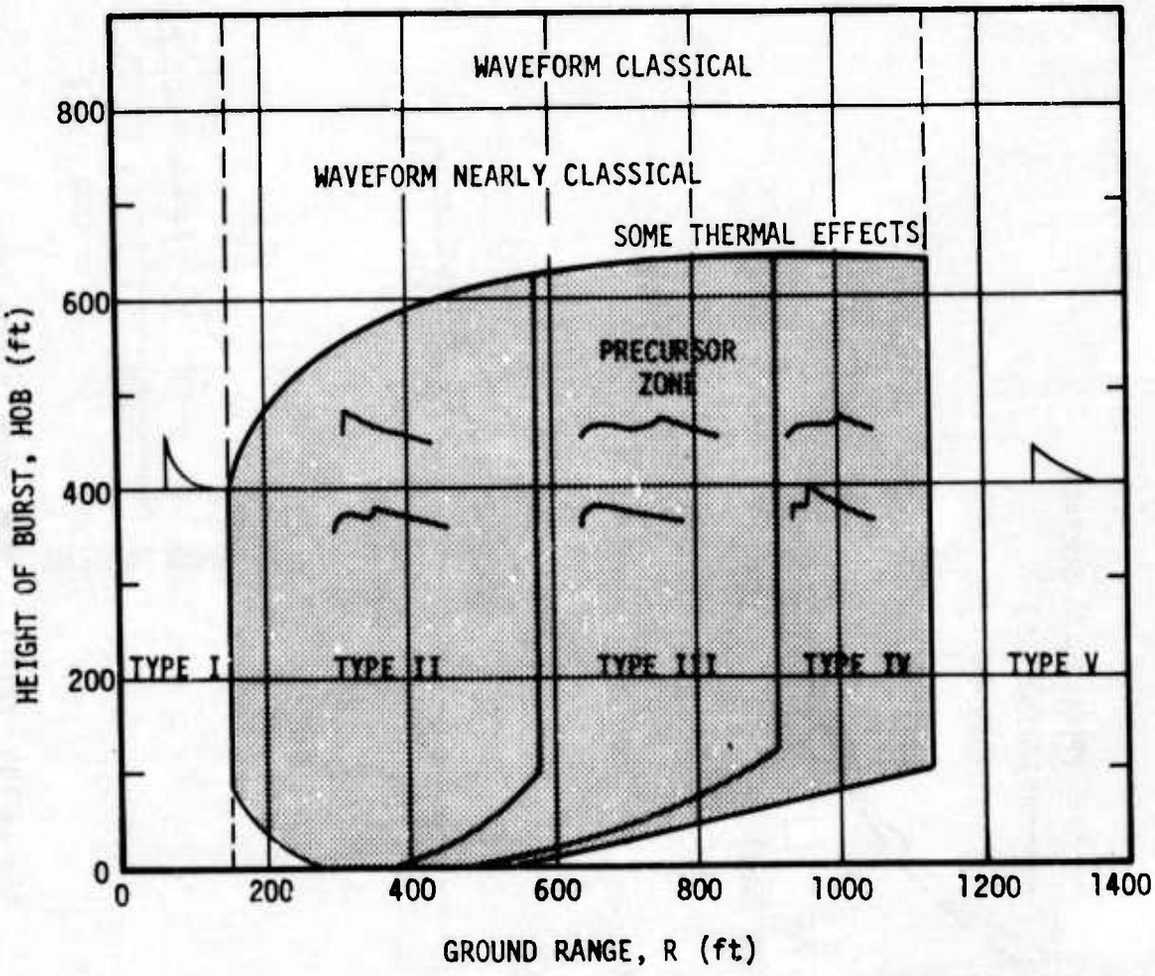

Figure 14. Precursor Formation Over Nonideal Surface for a 1-kT Burst

A lower-bound estimate for dynamic pressure effects for nonideal surfaces is that value predicted for an ideal surface. This estimate, used in the past, stands to reason because a precursor surface reduces the overpressure and increases the corresponding dynamic pressure. Uncertainties associated with the prediction of air blast effects on a precursor surface exceed a factor of 3, since few data or analytical results exist for such environments.

3.3 BERMED SURFACE EFFECTS

A particular case of interest to this study is the interaction of the free-field air blast with a bermed structure, defined as one whose front and rear surfaces are oriented at angles less than 45 degrees from the horizontal (Figure 15). This type of structure takes advantage of the lower reflected pressures associated with the Mach reflection region. Exact theoretical solutions describing the gas dynamics of this region do not exist, so that prediction of the pressure loading on the front face of the berm can only be approximated. The AFWL is currently performing AFTON calculations to determine loadings on such structures, the results of which should give a reasonably accurate picture of the interaction of the free-field air blast with a bermed structure.

Techniques for approximating loadings on different structure shapes have existed since the early 1950's (Reference 1). In addition, the current Air Force design manual reproduces a number of these prediction techniques. A reasonable prediction method, applicable for incident pressures greater than 100 psi, has been reported by the AFWL in a study related to MX.

Knowledge of the incident static and incident dynamic pressures are required to apply this prediction method (presented in Figure 15). The average loading on the front face of the berm is then given by

$$p_F(t) = p(t) + C_p\, q(t) \qquad (6)$$

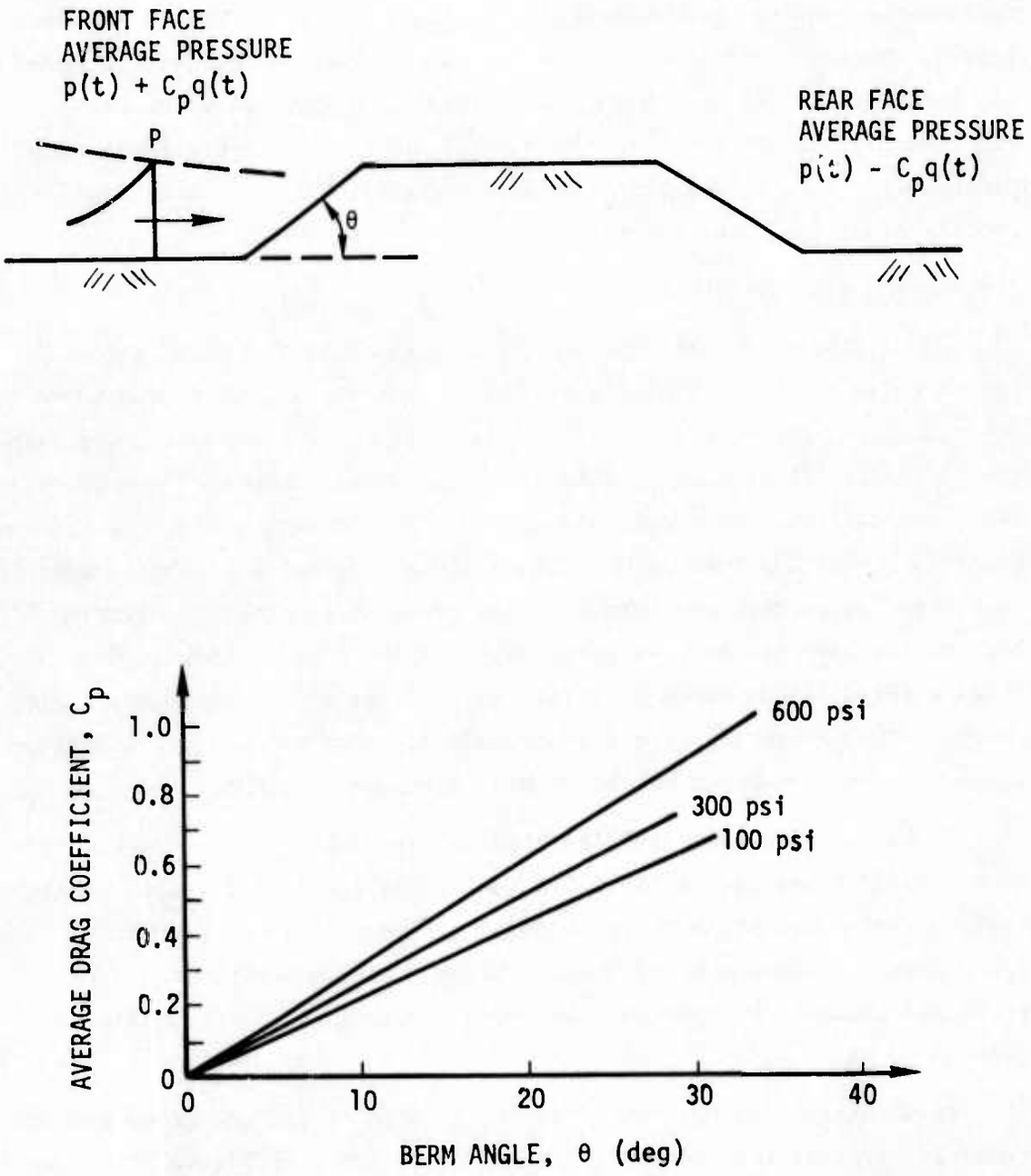

Figure 15. Pressure Loading on Bermed Surface

where C_p is the average pressure coefficient given on Figure 15, whose value has been established experimentally. A reasonable estimate for the loading on the top of the surface can be taken as the free-field overpressure history. The rear face of the berm will experience a loading which is estimated by

$$p_R = p(t) - C_p\, q(t) \tag{7}$$

The value of the pressure coefficient, C_p, is taken as the same for the rear face as it is for the front face. This is a commonly accepted practice for predicting loadings on symmetrical structures. As a result the net horizontal loading on the berm approaches $2\, C_p\, q(t)$.

The uncertainties associated with predicting the loadings on the bermed surface are the same or greater than those quoted for the other air blast effects. Current effort at AFWL seems to indicate that the values of C_p given on Figure 15 may be too low; however, they do represent available data.

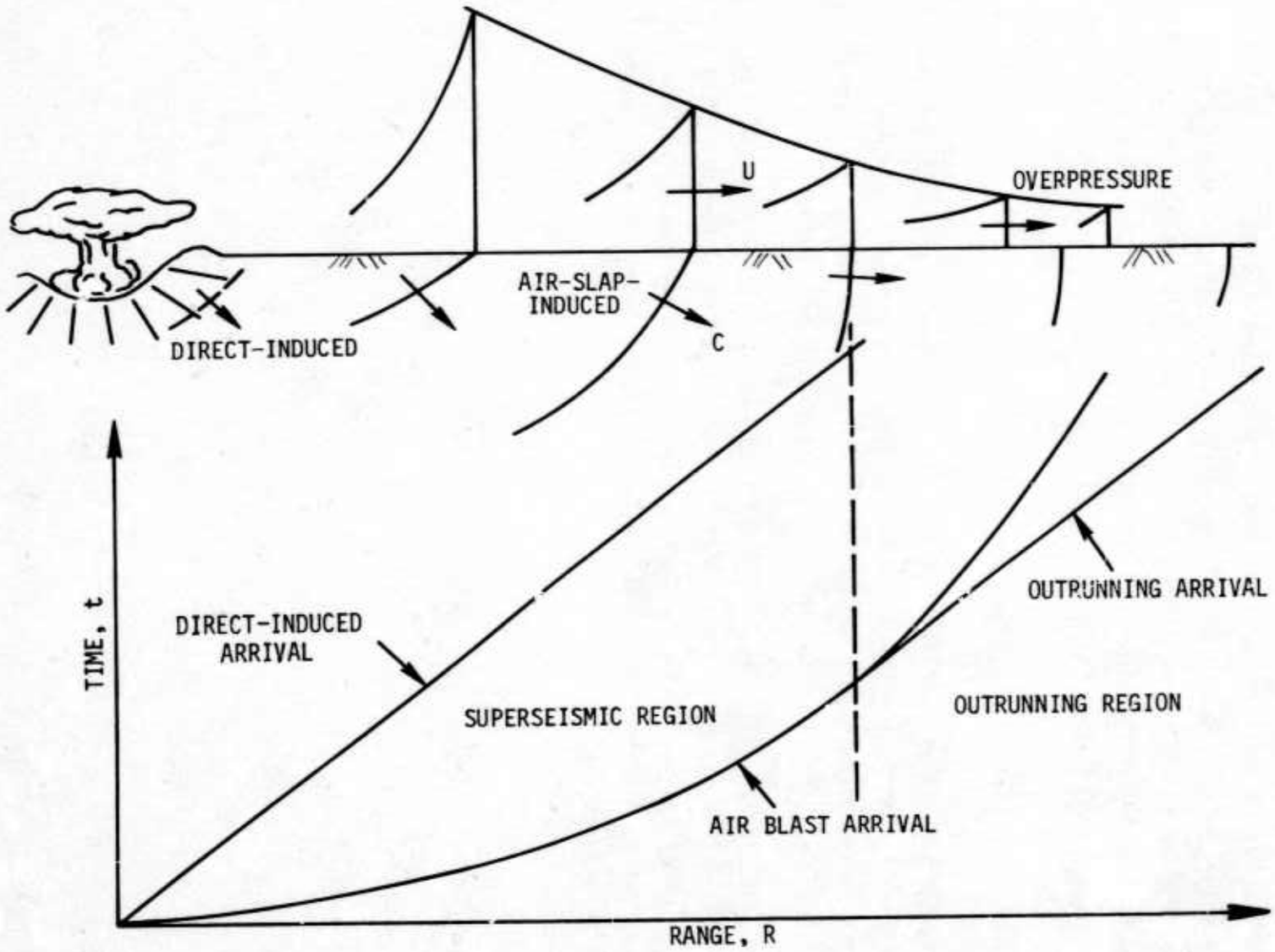

Figure 16. Surface Burst Ground Shock Phenomenology for Homogeneous Geology

4.0 GROUND SHOCK ENVIRONMENT

The amount of energy directly coupled into the ground depends on the weapon yield, design characteristics, and HOB, and the site properties. This direct coupling of energy and the air blast loading on the ground surface comprise the sources of the ground shock environment.

Figure 16 exhibits the ground shock phenomenology associated with a surface burst detonation in homogeneous geology. In the superseismic region, where the air blast wave speed exceeds the ground shock wave speed, effects from the overhead air blast (air slap) loading arrive first, producing initially downward and outward motion. The ground shock wave front is attached to the air blast front, having a fairly shallow angle at high overpressure and becoming more vertical with increasing range as the overpressure decays and the air blast front slows down. In the outrunning region, where the air blast speed lags behind the ground shock speed, more complex motion occurs on account of a more significant influence of upstream air blast sources. The ground shock wave front becomes detached from the air blast front and initial motion of a surface point precedes the air blast arrival. The response resulting from direct coupling of energy into the ground is termed "direct induced" (DI) when referring to early-time effects associated with the shock front, and "crater induced" (CI) when referring to later-time large outward and upward squish motion associated with the development of the crater and with other free surface effects. The DI/CI effects for surface burst ground shock occur in both the superseismic and outrunning regions, but follow the arrival of air-blast-induced (AI) effects.

For nonhomogeneous sites, geological layering can significantly affect the ground shock response. Shock signals travel faster in

underlying stiffer layers and the ground shock at depth can outrun the air blast while superseismic conditions still exist near the surface. Figure 17 exhibits the ground shock phenomenology for a two-layered medium. The shock wave in the lower stiff layer induces a refracted wave into the upper layer. At some range, defined as the onset of outrunning, the refracted wave will reach the ground surface at the same time as the air blast. Beyond this point, first arrivals are upstream AI signals, with the initial surface motion being up and out.

Figure 18 shows a typical response of a point, at a range $R = R_2$, located within the outrunning region. The point will initially feel the refracted wave, followed by the air slap and, finally, the DI effects. At a larger range, the DI arrival begins to outrun the air slap arrival. A near-surface point located within the superseismic region, at $R = R_1$, first experiences the arrival of the air-slap-induced wave, followed by the refracted wave from the lower layer; then comes the reflection of the air-slap-induced wave off the lower layer, and, subsequently, the DI arrival.

In the outrunning region, the primary motion is typically oscillatory and low frequency. The response has both AI and DI/CI components, but characteristics of the motion do not appear to be strongly linked to the source. These low frequency motions are termed "ground roll." Their presence is not limited to the outrunning region since similar types of motions can occur, at later time, within the superseismic region. However, this report primarily considers the ground roll response for the transition and outrunning regions, where it is more dominant.

Because of the complexity of the ground shock environment, attempts are made to separate the phenomenology into fundamental components. This is an engineering approach since the nonlinear interaction between

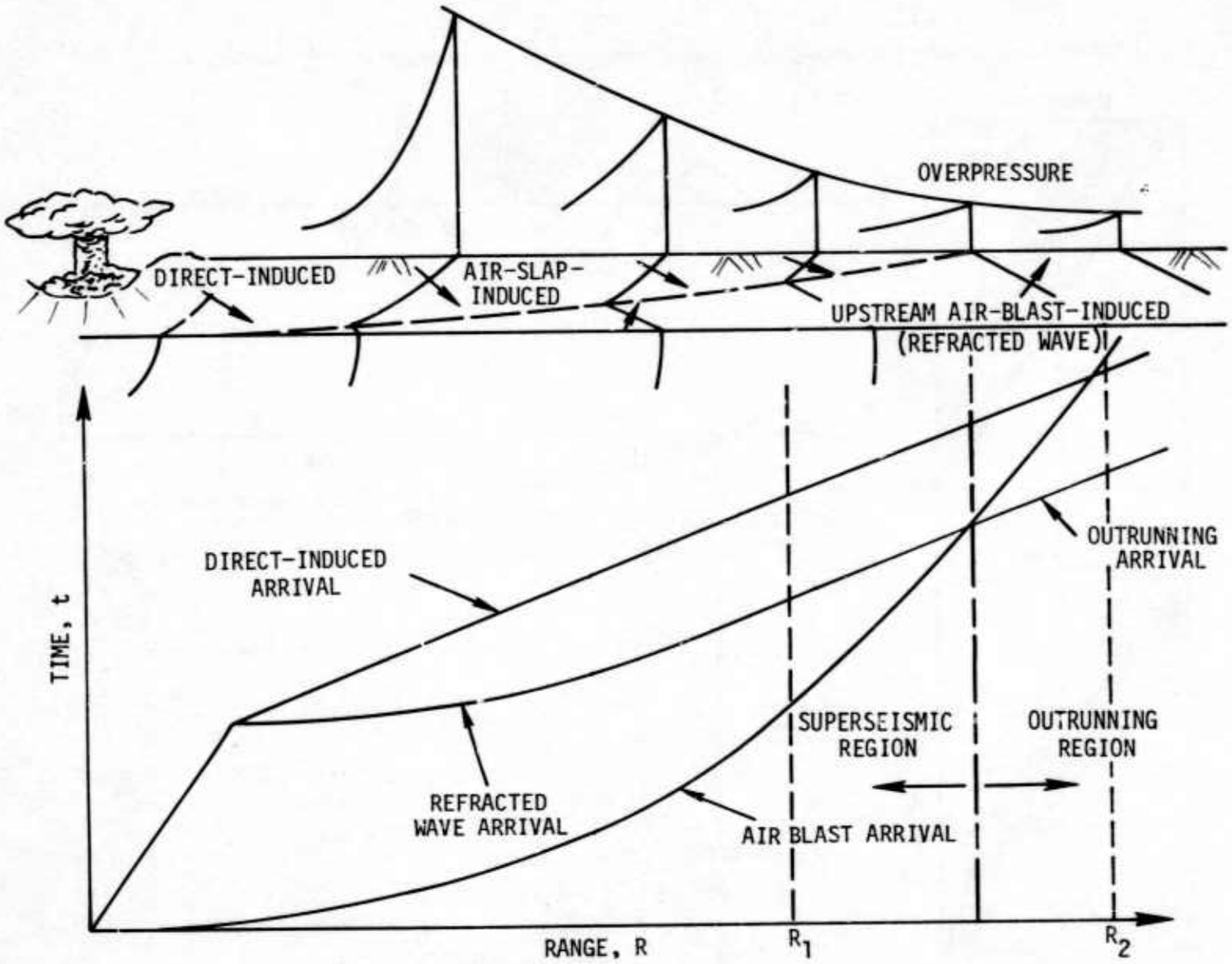

Figure 17. Surface Burst Ground Shock Phenomenology for Layered Geology

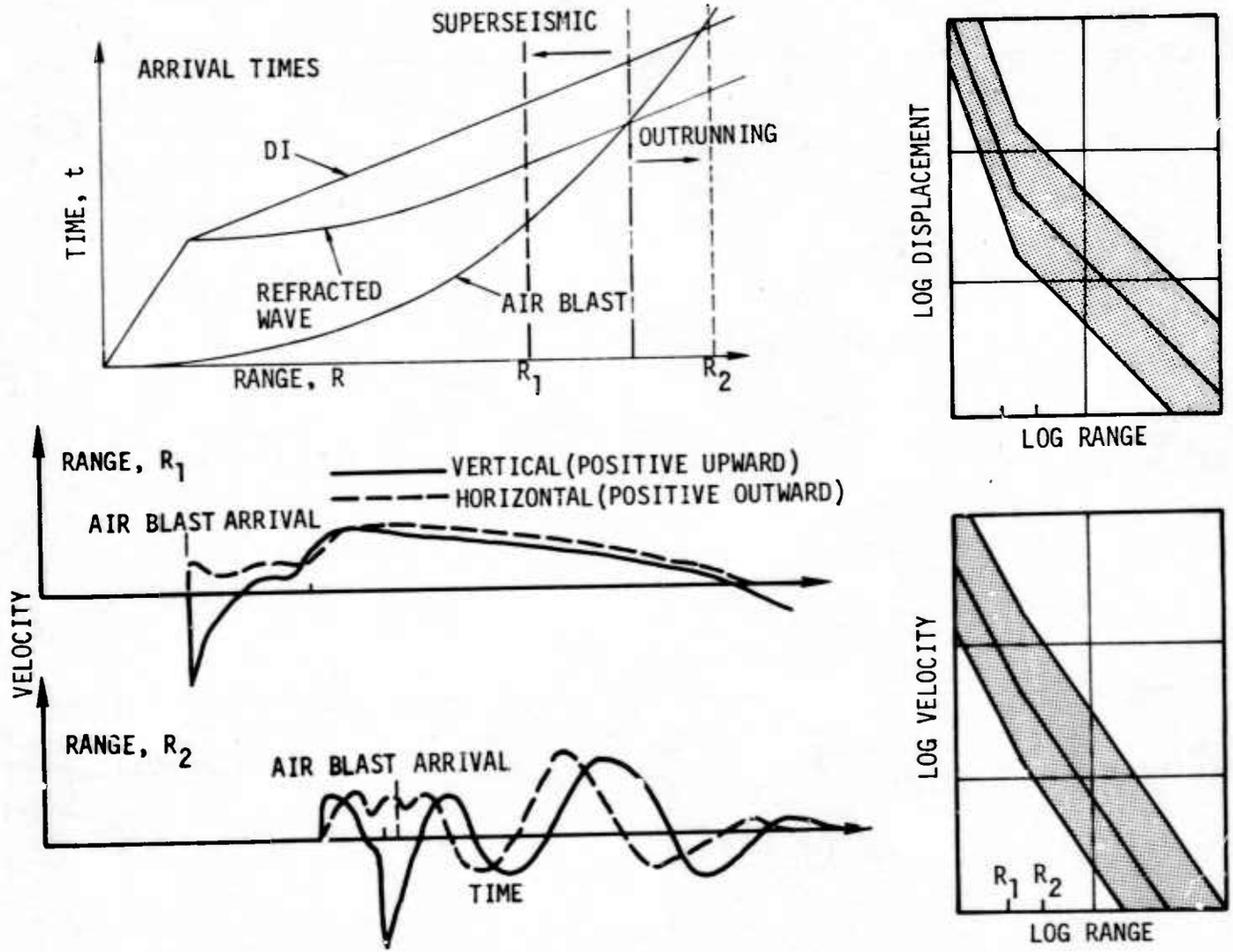

Figure 18. Representative Surface Burst Waveforms for Layered Geology

components does not allow for such separation on a theoretically sound basis. Phenomenologically, it is convenient to think of the ground shock environment as having components that are due to the AI and DI/CI sources. However, the test data, which are the primary basis for ground shock predictions, have components that are separable more by response characteristics such as frequency content and time phasing than by source.

For ranges closer in than the order of $5V^{1/3}$ (Reference 15), where V is the apparent crater volume, the motion due to a surface burst is predominately composed of (1) air slap effects associated with the overhead surface pressure history and pressure gradients, and (2) the DI/CI squish motions. For larger ranges, the low frequency ground roll oscillatory type of motion begins to dominate, with the air slap adding a higher frequency component. The transition between close-in and far-out regions is marked by a change in displacement attenuation with range, shown in Figure 18. The close-in squish motions attenuate rapidly, but the ground-roll-dominated motions attenuate much less severely.

4.1 DATA BASE

The ground shock data base for this study consists of nuclear and high explosive test results, calculational results, and material property data. This section provides a discussion of the data base for field test events and the associated sources of uncertainty.

4.1.1 Nuclear and High Explosive Test Events

Table 3 presents a summary of the primary surface and HOB field test data sources. The table lists the test site and geology, the source type, yield, and HOB, and the medium properties and ground shock data sources. Appropriate references of test event calculations are included in the table.

TABLE 3. GROUND SHOCK DATA BASE, NUCLEAR AND SINGLE-SOURCE LARGE-YIELD HIGH EXPLOSIVE EVENTS (Continued)

TEST SITE, MEDIUM		PROPERTIES		EVENT		SOURCE		HOB	DATA BASE					REFERENCE	
		Lab	Field			Type	Yield	(ft)	P (psi)	a	v	d	σ	Data	Analysis
Nevada Test Site (NTS) Frenchman Flat "Dry" Fine Grain Playa Silt (Alluvium)		U of I WES	AFWL (CIST)	SMALL BOY		NE		10	20-300	x	x	x	x		
				PRISCILLA		NE	37 kT	700	50-750	x		x	x	16,17	44,45
				TUMBLER 1		NE	1 kT	800	<50	x				2,18	46
				U/K 9		NE	26 kT	2400	<100	x					
				U/K 10		NE	15 kT	525	<100	x					
				FLAT TOP II		TNT	20 T	0	<420	x				19	
				FLAT TOP III		TNT	20 T	0	<300	x					
NTS Yucca Flat	"Dry" Silty Sand (Alluvium)		AFWL (CIST)	JOHNIE BOY		NE	0.5 kT	-1	<100	x	x	x			47
				JANGLE S		NE	1.2 kT	3.5	<100	x		x			
				JANGLE U		NE	1.2 kT	-1.7	<30	x		x			
				TUMBLER 2		NE	1.2 kT	1100	<50	x					
				TUMBLER 3		NE	30 kT	3450	<50	x					
				TUMBLER 4		NE	20 kT	1060	<50	x					
				U/K 1		NE	16 kT	300	<100	x					
	Playa	WES	(CIST)	PMT IV - 6		ANFO	100 T	R	<2500		x				
Suffield Experiment Station "Dry" Uniformly Layered Silts, Clay and Sandy Silt Depth to Rock is 200 ft Water Table is at 23 ft		WES		PRAIRIE FLAT		TNT	500 T	R	<2000	x	x	x	x	20,21,22	46,48
				DIAL PACK		TNT	500 T	R	<2000	x	x	x	x	23	48
				SNOWBALL		TNT	500 T	(1)	50-600	x	x	x		24,25	49
				DISTANT PLAIN	1	TNT	20 T	85	10-1000	x	x	x	x	26	
					1A	TNT	20 T	30	500-10,000	x	x	x	x	27,28	50,51
					2A	(2)	20 T	(1)	10-1000	x	x	x	x	26	
					3	TNT	20 T	0	20-300	x	x	x	x		
					5	TNT	20 T	0	20-300	x	x	x	x		
					6	TNT	100 T	R	10,2000	x	x	x	x	27,28	

TABLE 3 (Concluded)

TEST SITE, MEDIUM	PROPERTIES		EVENT		SOURCE		HOB (ft)	DATA BASE					REFERENCE	
	Lab	Field			Type	Yield		P (psi)	a	v	d	σ	Data	Analysis
Ordway, Colorado "Wet" Clay/Shale	WES	AFWL (CIST) (DISK HEST)	MIDDLE GUST	I	TNT	20 T	0	<600	x	x	x	x	30,29	
				II	TNT	100 T	17	<2500	x	x	x	x	31,29	
				III	TNT	100 T	R	<2500	x	x	x	x	32,29	52
Ordway, Colorado "Dry" Clay/Shale	WES	AFWL (CIST)	MIDDLE GUST	IV	TNT	100 T	R	<2600	x	x	x	x	33,29	53
				V	TNT	20 T	0	<600	x	x	x	x	34,29	
Ordway, Colorado	WES	AFWL	MG CAL (3)		TNT	0.5 T	(3)	10-1000	x	x	x	x	35	
Grand Junction, Colorado Sand Over Sandstone, Siltstone, and Mudstone	WES	AFWL (CIST) Terra Tech	MIXED COMPANY	1	TNT	20 T	0	<600	x	x	x		36	
				2	TNT	20 T	R	<600	x	x	x			
				3	TNT	500 T	R	<800	x	x	x		37	54,55,56
			CENSE (4)		TNT	0.5 T	(4)		x	x				
Eniwetok Proving Ground Coral	WES	AFWL (CIST)	KOA		NE	1.4 MT	3	50-2000	x					
			CACTUS		NE	18 kT	3	100-250	x					57
			IVY MIKE		NE	10.4 MT	10	<40	x				38	
			LACROSSE		NE	39 kT	17	<100	x					
			BLACKFOOT		NE		200	<100	x					
			CASTLE KOON		NE	130 kT	14	10-50	x					
			EASY		NE	47 kT	300	10-50	x					
			GEORGE		NE		200	10-50	x					
			PACE (5)		TNT	0.5 T	(5)	20-1000	x	x	x		39	
Cedar City, Utah Tonalite	Terra Tech WES CERF	Terra Tech	MINE ORE		TNT	100 T	0.9 R	20-2500	x	x	x	ε	40,41	58
			MINE UNDER		TNT	100 T	1.8 R	20-2500	x		x	ε		
			MINERAL ROCK		TNT	100 T	0.9 R	20-2500	x	x	x		42,43	58

(1) Hemisphere
(2) 62.5-ft Radius Hemispherical Propane and Oxygen Gas Bag
(3) 9 Tests, Half-Buried, Surface Tangent, and Fully Buried
(4) 7 Tests, 7 Charge Radii DOB to 4 Charge Radii HOB
(5) 7 Tests, Half-Buried and Surface Tangent

R One-Source Radius HOB (Surface Tangent)
ε Strain

The nuclear data consist of low yield near-surface and HOB tests at the Nevada Test Site (NTS) and higher yield, primarily near-surface, tests at the Eniwetok Proving Grounds (EPG). These data are largely acceleration histories and permanent displacement passive measurements. The tests at NTS were primarily performed in or over fairly homogeneous fine grain silt (Frenchman Flat Playa) or silty sand (Yucca Flat alluvium) medium with a deep water table and a very large depth to bedrock. The coral over limestone, typically ring-shaped, geology of the EPG area has not been representative of strategic sites of interest.

Since the Nuclear Test Ban treaty, ground-shock-related testing has been performed with high explosive energy sources. These tests have used (a) single high explosive sources (generally spherically packed TNT) up to 500 tons which have provided low yield AI effects and enhanced DI/CI effects (with respect to the nuclear environment for the same yield and HOB), (b) a High Explosive Simulation Technique (HEST) for providing a simulated nuclear traveling air blast environment over a limited area, (c) a Berm-Loaded Explosive Simulation Technique (BLEST) which provides an equivalent (with respect to ground shock) nuclear surface loading over a large area, surrounding a HEST loading, through near-surface time-phase-detonated high explosive charges, (d) a Direct-Induced/HEST (DIHEST) which employs a buried vertical planar array of high explosive charges to produce calculated DI peak velocities and stresses at a point of interest, and (e) a cratering and related ground shock simulation technique which employs high explosive loading to produce the environment within the hydrodynamic region.

Numerous single-source high explosive tests have been performed in various geologies. The most significant series include tests in thinly layered sandy silts and clays at the Suffield Experiment Station

(SES), Alberta, Canada; in tonalite at the MINE SHAFT site near Cedar City, Utah; in wet and dry (unsaturated) layered clay over stiff shale geologies at the MIDDLE GUST site in Colorado; in hard sandstone at the MIXED COMPANY site in Colorado; in coral at the PACE site in EPG and recently the PRE-MINE THROW IV tests in dry playa silt at NTS. Currently, the DICE THROW test series, being conducted in clay and alluvium media in New Mexico, will provide cratering and ground shock data of value to the SAMSO MX Program.

The HEST, developed by the AFWL, has been applied to four MINUTEMAN operational sites, the PRAIRIE FLAT, and other sites. However, the relatively short ground shock simulation duration (compared with the air blast simulation duration) brought about by relief wave effects from the edges of the HEST loaded area has been a limitation of the technique. To provide the loading outside the HEST cavity required to obtain longer ground shock simulation durations, the AFWL recently developed the BLEST for DNA. A HEST/BLEST simulation, currently being used in the HARD PAN test series of the SAMSO Structure-Medium Interaction Program, will provide an important data base for AI high yield ground shock effects in strongly layered soft rock media.

The DIHEST, also developed by the AFWL, has been used in testing related to the HARD ROCK SILO Development (HRSD) Program. This technique has a simulation uncertainty which is related to the large uncertainty in calculating the DI environment. To provide a more complete DI/CI simulation, Physics International (PI) developed for DNA the technique to emplace distributed high explosives on a surface located within the hydrodynamic region of the ground response to produce a calculated environment. This technique was demonstrated in the MINE THROW I event at NTS, designed to simulate the JOHNIE BOY event.

4.1.2 Calculational Results

In the late 1960's, the development of continuum computer codes matured to the point where they could be used for the calculation of layered nonlinear ground shock response. A number of axisymmetric calculations were performed by several organizations. The primary data base includes AI calculations performed by Applied Theory, Inc. (ATI) for the HRSD Program; by ATI and the AFWL for the MINUTEMAN Program; by Weidlinger Associates (WA) and R & D Associates (RDA) for the SAFEGUARD and SITE DEFENSE Programs; and by the AFWL and RDA for the MX Ground Mobile Program. This calculational data base is summarized in Table 4. Other ground shock calculational studies have been performed for DNA by Shock Hydrodynamics, PI, and WES.

The ATI calculations for the MINUTEMAN Program have considered a nonlinear, elastic, ideally plastic material model which includes a yield surface, flow rule, and tensile cracking criteria. Other calculations have used the CAP model, developed by WA (Reference 59). This model, based on incremental plasticity theory, contains a loading function that serves as both a yield surface and a plastic potential. Comparison calculations performed with both models (e.g., those for MIDDLE GUST II and the hypothetical DNA site U-2) show reasonable agreement.

4.1.3 Material Properties

In developing constitutive models for a nuclear or high explosive calculation, the typical procedure for the analyst is to start with uniaxial strain and triaxial stress mechanical properties for the strain rates of interest for layers down to a maximum of about 300 feet. When sufficient funding has been available, these properties have generally been obtained from analyses of laboratory test data on field samples, for at least initial calculational studies. The site layer properties for the above specific laboratory load paths are then generalized to a rate-independent constitutive model which governs the mechanical

TABLE 4. NUCLEAR GROUND SHOCK CALCULATIONAL DATA BASE

PROGRAM	SITE CONDITIONS				AGENCY	COMMENTS
	DRY SOIL	WET SOIL	SOFT ROCK	HARD ROCK		
MINUTEMAN	X	X	X		ATI AFWL	Large-yield surface burst air-blast-induced calculations, primarily for superseismic region
MINUTEMAN MX Ground Mobile	X				AFWL RDA	Large-yield surface burst air-blast-induced calculations. Isothermal sphere sources have been considered for parametric AI/DI studies
Site Defense	X	X	X		WA RDA	Large-yield HOB air-blast-induced calculations, primarily for out-running region
Hard Rock Silo				X	ATI	Large-yield surface burst air-blast-induced calculations for high pressure region

behavior of the medium for whatever stress path histories are experienced during the calculated ground shock response. Properties at depth, if required, are generally determined from the site profile, including geological definition, depths to water table and bedrock, and available seismic velocity information.

Recent analysis of high explosive test events (e.g., MIDDLE GUST III and IV and MIXED COMPANY 3) has pointed out the importance of in situ test data for determination of site properties. At a number of field sites, dynamic in situ tests have been performed, including (a) the Cylindrical in Situ Test (CIST), which applies an axisymmetric pressure loading on a vertical cylindrical hole, with a typical depth of 40 to 70 feet, and (b) the DISK HEST, which applies an axisymmetric pressure loading on the ground surface. For the DISK HEST loading, the response is one-dimensional for some time-space region. If good field data are obtained this is the best test that can be performed to determine the vertical uniaxial strain behavior. Performing a CIST, which provides data more related to the horizontal properties, is significantly less expensive. However, a large stress attenuation with range is experienced and the stress paths are more complex than for DISK HEST. Data from both a CIST and DISK HEST can be used to determine material anisotropy at a site. Seismic survey data are also important for determining site properties. Analysis of data for tests performed in soft rock (MIDDLE GUST and MIXED COMPANY) indicates that the ground shock peak stress speeds correlate better with seismic data than with speeds calculated from laboratory modulus data (e.g., Reference 60). Tests performed in soft soils generally reflect peak stress speeds slower than seismic speeds.

The site constitutive model is by far the primary cause of uncertainty in AI calculations. This uncertainty lies both in the site properties used and in the manner in which the site properties are generalized to establish the constitutive model.

Primary sources of error associated with properties developed from laboratory testing are sample disturbance effects and uncertainty of in situ initial (lithostatic) stress conditions. A small loss of water during sampling of saturated soils can result in a significant reduction in stiffness. For cemented soils the sampling process can break down the cementation, also resulting in a softer laboratory modulus. Comparison between WES laboratory uniaxial strain tests on 5-in. Shelby tube samples and on hand-carved samples for cemented sands, for a MINUTEMAN site, has demonstrated this effect. Vertical lithostatic stress is simply determined from the weight of material above the sample. However, significantly larger horizontal lithostatic stresses can be present that introduce an apparent anisotropic effect. This may be a primary contributor to the reason for the laboratory data underpredicting the ground shock speeds for the MIXED COMPANY site (Reference 54).

Another laboratory testing consideration has been the range of stress path histories that could be considered. For strongly superseismic loading conditions, the uniaxial strain and triaxial stress data are probably adequate. However, the stress paths are more complex for outrunning AI and for DI/CI motions. Tests on samples where all three principal stresses are independently controlled require cubical samples, a situation which may result in an unacceptable disturbance for soil materials except for sands that are rained in place (Reference 61). Another key material property difficult to obtain in the laboratory is the

tensile failure criteria and post-cracking behavior. Tensile spallation has occurred in high explosive tests such as MIDDLE GUST III; however, there are few data on which to base this aspect of material behavior.

If the constitutive model is based on any generalization of properties developed from laboratory data, which does not violate any physical principles such as conservation of energy, some important aspects of the material behavior may not be included. To develop an adequate constitutive model for a site, both laboratory and in situ studies are required. In situ tests should be aimed at loading the material as close as possible to the stress paths of interest and the gage layout should be designed to help establish, as best as possible, fundamental aspects of the medium response (e.g., vertical and horizontal wave speeds). Depending on the site of interest, the dynamic testing previously discussed and, possibly, static testing such as flat jack or Menard pressure meter tests might be considered. At the MIXED COMPANY site, static testing of large sandstone blocks were performed (Reference 62).

Constitutive model development is an iterative process that is completed when satisfactory agreement is obtained between continuum code calculational results for the in situ tests and the data. The form of the constitutive model should allow for modeling the key aspects of the material behavior determined from the laboratory testing and from analysis of the in situ test data.

A constitutive model developed in this manner can then be tested against data for a large-scale high explosive or nuclear test for the site of interest. Good test/analysis correlation is essential for (a) establishing confidence in nuclear computer code calculations for

related geologies, and (b) for validating scaling techniques for extrapolating data beyond the range of the existing base.

4.1.4 Test Data Applicability

Since calculational models are measured against their ability to unravel the phenomenology of field tests, it is important to evaluate the quality of the test data. A proper evaluation can be made only for test events where there is some measure of redundancy in the instrumentation; namely, data for the same range and depth but for different azimuths (for essentially axisymmetric sites) or for different gage types (such as velocity and accelerometer gages) in the same canister or in neighboring locations. Since the medium response can have non-axisymmetric characteristics, and gages in the same canister can record the same response with the canister response being different from that of the medium, this evaluation requires capabilities in both instrumentation and ground shock phenomenologies.

The most extensively instrumented test series to date is MIDDLE GUST. PRAIRIE FLAT and MIXED COMPANY also contained redundant measurements that can be used for evaluation. The only nuclear test with useful redundant data is PRISCILLA. Figure 19 shows a comparison of peak velocity data for the 500-ton PRAIRIE FLAT event (Reference 20 and 21). Both AI and initial peaks subsequent to DI arrival are shown. The figure compares integrated accelerometer data with velocity gage data for measurements in close proximity. Also compared are WES and Stanford Research Institute (SRI) measurement results for azimuths which are 120° apart. The data indicate that the accelerometer results are about 20% higher than the velocity gage results and the majority of the WES and SRI data are within 30% of each other.

A comparison of PRAIRIE FLAT waveforms for the 84-ft range and 5-ft depth (Figure 20) shows that the WES and SRI velocity gage data are in reasonable agreement for both vertical and horizontal measurements.

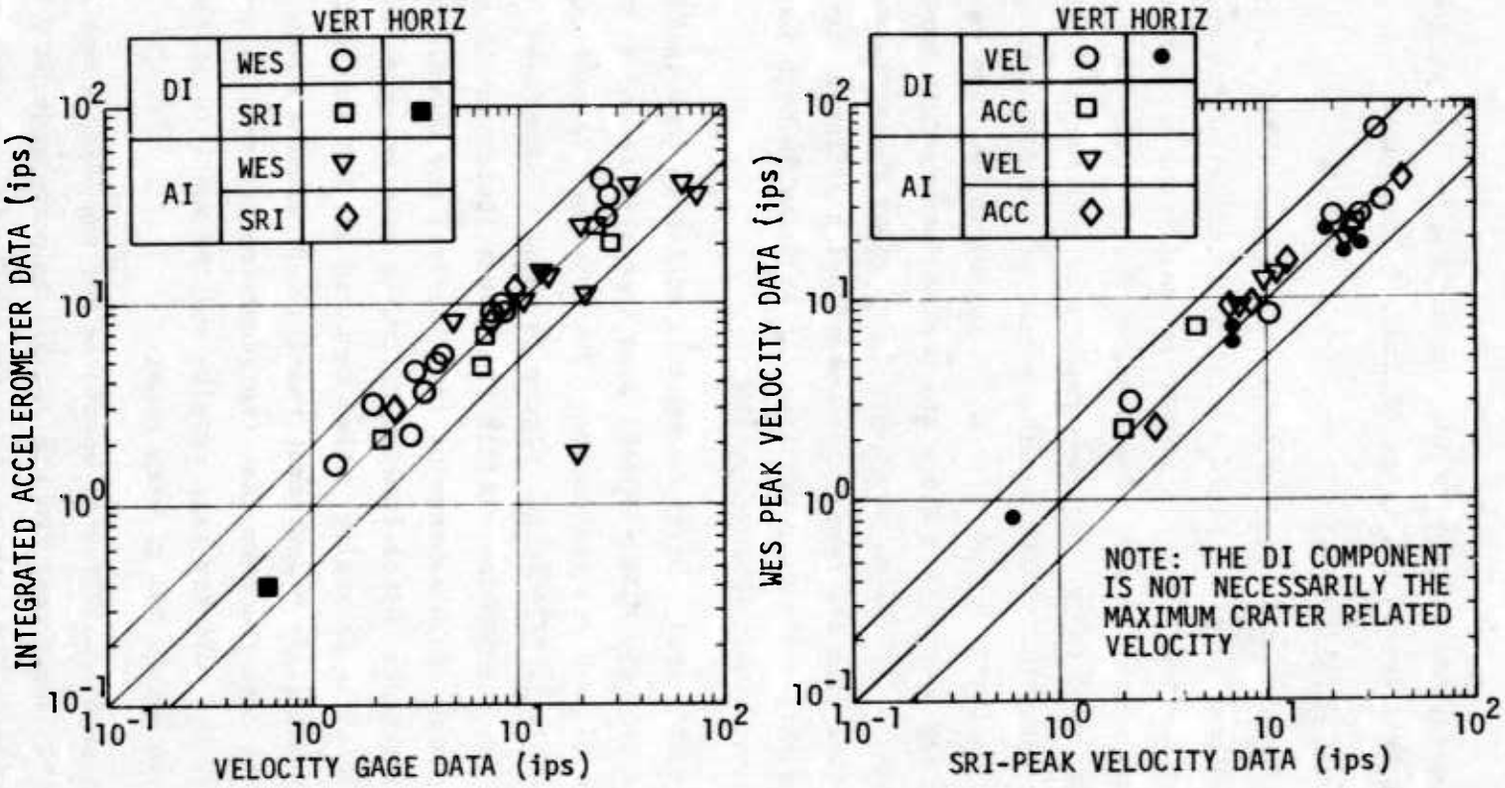

Figure 19. Comparison of PRAIRIE FLAT Peak Velocity Data

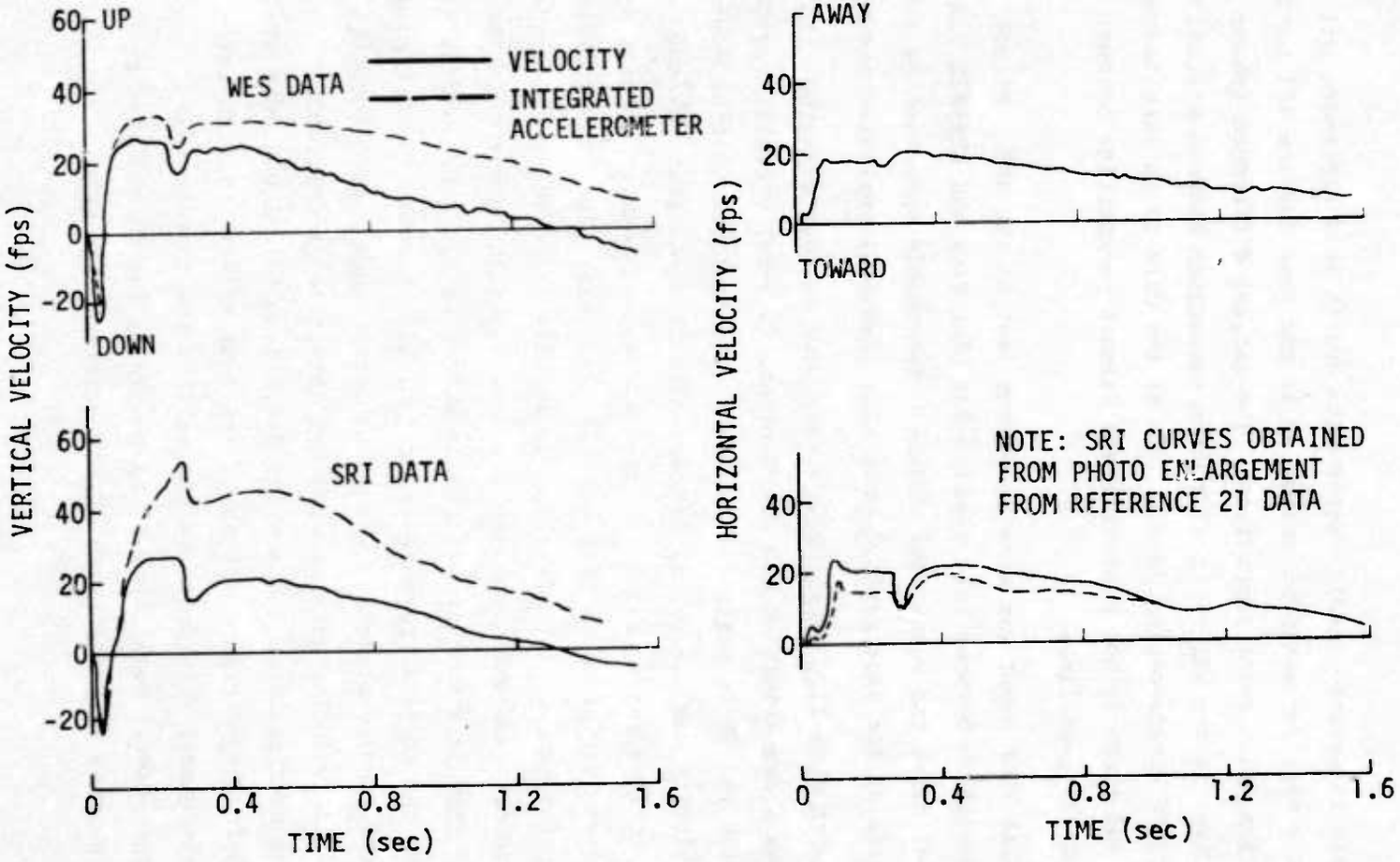

Figure 20. PRAIRIE FLAT Waveform Comparison, 84-ft Range, 5-ft Depth, ~1600-psi Overpressure

Also the WES integrated accelerometer data are in good agreement with the velocity data for vertical motion as is the case for the SRI horizontal motion measurement comparison. The largest difference (about a factor of two) is the SRI vertical motion comparison between velocity and integrated accelerometer data. Most of the data is in much better agreement and there is not a significant azimuth sensitivity between the WES and SRI gage lines.

The DIAL PACK event was also a 500-ton test at the SES. Figure 21 shows a comparison between test results for DIAL PACK and PRAIRIE FLAT for the 5-ft depth and equivalent ranges. Reasonable agreement is seen for two tests at the same general area with identical explosive sources.

In MIDDLE GUST III, measurements were made on four azimuths. Figure 22 shows a comparison of the near-surface (1.5-ft) vertical velocity histories for the 80-ft range for all four azimuths; the initial peak downward velocity has a very significant azimuth variation; but the subsequent motions out to about 150 msec are in much better agreement. A large azimuth variation in this peak is plausible, since the initial downward motion, due to the air slap, is shortly followed by the arrival of the refracted wave which opposed the air-slap-induced motion. Thus, the initial peak is a function of the impedance of the near-surface material and the small difference in arrival time between the air slap and refracted wave components. The figure also shows a good comparison between the velocity gage records and integrated accelerometer data for the same canister. A similar comparison for MIDDLE GUST IV for the 160-ft range (Figure 23) shows the peak velocities from integrated accelerometer records to be larger than the corresponding velocity gage peaks. Such a result is generally due to the higher frequency response characteristic of the accelerometer gages.

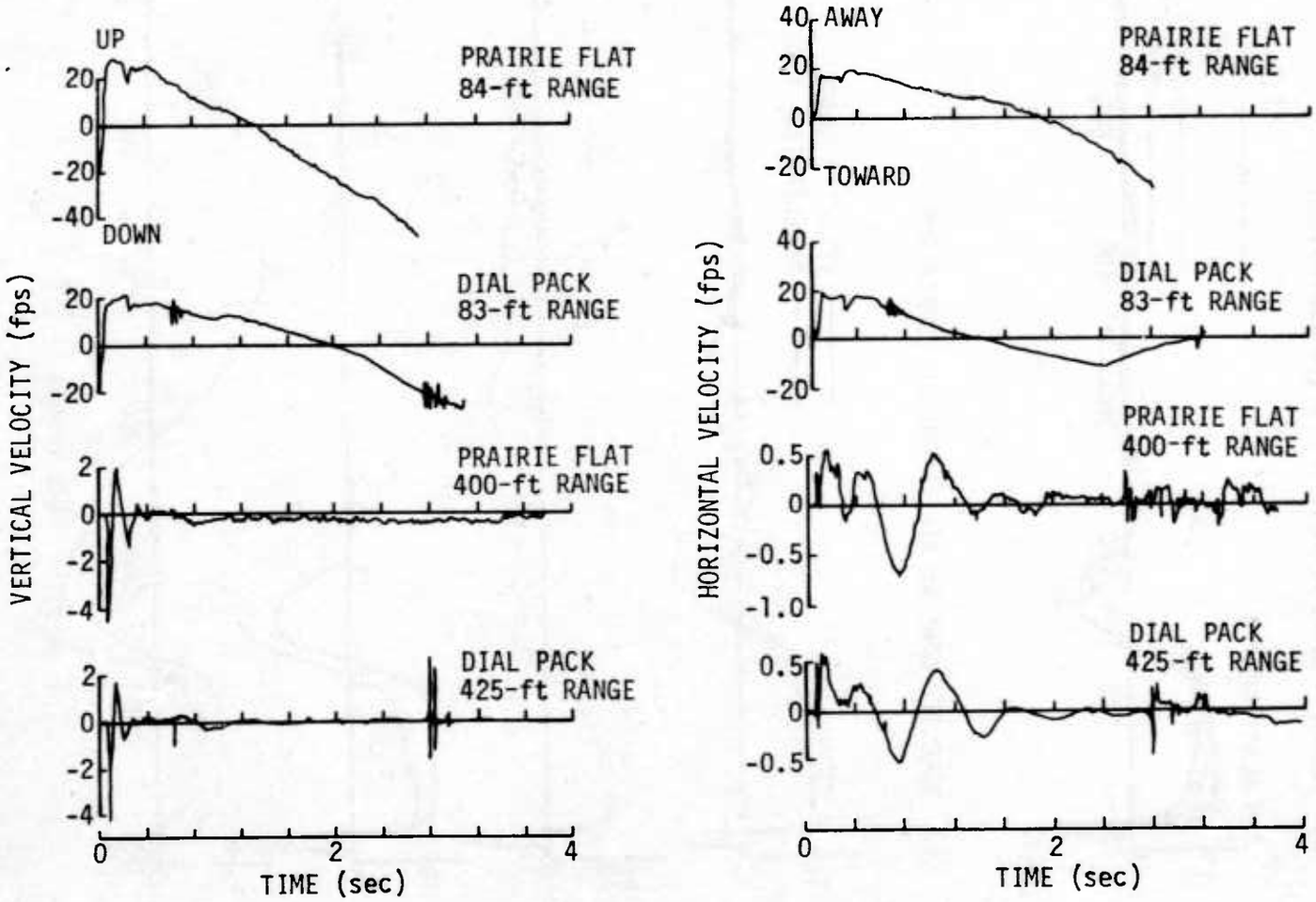

Figure 21. Comparison of SES 500-T Velocity Waveforms, 5-ft Depth (Reference 15)

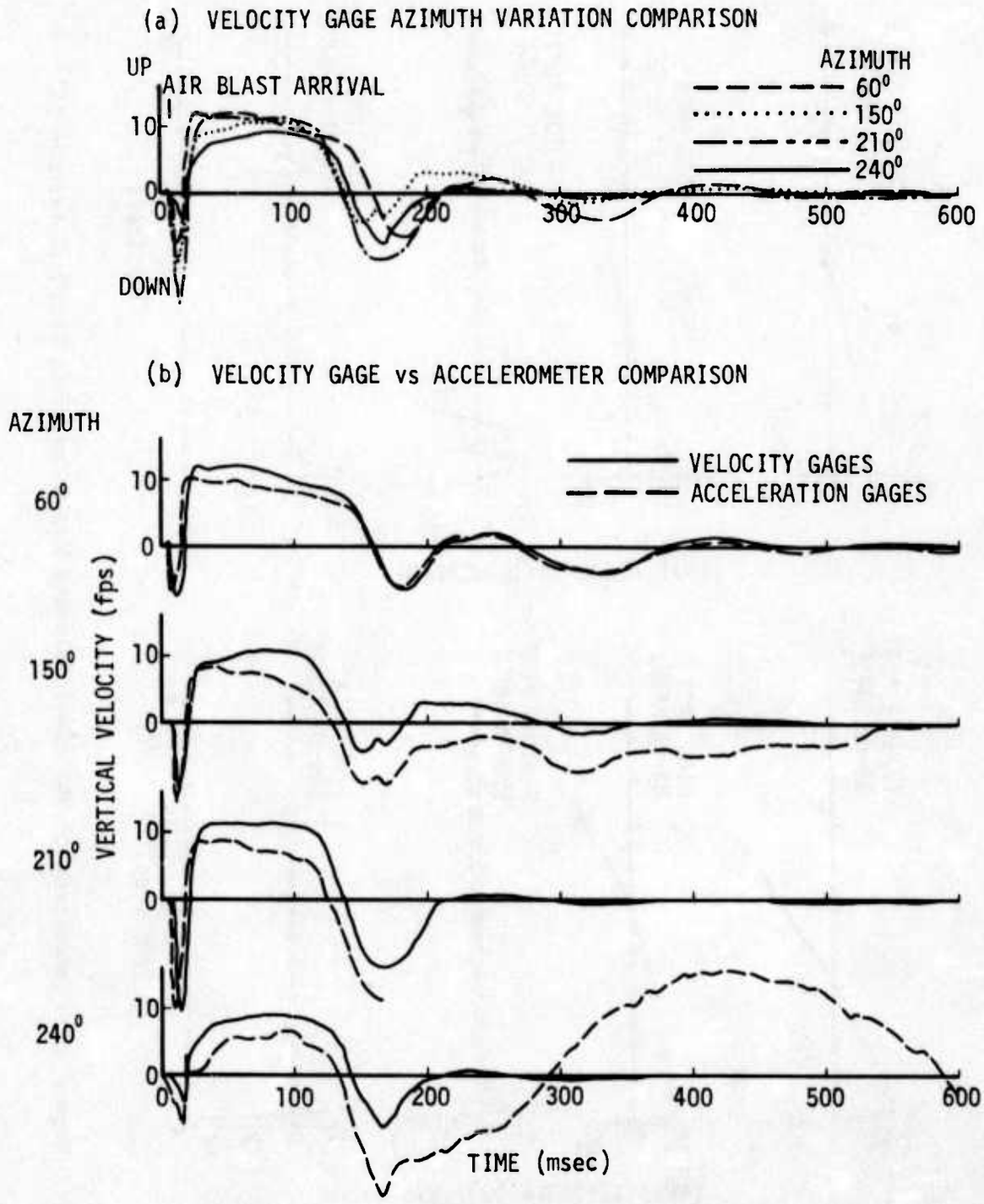

Figure 22. MIDDLE GUST III Vertical Velocity Azimuth Variation, 80-ft Range, 1.5-ft Depth, ~1000-psi Overpressure

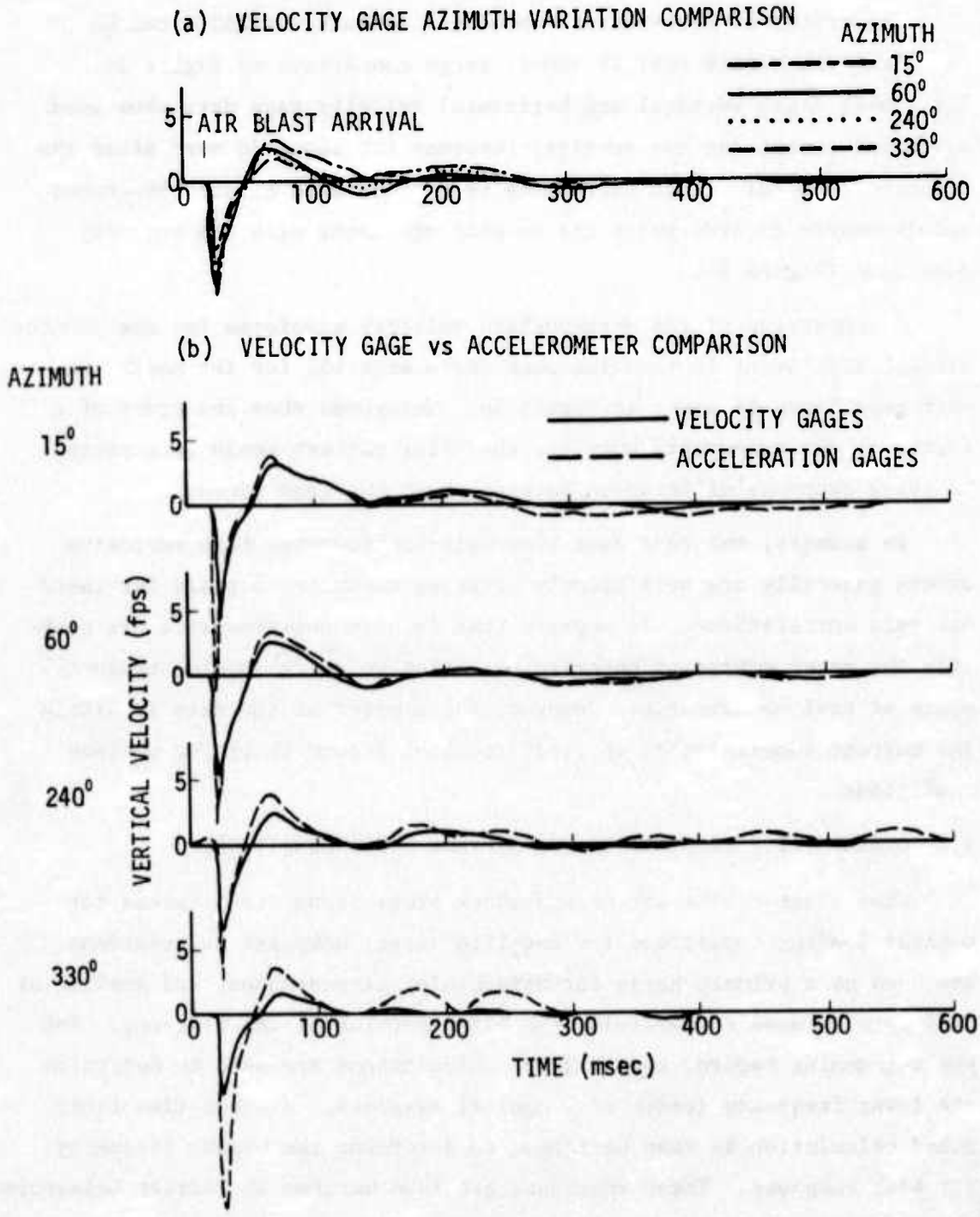

Figure 23. MIDDLE GUST IV Vertical Velocity Azimuth Variation, 160-ft Range, 1.5-ft Depth, ~350-psi Overpressure

The effect of near-surface-impedance azimuth variation can be seen from the MIDDLE GUST IV 400-ft range comparison of Figure 24. The 1.5-ft depth vertical and horizontal velocity gage data show good agreement except for the vertical response for about 30 msec after the air blast arrival. That difference is corroborated by the integrated accelerometer records which are in good agreement with the velocity gage data (Figure 25).

A comparison of the near-surface velocity waveforms for the 100-ton MINERAL ROCK event in tonalite rock (Reference 15) for the north and east gage lines is given in Figure 26. Waveforms show the order of a factor of two agreement; however, the joint pattern would be expected to cause response differences between these two gage lines.

In summary, the test data from well-instrumented high explosive events generally are sufficiently accurate to use as a basis for test/analysis correlations. It appears that in situ nonsymmetries are probably the major source of observed variation in corresponding measurements at various azimuths. However, the scatter of the data is within the current uncertainties in predictions of ground shock for nuclear conditions.

4.2 GENERIC SITE PREDICTIONS FOR SURFACE BURST CONDITIONS

When state-of-the-art ground shock predictions are required for nuclear loading conditions for specific sites, computer calculations are used as a primary basis for determining AI responses; and scaling of test data is used to determine the DI/CI portion of the response. For the outrunning region, coarse-zoned calculations are used to determine the lower frequency (order of 1 cps) AI response. A short-time finer zoned calculation is then performed to determine the higher frequency air slap response. These responses are then matched in Fourier transform space to determine the total AI response.

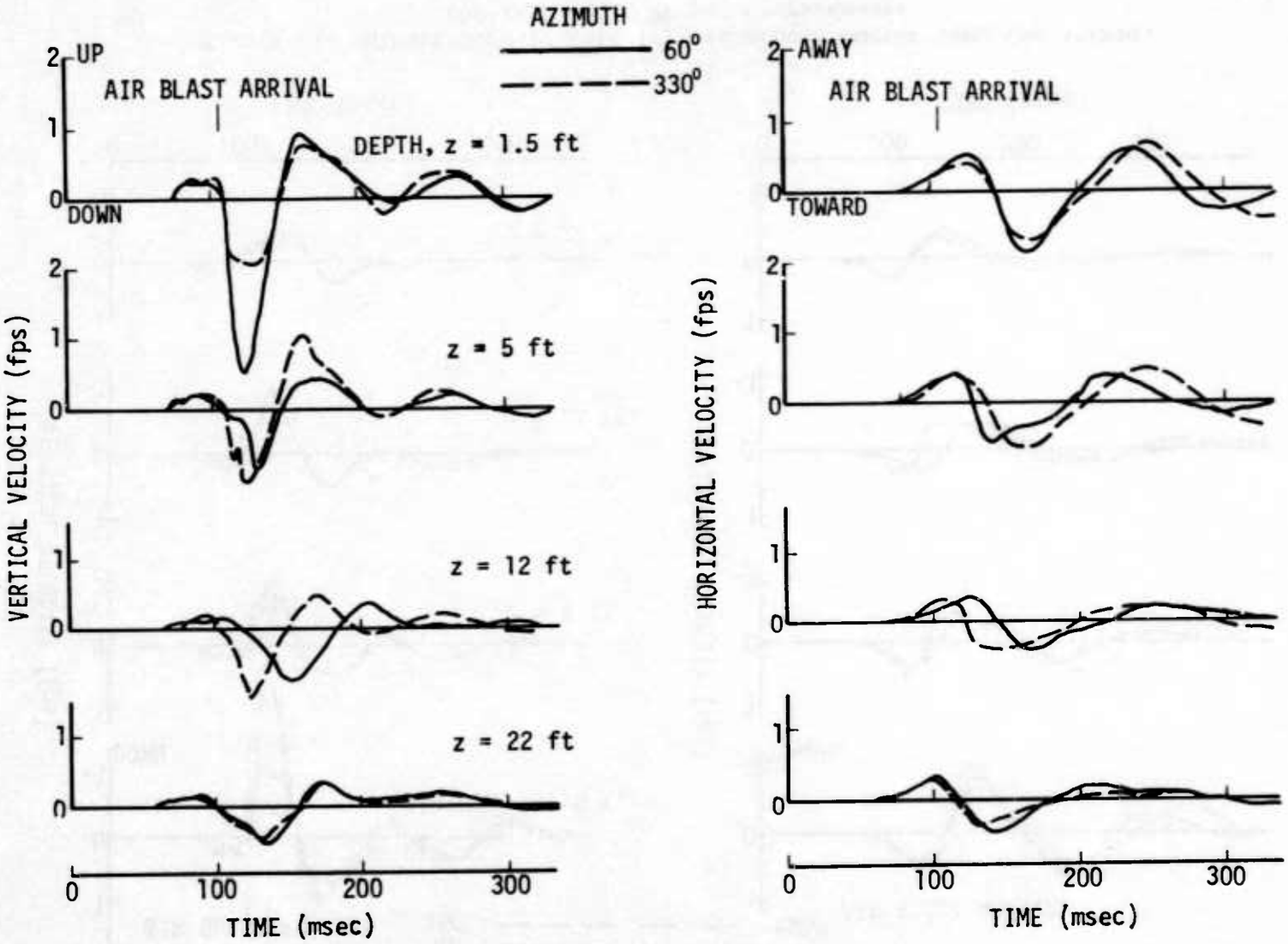

Figure 24. MIDDLE GUST IV Velocity Gage Azimuth Variation Comparison, 400-ft Range, ~20-psi Overpressure

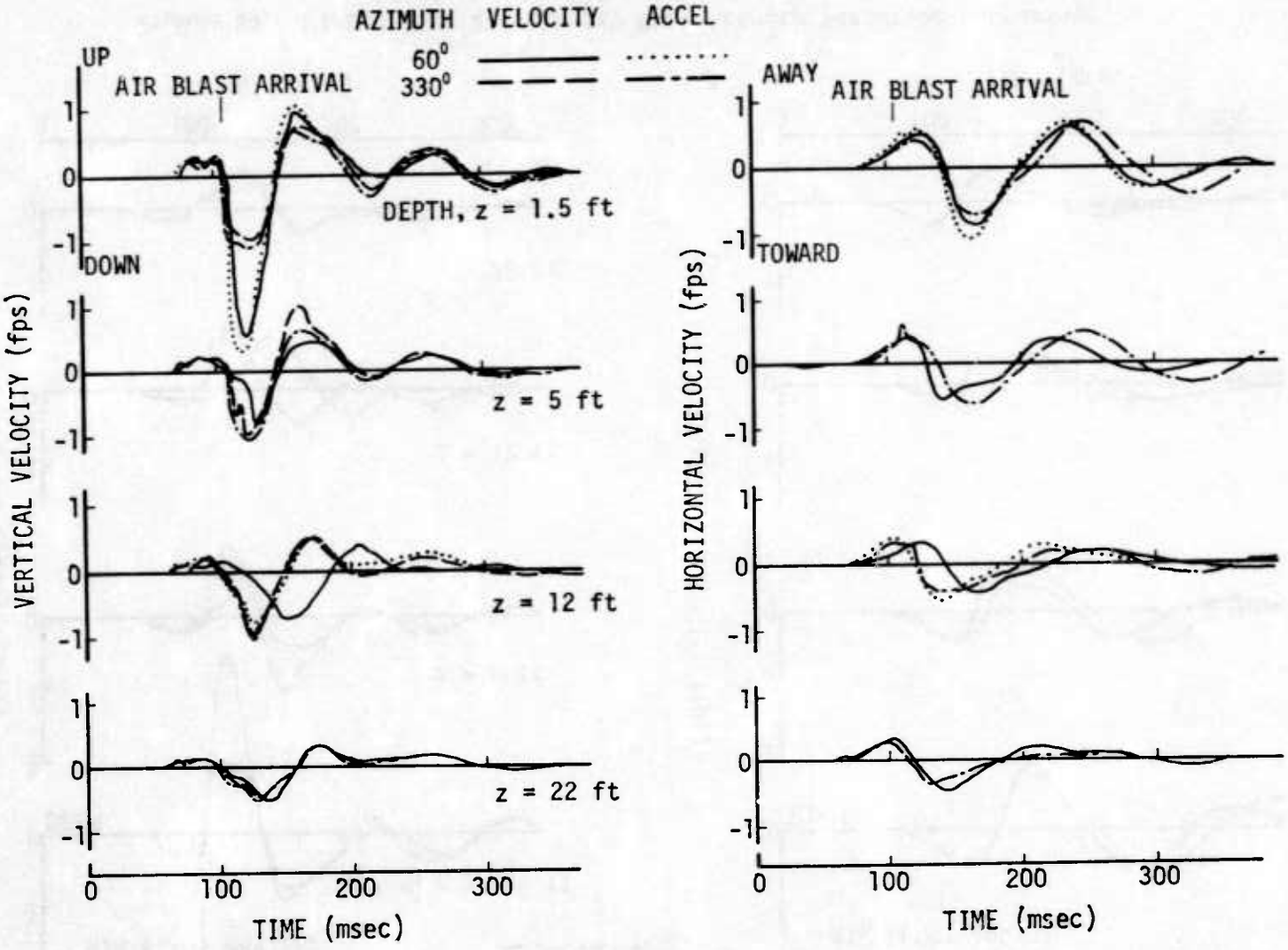

Figure 25. MIDDLE GUST IV Velocity and Accelerometer Gage Comparison, 400-ft Range, ~20-psi Overpressure

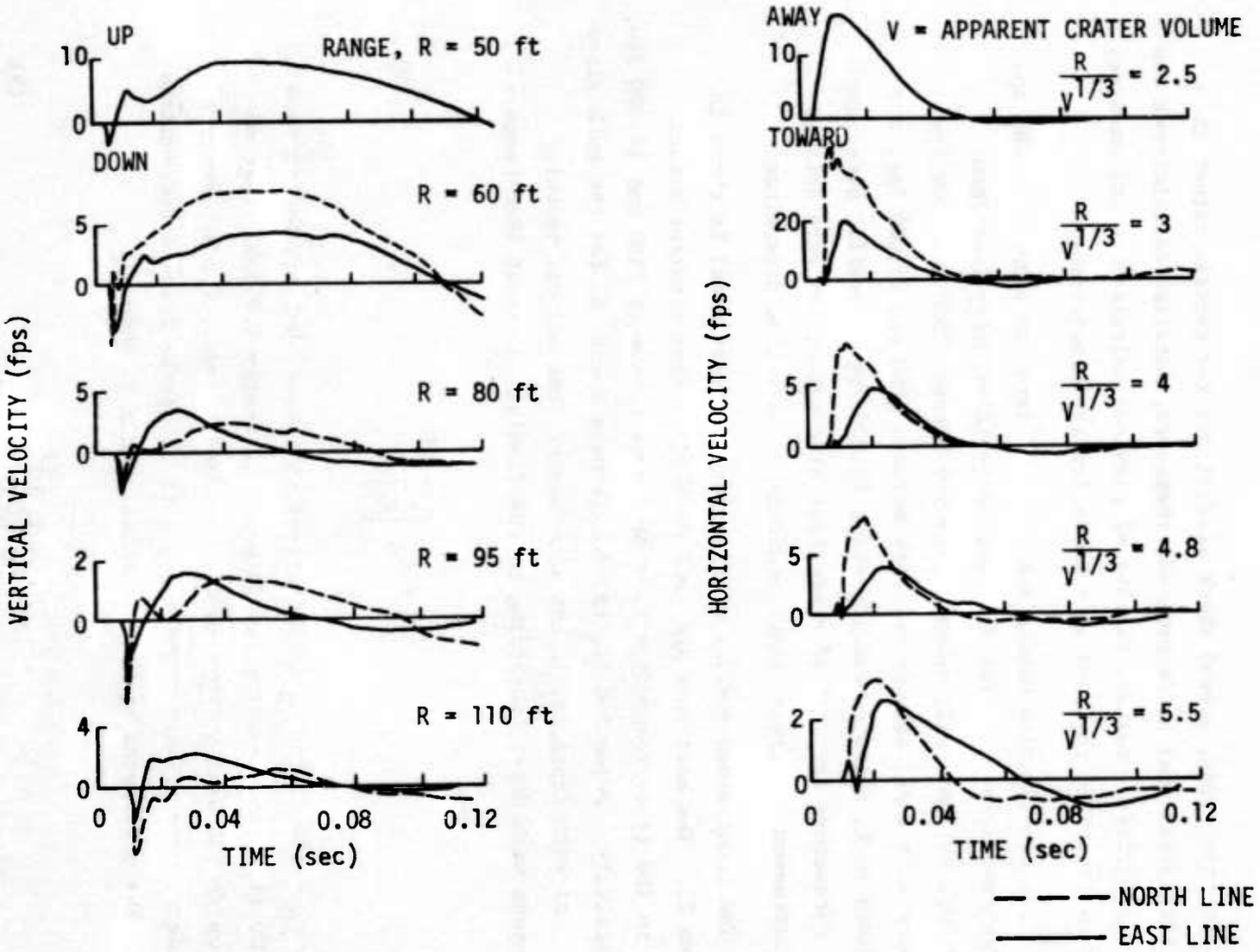

Figure 26. Close-In Particle Velocity Waveforms for MINERAL ROCK, 2-ft Depth (Reference 15)

In this study, ground shock predictions for generic rather than specific sites must be determined; therefore, detailed calculations are not appropriate. Rather, results of previous calculations and analyses of data have been reviewed as a basis for the predictions.

Four generic site conditions are considered in support of DNA and DIA/VAS requirements: (a) dry soil; seismic velocity less than 3000 fps, (b) wet soil; seismic velocity between 3000 and 6000 fps, (c) dry soft rock; seismic velocity between 6000 and 12,000 fps, and (d) hard rock; seismic velocity above 12,000 fps. Specific site property parameters for each of these four site categories were defined and corresponding ground shock predictions were then determined.

The constrained modulus profile for each site model is shown in Figure 27. The soft rock and hard rock sites have constant moduli down to 100 ft corresponding to stress wave speeds of 7500 and 14,000 fps, respectively. Below 100 ft, the stress wave speed, C, for the rock sites increases with depth, z, in the same manner that seismic velocity increases with depth, according to the findings of Faust (Reference 63),

$$C = C_0 \left[\frac{z}{z_0}\right]^{1/6} \tag{8}$$

where z_0 = 100 ft and C_0 is the stress wave speed between the surface and 100 ft depth. Faust's Law is based on nearly 1,000,000 feet of section in 500 well surveys in the U.S. and Canada. The materials considered were primarily shale and sand at depths below a few hundred feet. The corresponding modulus relationship is then

$$M = M_0 \left[\frac{z}{z_0}\right]^{1/3} \tag{9}$$

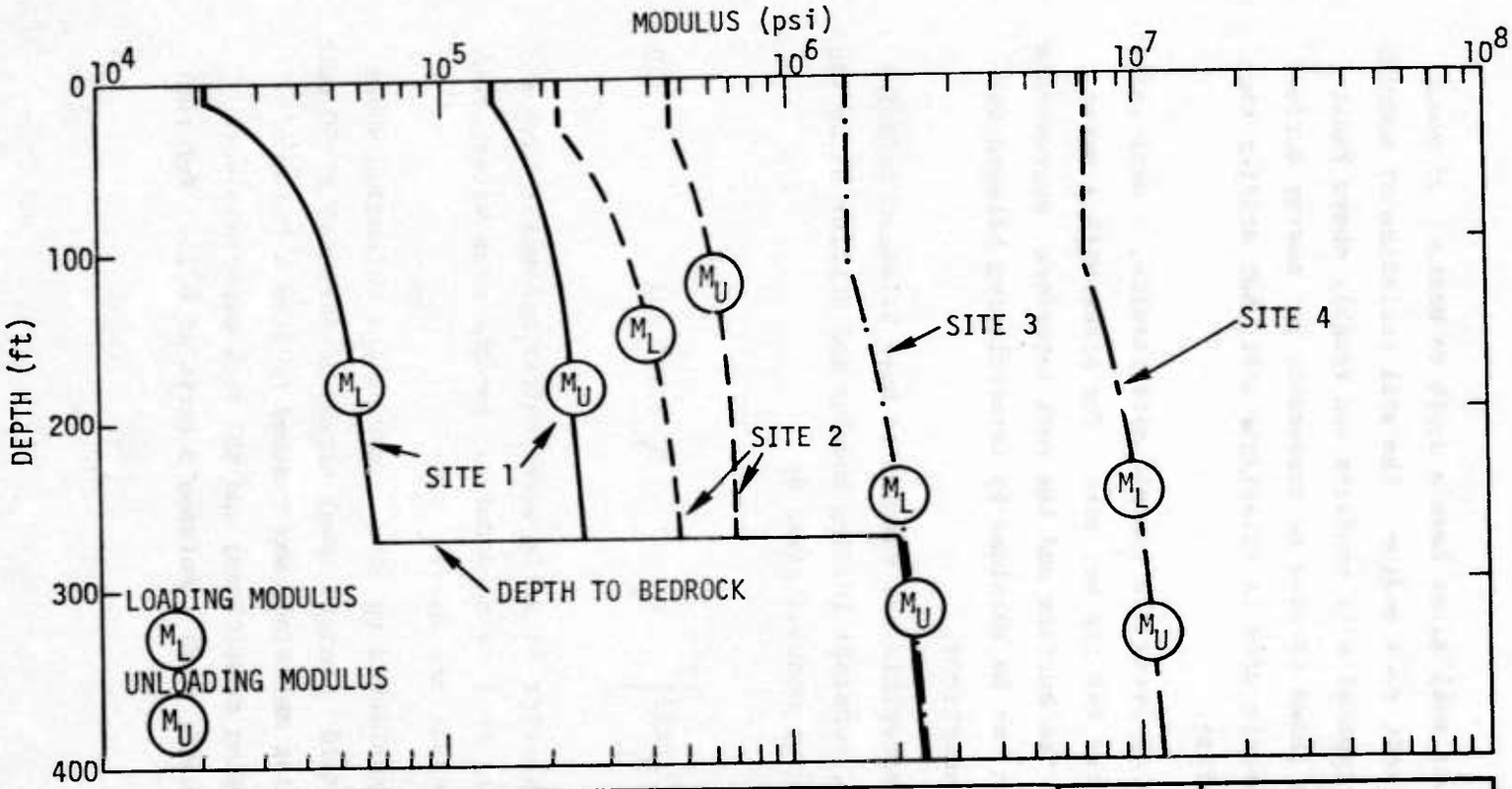

SITE	DESCRIPTION	SURFACE PARAMETERS				RQD (%)	CRATERING EFFICIENCY (10^6 ft^3/MT)
		DENSITY (pcf)	C_0(fps)	M_{LO} (ksi)	E(ksi)		
1	DRY SOIL	100	1000	21	—	—	50
2	WET SOIL	115	3000	220	—	—	170
3	SOFT ROCK	140	7500	1500	1250	50	40
4	HARD ROCK	165	14,000	7300	6100	85	30

Figure 27. Generic Site Properties

The dry soil and wet soil sites have a depth to bedrock of about 270 ft and overlie the soft rock medium. The soil variation of modulus with depth is based on typical site profiles and roughly obeys Faust scaling, which has been shown to also be reasonable for nearer surface media. The dry soil generic site is relatively soft, but stiffer than the playa at Frenchman Flat.

For convenience in applying the generic site results, a near-surface water table was considered for the wet site. For sites with a water table somewhere between the surface and the rock interface, approximate ground shock predictions can be obtained by interpolating between wet and dry generic site predictions.

Generic site soil materials are assumed to have bilinear uniaxial strain properties, i.e., constant loading modulus and stiffer unloading modulus, with the unloading modulus given by

$$M_U = \left[\frac{10^6 \text{ psi}}{M_L}\right]^{1/2} M_L \qquad M_L < 10^6 \text{ psi} \qquad (10)$$

This approximates the behavior of soils where softer materials have a larger ratio of unloading to loading modulus. For the rock sites, both loading and unloading moduli are equal.

The wet soil was considered to have a loading and unloading shear modulus of 30 ksi and yield strength (peak stress difference) of 50 psi; the dry soil, a compacting material, was assumed to have a Poisson's ratio of 0.33 under loading conditions; and the rock materials were assumed to be linear elastic with a Poisson's ratio of 0.25. For rock

sites, Young's modulus is a more frequently used material parameter than is the constrained modulus. Young's modulus and the rock quality designation (RQD) for the generic rock sites considered in this study are also shown in Figure 27.

In a typical situation, dry soil materials with some cementation exhibit initial softening followed by a hardening behavior at higher stress. At low stress, before cementation has broken down, the modulus tends to be more related to the seismic velocity. After cementation breaks down, the material softens significantly until lock-up occurs when the soil grains become compacted. In this study the modulus was considered to be independent of stress for all materials, which is believed adequate for consideration of generic sites.

The cratering efficiency for the hard rock is similar to that recommended by the Air Force design manual (Reference 7) and 20% lower for the dry soft rock site. The dry and wet soil generic sites have a rock interface at a depth of approximately 270 ft and, therefore, a somewhat lower cratering efficiency is used compared with the values recommended by the design manual for uniform site conditions. However, the yield dependence on cratering efficiency is not considered in this study.

The development of generic site ground shock predictions is discussed for air slap, close in DI/CI, and further out AI and DI/CI ground-roll-related effects. Subsequently, the synthesis of these components into waveforms for specific overpressure and yield conditions is considered.

4.2.1 Air Slap Effects

Data for ground shock due to air slap effects alone are obtained from the limited air burst test results. For the high pressure region, the main source of meaningful data is from the DISTANT PLAIN 1A high explosive test event, which was a 20-ton TNT tower shot (30-ft HOB) at

SES. At lower pressure, the nuclear event PRISCILLA, a 37-kT balloon shot at 700-ft HOB over Frenchman Flat provides the main data base.

The DISTANT PLAIN 1A event provides a good basis for evaluating the air slap calculational capability. Since the site is layered, sufficient material property data have been generated and good quality measurements for both the vertical and horizontal ground shock components have been obtained.

Figure 28 (Reference 50) shows the near-surface (1.5-ft) and 10-ft depth responses at the 35-ft range (1840 psi) for DISTANT PLAIN 1A. The 10-ft depth corresponds to a scaled depth (370 ft/$MT^{1/3}$), much greater than is of interest in this study. However, the response for this depth can be used in a study of the variation of effects with depth.

Near the surface, the peak horizontal velocity is about an order of magnitude lower than the peak vertical velocity since the wave front angle is shallow at high overpressure. The decay in peak velocity with depth is much less steep for the horizontal component than for the vertical. At the 10-ft depth, the ratio of horizontal-to-vertical peak velocity is about 0.3.

The waveform shape is also different for both components. The vertical velocity decays rapidly when reflections from lower layers reach the point of interest. Thus, the vertical motion at the 10-ft depth reaches peak displacement earlier than at the surface. This is contrasted with the longer duration of the horizontal velocity pulse.

Near the surface, there is an initial rapid horizontal velocity decay attributable to the surface overpressure decay and possibly shear wave effects. However, the stress gradients, caused by the overpressure gradient, have the effect of maintaining an outward velocity for times considerably longer than the duration of the vertical velocity. At the time that the reflected wave cuts off the vertical velocity, the horizontal

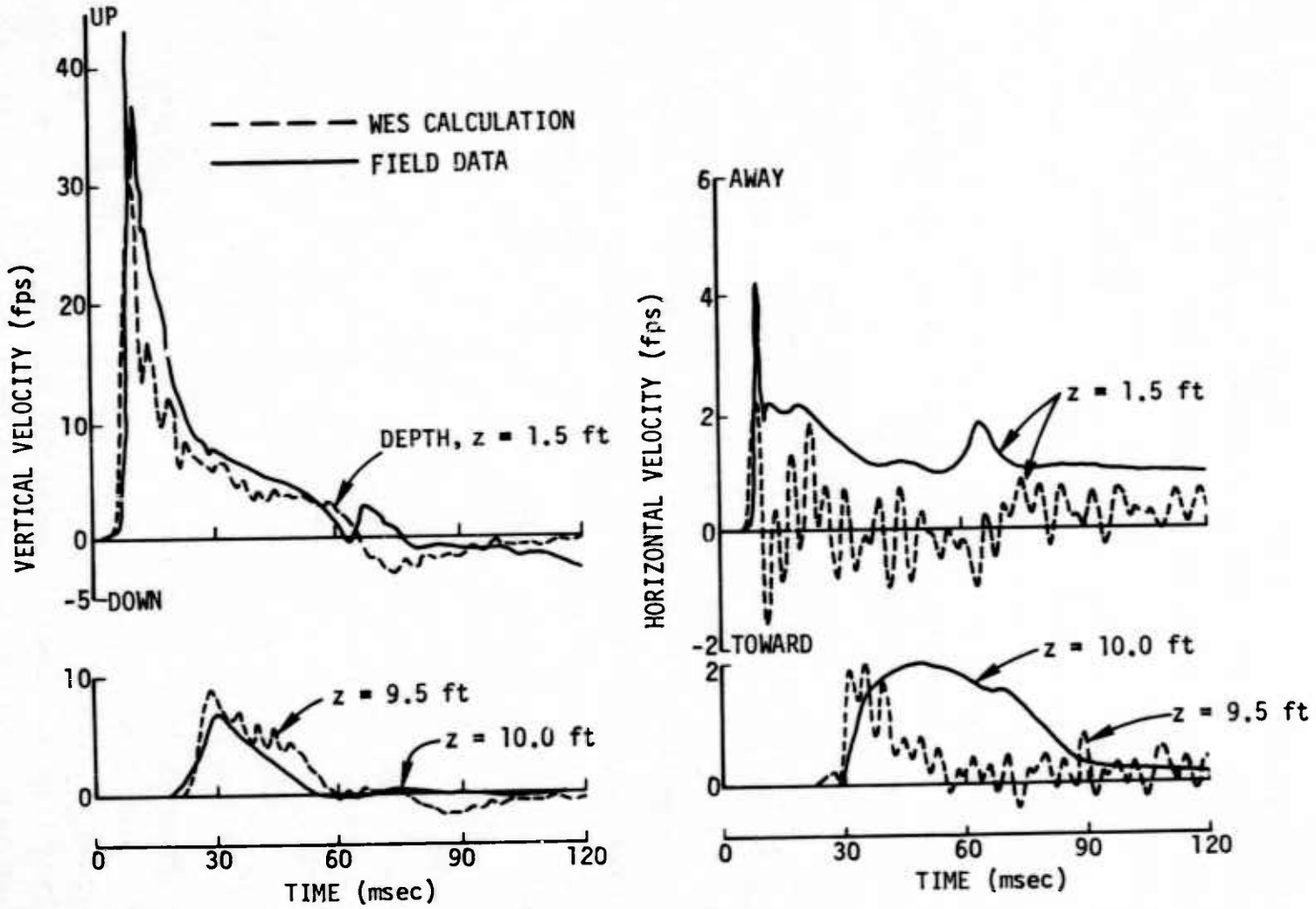

Figure 28. Comparison of WES-Computed Velocity Waveforms with Field Measurements for DISTANT PLAIN 1A, 35-ft Range, ~1840-psi Overpressure (Reference 50)

velocity is enhanced, as is noted in the figure. At the 10-ft depth the peak vertical and horizontal displacements are about equal.

Figure 28 also compares the data with computer code calculations performed by WES (Reference 50) based on soil models developed from laboratory test data for field samples. Very good agreement between test and analysis can be seen for the vertical response. The peak horizontal velocities are in good agreement for the 10-ft depth, but may require finer zoning to calculate the near-surface peak. However, the horizontal waveforms are not in agreement, as smaller displacements are obtained from the calculation.

This correlation alone might tend to imply that the laboratory soil test data base is of high quality but incomplete. The vertical response is primarily dependent on the uniaxial strain properties which are measured in the laboratory, while the horizontal response is more dependent on material behavior not directly measured in the laboratory.

Figures 29 and 30 show the test/analysis comparison for the DISTANT PLAIN 1A 80-ft range (400 psi) for both velocity and displacement histories. For this range very good agreement is obtained.

The stress data at the 5-ft depth are compared with the computer code calculations for both the 400- and 1100-psi overpressure stations on Figure 31. For the DISTANT PLAIN 1A 20-ton yield, a significant stress attenuation occurs between the surface and a depth of 5 ft. There is reasonable test/analysis comparison except for the vertical stress at the 400-psi station where the data are suspect because higher stresses were recorded than for the 1100-psi station.

A similar study was performed for PRAIRIE FLAT (Reference 48) for the AI portion of the response. The agreement between test and analysis for vertical and horizontal velocity is about the same as that observed for DISTANT PLAIN 1A. Thus it appears that air slap ground shock responses can be computed reasonably well for a soft, nonsaturated layered

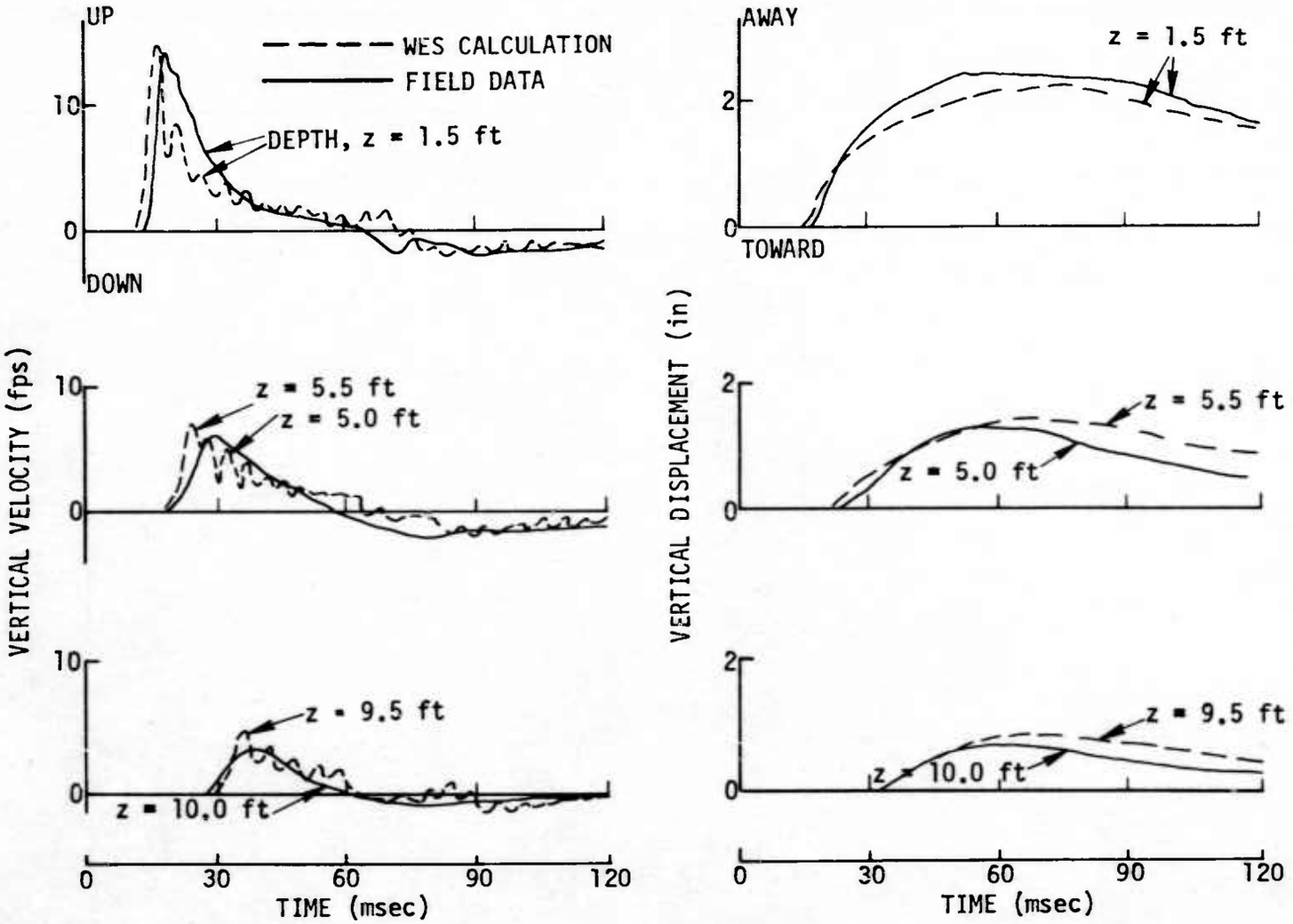

Figure 29. Comparison of WES-Computed Vertical Motion Waveforms with Field Measurements for DISTANT PLAIN 1A, 80-ft Range, ~400-psi Overpressure (Reference 50)

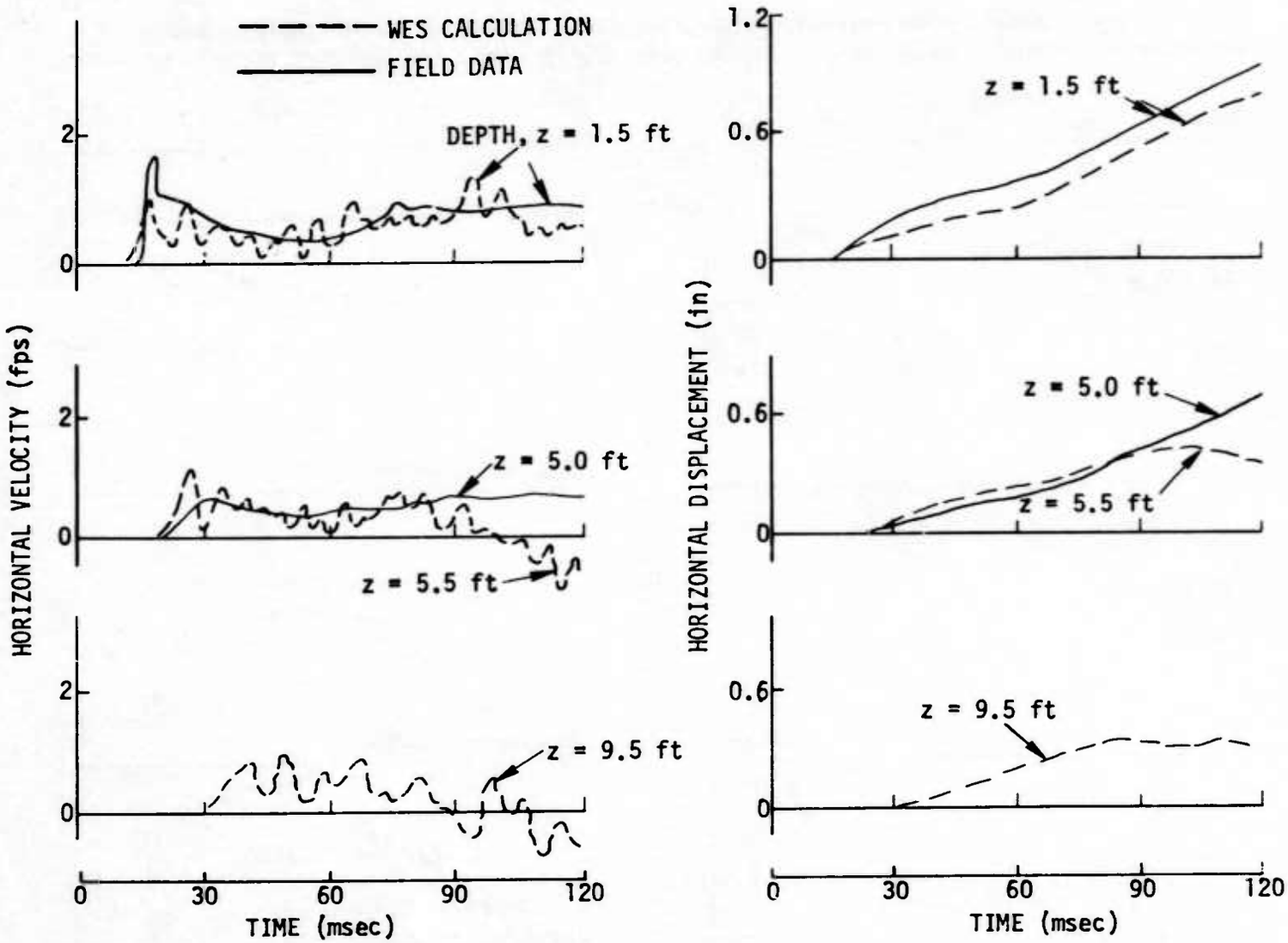

Figure 30. Comparison of WES-Computed Horizontal Motion Waveforms with Field Measurements for DISTANT PLAIN 1A, 80-ft Range, ~400-psi Overpressure (Reference 50)

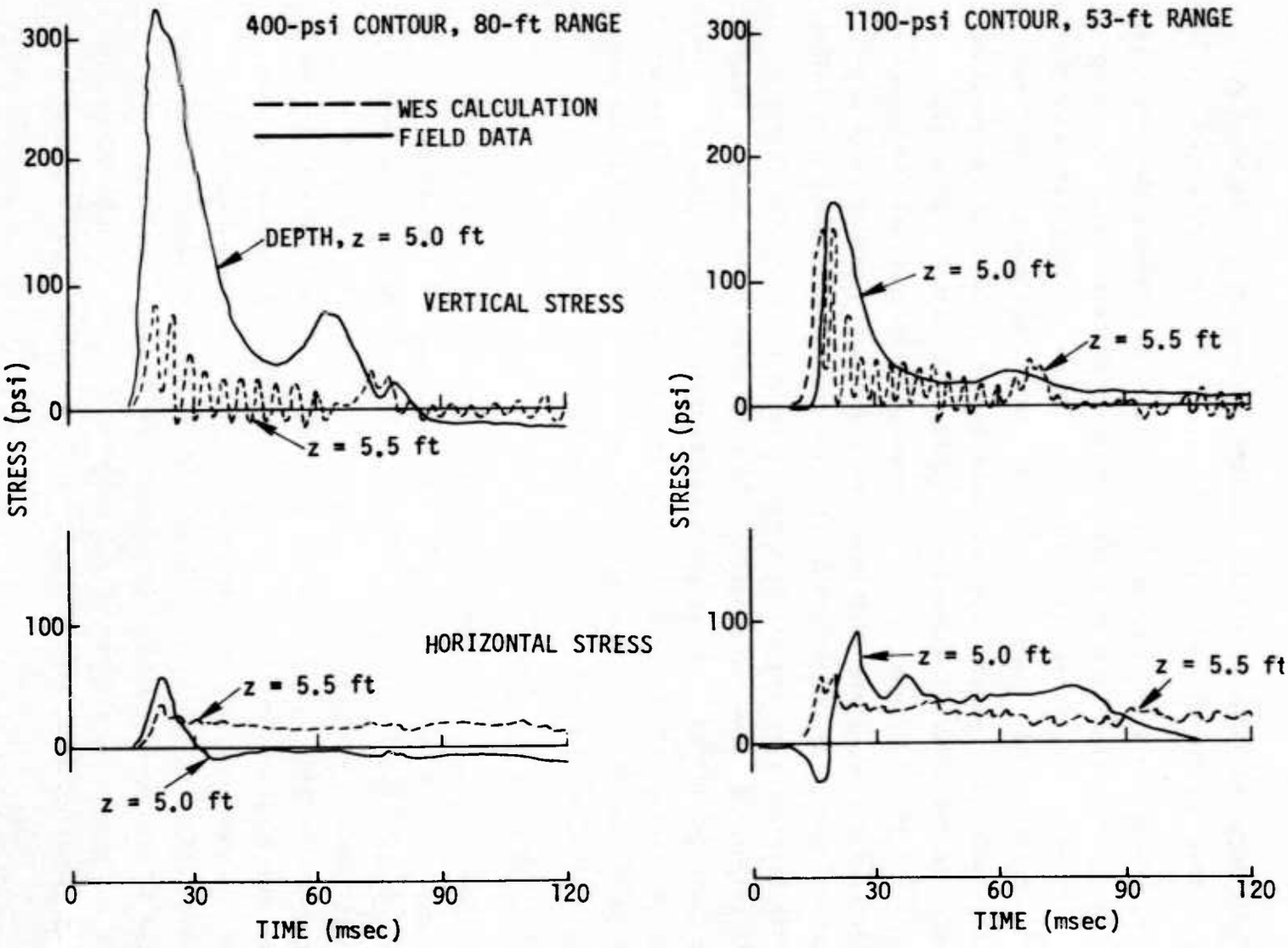

Figure 31. DISTANT PLAIN 1A Test/Analysis Stress History Comparison (Reference 50)

soil medium using state-of-the-art laboratory properties. Better accuracy is expected for the vertical response than for the horizontal.

The PRISCILLA event is significant because it provides the data base for the semi-empirical vertical displacement prediction technique recommended by Wilson and Sibley (Reference 64) and by the 1962 Air Force design manual (Reference 4). More recently, one-dimensional finite difference computer code calculations have been used for predictions of the vertical response in the strongly superseismic region. To help establish the validity of this approach, Cooper and Bratton (Reference 44) formulated a site property model and performed a one-dimensional ground shock calculational study for the PRISCILLA site. A comparison between peak velocity and displacement data and calculational results for the 37-kT PRISCILLA event (Figure 32) show the measured peak velocities to be about 40% higher than those calculated, and the peak displacements to be in good agreement. This correlation is within the accuracy expected according to the uncertainties in the air blast and ground shock data. Other calculations performed by Jackson (Reference 45) show similar correlation.

4.2.1.1 Vertical Motions

Figure 33 shows the peak near-surface air slap vertical acceleration and velocity for high explosive events at the SES (Reference 15). It is generally possible to separate the air slap near-surface peak vertical acceleration and velocity from the rest of the data, with a primary exception occurring when the air slap and refracted wave effects arrive at a point at about the same time. The scatter of the acceleration data is on the same order for individual events as for all SES events. The 500-ton PRAIRIE FLAT and DIAL PACK events tend to have higher velocities at the 1.5-ft depth than the other events which have lower yields of 20 or 100 tons. The scatter of the velocity data is slightly larger than for acceleration data, probably because of the higher yield sensitivity

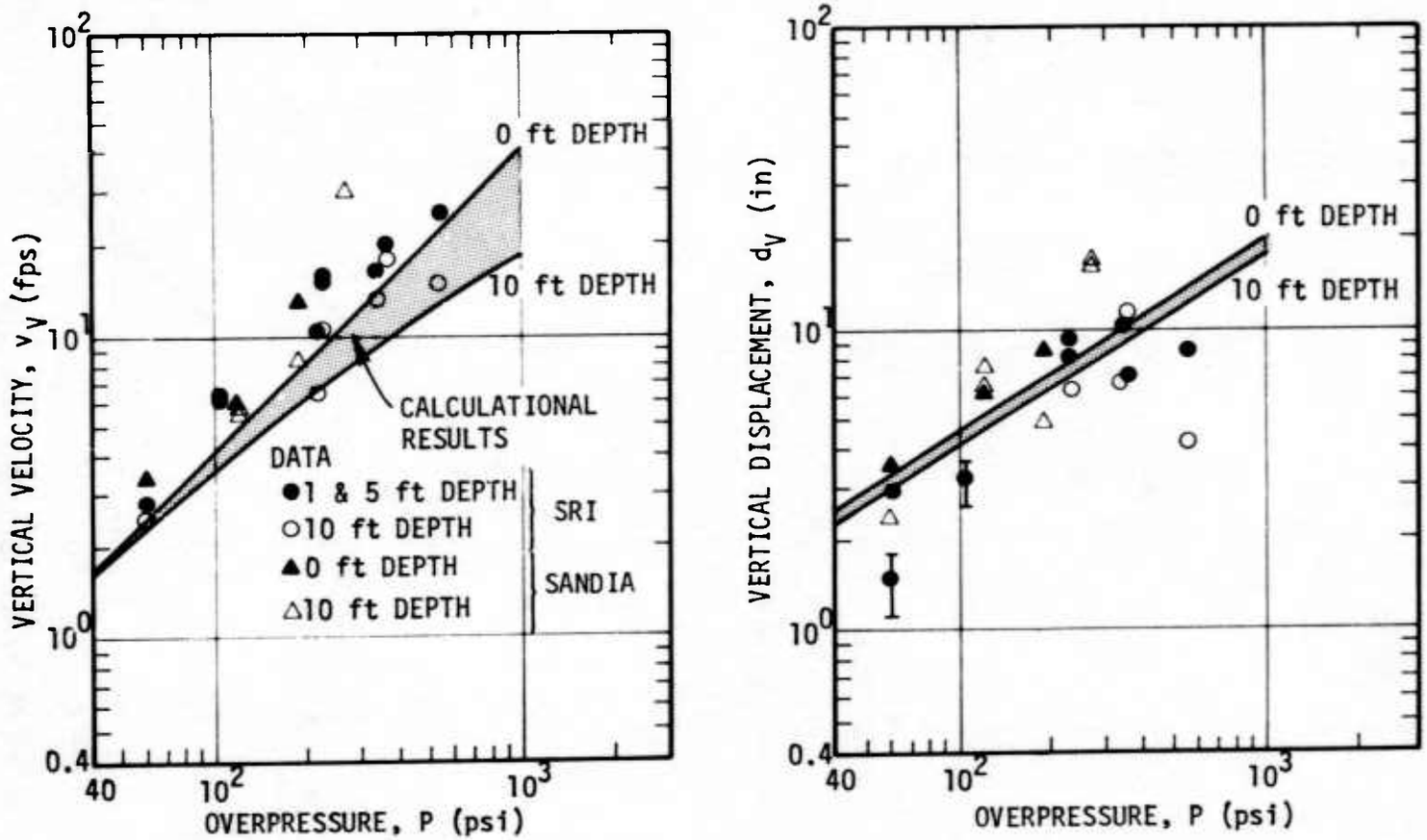

Figure 32. Comparison of Near Surface PRISCILLA Ground Motion Peak Value Data and One-Dimensional Calculational Results (Reference 44)

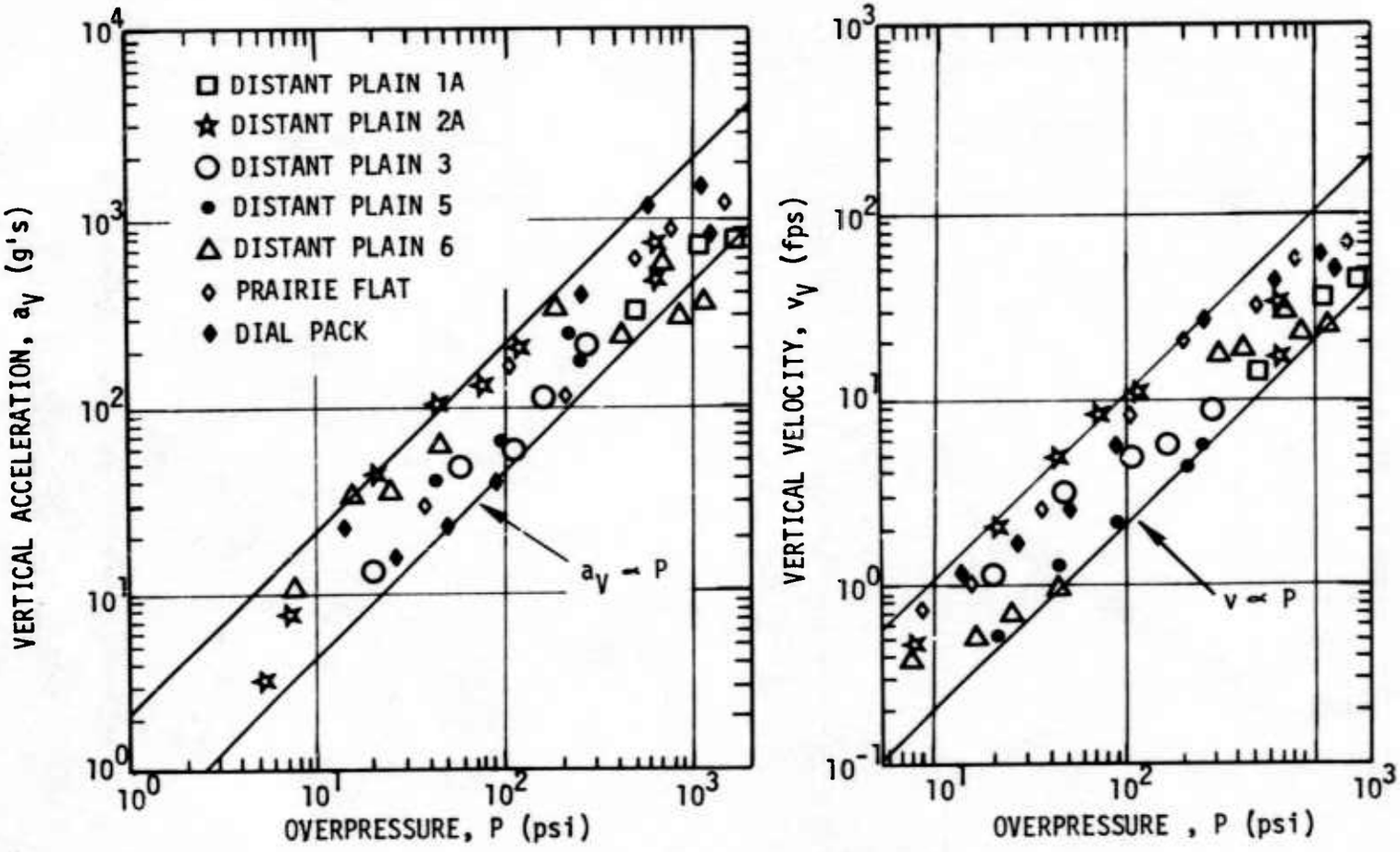

Figure 33. Peak Vertical Air Slap Acceleration and Particle Velocity for SES Events, 1.5-ft Depth (Reference 15)

of peak velocity. However, both sets of data essentially fall within bands about a factor of five apart. The root-mean-square of these bands, given by the following expressions, reasonably represent the data:

$$a_V = 950 \text{ g's } \left(\frac{P}{1000 \text{ psi}}\right) \tag{11}$$

$$v_V = 540 \text{ ips } \left(\frac{P}{1000 \text{ psi}}\right) \tag{12}$$

The near-surface peak vertical acceleration and velocity data for MIXED COMPANY 3 and MIDDLE GUST III and IV are shown in Figure 34 (Reference 15) and compared with the SES data band. Between 10 and 300 psi, the MIDDLE GUST data are within the SES scatter bands but tend to be lower at higher pressure, possibly due partly to the clipping of the air slap downward velocity by the upward moving upstream AI refracted wave. For MIXED COMPANY, all the data are within the SES bands. Thus the near-surface material for these high explosive test sites apparently does not have significant impedance differences for stress levels to at least 300 psi.

In Reference 7, the peak vertical acceleration is given as

$$a_V = n \frac{v_V}{t_R} \tag{13}$$

$$t_R = 0.001 \text{ sec} + \frac{z}{C_L} - \frac{z}{C_i}$$

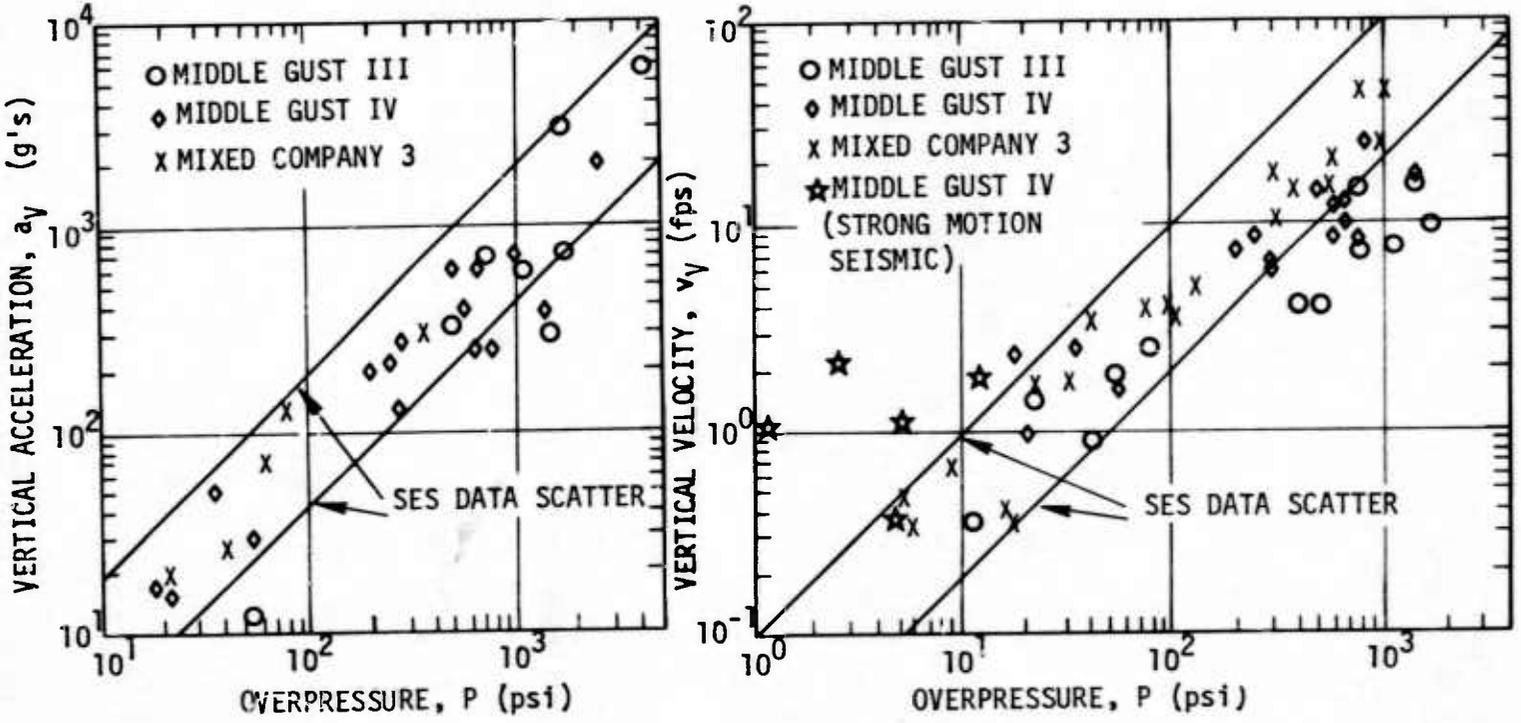

Figure 34. Peak Vertical Air Slap Acceleration and Particle Velocity for MIDDLE GUST III and IV and MIXED COMPANY 3, 1.5-ft Depth (Reference 15)

where t_R is the rise time to peak velocity, C_L is the peak stress speed, C_i is the seismic speed, and n is a factor greater than or equal to one that accounts for a nonlinear rise to peak velocity. This reference recommends a value for n of 1.2 for surface points, and n of 2.0 for points at depth. The rise time to peak velocity at the surface of 0.001 sec is based on estimates of the rise time of the overpressure pulse. Where detailed site data are not available, the peak stress speed C_L can be approximated as half the seismic velocity C_i.

For the DIA/VAS environments, these equations are used for acceleration predictions. The value of n is taken as 2 for all depths because a continuous variation of acceleration is obtained and because the acceleration of free-field surface points is rarely of interest. The approximation that C_L is one-half C_i is also used.

Acceleration and velocity data from SES in Figure 33 are consistent with Equation (13) using the near-surface seismic velocity of 1150 fps and n = 2. In considering deeper gages, Hadala (Reference 46) documented an analysis of data for the 1.5-, 2-, and 10-ft depths for test events at SES and at Cedar City. He concludes that a better fit to the data is obtained by using a 0.002-sec rise time at the surface. However, the effect of this modification is well within the prediction uncertainty.

The vertical acceleration prediction equations are most accurate when the air blast is superseismic with respect to the near-surface medium. When this superseismic condition does not exist, then the air slap response is more complex. However, it is not the dominant effect and the expression just given should be conservative for predicting acceleration.

The peak air slap vertical velocity at the surface is determined from the Hugoniot relationship

$$v_V = \frac{P}{\rho C_L} \tag{14}$$

which yields values of 540, 160, 65, and 23 ips for dry soil, wet soil, soft rock, and hard rock, respectively, for the 1000-psi overpressure reference environment.

At depth, the velocity is given by

$$v_V\ (z) = \frac{\sigma_{Vi}}{\rho C_L} \tag{15}$$

where σ_{Vi} (peak incident stress) and ρC_L (impedance) are both a function of depth. The variation of stress with depth is due to the peakedness of the surface overpressure history and the medium hysteresis and impedance variation with depth.

One-dimensional stress (and velocity) attenuation has been evaluated (Reference 65) for an exponentially decaying, uniform, overpressure loading, $P \exp(-t/T_0)$, on a homogeneous bilinear (linear loading, linear unloading) medium. This attenuation, for shallow depths, can be approximated by

$$\frac{\sigma_V}{P} = \exp\left[-k\ \frac{z}{C_L T_0}\right] \tag{16}$$

where k is a function of the ratio of loading to unloading speeds and T_0 is the initial decay slope time intercept of the overpressure history (similar to t_{00} for the nuclear overpressure). For nonhomogeneous media, enhanced stresses can be obtained on account of reflections at layer

interfaces for significant impedance increase with depth. For most conditions of interest to DIA/VAS, the peak stress is within a factor of about one and a half of the surface overpressure. Higher stress ratios are associated with sites with large impedance increase with depth and low overpressure and high yield loading. Lower stress ratios are associated with soft homogeneous media, and high overpressure and low yield conditions.

In the DIA/VAS environments, the peak vertical stress to the shallow depths of interest is taken to be equal to the surface overpressure. The vertical velocity attenuation, then, primarily results from the impedance variation with depth. For wet soil and soft rock this attenuation is expressed in the form

$$v_V(z) = v_V(0) \exp\left[-\frac{z}{L_0}\right] \tag{17}$$

where L_0 is 250 ft for wet soil and 600 ft for soft rock. The velocity attenuation with depth is neglected for hard rock.

The effect of overpressure and yield on the vertical velocity attenuation for dry soil can be important. This attenuation was assumed to have the following form, suggested by Equation (16), of

$$v_V(z) = v_V(0) \exp\left[-\frac{z}{L_1}\left(\frac{P}{1000\ \text{psi}}\right)^{\alpha}\left(\frac{W}{1\ \text{MT}}\right)^{\beta}\right] \tag{18}$$

where the values of α is 1/4, β is -1/12 and L_1 is 50 ft were determined from one-dimensional calculations for the dry soil site.

Peak vertical displacement for a linear elastic homogeneous medium would be proportional to total impulse, or (for the high pressure region),

$$d_V \sim P^{1/2} W^{1/3} \tag{19}$$

However, for a soft compacting medium (with loading modulus independent of overpressure) overlying a shallow stiff bedrock, the near-surface displacements would be nearly proportional to overpressure and nearly independent of yield. In general, the scaling of peak displacement is related to the ratio of the ground shock transit time between the response point of interest and the effective bedrock to a characteristic time of the overpressure history decay. The Frenchman Flat site exhibited a scaling with yield to the 0.15 power at 100 psi and the 0.22 power at 1000 psi (Reference 44). Other calculational studies have indicated that one-sixth power yield scaling is approximately valid for most sites with significant layering.

One-dimensional calculations for the generic dry soil site resulted in the following peak vertical surface displacement scaling,

$$d_V = 42 \text{ in.} \left(\frac{P}{1000 \text{ psi}}\right)^{2/3} \left(\frac{W}{1 \text{ MT}}\right)^{A} \tag{20}$$

$$A = \frac{1}{6} \left(\frac{P}{1000 \text{ psi}}\right)^{0.23}$$

or 42 in. of displacement for the reference condition of 1 MT yield and 1000-psi overpressure. Parameter calculations varying depth to bedrock, H, have shown the displacement to scale as $H^{0.5}$. According to calculations, the same scaling applies to the wet soil site with a displacement of 12 in. for the reference condition.

The rock sites are nearly homogeneous and the displacements are computed from the uniform elastic medium relationship

$$d_V = \frac{I}{\rho C} \tag{21}$$

where I is the total impulse and ρC is the medium impedance. The reference values for the soft and hard rock sites are 4 and 1.3 in. respectively.

13

These expressions define the air slap component of vertical surface displacement, which is essentially the total AI displacement in the strongly superseismic region. In the outrunning region, the air slap response is superimposed on the ground roll motions. Therefore, the air slap response is not nearly as well defined as for the superseismic region. Until additional analysis is performed, the one-dimensional response is a reasonable estimate of the peak air slap vertical displacement for both regions.

An exponential displacement attenuation with a depth of a form similar to Equation (17) is used. The attenuation constant, L_0, is 150 ft for dry soil, 250 ft for wet soil, and 400 ft for soft rock. No attenuation of displacement from the surface through the 50-ft depth occurs for the hard rock site.

The DIA/VAS air slap ground shock parameter definition for the dry soil, wet soil, soft rock, and hard rock sites is summarized in Tables 5 to 8 respectively. The tables give best estimate peak values for displacements, velocities, accelerations, and stresses; and scaling with yield, overpressure, and depth. In addition, 2σ uncertainty factor estimates are specified.

TABLE 5. SURFACE BURST DRY SOIL PEAK AIR SLAP PARAMETERS

$$\text{Environment Value} = \left(\text{Reference Value}\right)\left(\frac{W}{1\ \text{MT}}\right)^{A}\left(\frac{P}{1000\ \text{psi}}\right)^{B}\exp\left|-\frac{z}{L_0}\right|$$

ENVIRONMENT PARAMETER	REFERENCE VALUE	SCALING FACTORS*			2σ UNCERTAINTY FACTOR
		A	B	L_0 (ft)	
d_V (in)	42	(1)	2/3	150	2.5
d_H (in)	7	(1)	1/3	500	3.0
v_V (ips)	540	0	1	(2)	2.5
v_H (ips)	80	0	0.6	∞	2.5
a_V (g's)	2800	0	1	(3)	3.0
a_H (g's)	400	0	0.6	(3)	3.5
σ_V (psi)	1000	0	1	∞	2.0
σ_H (psi)	350	0	0.8	∞	3.0

*Scaling Range: 20 kT ≤ W ≤ 50 MT
10 psi ≤ P ≤ 5000 psi
z ≤ 50 ft

(1) $A = \frac{1}{6}\left(\frac{P}{1000\ \text{psi}}\right)^{0.23}$

(2) $L_0 = 50\ \text{ft}\left(\frac{P}{1000\ \text{psi}}\right)^{-1/4}\left(\frac{W}{1\ \text{MT}}\right)^{1/12}$

(3) $a_{V,H} = \frac{5v_{V,H}}{\left(1 + \frac{z}{4\ \text{ft}}\right)}$ g's/ips , $z > 0$

TABLE 6. SURFACE BURST WET SOIL PEAK AIR SLAP PARAMETERS

$$\text{Environment Value} = \left(\text{Reference Value}\right) \left(\frac{W}{1\ \text{MT}}\right)^{A} \left(\frac{P}{1000\ \text{psi}}\right)^{B} \exp\left[-\frac{z}{L_0}\right]$$

ENVIRONMENT PARAMETER	REFERENCE VALUE	SCALING FACTORS*			2σ UNCERTAINTY FACTOR**
		A	B	L_0 (ft)	
d_V (in)	12	(1)	2/3	250	2.5
d_H (in)	15	(1)	2/3	∞	3.0
v_V (ips)	160	0	1	250	2.5
v_H (ips)	60	0	0.6	∞	2.5
a_V (g's)	830	0	1	(2)	3.0
a_H (g's)	420	0	0.6	(2)	3.5
σ_V (psi)	1000	0	1	∞	2.0
σ_H (psi)	1000	0	1	∞	2.0

*Scaling Range: 20 kT ≤ W ≤ 50 MT
10 psi ≤ P ≤ 5000 psi
z ≤ 50 ft

(1) $$A = \frac{1}{6} \left(\frac{P}{1000\ \text{psi}}\right)^{0.23}$$

(2) $$a_{V,H} = \frac{5 v_{V,H}}{\left(1 + \frac{z}{9\ \text{ft}}\right)} \quad \text{g's/ips}, \ z > 0$$

TABLE 7. SURFACE BURST SOFT ROCK PEAK AIR SLAP PARAMETERS

$$\text{Environment Value} = \left(\text{Reference Value}\right)\left(\frac{W}{1\ \text{MT}}\right)^{A}\left(\frac{P}{1000\ \text{psi}}\right)^{B}\exp\left[-\frac{z}{L_0}\right]$$

ENVIRONMENT PARAMETER	REFERENCE VALUE	SCALING FACTORS*			2σ UNCERTAINTY FACTOR**
		A	B	L_0 (ft)	
d_V (in)	4	1/3	0.4	400	2.5
d_H (in)	4	1/3	0.4	400	3.0
v_V (ips)	65	0	1	600	2.5
v_H (ips)	40	0	0.6+	∞	2.5 to 3.5
a_V (g's)	330	0	1	30	3.0
a_H (g's)	330	0	1	30	3.5 to 4.5
σ_V (psi)	1000	0	1	∞	2.0
σ_H (psi)	1000	0	1	∞	3.0 to 4.0

*Scaling Range: 20 kT ≤ W ≤ 50 MT
10 psi ≤ P ≤ 5000 psi
z ≤ 50 ft

+$v_H = v_V$ for P < 300 psi

**When ranges of values are given, the uncertainties are largest for the lower overpressure, outrunning region; and smallest for the high overpressure, superseismic region.

TABLE 8. SURFACE BURST HARD ROCK PEAK AIR SLAP PARAMETERS

$$\text{Environment Value} = \left(\text{Reference Value}\right) \left(\frac{W}{1\ \text{MT}}\right)^{A} \left(\frac{P}{1000\ \text{psi}}\right)^{B} \exp\left[-\frac{z}{L_0}\right]$$

ENVIRONMENT PARAMETER	REFERENCE VALUE	SCALING FACTORS*			2σ UNCERTAINTY FACTOR**
		A	B	L_0 (ft)	
d_V (in)	1.3	1/3	0.4	∞	2.5
d_H (in)	1.3	1/3	0.4	∞	3.0
v_V (ips)	23	0	1	∞	2.5
v_H (ips)	30	0	1	∞	2.5 to 3.5
a_V (g's)	120	0	1	60	3.0
a_H (g's)	120	0	1	60	3.5 to 4.5
σ_V (psi)	1000	0	1	∞	2.0
σ_H (psi)	1000	0	1	∞	3.0 to 4.0

*Scaling Range: 20 kT ≤ W ≤ 50 MT
20 psi ≤ P ≤ 5000 psi
z ≤ 50 ft

**When ranges of values are given, the uncertainties are largest for the lower overpressure, outrunning region; and smallest for the high overpressure, superseismic region.

4.2.1.2 Horizontal Motions

In the superseismic region an initial outward peak horizontal velocity occurs because of the compressional wave induced by the air slap. Analytical solutions exist for the response of elastic and certain nonlinear media to a uniformly traveling constant overpressure profile air blast loading. This steady state loading is a reasonable approximation for determining air slap peak velocities in the superseismic region.

Sackman developed a solution (Reference 66) for the ground shock response to a steady state load on a layered elastic medium. Results for this solution indicate that the peak air slap near surface horizontal velocity (Figure 35) for most of the superseismic region is given approximately by

$$v_H = \frac{P}{\rho U} \tag{22}$$

where U is the air shock velocity. The horizontal velocity is larger in the lower layer, but still within a factor of two of this equation until near transseismic conditions are achieved. This trend agrees with test data for some events where the horizontal velocity does increase with depth, although it is not always due to air-slap-induced effects.

The accuracy of horizontal air slap velocity measurements is not as good as the vertical response since the direct shear wave which follows the compressional wave causes an inward component resulting in a short pulse width (higher frequency) response. For a low value of Poisson's ratio, the shear wave component is quite large and the elastic solution produces inward displacements. This type of response has been observed in test events such as MINERAL ROCK, where the medium has a high shear strength and modulus.

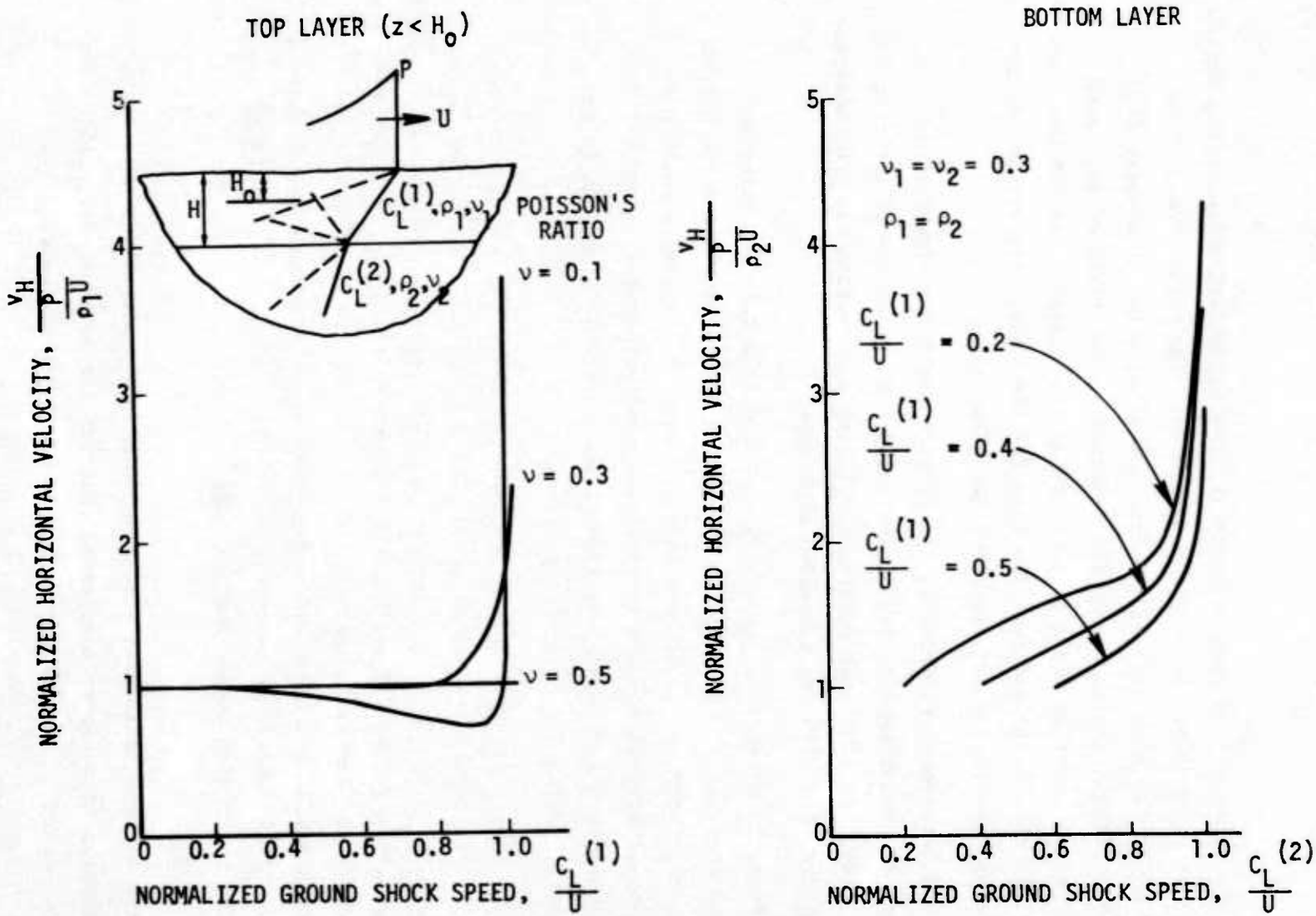

Figure 35. Peak Horizontal Velocity for Uniformly Moving Load on Layered Elastic Half-Space

The near-surface peak air-slap-induced horizontal velocity for high explosive test events is shown in Figure 36. The expression $P/\rho U$ is somewhat on the high side of the data for sites other than Cedar City. Velocity attenuation caused by the compaction hysteresis of soft material near the surface would be expected at the 1.5-ft depth for the very low yield air blast loading. The data for the Cedar City events are for the transition region and are above the $P/\rho U$ curve.

The horizontal velocity variation with depth for higher yield nuclear air blast loading can be neglected for the depths of interest in this study. In some test events, a velocity attenuation has been observed; for others, the velocity increased with depth.

There is minimal calculational or field data base for air-slap-induced horizontal velocities in the outrunning region, where the ground shock wave speed, C, is greater than U. In such cases $P/\rho U$ would predict larger horizontal than vertical air slap velocities. However, test data indicate that the peak horizontal and vertical velocities in the outrunning region are on the same order.

For the reference condition of 1000 psi and 1 MT, the peak surface air slap horizontal velocities are 80 ips for dry soil, 60 for wet soil, 40 for soft rock, and 30 for hard rock. This velocity scales as $P^{0.6}$, which is approximately the P/U scaling for the overpressure region of interest. This decay is maintained until the horizontal and vertical velocities are about equal, and then both decay linearly with overpressure thereafter. At the reference overpressure level, the soft rock medium is near the outrunning region and the hard rock medium is well into outrunning.

The surface horizontal acceleration and its attenuation with depth are computed in a manner similar to that for the vertical component. For the soil medium, the same expression is used with the modification

$$a_H = 2 \frac{v_H}{t_R} \tag{23}$$

and the horizontal acceleration is taken to be equal to that of the vertical for the rock medium.

Calculations of the response of layered media to the air blast loading due to a high yield nuclear weapon for dry soil over rock, wet soil over rock, and clay over interbedded shale and limestone media were performed by ATI. The computations were performed out to approximately the positive phase duration of the air blast for overpressure stations down to 150 psi. An analysis of the peak horizontal displacements in the superseismic region indicates that they correlate reasonably well with unloading shear modulus of the medium. The following relationship has been developed for the near-surface displacement

$$d_H = 40 \text{ in.} \left[1 + \frac{z_{BR}}{200 \text{ ft}}\right] \left(\frac{P}{G_M}\right)^{1/2} \left(\frac{W}{1 \text{ MT}}\right)^{1/6} \tag{24}$$

where G_M is the unloading shear modulus and z_{BR} is the depth to bedrock. Only a small dependence of shear strength on displacement was observed. However, for most materials there will be a strong correlation between shear modulus and the better defined shear strength. Thus the horizontal displacement is primarily dependent on shear properties of the medium, while the vertical displacement is primarily dependent on uniaxial strain properties.

Using representative unloading shear moduli of 100 ksi for dry soil and 30 ksi for wet soil gives 1 MT displacements for overpressures of 1000 and 100 psi, of 9 and 3 inches, respectively, for dry

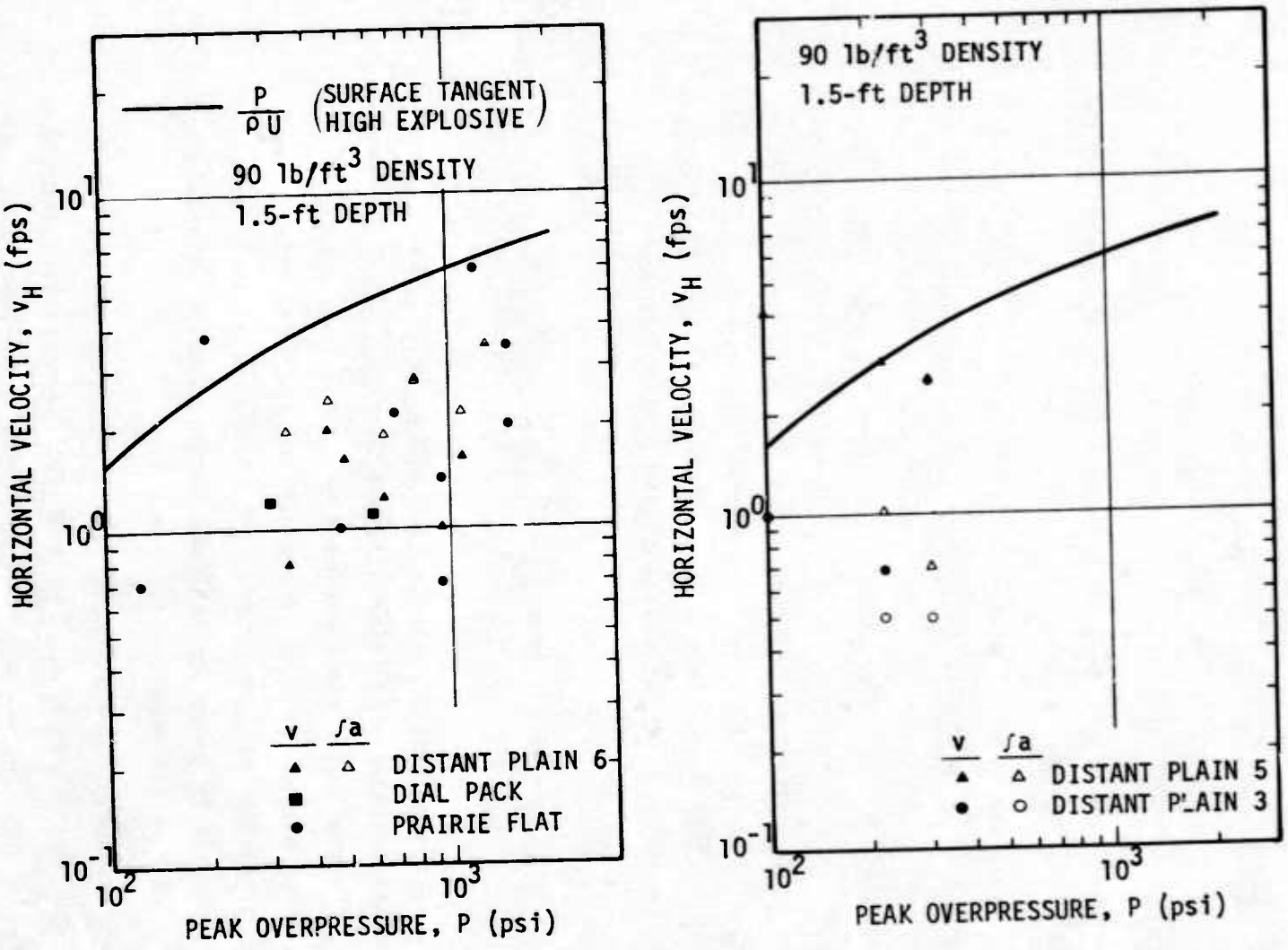

Figure 36. Peak Air Slap Horizontal Velocity High Explosive Test Data (Continued)

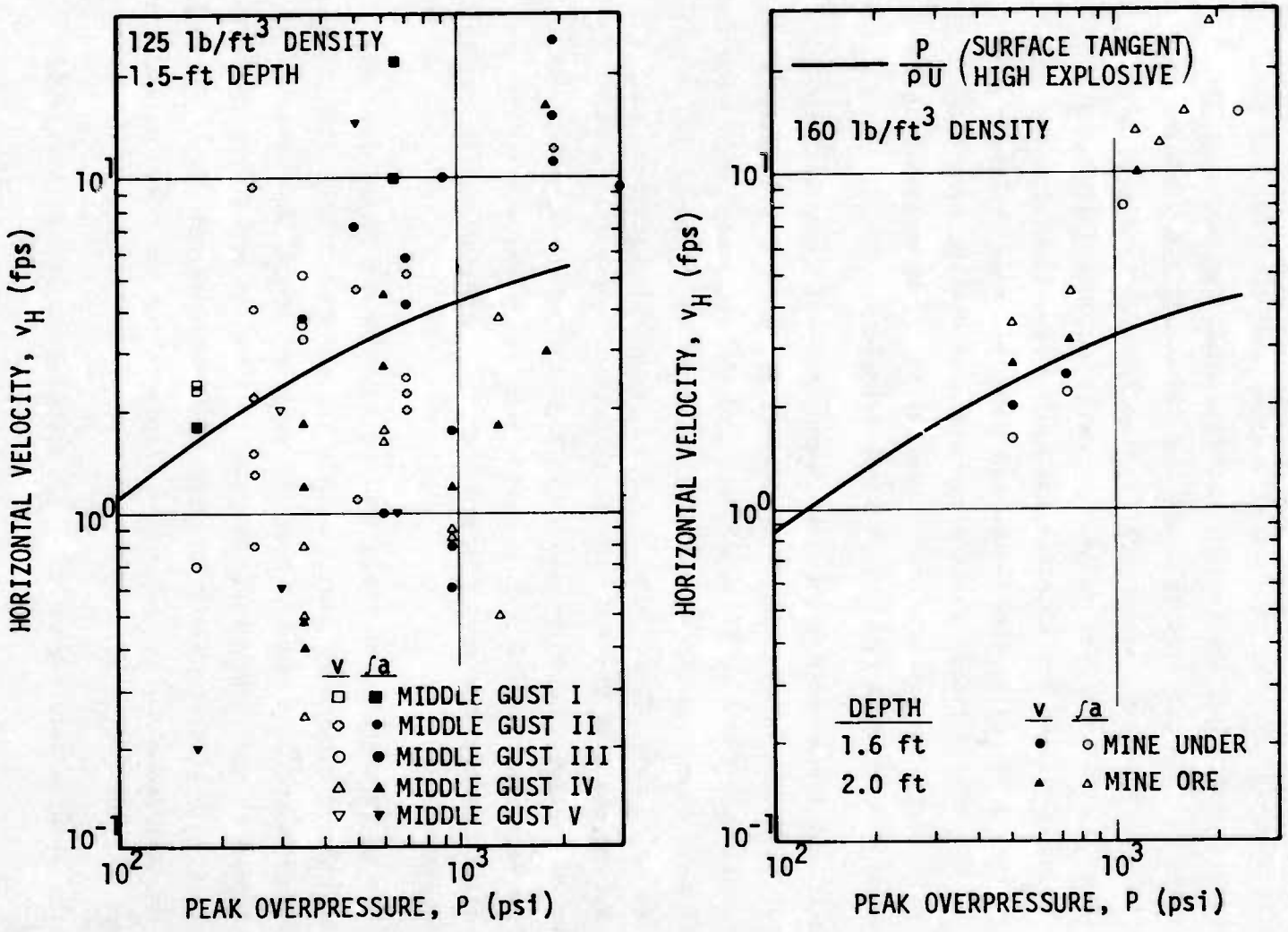

Figure 36. Peak Air Slap Horizontal Velocity High Explosive Test Data (Concluded)

soil; and 17 and 6 inches, respectively, for wet soil. At the 1000-psi overpressure, the horizontal displacement for dry soil is considerably lower than the vertical displacement; for wet soil the peak horizontal displacement is about one and a half times higher than the vertical. The large horizontal displacements for wet soil are due to the low capability of the medium to resist horizontal stress gradients in the soil and for decelerating motion resulting from the air slap horizontal velocity; therefore, the material tends to keep moving outward. There is a fairly small attenuation of displacement with depth, down nearly to bedrock, since the motion is predominantly a shearing of the wet soil near the bedrock interface.

In calculations performed by WA (Baron, private communication), ratios of horizontal-to-vertical peak air-slap-induced displacements for wet soil were found to be about one, and the corresponding ratios for dry soil were about one-sixth at 1000 psi, about one-third at 100 psi, and about one at 10 psi. These results are in reasonable agreement with the ratios determined from the ATI calculations considering the large uncertainties in horizontal displacement. In the DIA/VAS environments, the WA ratios were used for dry soil displacement, while the wet soil horizontal displacements were taken as one and one quarter times the vertical at the surface.

There is no significant field test or calculational data base for air-slap-induced horizontal displacements for the rock sites. The design manual (Reference 7) recommends that the peak horizontal and vertical AI displacements in the superseismic regions be taken as equal when the stress wave velocity is greater than 0.71 times the air shock velocity. On this basis, the DIA/VAS air slap horizontal displacements are taken as equal to the vertical, for the rock sites.

In the superseismic region the peak air slap horizontal stress is given by

$$\sigma_H = K\sigma_V \tag{25}$$

where K is a dynamic lateral stress coefficient. This coefficient is generally low for dry soils (Reference 7) and a value of 0.35 is used for the superseismic 1000-psi overpressure reference condition for the dry soil site. The scaling with overpressure is such that at 10 psi both components of stress are approximately equal. Low shear strength wet soils cannot maintain significant stress differences and the vertical and horizontal components of stress are approximately equal for the whole overpressure range.

The rock sites are in the outrunning or weakly superseismic region throughout most of the region of interest in this study and the horizontal stress has significant uncertainty for such conditions. Steady state elastic analyses (e.g., Reference 66) predict large horizontal stresses near the outrunning region, but finite difference calculations for the HRSD Program exhibited horizontal stresses on the order of the vertical stresses. The DIA/VAS horizontal stresses are taken to be equal to that of the vertical for the rock sites. However, both the stress and motion environments for the transseismic region is an area where the phenomenology needs better definition.

The peak air slap horizontal ground shock parameter scaling and 2σ uncertainty factor estimates are given in Tables 5 to 8.

4.2.2 Directly Coupled Effects

Only a small fraction of the total nuclear weapon energy is directly coupled to the ground. This fraction is composed of internal energy primarily from radiative coupling and kinetic energy associated with weapon debris. The energy coupling decreases rapidly with increased HOB, since the air absorbs radiative energy (which results in the fireball formation) and dissipates kinetic energy.

Kinetic energy is fairly efficient in producing craters, and source details must be considered when direct coupling effects are evaluated. For

example, the KOA event, fired in a water tank, had a cratering efficiency about three times that of "hot" devices for comparable HOB and geological conditions. This was due to the enhanced kinetic energy associated with effects due to the water tank.

Early predictions for directly coupled effects (Reference 4) were based on accelerometer data for underground nuclear tests (primarily RAINIER fired in tuff). Predictions for surface bursts were determined by applying (a) an equivalent yield factor to these data to obtain surface burst predictions, (b) empirical ratios of ground shock arrival time to peak velocity rise time and positive phase duration, to obtain peak velocity and displacement from acceleration, (c) hydrodynamic yield scaling, and (d) seismic velocity scaling, based on high explosive data, to apply these results to materials other than tuff. At that time, the velocities and displacements from near-surface nuclear events were not studied in detail since the uncertainties associated with integrating the accelerometer records were considered too large. The engineering approximations used to develop this methodology have proven to be good, considering the limited data base at that time, for the prediction of directly coupled effects in the far-out region. Close in, the methodology did not account for the significant variation with range of the ratio of velocity pulse duration to arrival time, caused by free surface effects. This ratio remained constant in the far-out region.

When the need developed for strategic systems to survive closer-in to ground zero, it became critical to develop higher confidence predictions for DI/CI effects. At this time, continuum code calculational techniques had been developed that could be used to calculate these effects. Initial efforts addressed the HRSD program requirements, with more recent calculations performed for a generic clay/shale site termed U-2. However, to date the theoretical techniques are not at the point where

credible calculational results can be obtained. Ground shock calculations for Site U-2 performed by ATI show little difference between the response to air blast loading only and the response to combined air blast loading and initial energy deposition (direct coupling) conditions. The latter calculation considered directly coupled effects using the DNA Source 3 model developed by Systems, Science and Software (S^3). However, significant crater-related motions would be expected for this site. Preliminary results of similar calculations performed by PI show agreement with the ATI results.

When the limitations in the calculational state-of-the-art became apparent, emphasis was again placed on empirical analysis of the test data. This effort was aided by data from better-instrumented high explosive tests at the SES and Cedar City test sites in the late 1960's.

In analyzing the project MOLE horizontal displacement data from the early 1950's, Cooper determined that the cube root of apparent crater volume scaled the data better than all other parameters considered. This scaling parameter was then tested against the available nuclear and high explosive data and found to correlate quite well, as shown in Figure 37 (Reference 7).

For a given crater volume, above-surface detonations were found to be more efficient in producing horizontal displacement than half-buried and below-surface detonations. Cooper indicates that this is possibly due to the fact that material ejecta is more predominant in the cratering process for surface and below-surface detonations. This process could be less efficient in producing horizontal displacement than a compression-induced crater would be.

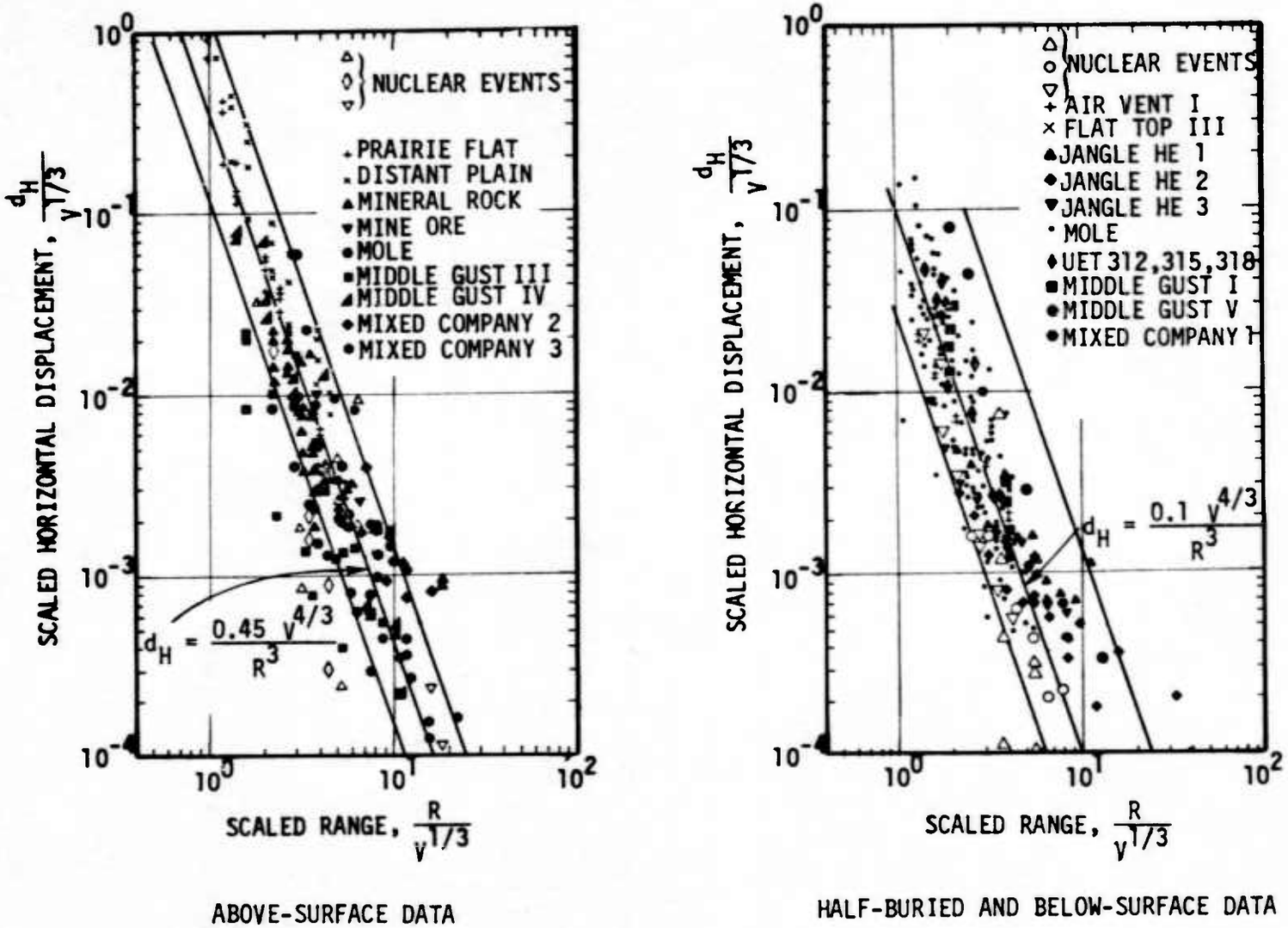

Figure 37. Crater Volume Scaled Peak Horizontal Displacement Correlation

A fit to the data in log space was given by

$$d_H = 0.45 \frac{V^{4/3}}{R^3} \qquad \text{HOB} > 0 \qquad (26)$$

and

$$d_H = 0.10 \frac{V^{4/3}}{R^3} \qquad \text{HOB} \leq 0 \qquad (27)$$

where V is the apparent crater volume and R is the ground range. The data available are not sufficient to accurately define a continuous transition from above-surface to buried-source conditions. A surface contact burst is considered to be at a slight HOB, while a true surface burst is one where the center of mass of the explosive is coincident with the ground surface.

The data scatter in the correlation (Figure 37) is approximately an order of magnitude. However, the correlation achieved is quite good considering the wide range of geology and explosive sources included and the significant scatter of test data for individual events.

Reference 7 also presents Cooper's permanent horizontal displacement data correlation for high explosive tangent spheres for events at SES and Cedar City and for the MOLE series. This correlation indicates that

$$d_{HP} = 0.2 \frac{V^{4/3}}{R^3} \qquad \text{HOB} > 0 \qquad (28)$$

For surface burst conditions, the close-in near-surface vertical response consists of downward motion brought about by the air slap and

followed by the upward motions associated with DI/Cl effects. Figure 38 (Reference 15) shows a comparison between vertical and horizontal scaled displacement data for SES and Cedar City high explosive events, where close-in the crater-related effects dominate the response. The Cooper crater volume scaled peak horizontal displacement data are on the high side of Equation (26); and the vertical and horizontal peak displacements are approximately equal, with both data sets being essentially within scatter bands a factor of ten apart. Analysis of nuclear data, by Cooper, for above-surface bursts in the EPG shows much scatter in limited data, but the trend is consistent with horizontal and vertical displacements being equal.

Figure 39 shows the vertical and horizontal scaled displacements for the two 100-ton MIDDLE GUST and the 500-ton MIXED COMPANY surface tangent high explosive events. Also shown, for comparison, are the scatter bands for the SES and Cedar City data and the Equation (26) prediction line. These horizontal displacement data on the average agree with the prediction equation; however, a marked geology dependence is shown. The scaled displacements for MIXED COMPANY 3 (dry hard sandstone) are the largest, with the MIDDLE GUST dry clay/shale site having nominal values and the MIDDLE GUST wet clay/shale site having the smallest values. The peak vertical displacements are about a factor of two lower than the horizontal with the same geological separation.

The MIDDLE GUST and MIXED COMPANY events are the first significant tests in medium with strong near-surface impedance mismatches. Since many strategic sites of interest have strong layering features at comparable scaled depths, it is important to better define the effects of layering on ground shock response. Possibly geological correction factors to crater volume scaling could be determined.

Scaled displacement data for five of the eight 1000-lb calibration shots fired at various depths in the MIDDLE GUST wet site are shown in

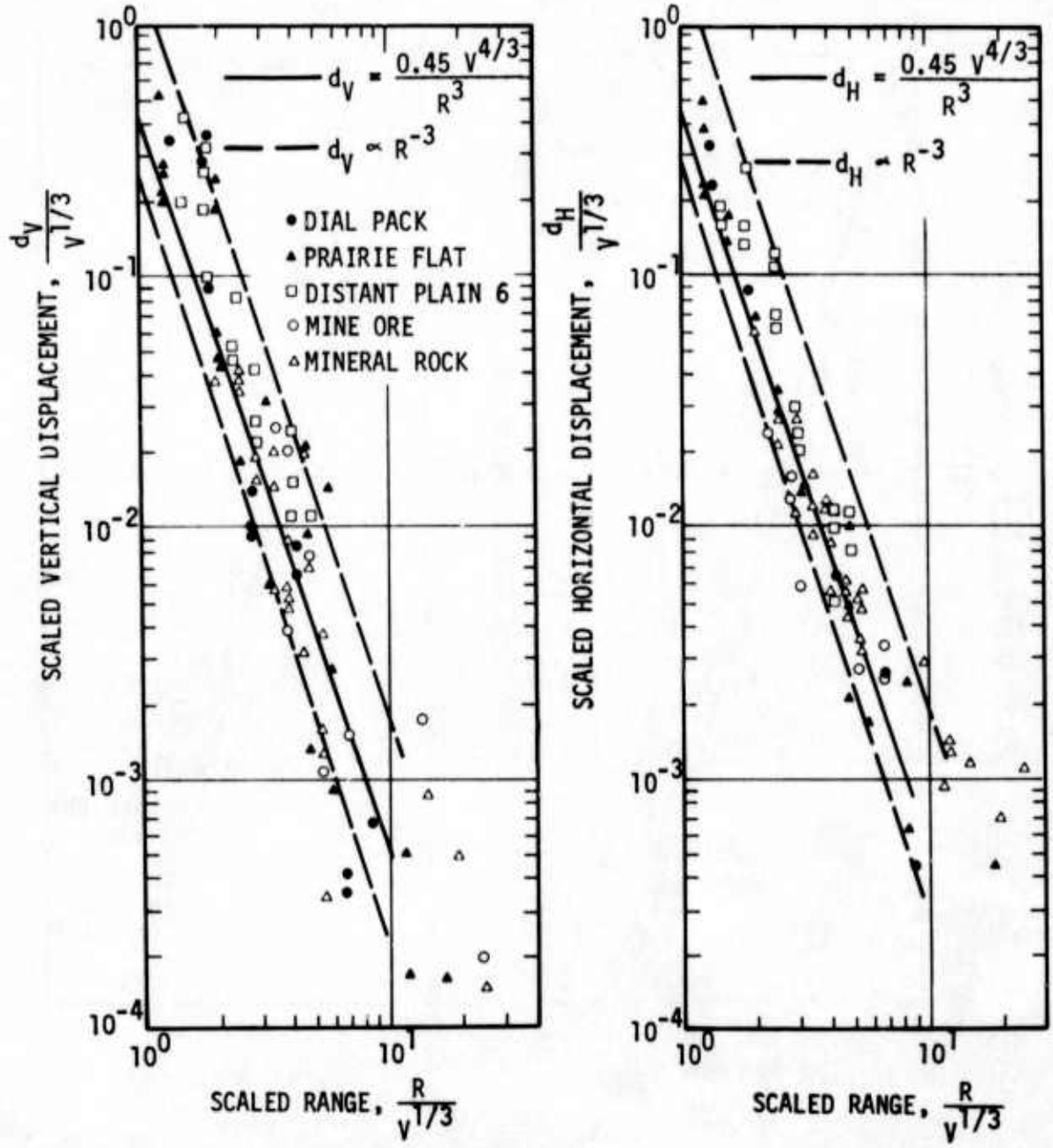

Figure 38. Crater Volume Scaled Peak Displacement Correlation for Surface Tangent High Explosive Events at SES and Cedar City (Reference 15)

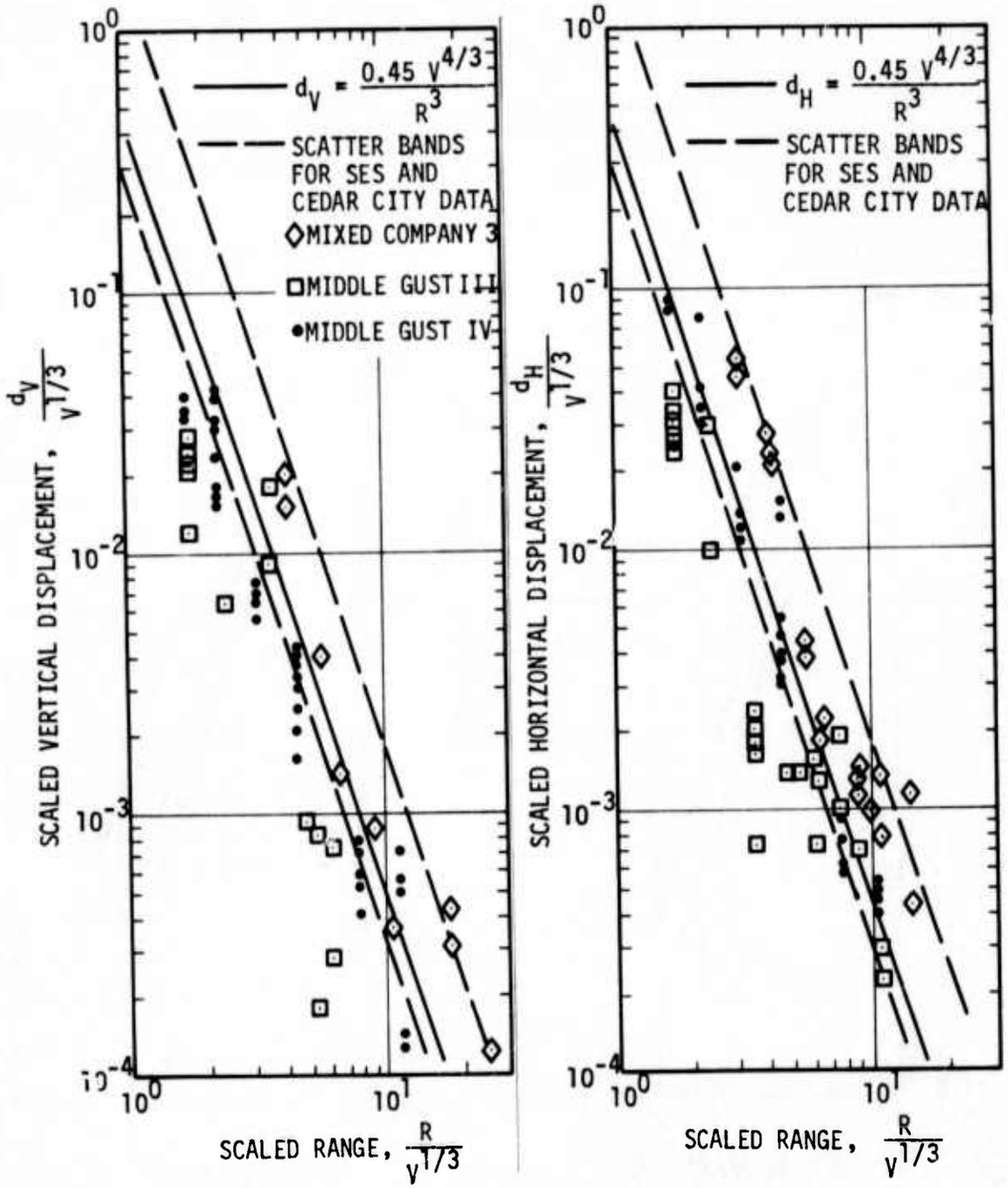

Figure 39. Crater Volume Scaled Peak Displacement Correlation for Large Surface Tangent High Explosive Events at MIDDLE GUST and MIXED COMPANY

Figure 40. Surface tangent and half-buried conditions were obtained by excavating down to the depths of interest. The site is not as strongly layered, in a scaled sense, for these smaller high explosive charges; and data for the surface tangent events are slightly lower than, but in reasonable agreement with, the prediction equation. However, the half-buried event data are high compared with the prediction equation. Actually, the calibration data do not exhibit a difference in crater volume scaling between half-buried and surface tangent events.

Test events generally have data for gages from various depths. However, dimensional scaling considerations indicate that if the response is a function of depth, then it is more appropriate (for at least nearly homogeneous sites) to compare data from similar scaled depths. Figure 41 (Reference 67) shows that when SES data for only the top 0.1 $V^{1/3}$ are considered, then the scatter about the best fit line is considerably reduced. Figures 42 and 43 show these data for MIDDLE GUST IV and MIDDLE GUST III, respectively.

The data base has received extensive study of various possible scaling parameters. In Reference 67, Cooper presents a dimensional analysis for crater-related ground motion response in "uniform" geologies. The analysis considers as independent variables: crater volume, V; medium density, ρ; and characteristic wavespeed, C; gravitational acceleration, g; range from burst, R; depth, z; and weapon HOB. The influence of material strength is assumed to be considered through the crater volume and, therefore, is not an independent parameter. Crater-related displacements can then be written in the form

$$\frac{d}{V^{1/3}} = f\left[\frac{R}{V^{1/3}}, \frac{z}{V^{1/3}}, \frac{HOB}{V^{1/3}}, \frac{gV^{1/3}}{C^2}\right] \qquad (29)$$

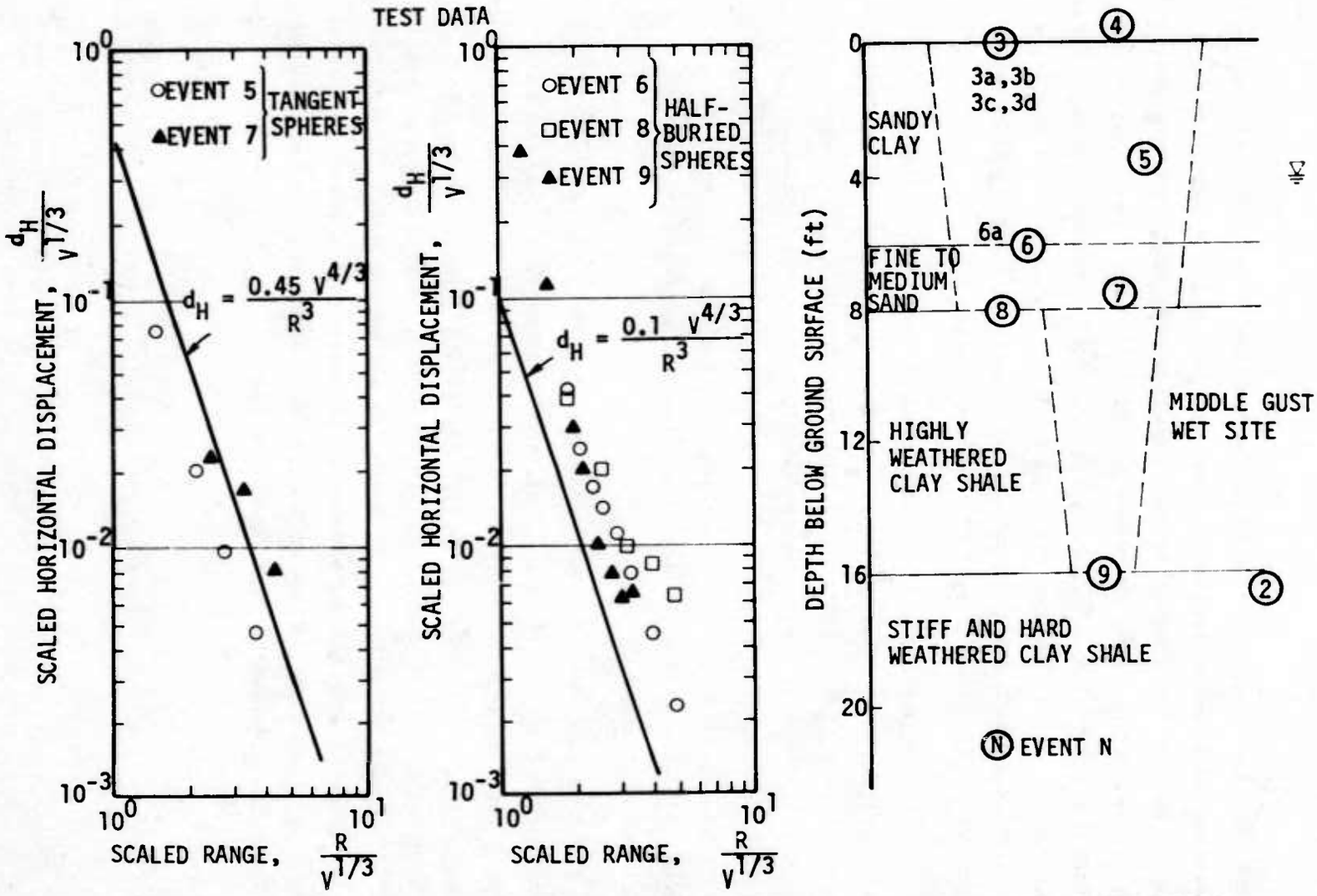

Figure 40. Crater Volume Scaled Horizontal Peak Displacement Correlation for MIDDLE GUST, Wet Site Calibration Events (Cooper, Unpublished Data Analysis)

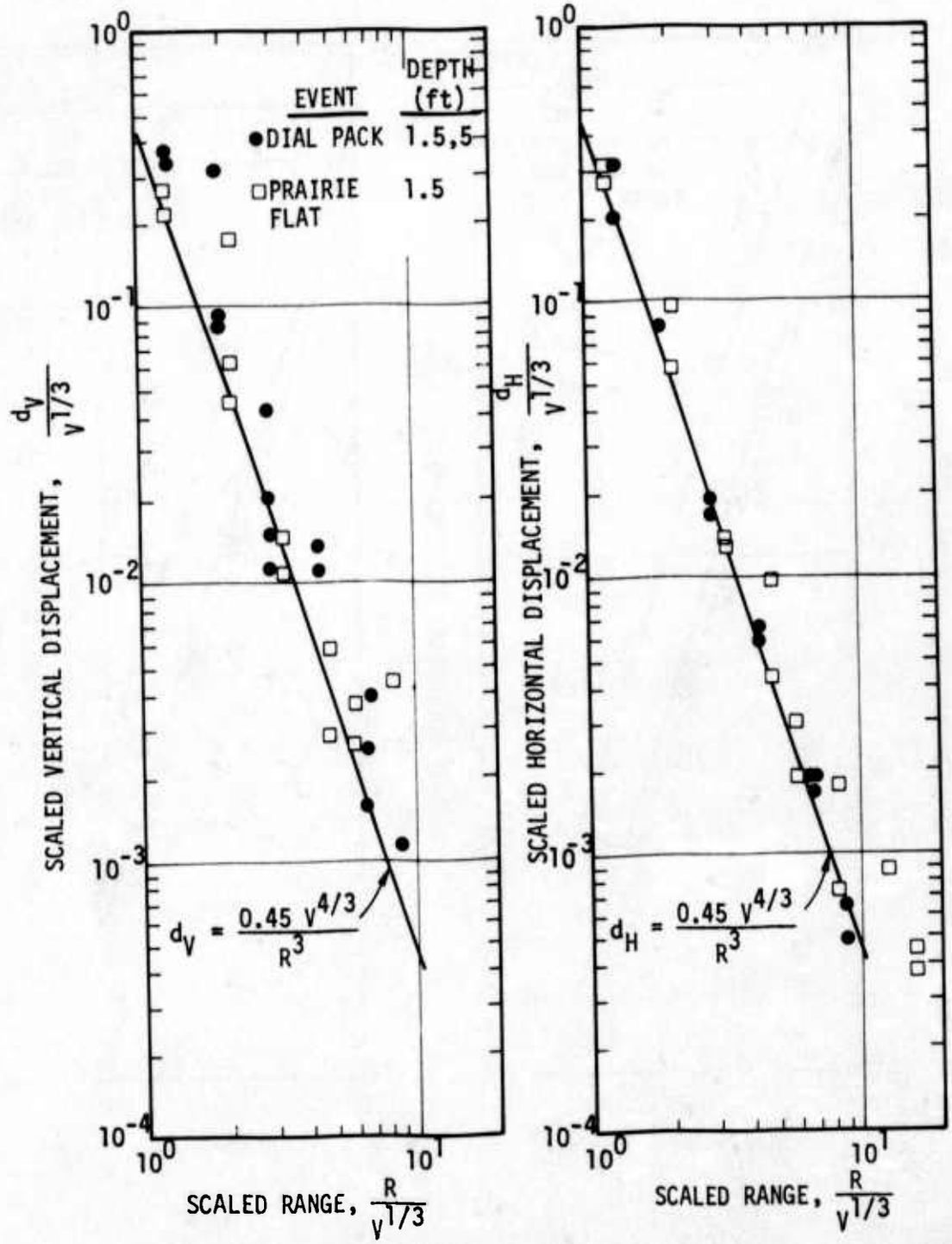

Figure 41. Crater Volume Scaled Peak Displacement Correlation for Top 0.1 $V^{1/3}$ for SES Events (Reference 67)

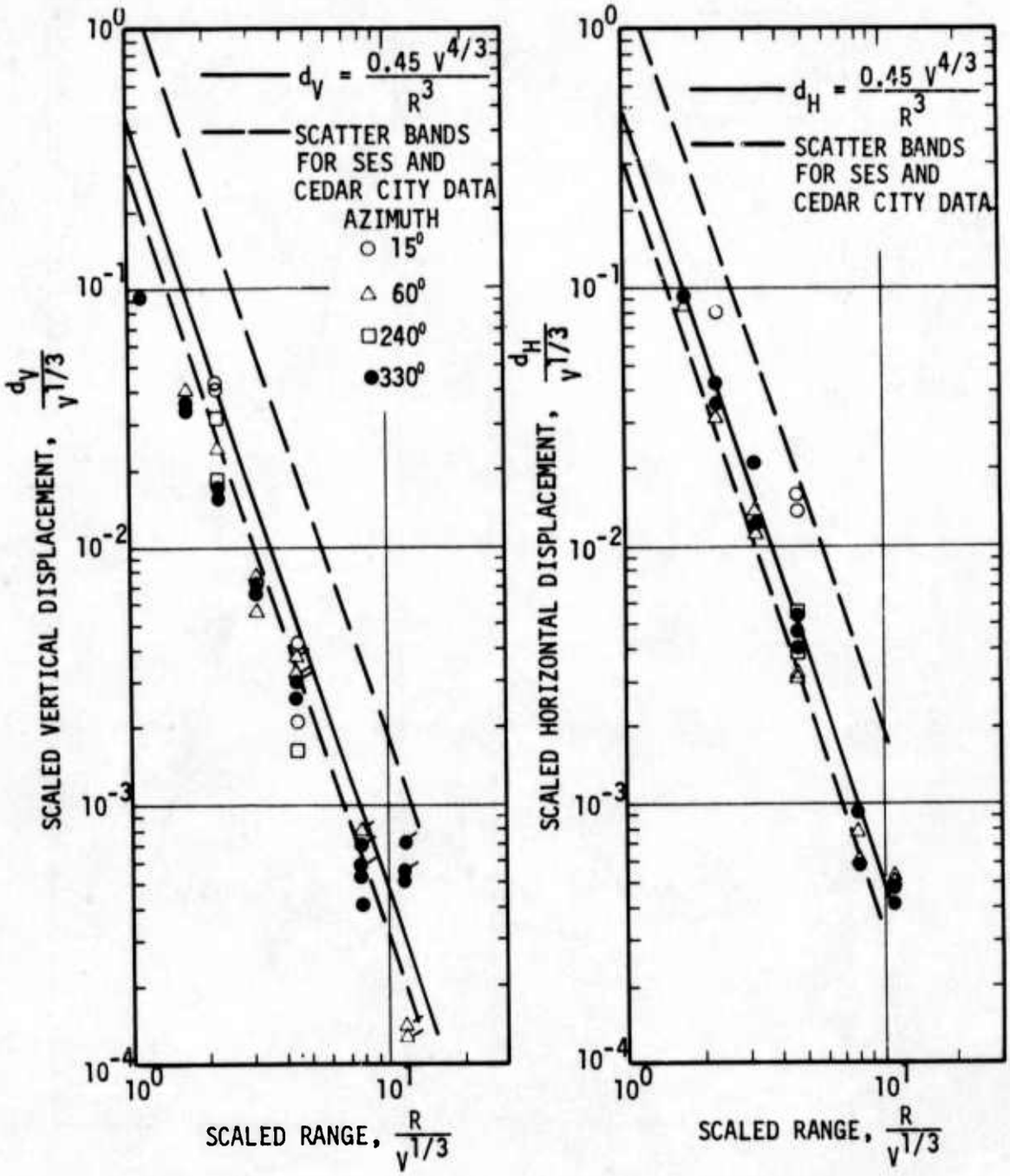

Figure 42. Crater Volume Scaled Peak Displacement Correlation for Top 0.1 $V^{1/3}$ for MIDDLE GUST IV (Cooper, Unpublished Data Analysis)

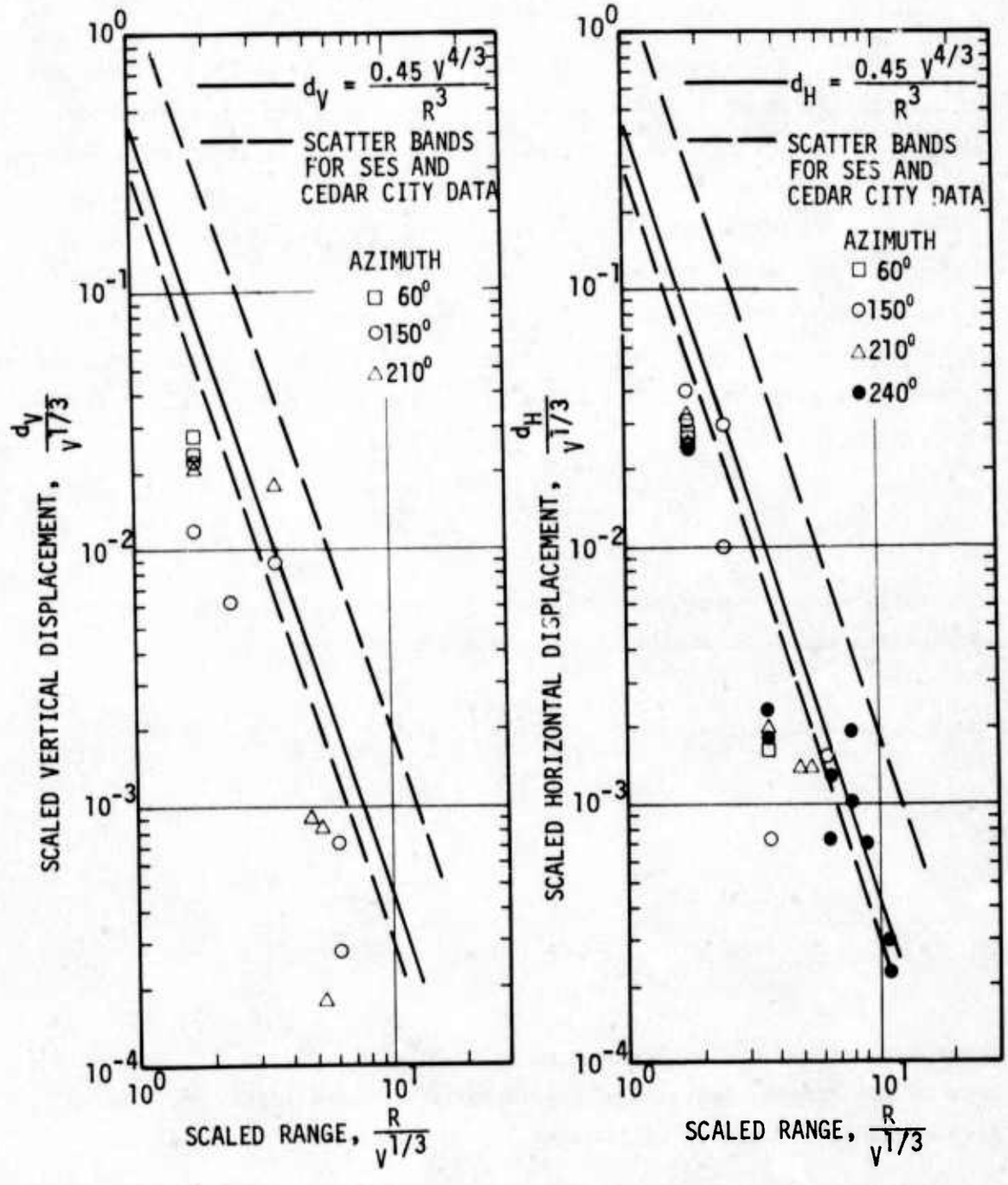

Figure 43. Crater Volume Scaled Peak Displacement Correlation for Top 0.1 $V^{1/3}$ for MIDDLE GUST III (Cooper, Unpublished Data Analysis)

The last term is analogous to the Froude Number used in fluid mechanics. In a report by Sauer (Reference 68), he indicated that crater-related motions are at least as well correlated with quarter-root of crater volume scaling as with cube root scaling. This would imply that gravitation effects are dominant and that the Froude type of scaling is applicable. However, a more extensive analysis of the data (Reference 69), including results of buried cratering bursts in alluvium and considering scaled depth effects, has led to a general acceptance of Cooper's cube root crater volume scaling for displacements which incorporates reciprocal R^3 attenuation: i.e.,

$$\frac{d}{V^{1/3}} = f\left[\frac{z}{V^{1/3}}, \frac{HOB}{V^{1/3}}\right]\frac{V}{R^3} \tag{30}$$

Applying the dimensional analysis to peak velocity results in two alternative forms for the scaling relationship, namely,

$$\frac{v}{C} = k\left[\frac{R}{V^{1/3}}, \frac{z}{V^{1/3}}, \frac{HOB}{V^{1/3}}, \frac{gV^{1/3}}{C^2}\right] \tag{31}$$

or

$$\frac{v}{\sqrt{gV^{1/3}}} = k\left[\frac{R}{V^{1/3}}, \frac{z}{V^{1/3}}, \frac{HOB}{V^{1/3}}, \frac{gV^{1/3}}{C^2}\right] \tag{32}$$

These expressions are equivalent since they merely differ by the square root of the Froude type of scaling parameter. Similarly, time-to-peak displacement, t_d, can be written as

$$\frac{Ct_d}{V^{1/3}} = q\left[\frac{R}{V^{1/3}}, \frac{z}{V^{1/3}}, \frac{HOB}{V^{1/3}}, \frac{gV^{1/3}}{c^2}\right] \quad (33)$$

or

$$t_d \sqrt{\frac{g}{V^{1/3}}} = q\left[\frac{R}{V^{1/3}}, \frac{z}{V^{1/3}}, \frac{HOB}{V^{1/3}}, \frac{gV^{1/3}}{c^2}\right] \quad (34)$$

For a consistent prediction technique, the scaling for peak velocity and time to peak displacement must be compatible with the peak displacement scaling.

The vertical and horizontal near-surface ($<0.1\ V^{1/3}$) velocity data for surface tangent events at SES are shown in Figure 44 (Reference 15), plotted against scaled range. No trend separates the 500-ton PRAIRIE FLAT and DIAL PACK data from the 100-ton DISTANT PLAIN 6 data. In addition, vertical velocities are about a factor of two higher than the horizontal velocities. This difference is possible due to the fact that the DI/CI motions are initially caused by a refracted wave which has a front directed primarily upward.

The Cedar City near-surface-tangent event velocity data are shown in Figure 45 along with the SES data scatter bands. The horizontal velocity is larger than the vertical for these events, fielded in the much stiffer medium.

In order to determine geological effects, it is useful to compare data for events with comparable explosive source and differing geological conditions. Figure 46 shows the velocity data for 100-ton surface tangent and near-surface-tangent events for conditions from soft soil to rock. The peak horizontal velocity for this charge configuration is not very dependent on geology, a trend also observed for air-slap-induced motions. Vertical velocities do depend on geology, being largest

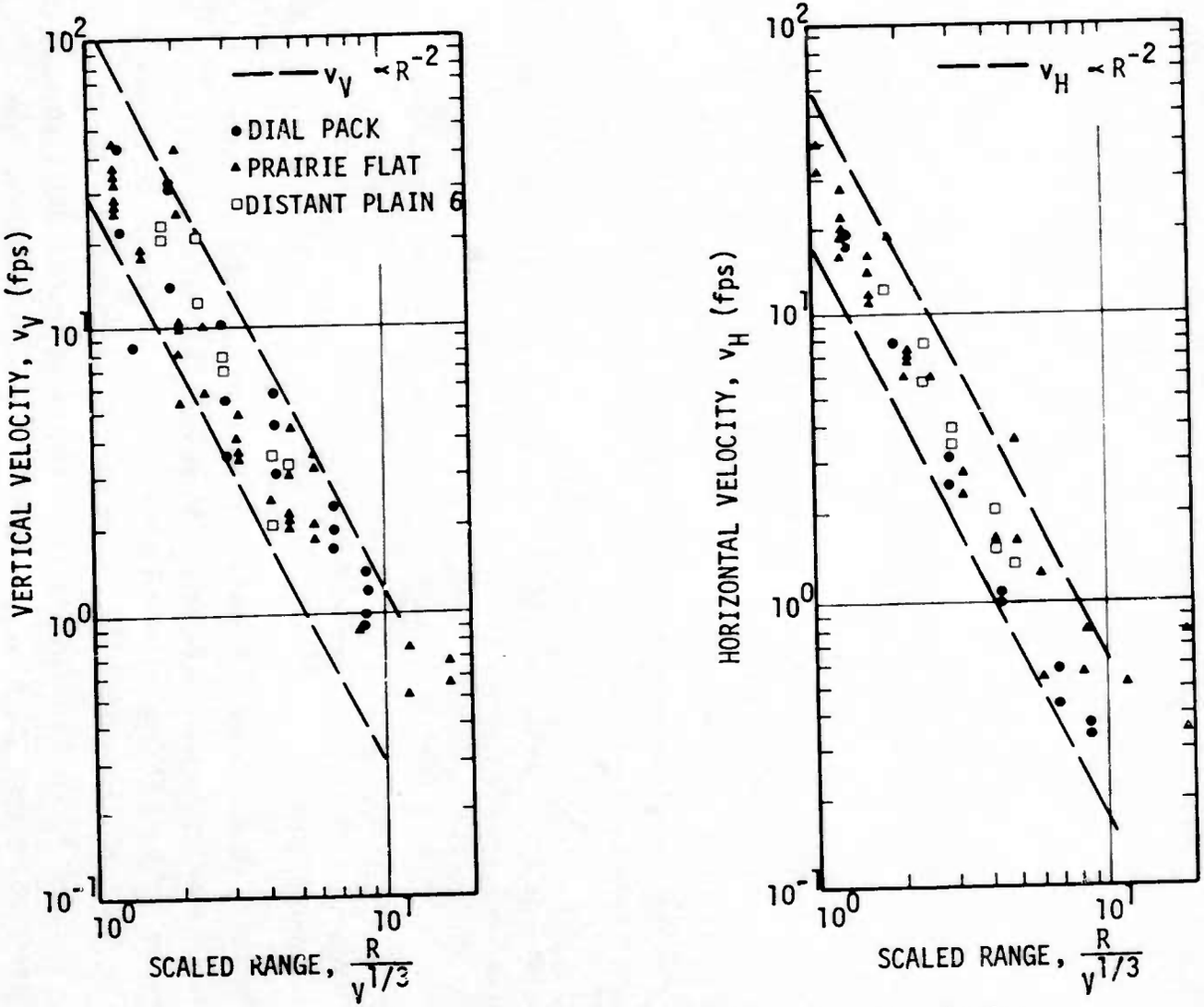

Figure 44. Peak Velocity Crater Volume Scaling Correlation for Surface Tangent SES Events (Reference 15)

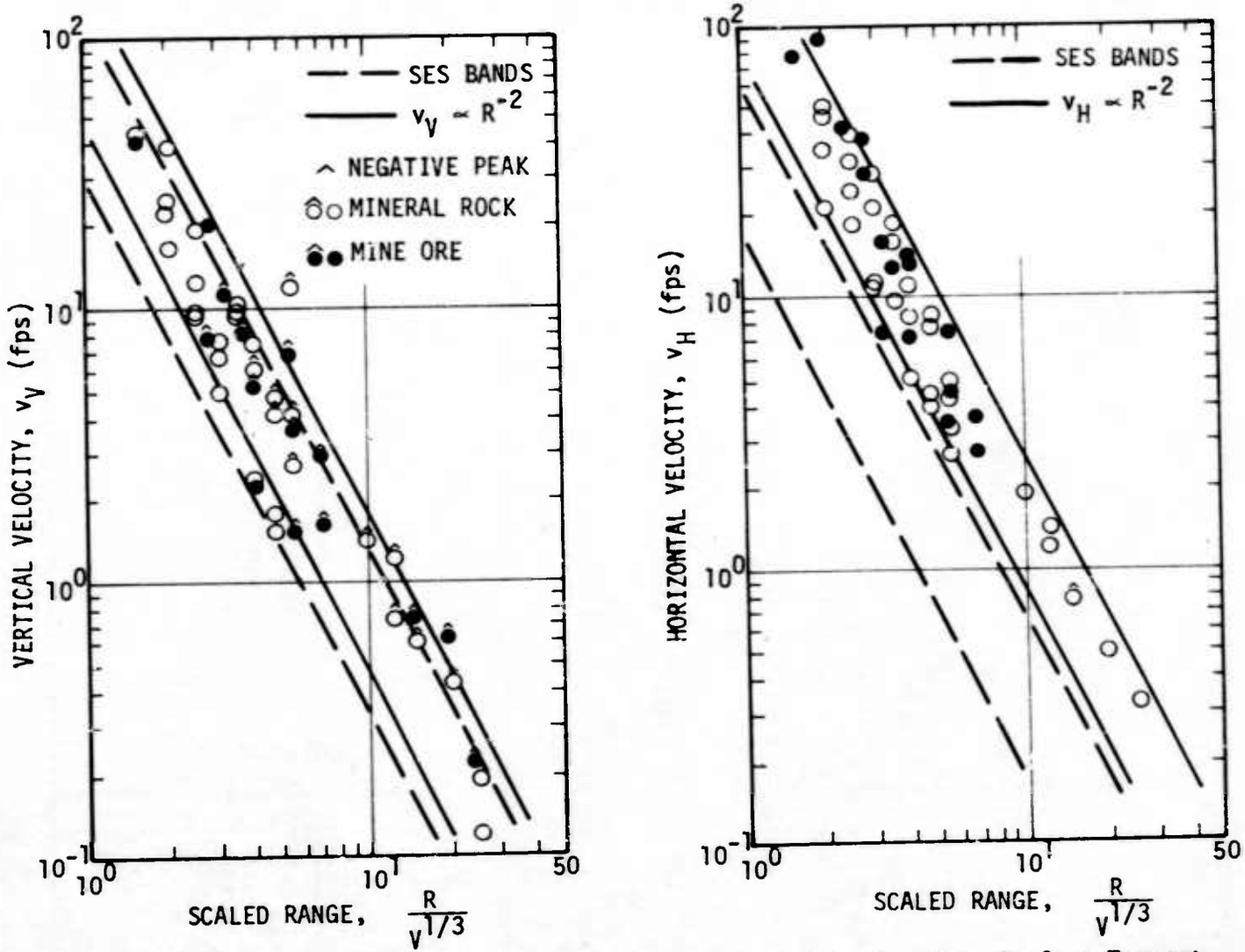

Figure 45. Velocity Crater Volume Scaling Correlation for Near-Surface Tangent Cedar City Events (Reference 15)

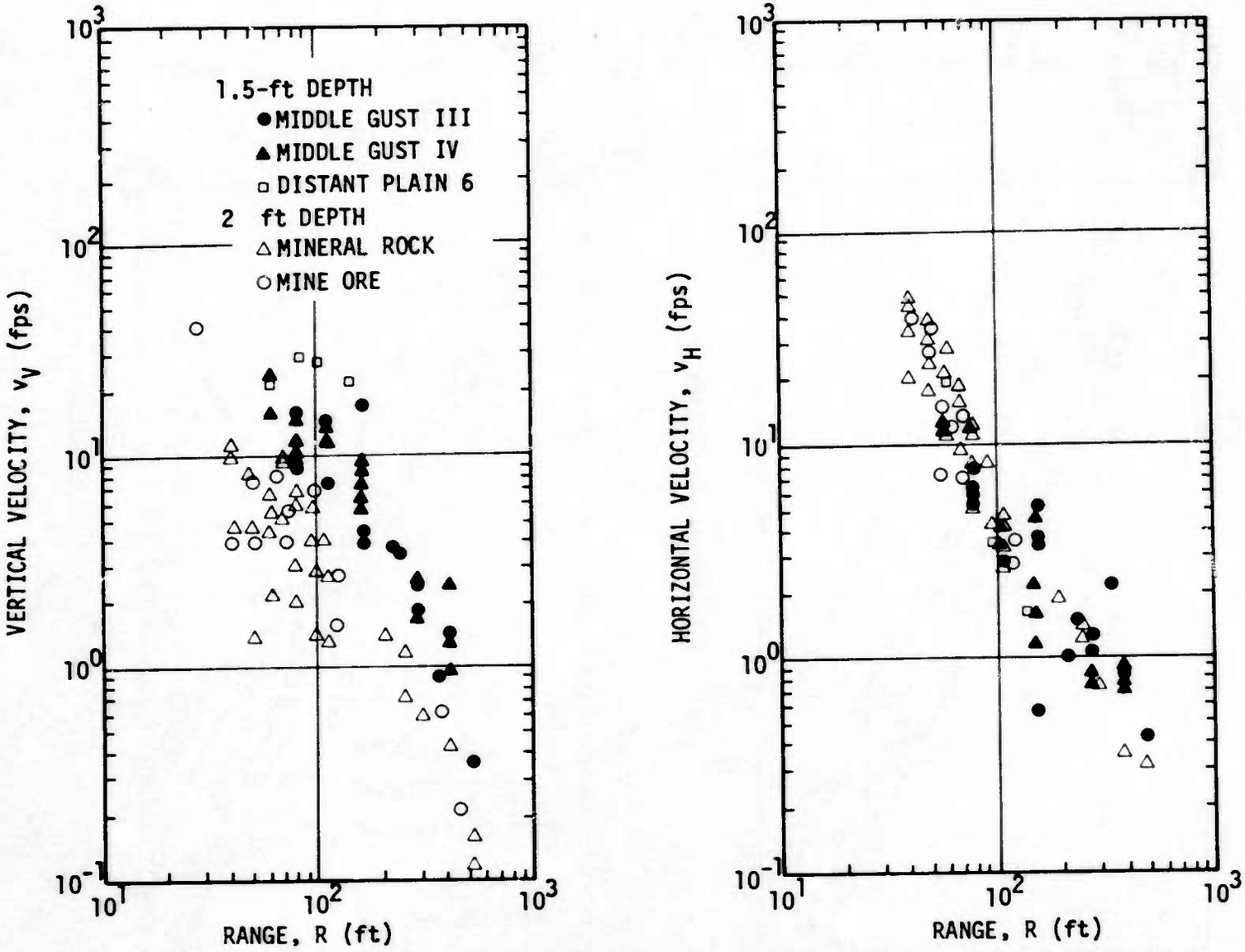

Figure 46. Near-Surface Peak Velocity Geology Sensitivity for "Surface Tangent" 100-ton High Explosive Events (Reference 29)

for the softest medium. The 20-ton half-buried events data (Figure 47) show horizontal velocities to be higher in the stiffer MIDDLE GUST sites. As the HOB decreases, this trend is expected since higher velocities have been observed in stiffer medium for fully buried detonations. However, the geological separation of the horizontal half-buried data is not large. The corresponding data for 1.0- and 0.9-diameter HOB 100-ton events are given in Figure 48.

Initial analyses of crater-related velocities for test site geologies considered the Equation (31) scaling, with the seismic velocity at the depth of interest used as the scaling parameter, and reasonable correlation was obtained. The alternate form of Equation (32) accounts for gravitational effects which were not significant for displacement response and are also expected to lack significance for the higher frequency peak velocity response.

The current Air Force design manual (Reference 7) uses an equivalent seismic velocity scaling of the form

$$\frac{v}{C_e} = 0.01 \frac{V^{2/3}}{R^2} \tag{35}$$

where C_e is the range divided by the seismic arrival time at the point of interest, which applies to near-surface detonations. The scatter bands of available data shown in the reference are about a factor of 4 up and down. For the DIA/VAS analysis, Equation (35) is used with C_e taken to be constant for the generic sites considered.

For a "uniform" medium cube-root crater volume scaling implies that the time to peak displacement, t_d, scales with the cube-root of crater volume for a given scaled range. However, PRE-MINE THROW IV vertical motion data for Events 5 (1000 lb) and 7 (256 lb) in Yucca Flat

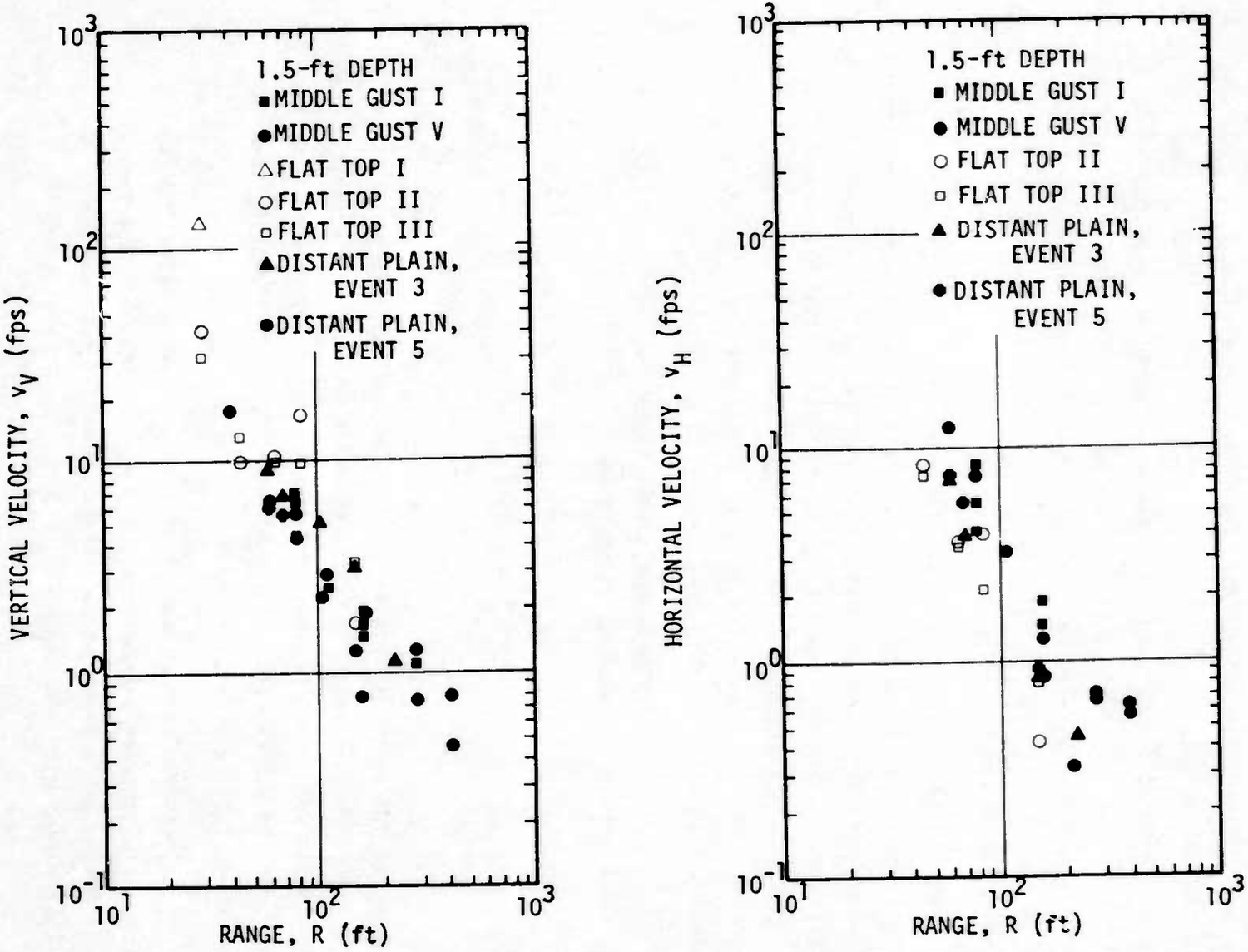

Figure 47. Near-Surface Peak Velocity Geology Sensitivity for Half-Buried 20-ton High Explosive Events (Reference 29)

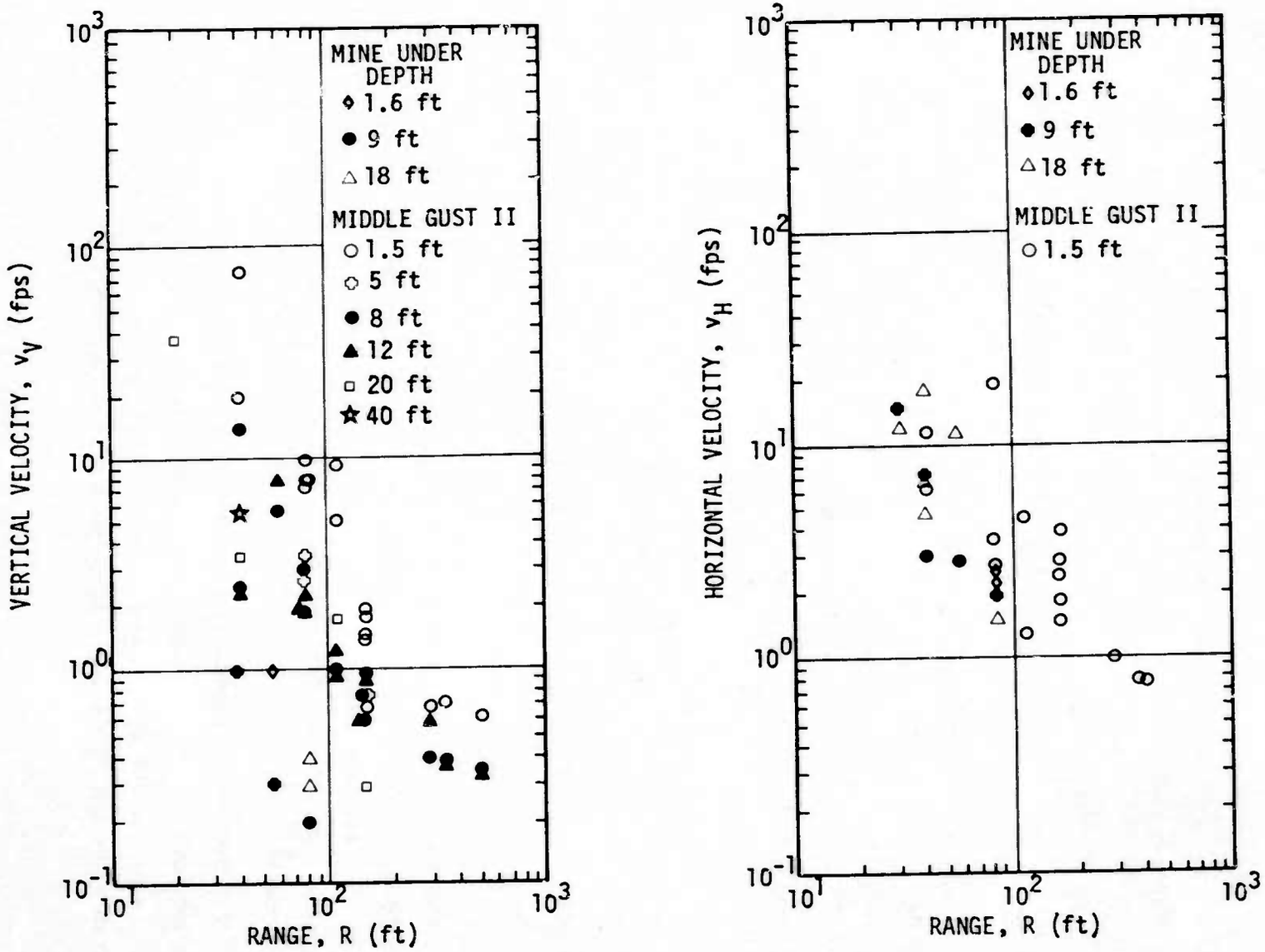

Figure 48. Peak Velocity Geology Sensitivity for "One-Diameter" HOB 100-ton High Explosive Events (Reference 29)

playa indicate that crater-related durations scale more like $W^{1/6}$ for the same cube-root yield scaled range (Reference 15). Thus consistency between scaling of d, v, and t_d has not been demonstrated and additional analysis of the available data base will be required as results of the PRE-MINE THROW IV scaling experiments become available. At this time, cube-root crater volume scaling is recommended.

The surface burst DI acceleration at a depth below ground zero equal to the range of interest is a conservative estimate of the DI/CI acceleration. On the basis of equivalent yield scaling of underground test data, the Air Force design manual (Reference 7) specifies this acceleration in the form

$$a = a_0 \left[\frac{W}{1\ MT}\right] \left[\frac{R}{1000\ ft}\right]^{-4} \tag{36}$$

where a_0 is 140 g's for hard rock, 25 g's for soft rock, and 5 g's for dry soil. The value for wet soil is between that for soft rock and dry soil.

The peak DI/CI accelerations, needed to construct ground shock waveforms, should not be critical to response of near-surface systems since they are significantly lower than those caused by the air slap. Therefore, these conservative expressions can be used for the DIA/VAS environments.

Few data exist regarding peak stresses associated with directly coupled effects. Stress gages have been placed in some high explosive test (e.g., MIDDLE GUST, PRAIRIE FLAT). However, these data are questionable for the DI/CI later time phase of the response.

The peak stress can be written in the form

$$\sigma = \rho C_{EQ} v \tag{37}$$

where ρC_{EQ} is the peak stress equivalent impedance. The peak particle velocity wave speed is a first-order estimate for C_{EQ}. For the PILEDRIVER event, the peak velocity wave speed was about 0.75 of the 19,000 fps seismic velocity (Reference 70).

If both velocity and stress measurements are obtained, then a direct determination of the equivalent impedance can be made. High quality data for both of these ground shock parameters were obtained in 50-lb calibration shots in dry clay for the design of the BLEST environment for the SAMSO HARD PAN series in Kansas. These data indicated a value of C_{EQ} of about half the seismic velocity. Thus, the peak DI/CI stress can be written in the form

$$\sigma = \gamma \rho C_i v \tag{38}$$

where C_i is the seismic velocity and γ is the ratio of the peak stress impedance to seismic impedance. A value for γ of 0.75 for the hard rock site and 0.5 for the other sites is used. Lower values can be obtained for cemented dry soils with high porosity.

The DI/CI ground shock parameter definition for the four generic sites is given in Table 9. The table gives best estimate peak values for displacements, velocities, accelerations, and stresses; and scaling with yield and range. Since scaled depths are within about 0.3 $W^{1/3}$ for most of the conditions considered in this study, no variation with depth is specified. The table also specifies 2σ uncertainty factor estimates.

TABLE 9. SURFACE BURST CLOSE-IN PEAK-DI/CI PARAMETERS

$$\text{Environment Value} = \left(\text{Reference Value}\right)\left(\frac{W}{1\ \text{MT}}\right)^{A}\left(\frac{1000\ \text{ft}}{R}\right)^{B}$$

ENVIRONMENT PARAMETER	REFERENCE VALUE				SCALING FACTORS		2σ UNCERTAINTY FACTOR
	Dry Soil	Wet Soil	Soft Rock	Hard Rock	A	B	
Crater Volume (10^6 ft^3)	50	170	40	30	1	0	1.8
Displacement (in)	100	510	75	50	4/3	3	3.5
Velocity (ips)	50	180	110	150	2/3	2	3.5
Acceleration (g's)	5	15	25	140	1	4	5
Stress (psi)	75	750	880	5000	2/3	2	4

4.2.3 Ground Roll Effects

Until quite recently, outrunning ground shock phenomenology has not received much systematic investigation. In the early 1960's, ground motion criteria for systems designed to survive overpressures of a few hundred pounds per square inch and higher were considered to be governed by the softest site conditions where the motion was generally superseismic. Detailed structural loading definition was not available nor required since very conservative structure design procedures were used. Hardened systems, designed for overpressures on the order of a few tens of pounds per square inch generally consisted of protruding structures, and the dynamic pressure effects would govern the design. However, SAFEGUARD and SITE DEFENSE systems, which have been designed for the outrunning region, are sensitive to ground shock. The development of these systems has spurred the study of outrunning ground shock.

Most of the more recent high explosive test events were fairly well instrumented in the outrunning region, where the ground roll response is the primary environment. An extensive review and analysis of these data has been performed for the SES and Cedar City events (References 46 and 71) and for the MIDDLE GUST and MIXED COMPANY events (Reference 71).

The primary source of nuclear data for outrunning motions is the TUMBLER 1 HOB event at NTS. Sauer (Reference 2) developed a vertical outrunning waveform definition based on the TUMBLER 1 integrated accelerometer records (Figure 49). These data are about the only purely airblast-induced outrunning records available, since all the high explosive event data exhibiting outrunning phenomenology also contain significant direct-induced effects.

Data in the region of interest were also obtained for the near-surface-burst IVY MIKE event in EPG. The integrated accelerometer records (Reference 38) for stations at 18,300 ft range ($\sim$14 psi) and 21,300 ft

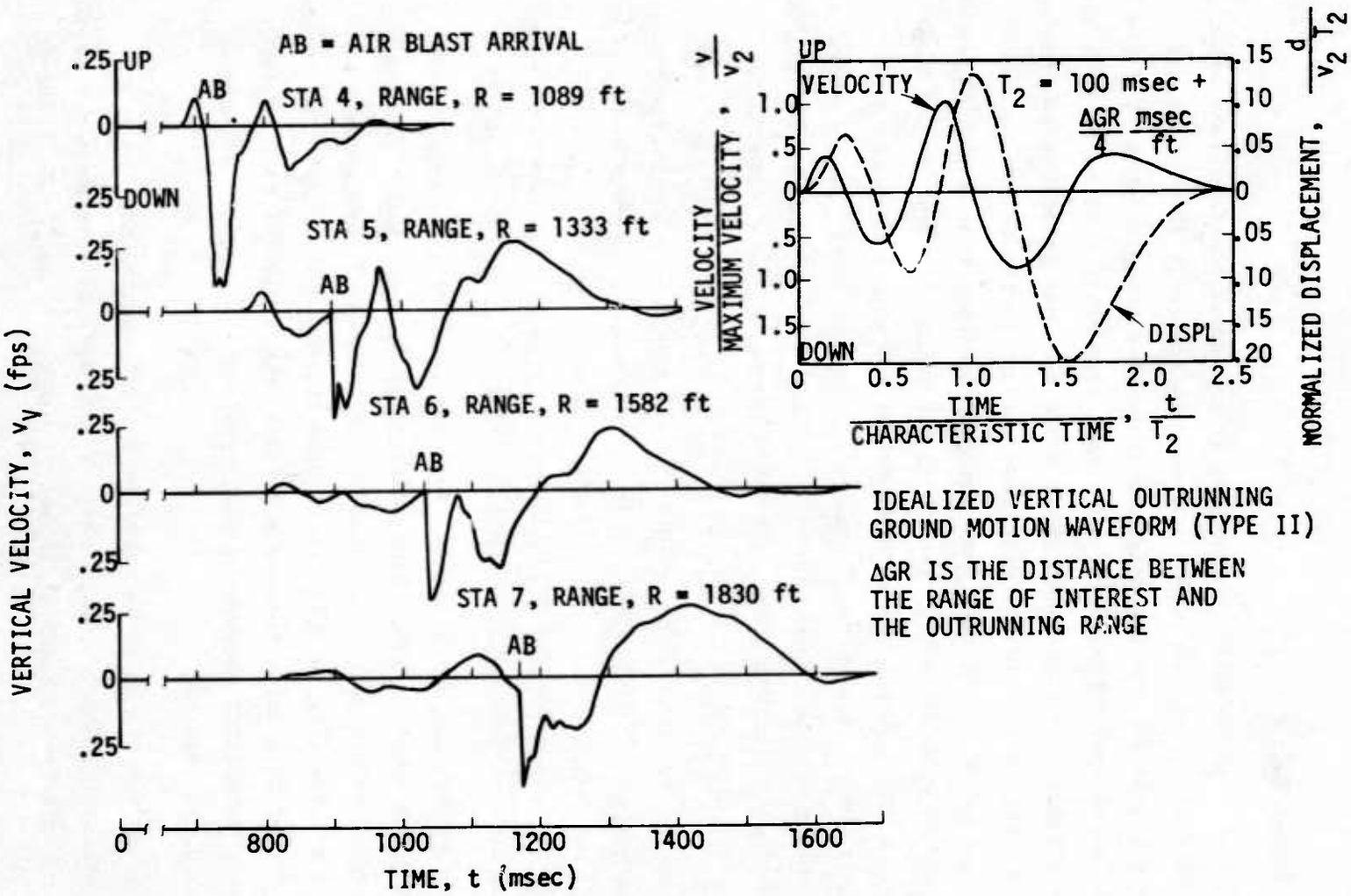

Figure 49. TUMBLER 1 Vertical Velocity Data and Idealized Outrunning Waveform (Reference 2)

range (∿12 psi) are shown in Figure 50. These stations are located on different atolls, quite distant from one another. Since the outrunning range for EPG (2000 to 4000 ft/$MT^{1/3}$) is about one-half that for NTS playa, the 10-psi IVY MIKE ground roll motions are more fully developed than the TUMBLER 1 motions for the same overpressure.

In Reference 46, Hadala presents results of calculations for the TUMBLER 1 event. Since there is uncertainty in the Frenchman Flat seismic velocity for the material between the 240 and 590-ft depths, different calculations were performed with nonlinear material properties consistent with the seismic velocity uncertainty band. Reasonable correlation was obtained for the stiffer site model. The test/analysis comparison shown in Figure 51 represents the first demonstration of the capability to compute outrunning motions.

Hadala also performed calculations for the SES ground shock response to a 500-ton high explosive air blast loading, for comparison with PRAIRIE FLAT and DIAL PACK data. The direct-induced response was investigated parametrically by considering high stress, short duration, loading near ground zero. These studies indicated that the horizontal, but not vertical, response in the outrunning region is very sensitive to the close-in boundary conditions. A number of calculations were performed, however, good test/analysis correlation was not obtained.

As previously discussed, reasonable test/analysis correlation has been obtained for the air slap response for PRAIRIE FLAT for a WES soil model. The lack of correlation for the Reference 46 study might be attributed to the fact that the basic soil property test data are developed for stress path histories that are more related to air slap loading. However, the capability to perform adequate calculations of ground shock response due to the direct high explosive coupling with the medium does not exist. Calculations have been performed for other test sites with reasonable crater results being obtained for some cases (e.g., MIXED

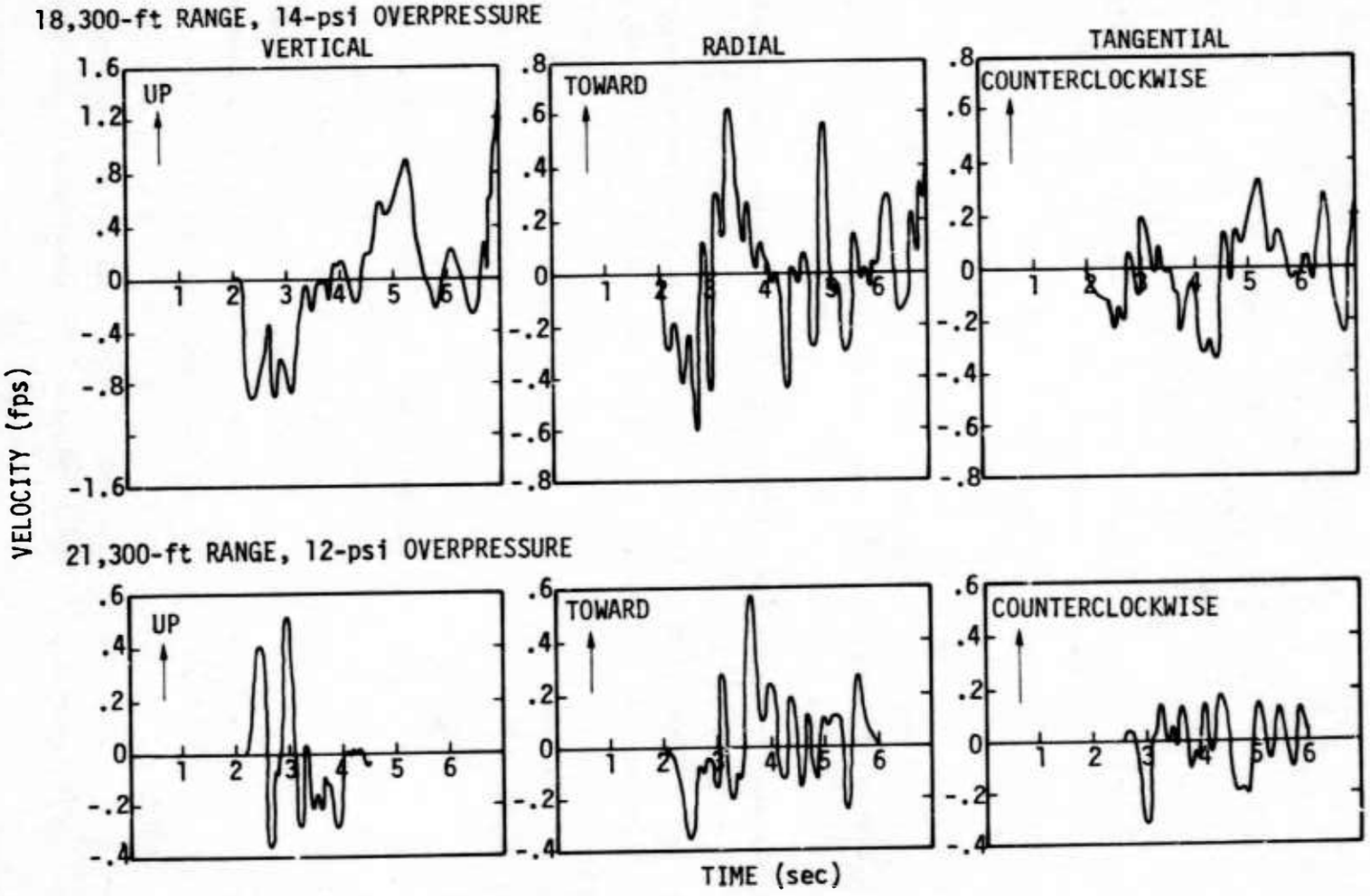

Figure 50. IVY MIKE Vertical Velocity Outrunning Waveforms (Reference 38)

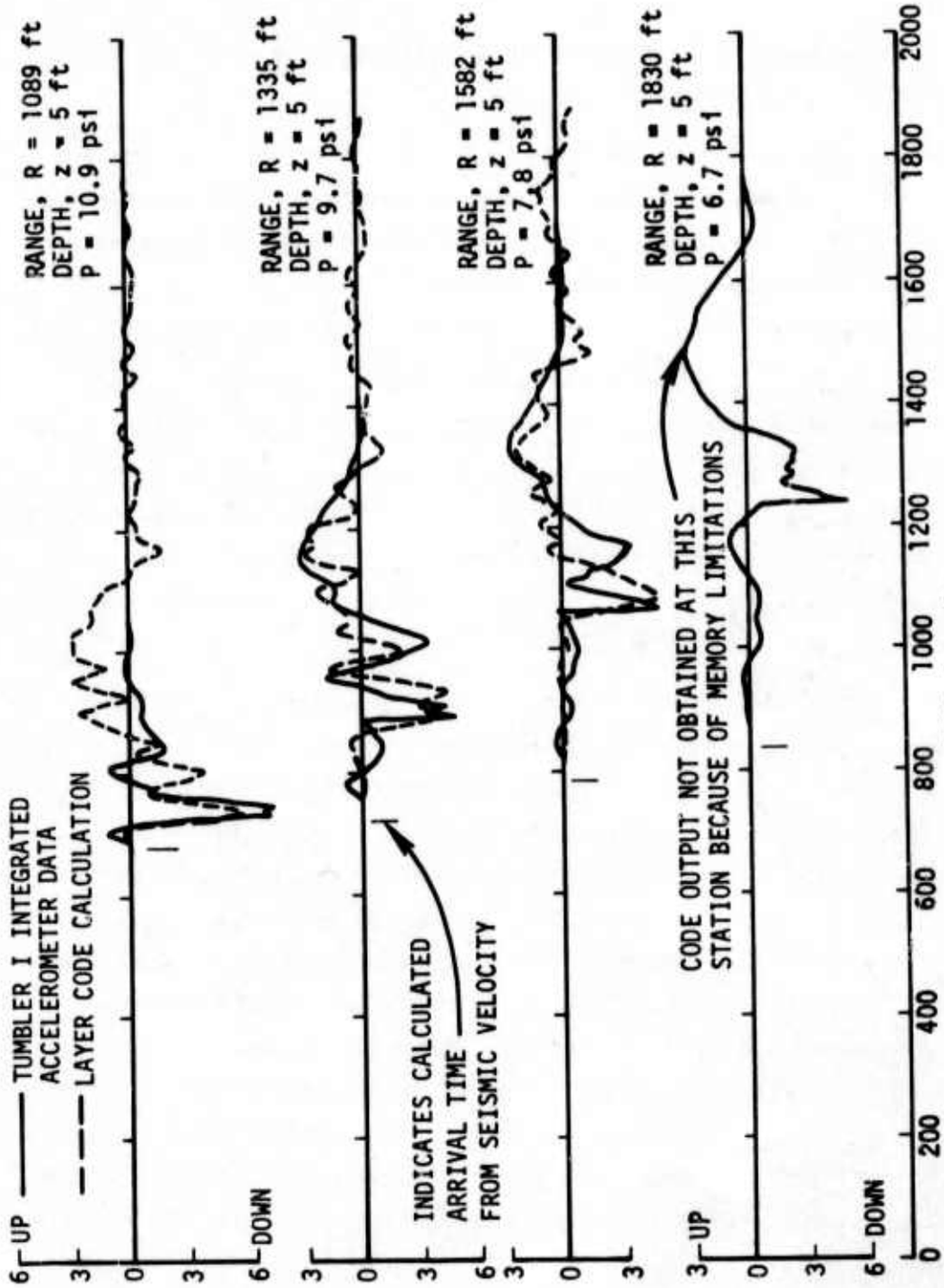

Figure 51. TUMBLER 1 Vertical Test/Analysis Waveform Comparison (Reference 46)

COMPANY, Reference 56). However, the ground shock response does not agree with data for these calculations.

Analysis of data from the high explosive events suffers from the difficulty of separating AI ground roll effects from DI/CI ground roll effects. Separation is particularly important if scaling techniques to predict nuclear motions are to be developed from the data, since source coupling effects are significantly enhanced in the high explosive tests.

As previously discussed, the initial response in the outrunning region, for layered media, is usually associated with a refracted wave caused by upstream air blast sources. However, for relatively homogeneous media, outrunning occurs when the air blast slows down below the ground shock speed and the initial response is associated with a near-surface wave path. In both cases, the initial motion is upward and outward.

Analysis of the initial upward vertical velocity (v_1) for high explosive events at SES, MIDDLE GUST, MIXED COMPANY, and Cedar City indicated the data to correlate best with cube root of yield scaling of range (Reference 71). The reference shows the specific data points for the individual events which indicate scatter bands varying from a factor of about 1.5 up and down for MIDDLE GUST II and III to a factor of about 2.5 for MIXED COMPANY 2 and 3. Separating near-surface from deeper gage data did not help reduce the scatter. The DISTANT PLAIN 6 100-ton-event data were significantly lower than the 500-ton SES events and were not included in the best fit. However, the scatter bands for MIXED COMPANY contained most of the DISTANT PLAIN 6 data. The initial peak decay with range varies from $R^{-1.5}$ to $R^{-1.65}$. Higgins and Schreyer indicate that an $R^{-1.5}$ decay is representative of most of the data. Figure 52 shows the Reference 71 fits to the data.

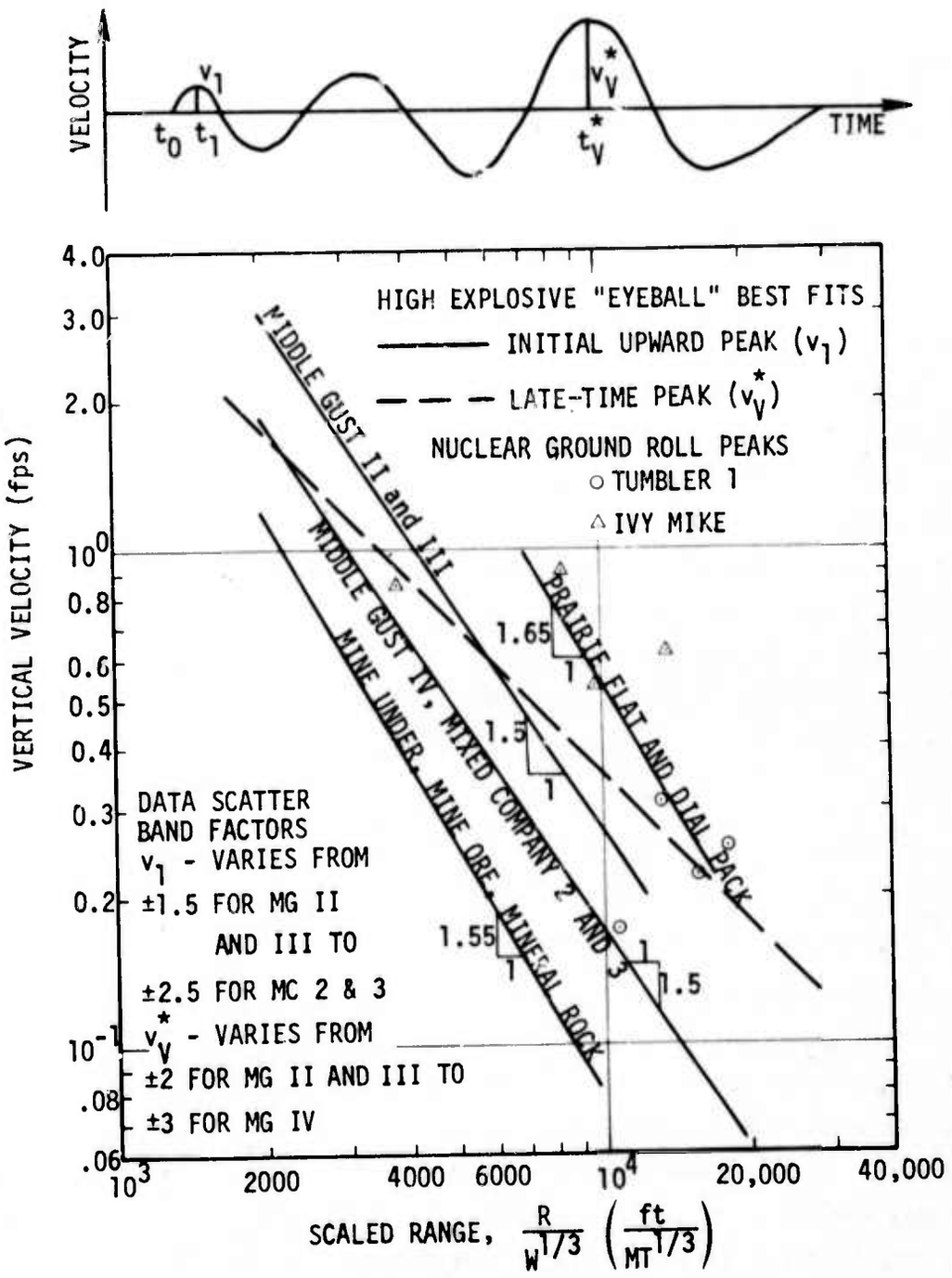

Figure 52. High Explosive Outrunning Vertical Velocity Peak Attenuation and Nuclear Data Comparison (Reference 71)

For the layered sites, the initial peak velocity is approximately proportional to the propagation velocity (phase velocity) of outrunning motions. These phase velocities (Reference 71) are about 11,000 fps for the MIDDLE GUST wet site; 10,500 to 13,500 fps for the MIXED COMPANY site; and 5,500 fps for the SES site.

The initial peak velocities for the Cedar City events are significantly below the MIXED COMPANY and MIDDLE GUST data even though the outrunning propagation velocities are comparable. The Cedar City site is a fairly homogeneous medium with outrunning being initiated at the surface. Therefore, the initial peak upward velocity may not be as large as if it were due to a refracted wave whose wave front normal is more vertical. The jointing of the medium at Cedar City resulted in direction-dependent wave speeds of 8800 fps for propagation perpendicular to the jointing and 11,000 fps in the parallel direction. The direction of propagation did not appear to significantly affect the initial peak vertical velocity; however, the horizontal response exhibited propagation direction-associated differences.

Additional analysis of vertical refracted wave velocity peaks for MIDDLE GUST is presented in Reference 72. This analysis indicates that the velocities normalized to a layer impedance factor correlate well with wave path length for a given event.

Representative wave forms for the MIDDLE GUST, MIXED COMPANY, and Cedar City sites for the outrunning region are shown in Figure 53. For these relatively stiff sites, the peak vertical velocity generally occurred after the first cycle of motion. For the SES events, the late-time vertical oscillatory peaks were generally less than the initial peak for stations above 10 psi. The motion for this softer site contained more cycles, with the predominant frequency decreasing with time on account of the dispersive effects.

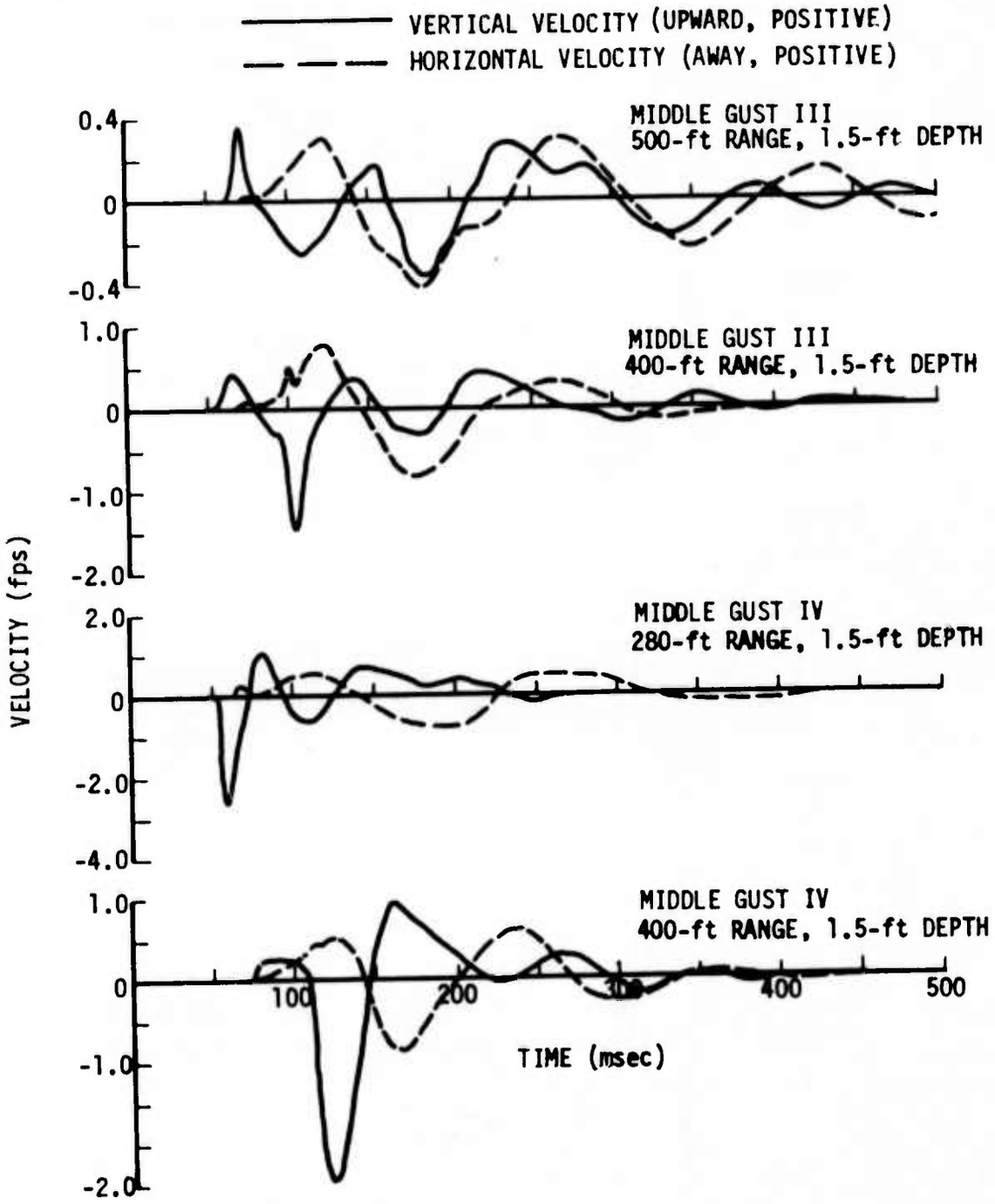

Figure 53. High Explosive Event Waveforms for Outrunning Region (Continued)

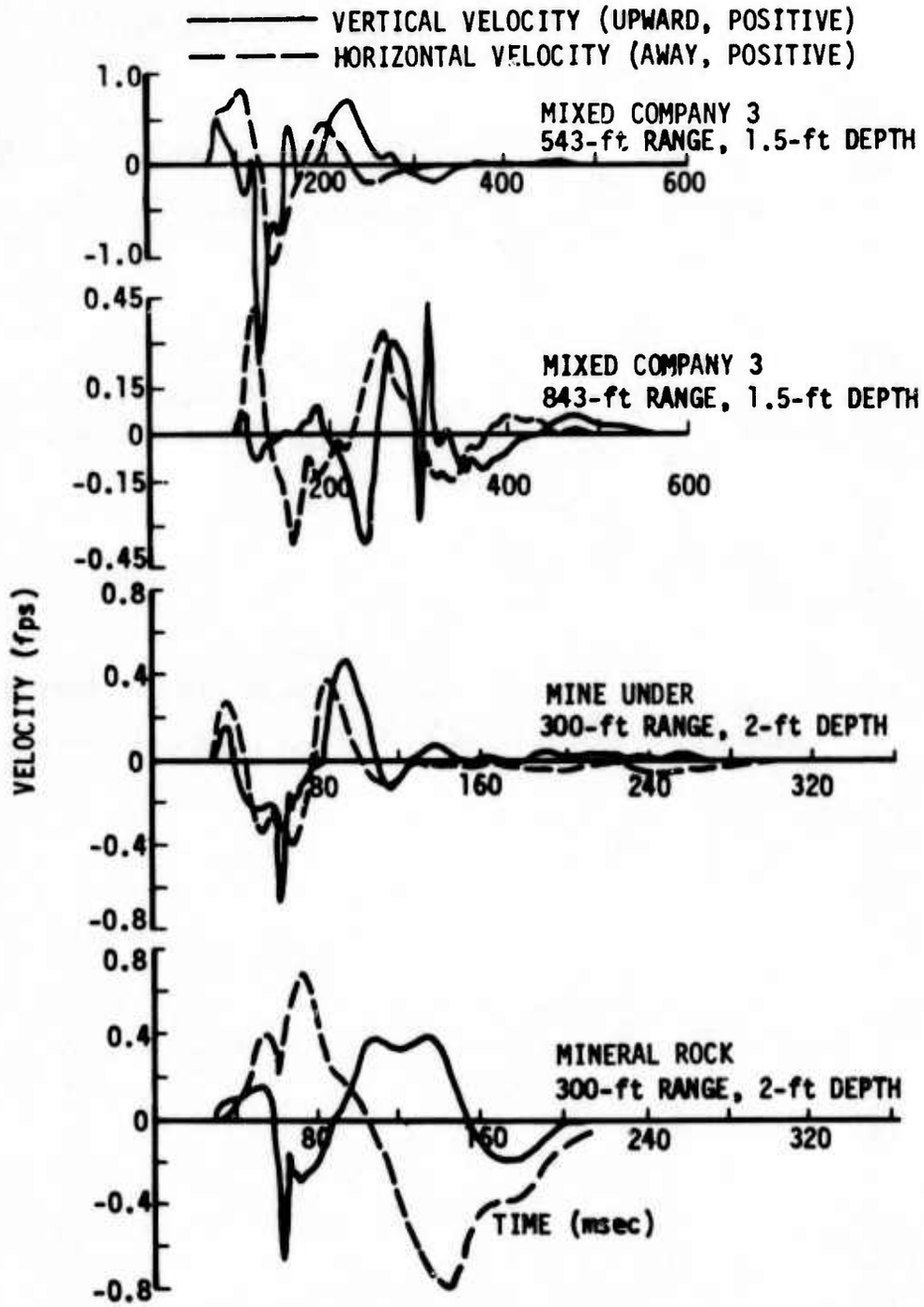

Figure 53. High Explosive Event Waveforms for Outrunning Region (Concluded)

The analysis of Reference 71 indicates that the late-time peak ground roll velocities were not very geology dependent. A fit to these data is also shown in Figure 52. The late-time peak vertical velocities attenuate slightly faster than R^{-1} and the data scatter varies from a factor of about 2 up and down for MIDDLE GUST II and III to a factor of about 3 for MIDDLE GUST IV and the Cedar City events, as discussed in the reference. A comparison of data for approximately surface tangent and one-diameter HOB conditions at the MIDDLE GUST wet site (Event II and III) with the Cedar City (MINE UNDER and MINE ORE or MINERAL ROCK) site did not show a significant HOB dependence for the vertical response at a given test site.

For completeness, peak ground roll vertical velocities for the TUMBLER 1 and IVY MIKE nuclear events are also shown in Figure 52. No equivalent yield adjustments have been made to account for differences between nuclear and high explosive efficiencies. The TUMBLER 1 data agree with the high explosive ground roll data. The IVY MIKE data are higher and are comparable to the SES initial upward vertical peaks.

The horizontal ground roll response is more complex than the vertical and has not been analyzed quite as extensively in Reference 71. The horizontal ground roll velocity response at MIDDLE GUST III was more severe and more rapidly attenuating than the corresponding response at MIDDLE GUST II, indicating a probable HOB effect associated with the close-in coupling for this motion component. A similar behavior was also observed for the Cedar City events.

The analysis of the high explosive data in Reference 71 considers only the peak velocity, which generally occurred on the initial pulse rather than both the initial and late time peaks. The analyses of both Reference 71 and 46 indicate that the initial peak horizontal velocity in

the outrunning region is due to both AI and DI effects; therefore, it would have an HOB dependence.

At the maximum scaled range of interest in the study, about 10^4 ft/$MT^{1/3}$, the peak horizontal velocities for all events are on the order of 0.3 fps except for the 0.9 diameter HOB MINE UNDER event which was about a factor of two lower. The horizontal and vertical late time peak velocities are about equal for this maximum scaled range with the primary differences between the two components occurring in the initial peaks. Additional analysis of the horizontal velocity data should be performed to determine the geology and HOB effects on both the initial and the late time peaks. The maximum horizontal velocity decayed with range ($R^{-1.4}$ to $R^{-2.0}$ for various events) more steeply than the initial vertical velocity ($R^{-1.5}$ to $R^{-1.65}$ for various events) possibly because the faster attenuating DI effects had more influence on the horizontal. It would be significant to determine whether the horizontal late-time peak velocities scale approximately according to R^{-1} as do the vertical.

In comparing the test data waveforms in Figure 53, one sees that the Sauer Type II waveform is representative. Even though it is apparent that the initial and late-time peaks scale differently, the understanding of ground shock phenomenology in the outrunning region has not reached the point where this difference has been implemented in a prediction technique. In this analysis, the peak outrunning velocity will be taken to decay with range as $R^{-1.5}$ and the Sauer waveform will be used. However, it seems that more detailed analysis of the presently available data could result in a prediction technique that considers the scaling difference between the initial and the late-time peaks.

On the basis of the available data shown in Figure 52, the ground roll peak velocity for dry and wet soils is taken as

$$v = 0.5 \text{ fps} \left[\frac{R}{W^{1/3}} \frac{MT^{1/3}}{10^4 \text{ ft}} \right]^{-1.5} \tag{39}$$

A velocity coefficient of 0.2 fps is used for the rock sites.

Peak displacement data for the outrunning region for NTS events are analyzed in Reference 73. The analysis indicates that the displacements shown in Figure 54 follow $W^{1/3}$ scaling. In the outrunning region data for air bursts, surface contact bursts, and optimum depth-of-burial bursts all attenuated as R^{-1}. The air burst data are about a factor of 1.8 lower than the surface contact burst data, with the depth-of-burial burst data a factor of 2.6 higher. Thus, in each of these cases the phenomenology should be similar since the attenuation rates are the same, the primary difference being the amount of energy causing the motions. For surface contact bursts, the peak outrunning displacement is given by

$$\frac{d}{W^{1/3}} = 1.3 \frac{\text{in.}}{MT^{1/3}} \left[\frac{R}{W^{1/3}} \frac{MT^{1/3}}{10^4 \text{ ft}} \right]^{-1.0} \tag{40}$$

with slightly higher motions expected for surface burst conditions. Since the Sauer outrunning waveform has approximately an equivalent period of

$$T \sim 5 \frac{d}{v} \tag{41}$$

we have

$$\frac{T}{W^{1/3}} = 1.1 \frac{\text{sec}}{MT^{1/3}} \left[\frac{R}{W^{1/3}} \frac{MT^{1/3}}{10^4 \text{ ft}} \right]^{0.5} \tag{42}$$

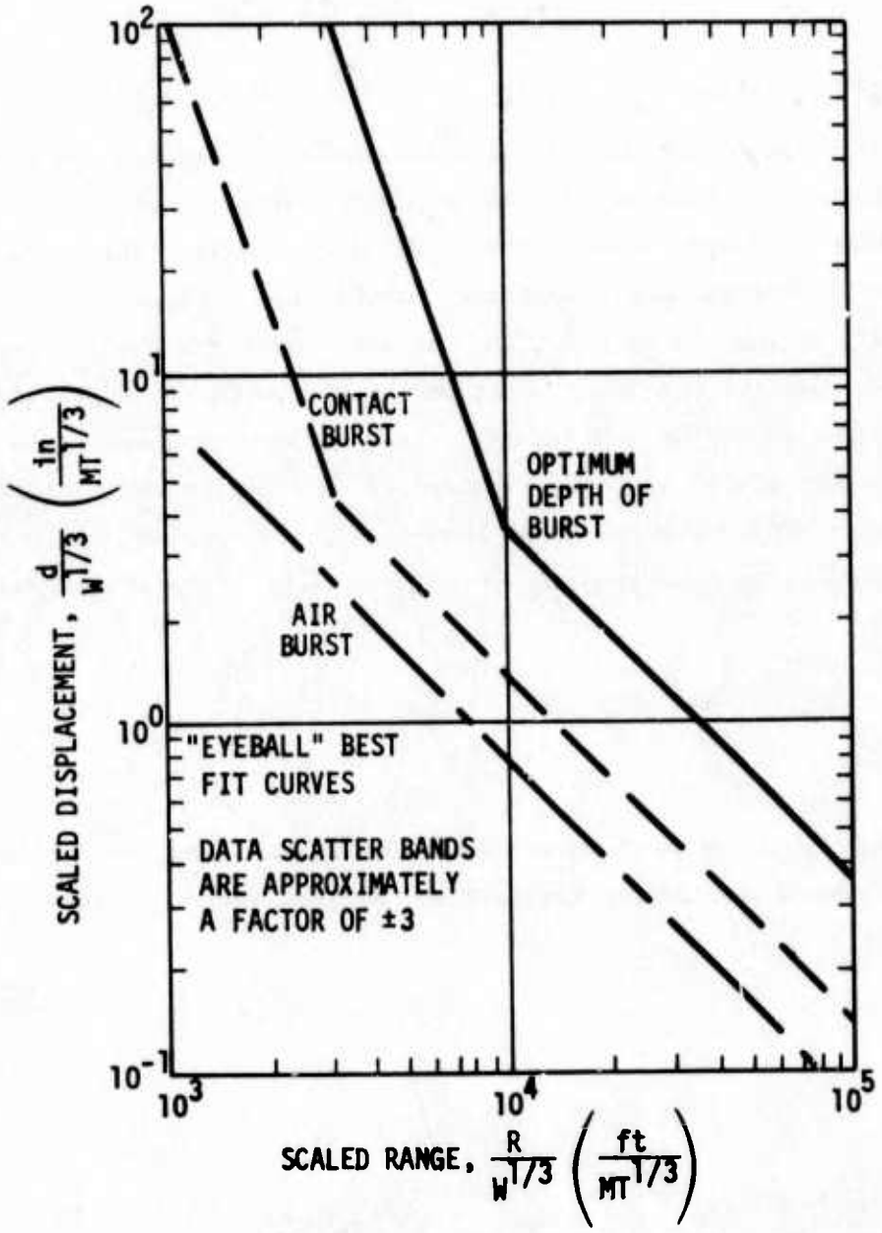

Figure 54. HOB Effects on Outrunning Peak Vertical Displacements for NTS Events (Reference 73)

This expression results in a period of 0.11 sec for 1-kT (TUMBLER 1) and 0.09 sec for 500 tons at the 10 psi station. The PRAIRIE FLAT and DIAL PACK events had periods of approximately the latter value but also had very late time motions with periods on the order of 0.5 sec. The peak displacements for these SES events decay as R^{-3} for $R/V^{1/3}$ out to nearly 20; therefore, the low frequency outrunning phenomenology for the high explosive events at SES is different from the nuclear NTS events. The predominant TUMBLER 1 period was about one and one-half times greater than that obtained from this equation.

Tests at the MIXED COMPANY site for events of 0.5 ton to 500 tons have shown periods that approximately scale by the cube root of yield at a given scaled range. However, other studies have indicated that the period scales according to the sixth or eighth power of the yield for for the outrunning region of interest.

The outrunning response modes are a function of the geological layering and shear wave velocities. However, those modes which are excited are governed by the applied loading characteristic periods which scale as the one-third power of yield. Thus if geological layering considerations are important, the periods should scale less than the one-third power of yield and the scaling implied by Equation (42) should be considered to have significant uncertainty. Correspondingly, peak displacements in the ground-roll-dominated region also have significant uncertainty.

The ground-roll-displacement scaling is of the form

$$\frac{d}{W^{1/3}} = \mu \left[\frac{R}{W^{1/3}} \; \frac{MT^{1/3}}{10^4 \text{ ft}} \right]^{-1} \tag{43}$$

and only distinction between soil and rock sites is made in the value of μ. On the basis of the analysis of the NTS data, the value of μ is taken as 1.5 in./$MT^{1/3}$ for surface bursts for the dry soil site. The high

explosive data indicate that the response frequencies are on the same order for the dry soil sites as for the soft rock sites. Therefore, the same ratio of velocity to displacement will be maintained for all sites, resulting in a value for μ of 0.6 in/$MT^{1/3}$ for the soft and hard rock sites, and 1.5 in./$MT^{1/3}$ for the wet soil site.

The DIA/VAS ground roll motion predictions for the four generic sites are given in Table 10. Again 2σ uncertainty factor estimates are also specified.

4.2.4 Waveforms and Shock Spectra

The 1-MT peak air slap, DI/CI and ground roll displacements and velocities are shown for the four generic sites in Figures 55 through 58. Cooper (Reference 15) indicates that the transition region should occur at a range of about $5V^{1/3}$, which is approximately where the vertical close-in DI/CI and the far-out ground roll dry soil displacements are equal in this analysis. For other conditions, the displacement crossover is farther out, as can be seen in the figures. In this study, the DI/CI displacements are considered applicable out to the region where the ground roll dominates. Both DI/CI and ground roll effects are derived from the same data base; therefore, the maximum horizontal or vertical upward displacement should not exceed the larger of the two components in the transition region.

However, a consistent theory has not been developed to synthesize waveforms from these components so that a continuous variation of waveform with ground range can be defined. To develop waveforms for a given weapon yield and range from ground zero, simplified waveforms were developed for each motion component. Waveform equations for peak acceleration, velocity, and displacement have been previously developed by TRW for application to hardened facilities analysis. These waveforms (Figure 59) do not exhibit all of the features of data but are representative. They have been used to construct near-surface vertical and

TABLE 10. SURFACE BURST PEAK GROUND ROLL PARAMETERS

$$\text{Environment Value} = \left(\text{Reference Value}\right)\left(\frac{W}{1\ \text{MT}}\right)^{A}\left(\frac{10{,}000\ \text{ft}}{R}\right)^{B}$$

PREDICTION PARAMETER	ENVIRONMENT PARAMETER	GENERIC SITE				SCALING FACTORS	
		Dry Soil	Wet Soil	Soft Rock	Hard Rock	A	B
REFERENCE VALUE	Displacement (in)	1.5	1.5	0.6	0.6	2/3	1
	Velocity (ips)	6.0	6.0	2.4	2.4	1/2	3/2
2σ UNCERTAINTY FACTOR	Displacement	3.5	4.0	5.0	5.0	–	–
	Velocity	3.5	3.5	4.0	4.0	–	–

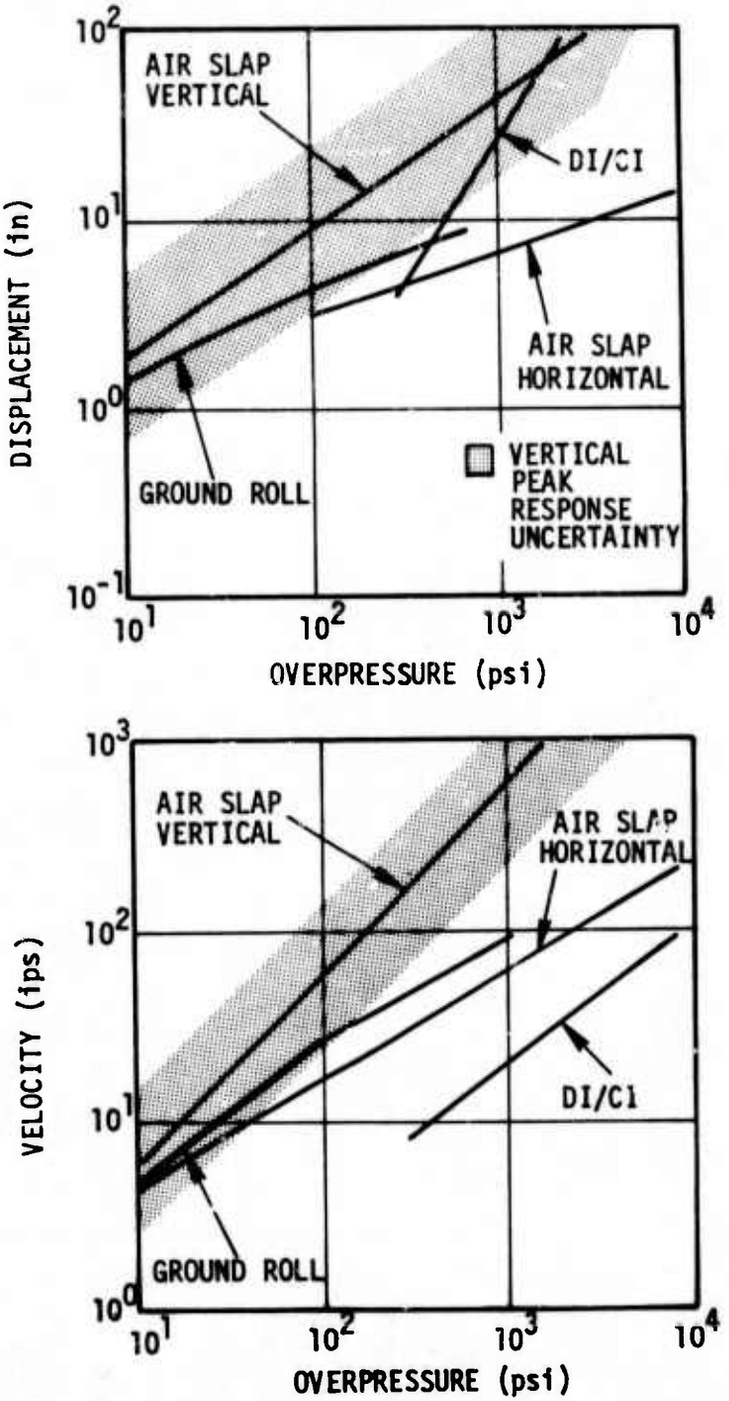

Figure 55. Dry Soil 1-MT Surface Burst
Near-Surface Motion Peak Values

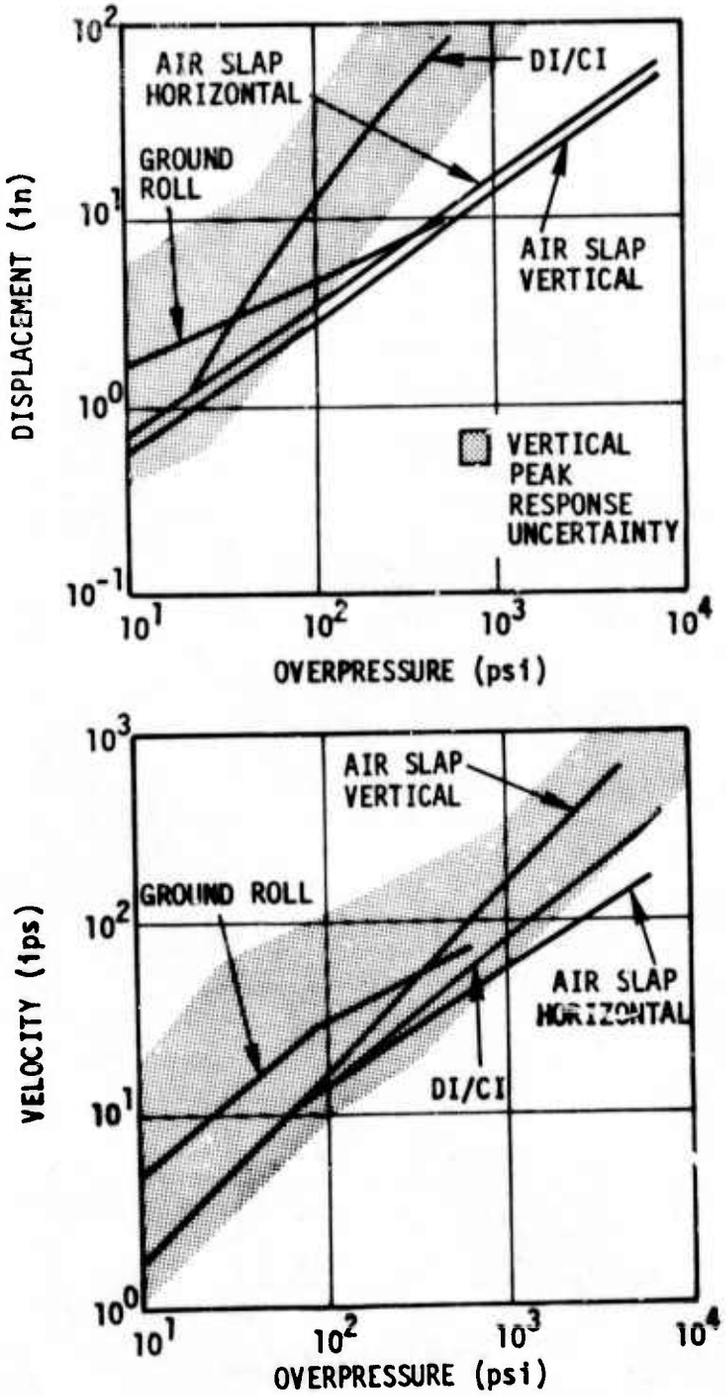

Figure 56. Wet Soil 1-MT Surface Burst
Near-Surface Motion Peak Values

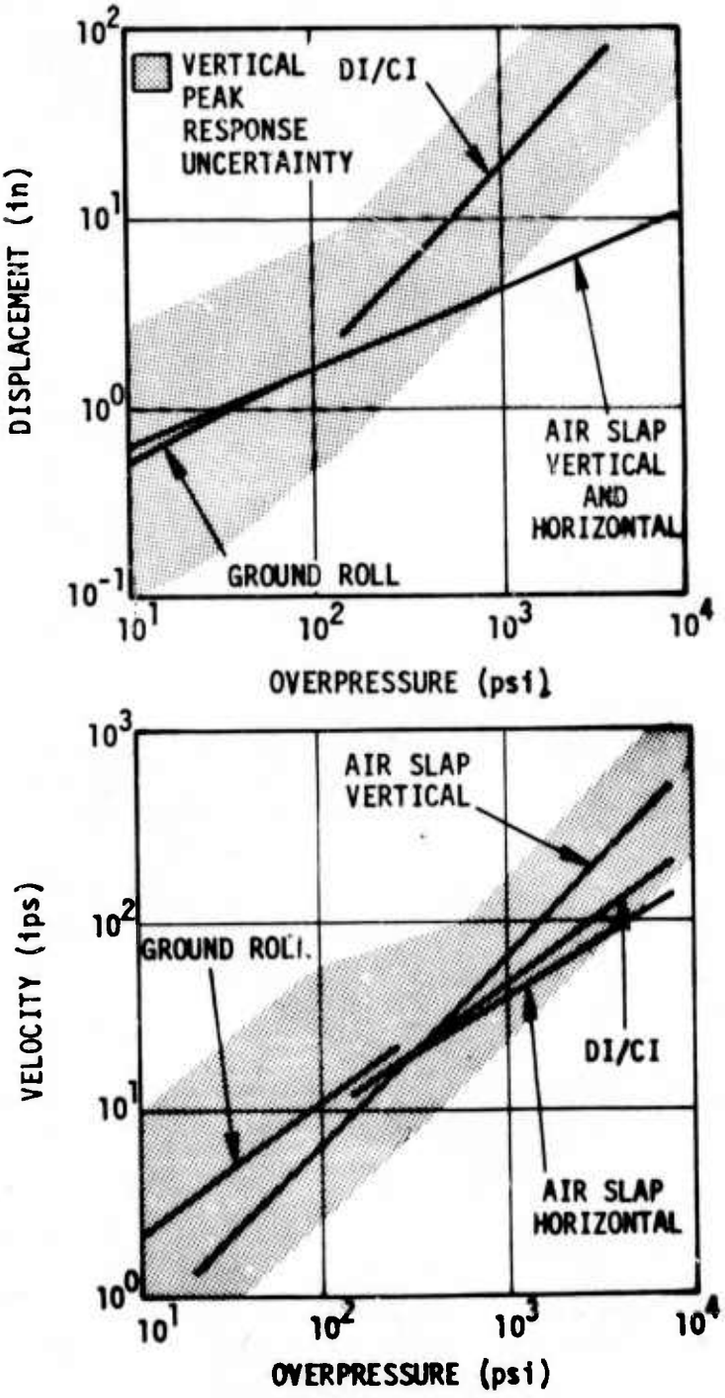

Figure 57. Soft Rock 1-MT Surface Burst
Near-Surface Motion Peak Values

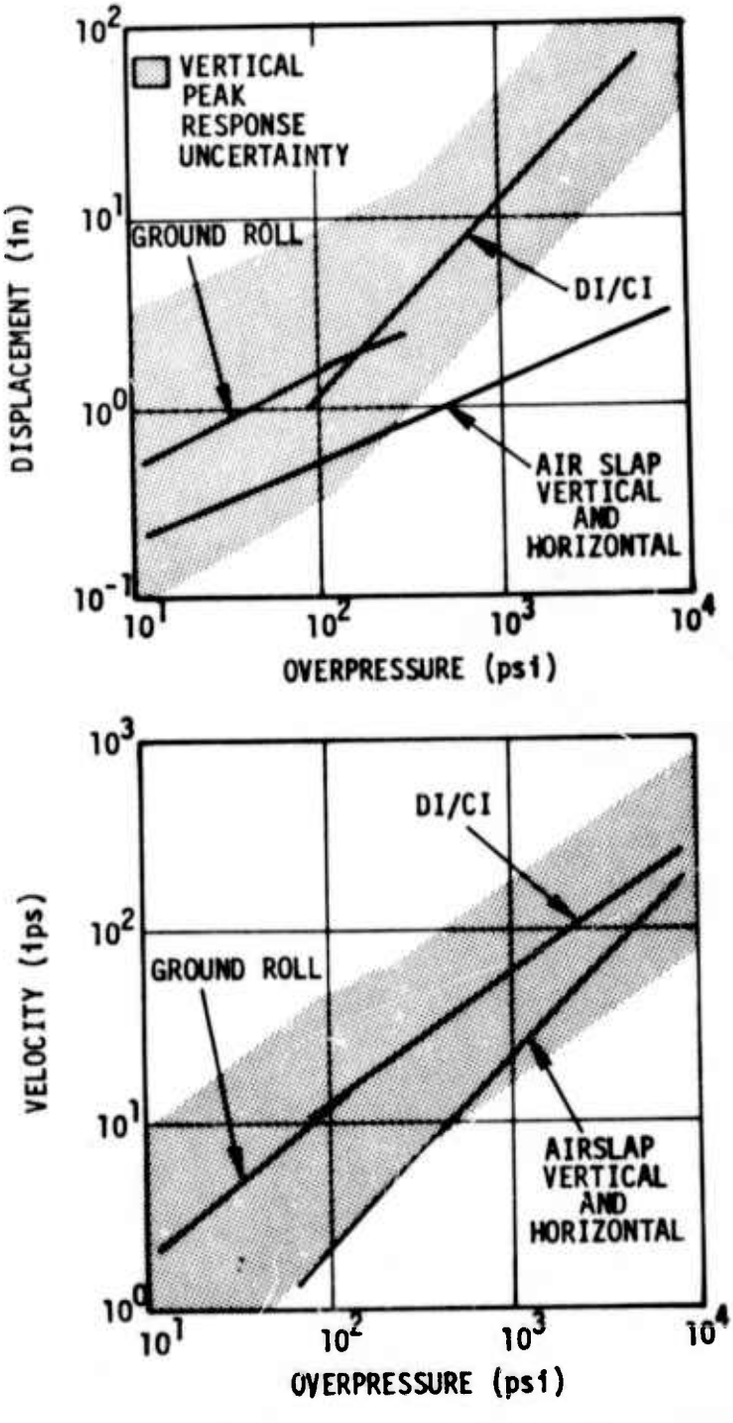

Figure 58. Hard Rock 1-MT Surface Burst Near-Surface Motion Peak Values

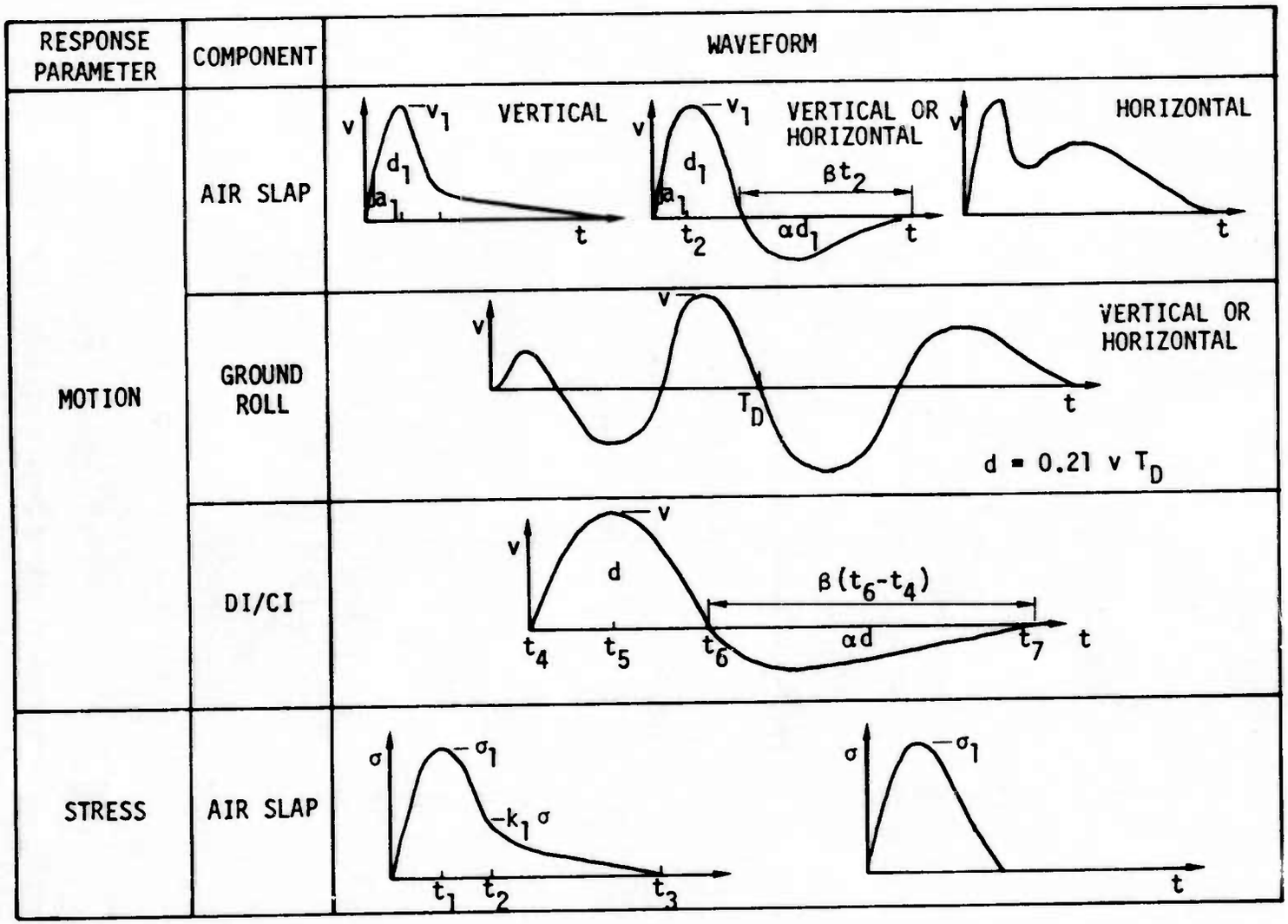

Figure 59. Idealized Ground Shock Waveforms

horizontal waveforms for the four generic sites, accounting for the phasing of the motion components.

The air slap motion arrivals are determined directly from the air blast arrival. The DI/CI arrival is based on the transit time from ground zero, and the ground roll arrival is based on the first outrunning or refracted wave arrival.

With arrival times and peak motion parameters established, representative waveforms can be constructed. Both horizontal and vertical waveforms for 1000, 100, and 10 psi (Figures 60 to 63), and corresponding shock spectra (Figures 64 through 71), were constructed for each generic site. The horizontal and vertical components of ground roll were phase-adjusted to correspond with data, i.e., taken as out of phase. Approximate shock spectra amplification factors are (1) air slap; 1 to 1.5 for displacement, 1.3 to 2 for velocity and 2 for acceleration, (2) ground roll; 2 to 3 for displacement, 3 to 4.5 for velocity and 4 to 5.5 for acceleration and (3) DI/CI; 1 to 1.5 for displacement and velocity.

For all site conditions, the 1000-psi waveforms contain the air slap and DI/CI components, and the 10-psi waveforms contain the ground roll and air slap components. However, the 100-psi waveforms for the soil sites were not as easily definable. The wet soil site was considered to have, in addition to the air slap component, both ground roll and DI/CI motions - adjusted so that maximum motion predictions were not exceeded. The duration of the dry soil waveform was reduced, since 100 psi is only the beginning of the outrunning region.

Stress waveforms have also been estimated for each of the generic sites. The air slap waveforms are based on characteristics of computer code calculational results and the peak stress values. Free surface effects tend to reduce the stress and increase the duration of the velocity pulse. The DI/CI stress duration is related to displacement time to peak for deep points not influenced by free surface effects.

(Text continues on page 164)

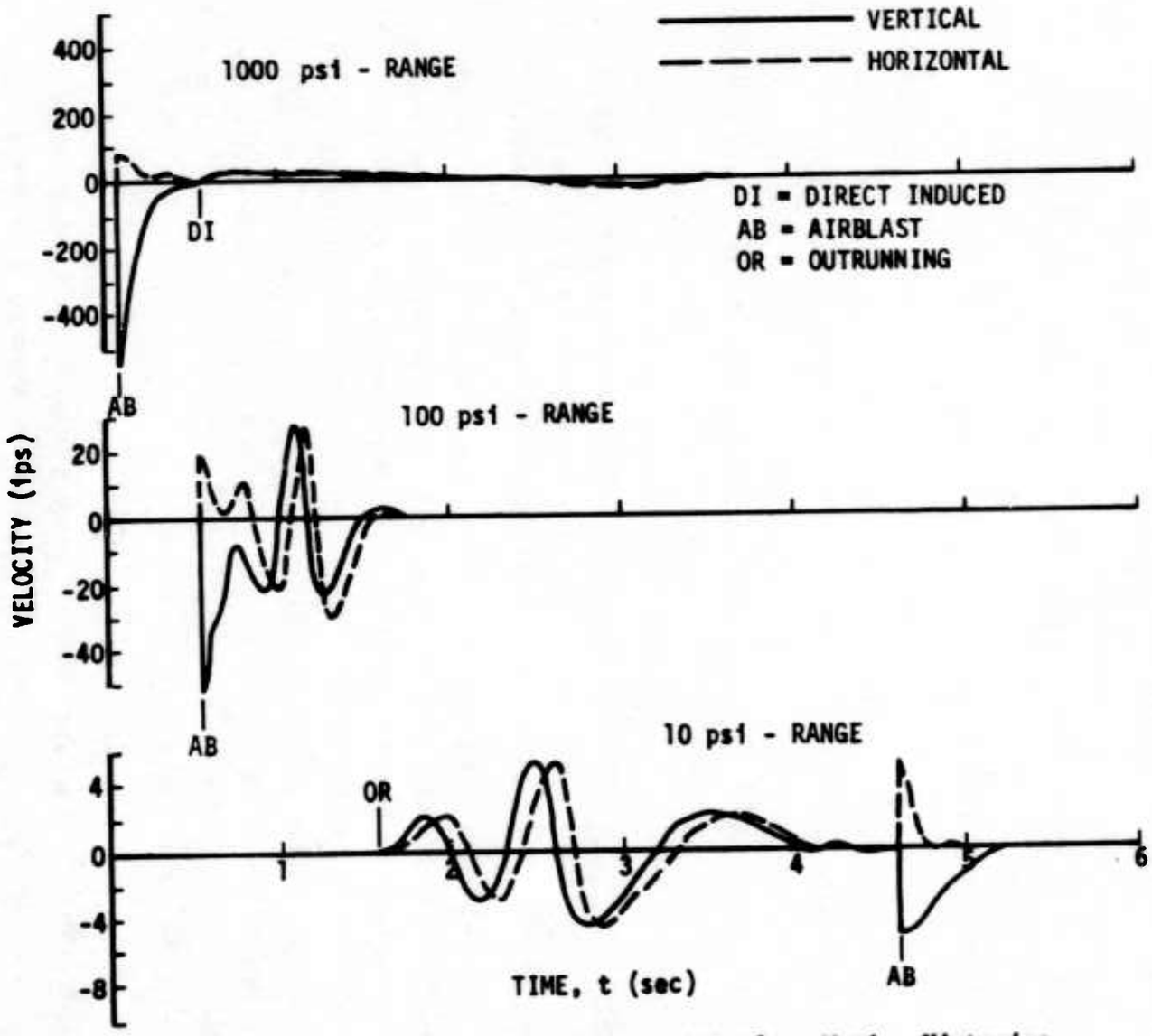

Figure 60. Dry Soil 1-MT Surface Burst Near-Surface Motion Histories

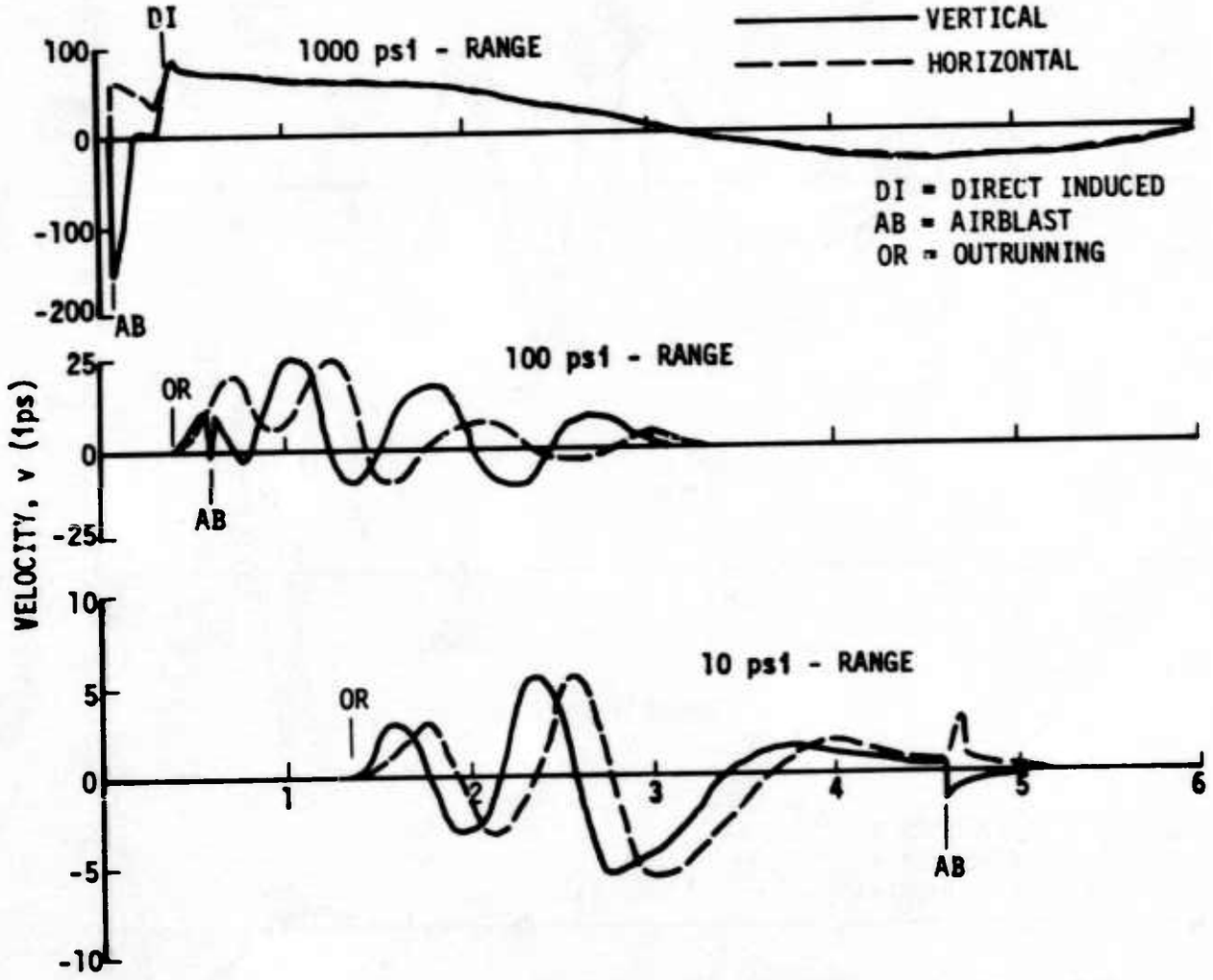

Figure 61. Wet Soil 1-MT Surface Burst Near-Surface Motion Histories

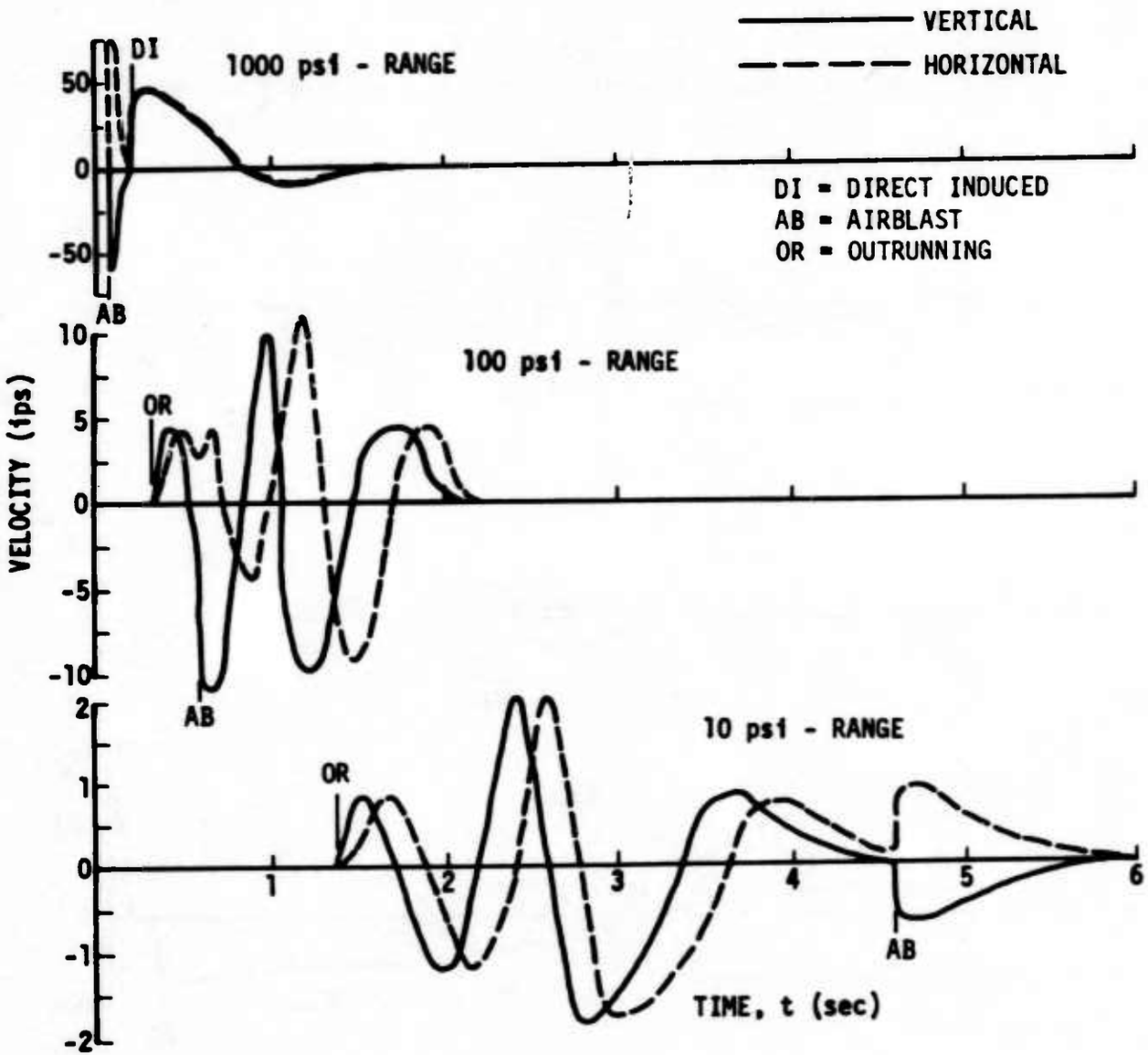

Figure 62. Soft Rock 1-MT Surface Burst Near-Surface Motion Histories

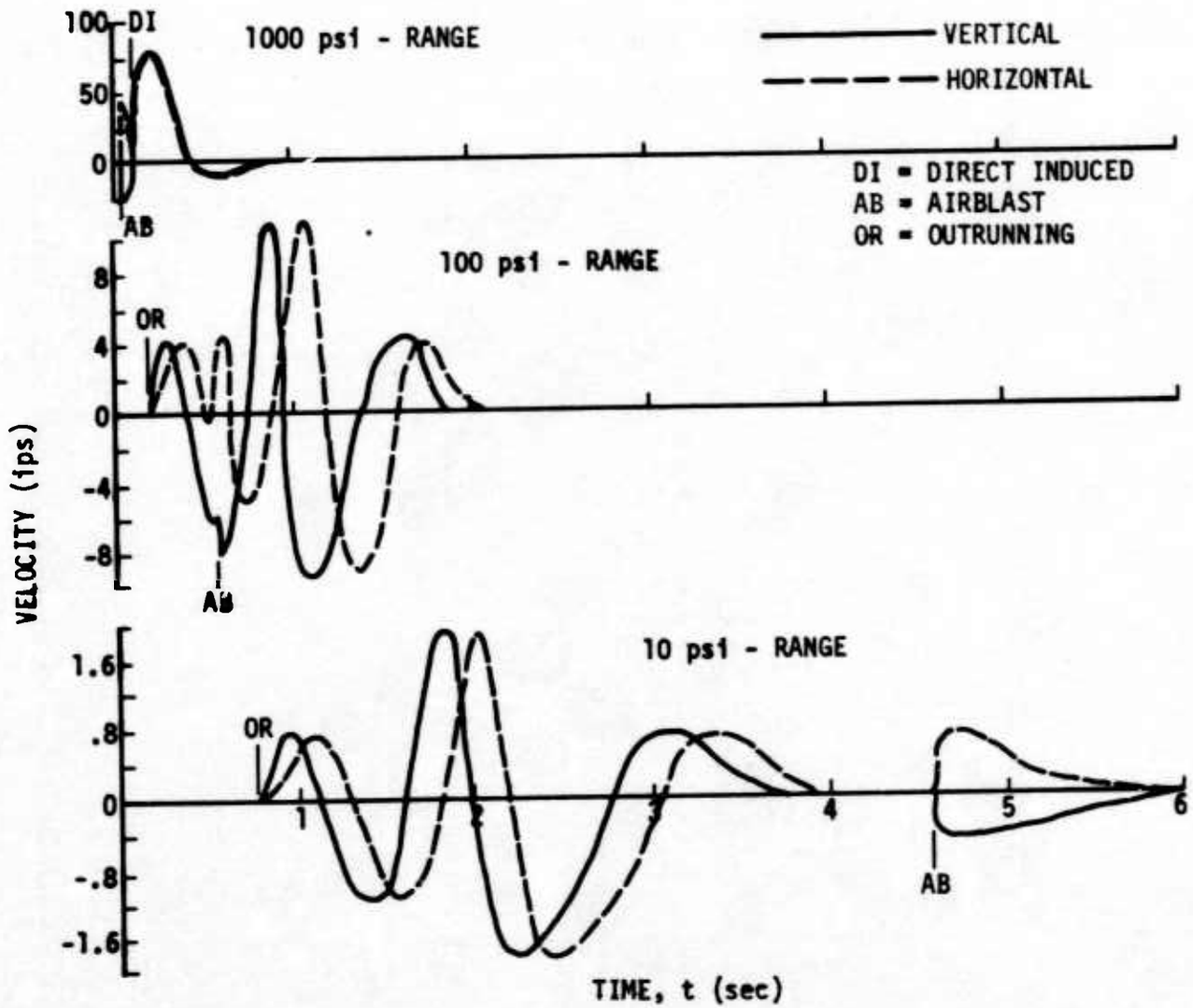

Figure 63. Hard Rock 1-MT Surface Burst Near-Surface Motion Histories

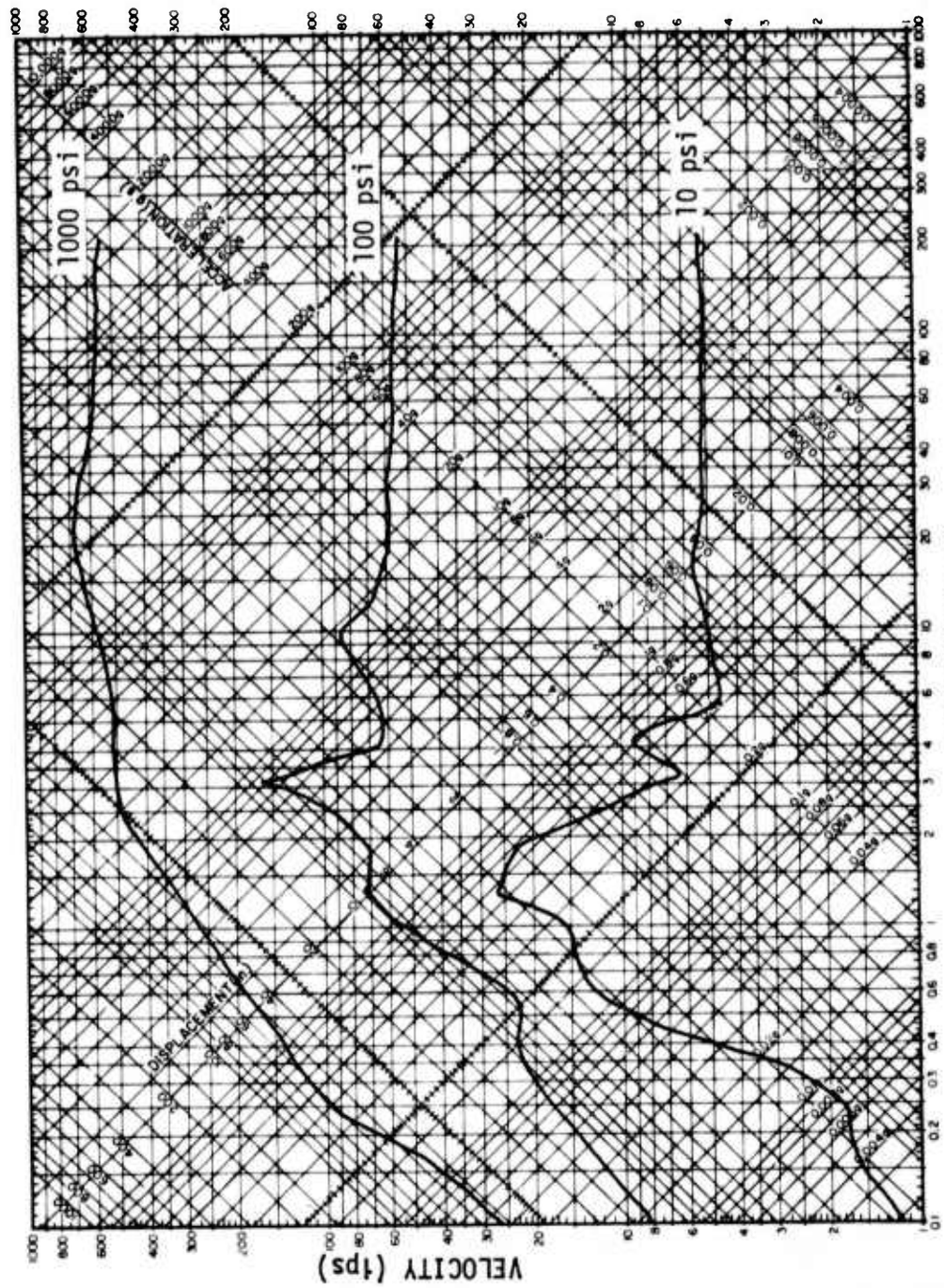

Figure 64. Dry Soil, 1-MT Surface Burst Near-Surface Vertical Shock Spectra

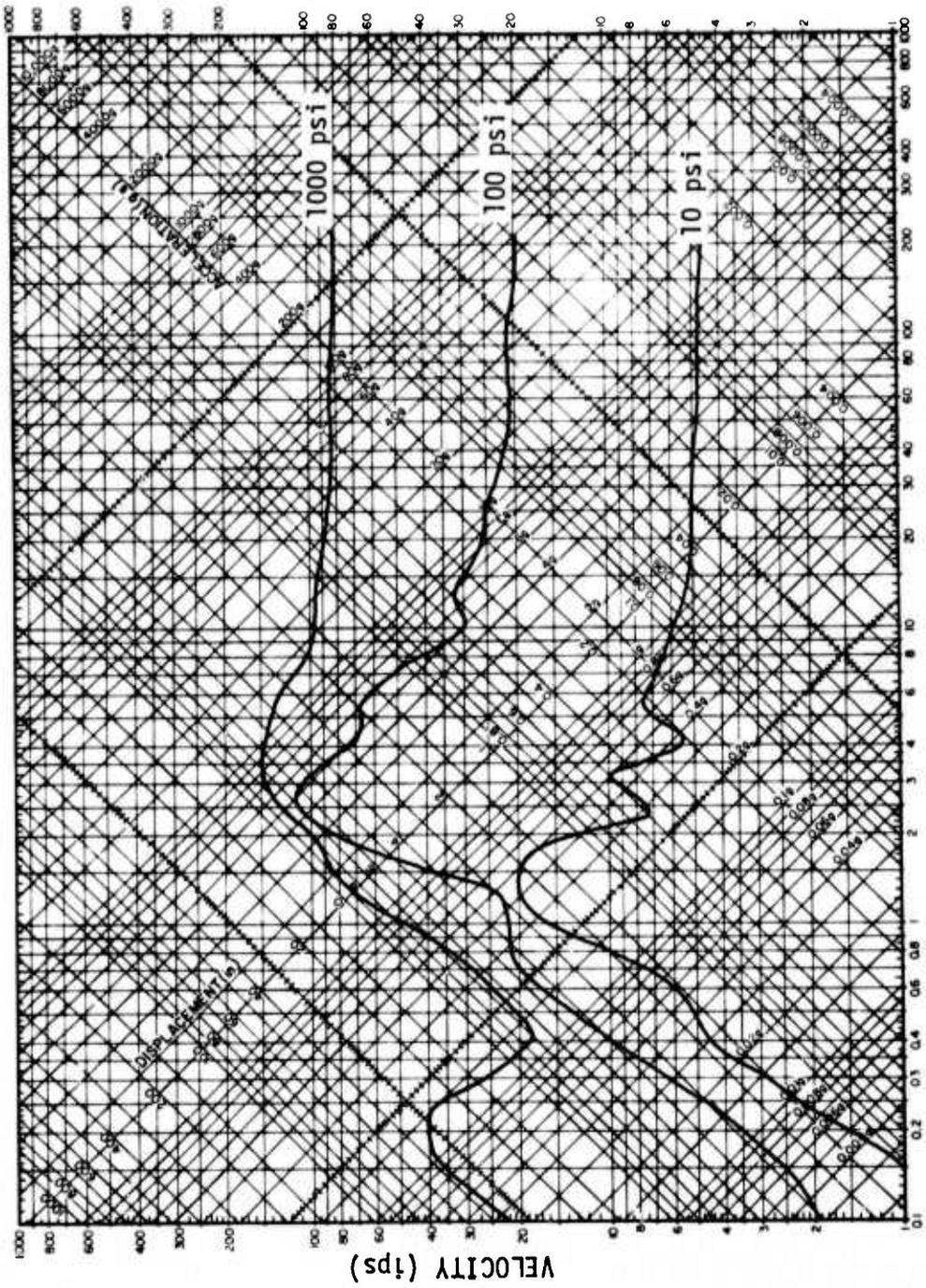

Figure 65. Dry Soil, 1-MT Surface Burst Near-Surface Horizontal Shock Spectra

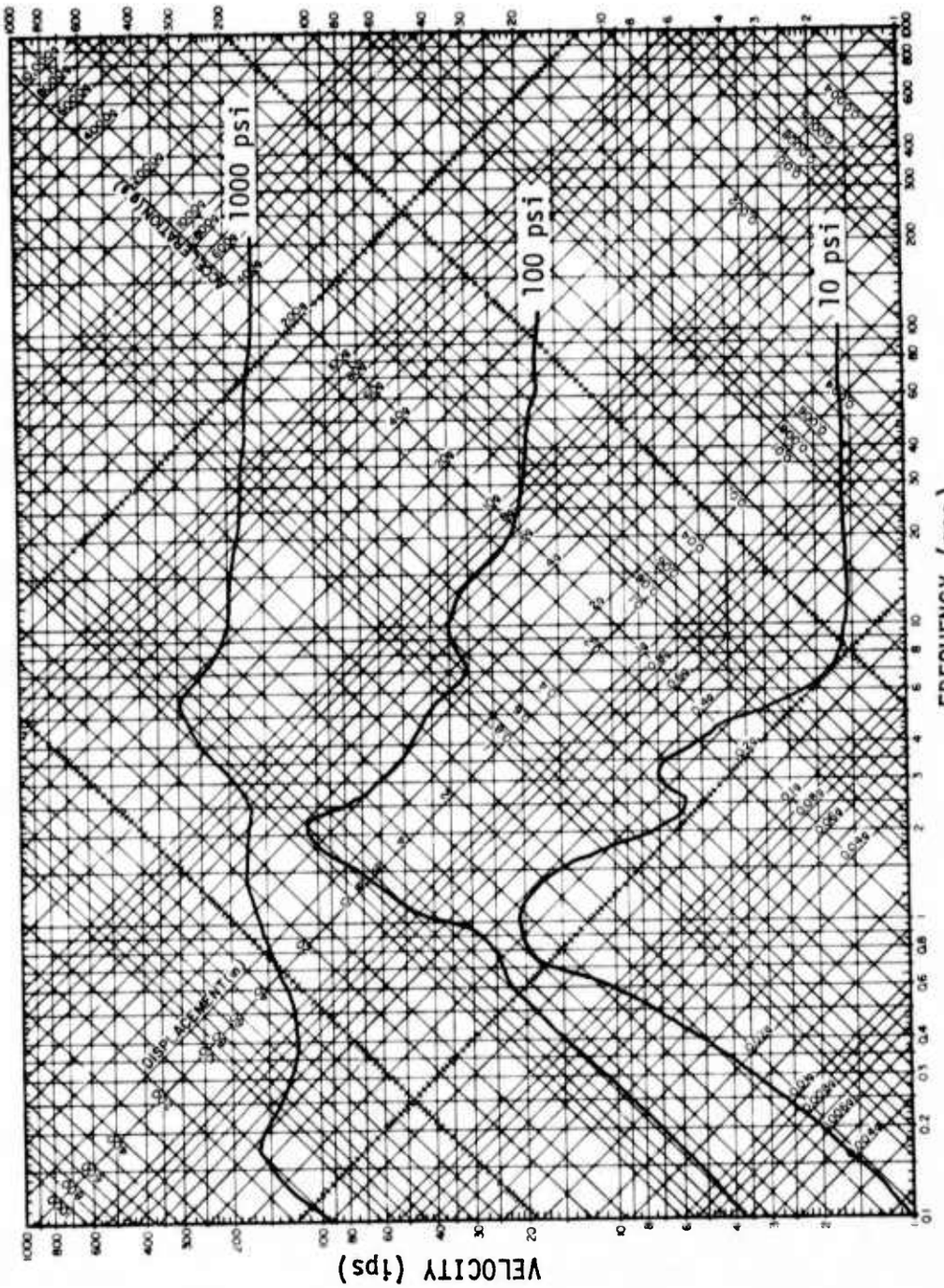

Figure 66. Wet Soil, 1-MT Surface Burst Near-Surface Vertical Shock Spectra

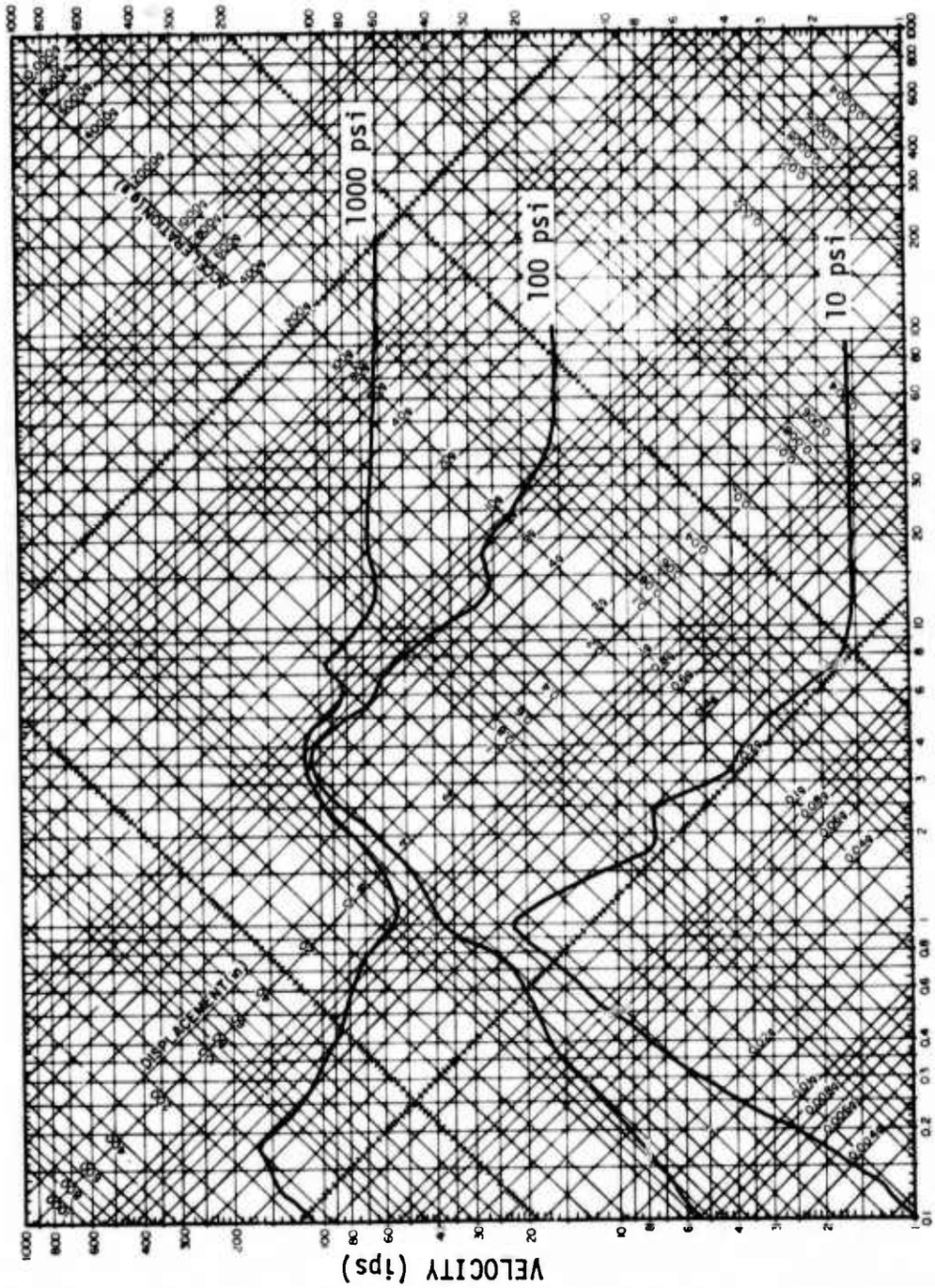

Figure 67. Wet Soil, 1-MT Surface Burst Near-Surface Horizontal Shock Spectra

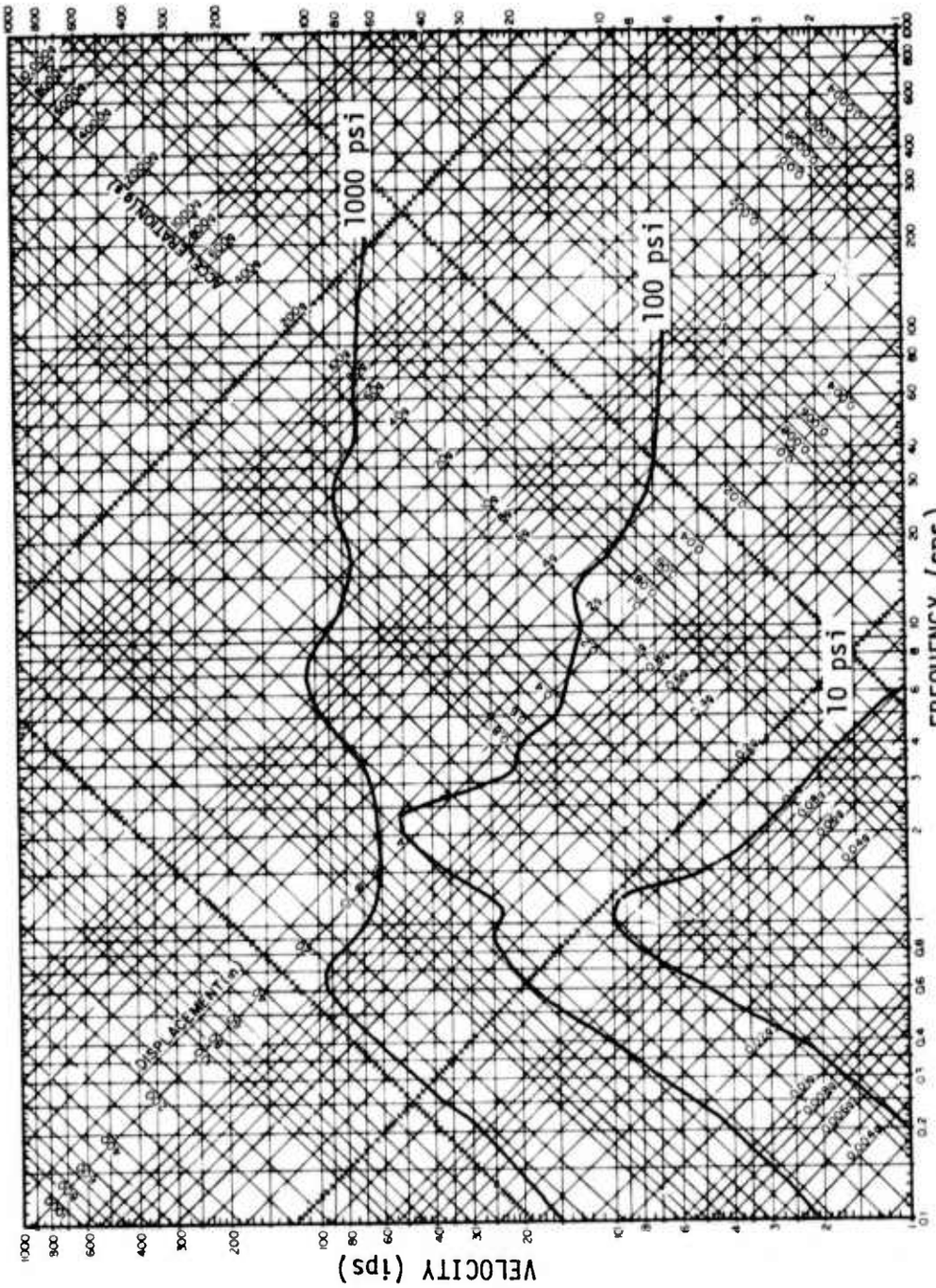

Figure 68. Soft Rock, 1-MT Surface Burst Near-Surface Vertical Shock Spectra

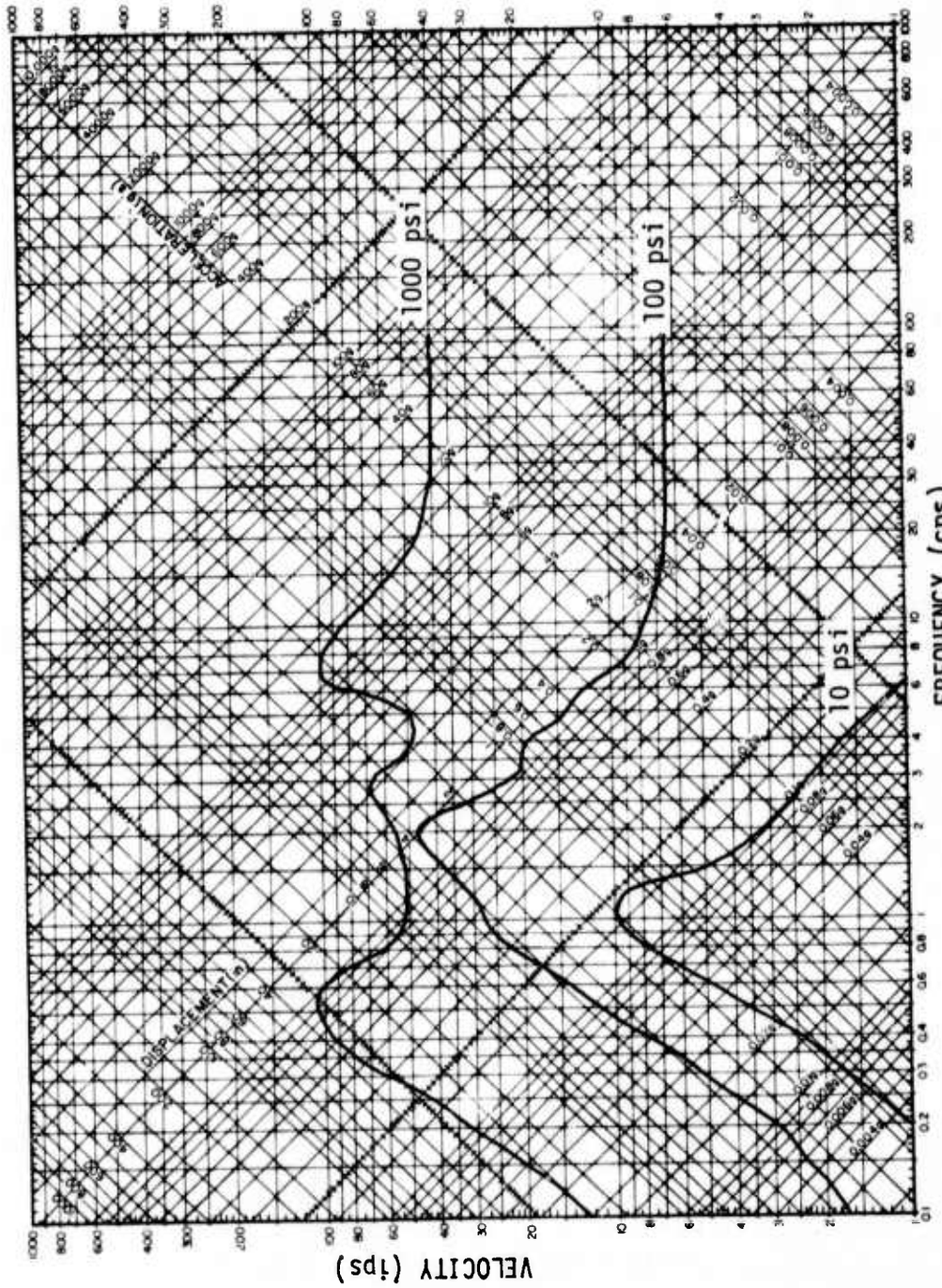

Figure 69. Soft Rock, 1-MT Surface Burst Near-Surface Horizontal Shock Spectra

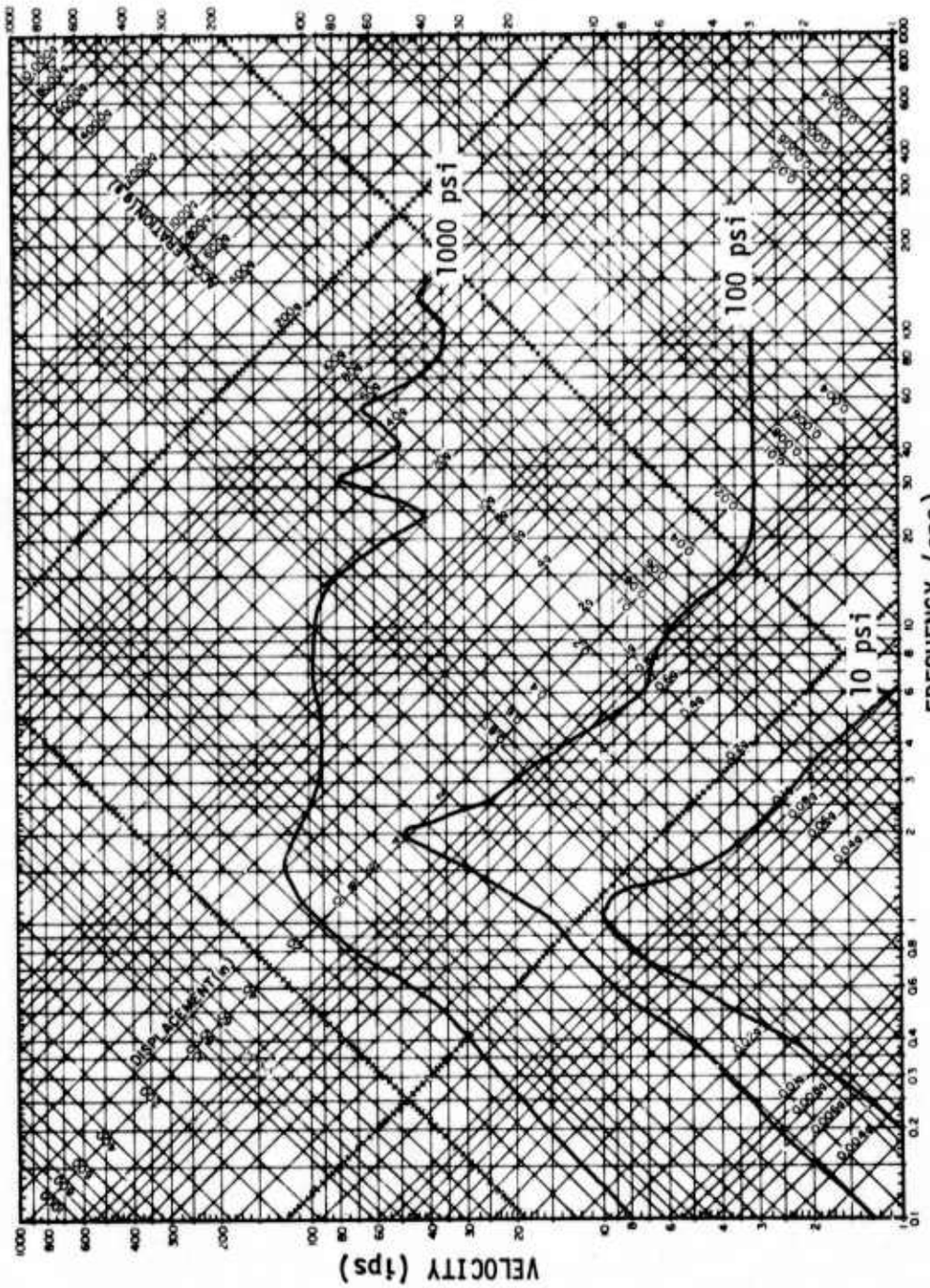

Figure 70. Hard Rock, 1-MT Surface Burst Near-Surface Vertical Shock Spectra

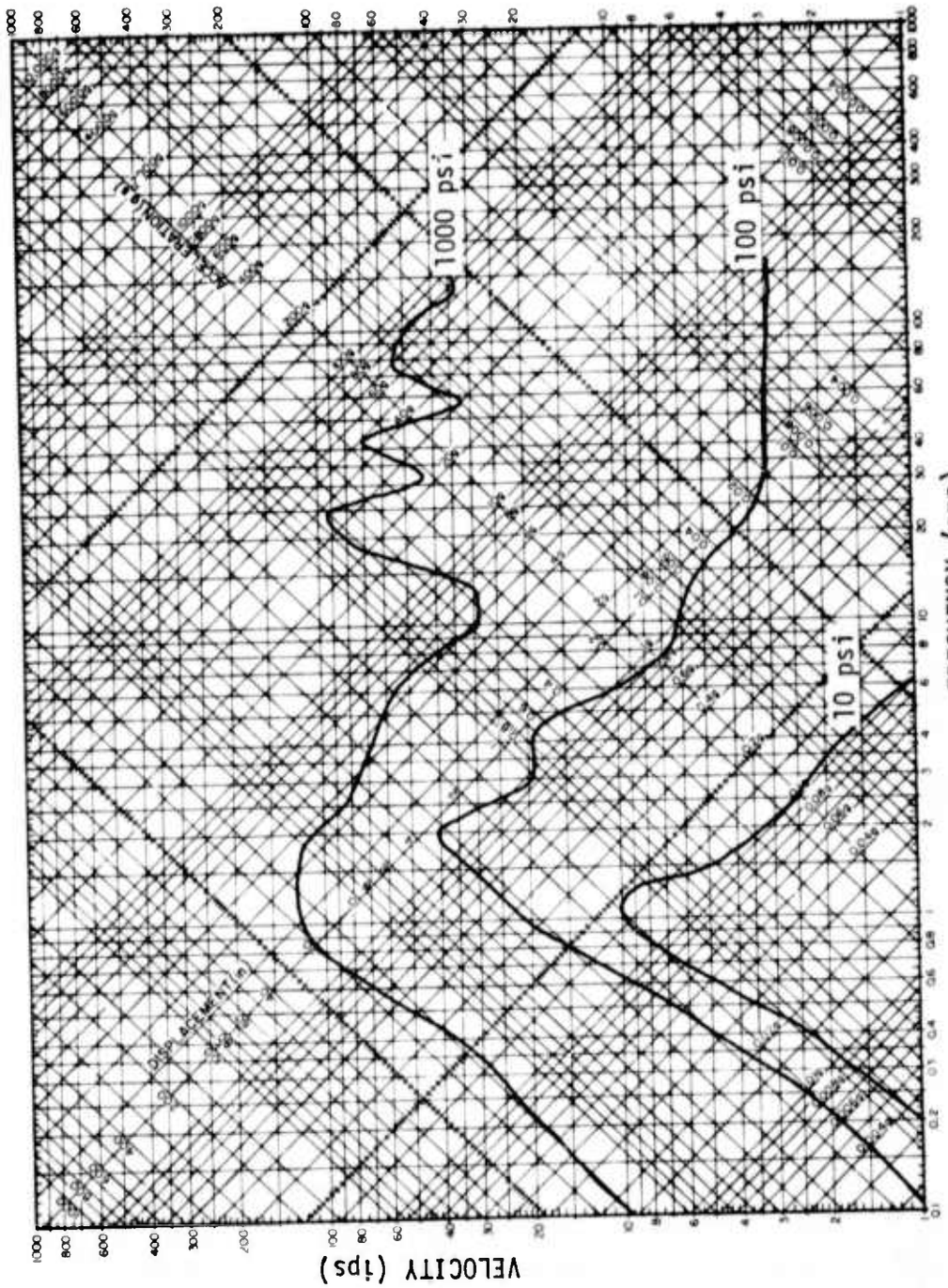

Figure 71. Hard Rock, 1-MT Surface Burst Near-Surface Horizontal Shock Spectra

Little analysis has been performed for stresses due to ground roll effects, which are not considered in this study. However, the peak stresses should be associated with either the air slap or DI/CI components of motion. Representative stress waveforms are shown in Figures 72 and 75, except for the 10-psi station for the rock sites. The uncertainties are currently too large to present waveform estimates for those conditions.

4.3 GENERIC SITE PREDICTIONS FOR HEIGHT-OF-BURST CONDITIONS

Use of a surface equivalent yield facilitates the prediction of air-slap-related ground shock, crater volume, and DI/CI motions, as well as ground roll effects. Air slap motions and stresses depend on the surface pressure loading. For a fixed peak pressure, several surface burst overpressure histories are compared with those for approximately optimum HOB (Figure 76). The major differences in the waveforms are in the value of t_{00}, the initial slope intercept. The impulse associated with the HOB case is generally within 50% of that associated with the corresponding surface burst.

Displacement, which is the only air slap motion parameter significantly scaling with yield, is related to the air blast impulse; consequently, one may determine an equivalent surface burst yield, W_{EQ}, by

$$W_{EQ} = W \left[\frac{I_{HOB}}{I_{SB}}\right]^3 \qquad (44)$$

where W is the actual yield, I_{HOB} is the impulse from the height-of-burst case, and I_{SB} is the impulse from the surface burst case. This equation represents a reasonable method for determining an equivalent yield for scaling air slap displacements which peak late time with respect to the air blast loading. However, for cases where higher frequency response is involved an improved method for determining a surface equivalent yield is given by Equation (45).

(Text continues on page 170)

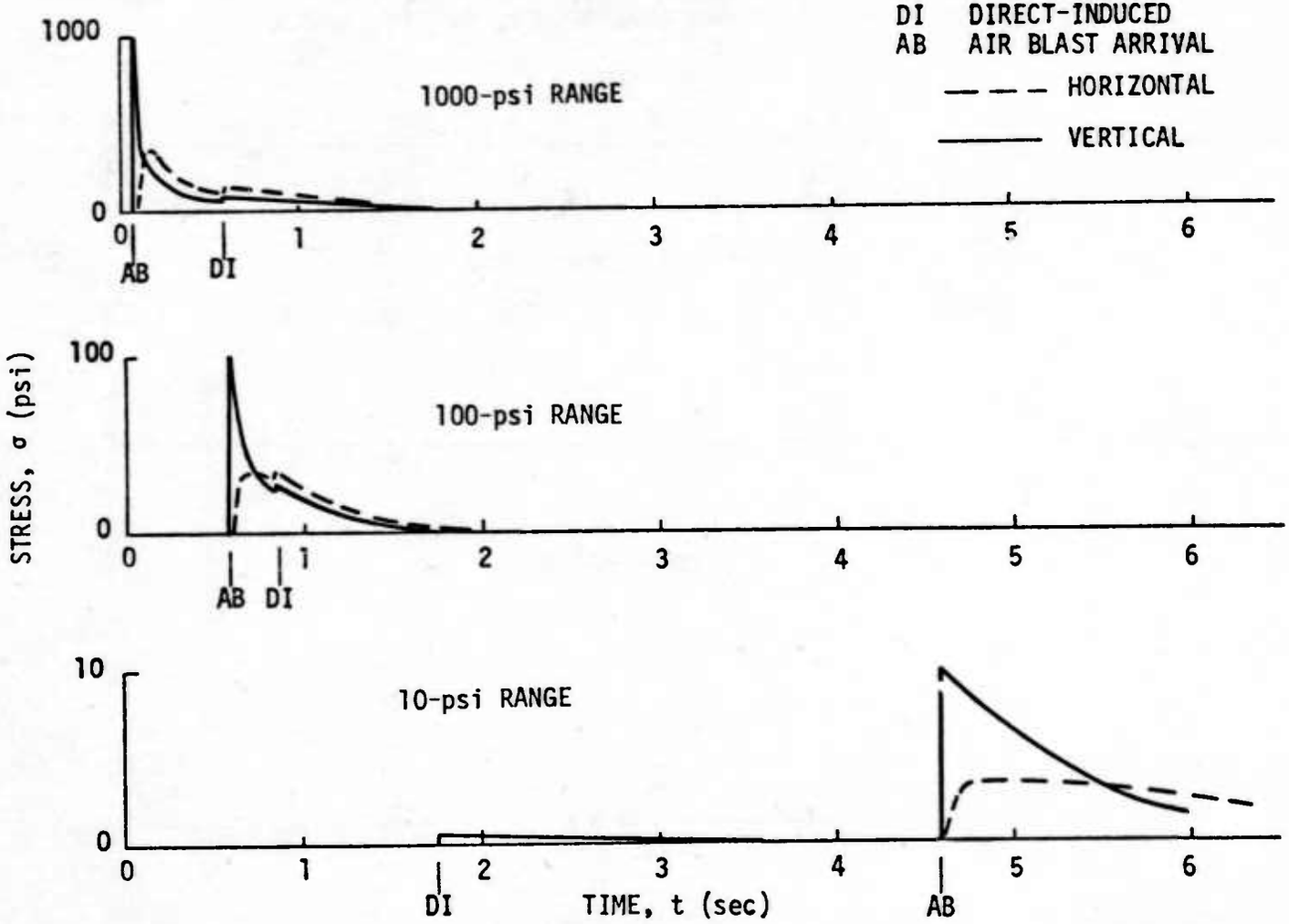

Figure 72. Dry Soil Surface Burst 1-MT Stress Waveforms

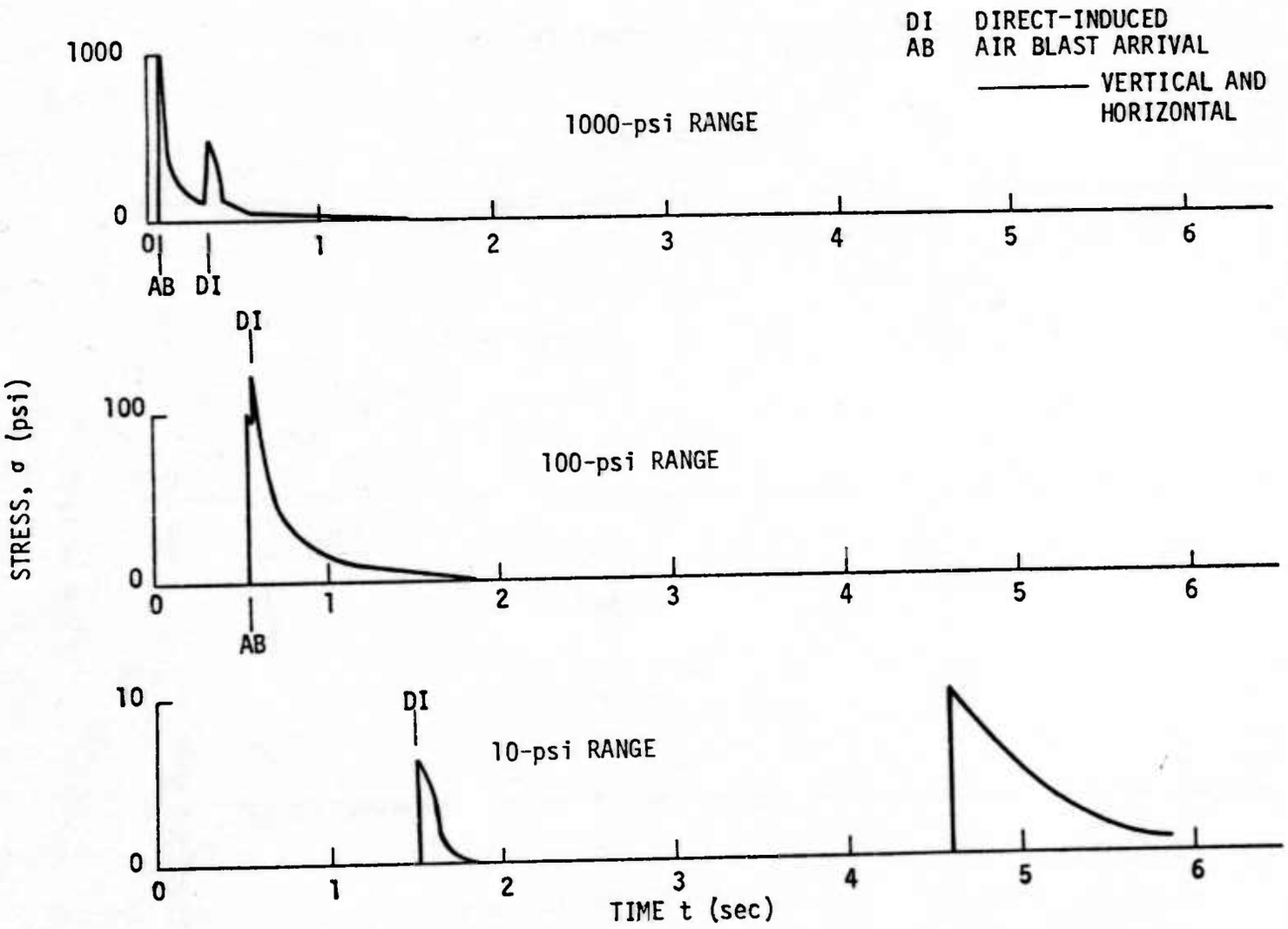

Figure 73. Wet Soil Surface Burst 1-MT Stress Waveforms

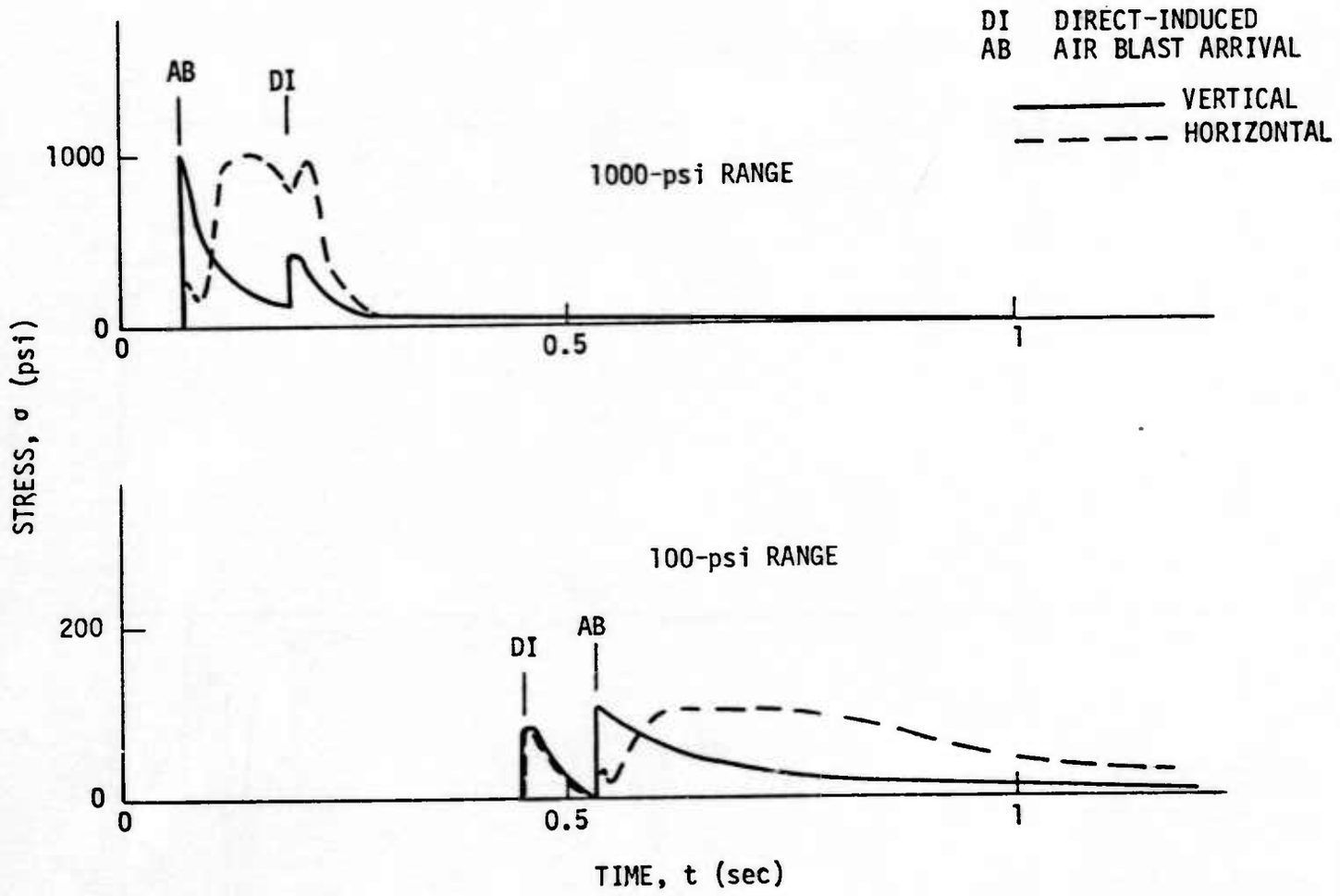

Figure 74. Soft Rock Surface Burst 1-MT Stress Waveforms

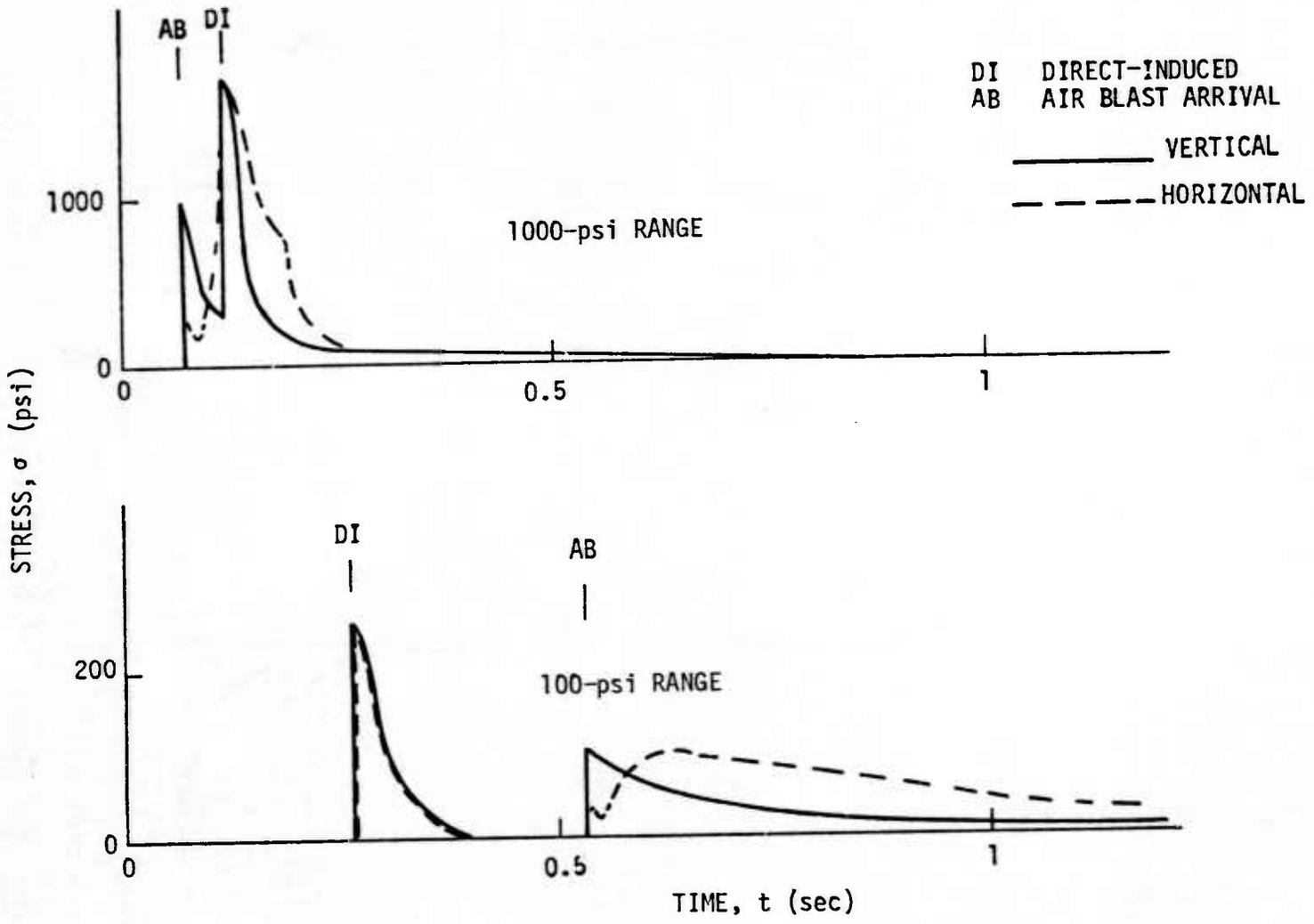

Figure 75. Hard Rock Surface Burst 1-MT Stress Waveforms

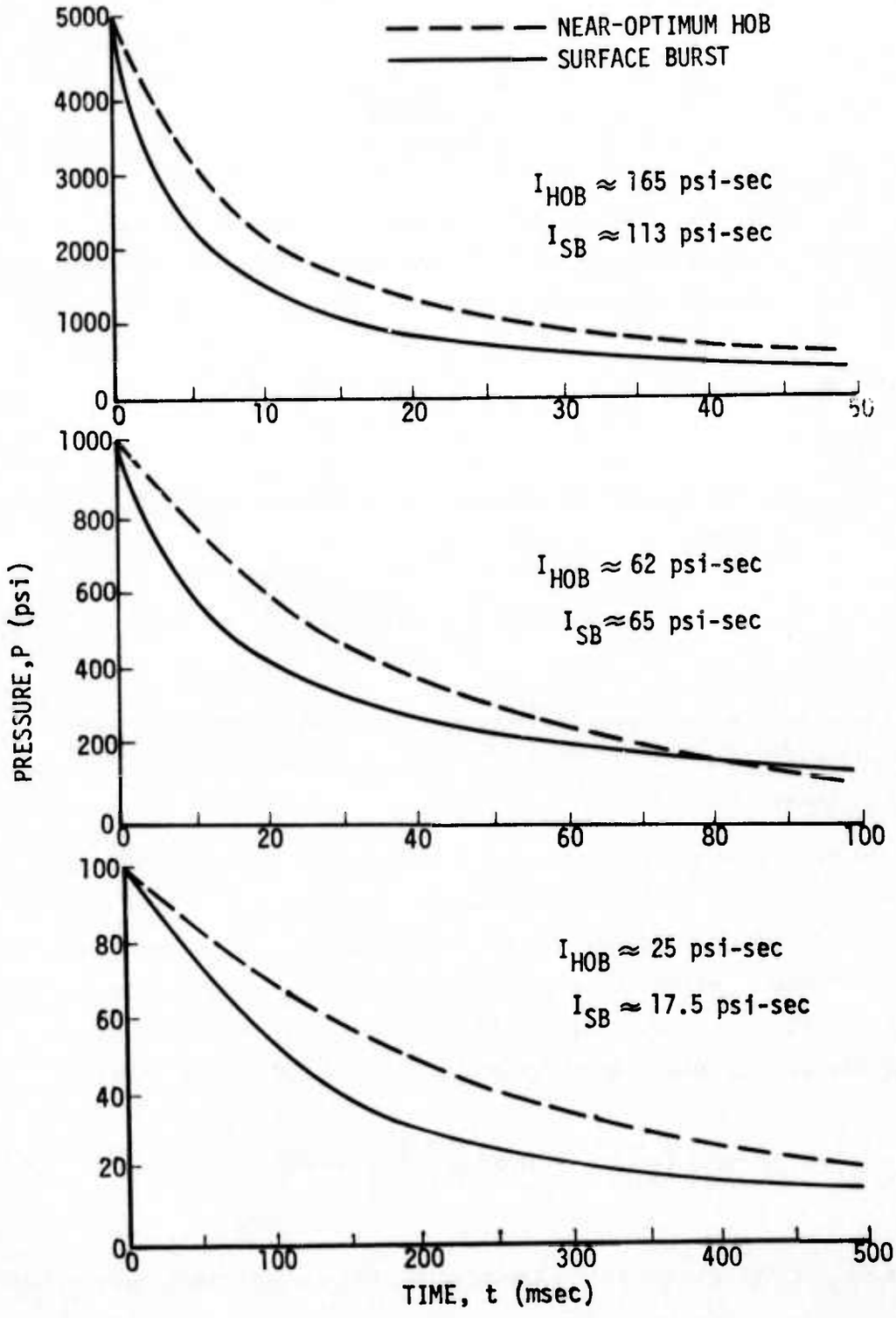

Figure 76. Comparison of Surface Burst and HOB Overpressure Waveforms

$$W_{EQ} = W \left[\frac{(t_{00})_{HOB}}{(t_{00})_{SB}}\right]^3 \tag{45}$$

The influence of HOB on DI/CI motions is directly related to the effect of HOB on crater volume. The Air Force design manual (Reference 7) gives the following relationship for wet soils,

$$V_{HOB} = V \exp\left[-\frac{HOB/W^{1/3}}{30\ ft/MT^{1/3}}\right] \tag{46}$$

where V_{HOB} is the HOB crater volume; the equivalent yield is then given by

$$W_{EQ} = W \exp\left[-\frac{HOB/W^{1/3}}{30\ ft/MT^{1/3}}\right] \tag{47}$$

This equation is then used for HOB scaling of DI/CI motions. The equivalent yield is simply used in place of the actual yield to calculate DI/CI parameters.

To determine the influence of HOB on ground roll motions, data reported by Cooper in Reference 73 have been examined. Figure 54 shows the scaled peak displacement range decay for three burst positions, i.e., optimum burial, surface burst, and air burst. The outrunning displacements for air bursts are reduced to 60% of the surface burst values. Thus, the ground roll displacements can be written in the form

$$d = d_{SB}\left[0.6\left(\frac{W}{1\ MT}\right)^A + 0.4\left(\frac{W_{EQ}}{1\ MT}\right)^A\right]\left[\frac{1000\ ft}{R}\right]^B \tag{48}$$

where d_{SB} is the ground roll displacement for the reference conditions.

5.0 SUMMARY

This section briefly summarizes conclusions and recommendations determined from this study of air blast and ground shock prediction techniques and indicates those areas which most influence the environment uncertainties.

5.1 AIR BLAST

The current standard for computing height-of-burst (HOB) overpressure waveforms for ideal surfaces is the Brode 1-kT free-air environment definition together with a surface reflection interpolation scheme (Reference 6). The resulting peak overpressure contours show that nearly optimum HOB detonations have a larger ground range to a specified overpressure than does a surface burst of the same yield. This phenomenon has received attention with regard to the vulnerability of overpressure sensitive targets to air bursts. However, there is uncertainty as to whether this enhancement would actually occur in the high overpressure region. To resolve the issue, the AFWL is currently performing a series of HOB finite difference computer code calculations. It has been necessary to rely largely on analysis and high explosive test data for air blast prediction for the higher overpressure region, since most nuclear air blast data have been recorded in the lower overpressure regions.

Recent high explosive HOB tests with 8-lb charges (Reference 10) have revealed the existence of a double-peak air blast waveform associated with slipstream effects which are averaged out in the Brode interpolation scheme. This double-peak phenomenon can have a significant effect on reducing the dynamic pressure when the first peak is not the maximum overpressure. In this study, a prediction methodology for double-peak waveforms has been devised from the 8-lb test data.

The dynamic pressure environment for surface burst, ideal surface conditions has been defined by a double exponential waveform expression developed by Brode. This expression contains a number of parameters which are functions of the peak overpressure. During the course of this study it was determined that the dynamic pressure history could be expressed more simply as a function of only the peak overpressure and the dynamic pressure peak and duration. The differences between the two expressions are small and, therefore, the simpler fit is adequate.

For HOB conditions, the dynamic pressure environment is quite complex and a waveform prediction technique has not been devised. Peak-pressure HOB curves have been developed, but they have very large uncertainty for high overpressures especially in the double-peak region. In this region, the peak dynamic pressure may be more related to the first peak (shock front) overpressure. The HOB ideal surface air blast calculations being performed by the AFWL will help to better define this environment.

A method for predicting the precursor overpressure history for non-ideal surfaces is contained in the Air Force design manual (Reference 7). In addition, the AFWL is currently performing first principle calculations for precursor air blast environments which consider an initial thermal profile based on a separate analysis of the dust/air interaction. These calculations will also define the dynamic pressure, which is enhanced in the precursor region. The initial thermal conditions are the primary source of uncertainty in this analysis since there are almost no relevant data. Calculations will be performed for the PRISCILLA event for validation of the approach.

Recent calculations have also been performed by the AFWL to determine the air blast loading on a perfectly reflective bermed surface. The results indicate that a significant nonuniform loading could occur

for berms with slopes of 1:4. Previously, slopes this shallow were not considered to influence the air blast loading.

5.2 GROUND SHOCK

This study has considered the ground shock environment for the near-surface region (between the ground surface and 50-ft depth) which results from both air-blast-induced (AI) and direct-induced/crater-induced (DI/CI) effects.

For the close-in (or strongly superseismic) region, the surface burst ground shock environment is caused primarily by effects from the surface overpressure history and overpressure gradients of the air slap (overhead air blast loading) portion of the AI loading and by DI/CI effects. However, the DI/CI effects diminish rapidly as the burst height above the surface increases.

In the outrunning region, the typical motion for both surface and above-surface bursts is that of low frequency oscillation, termed ground roll. The initial arrival is usually due to upstream AI loading. However, for surface bursts, later events are due to both AI and DI/CI sources.

Ground shock predictions are developed for peak motion and stress parameters related to air slap, close-in DI/CI, and AI and DI/CI ground roll effects for the four generic site conditions. They are expressed in the form of simplified prediction equations appropriate to the DIA/VAS analysis. Uncertainties in the predictions are estimated from uncertainties of the test data and of the scaling and computer code analyses which form the technology base for this study.

Of all ground shock effects, the vertical air-slap-induced response for superseismic conditions has the least uncertainty since it is based on first principle analysis validated by comparison with field test data. The uncertainty in this response is based primarily on

uncertainty in the properties of the medium and in the definition of the airblast. Available test data and analysis indicate that for superseismic conditions the horizontal air slap velocity is not very sensitive to the properties of the medium, while the horizontal displacement is very dependent on the shear properties of the medium and has large uncertainty even in the superseismic region.

In the outrunning region, the initial response is due to upstream AI loading. The phenomenology of the response has much uncertainty since good correlation of test results with analysis has not been obtained for the relevant high explosive events which comprise the primary data base. Calculation of response for layered sites with large impedance variations requires fine zoning to minimize numerical calculational errors. Lack of good correlation, however, is due primarily to the uncertainty in the in situ constitutive properties of the medium, both in the form of the constitutive equations and in the material properties used to fit these equations. It is quite important to have a laboratory program and a field test program for determining good in situ properties. Within the current state-of-the-art, adequate uniaxial strain definition can be obtained. However, there are not sufficiently adequate techniques for determining in situ shear stiffness, anisotropic effects, tensile failure criteria, and post-cracking behavior and interface conditions which can be significant factors in ground shock response.

To obtain a good definition of the ground shock response, it is important to first correlate test results with analysis for events in related media. Then material models can be validated and used for calculating nuclear response.

Both ground roll and close-in DI/CI effects are determined in this study primarily from scaling of test data. A principal area of uncertainty lies in the scaling of waveform durations with yield. Analyses

of peak DI/CI displacements and velocities indicate that although cube root of crater volume (or yield, for uniform geologies) scaling is reasonable, this scaling is not consistent with time to peak displacement results from the PRE-MINE THROW IV experiments at NTS. Further analysis of the data base will be required to resolve this issue. The peak ground roll velocity and displacement scaling imply cube root of yield time (and frequency) scaling. This situation is consistent with results of experiments at the MIXED COMPANY site. The uncertainty in this scaling is related to the fact that geological layering would be expected to make these frequencies less sensitive to yield. Furthermore, there are other data which imply $W^{1/5}$ or $W^{1/6}$ time scaling. For both the DI/CI and ground roll environments, peak velocity and displacement data have been weighted more heavily than frequency content.

Waveforms have been synthesized from air slap, close-in DI/CI, and further-out ground roll components, for three overpressure stations and the four site conditions. The ground roll waveform was developed by Sauer (Reference 2) from nuclear test data for NTS. However, for some high explosive events differences are observed between the scaling of peak velocities associated with the initial portion of the pulse and with the later time motion. These data must be further analyzed to develop waveforms that consider these scaling differences.

Adequate waveforms can be developed for the vertical response brought about by superseismic air blast effects. But nuclear waveforms for other conditions are based primarily on test data for low yield high explosive events and have significant uncertainty. To improve the capability of predicting waveforms for generic site conditions, it would be important to obtain correlation between data and valid calculational results and a simplified prediction scheme for the geologies and overpressure levels of interest. Such investigations would

also further the understanding of the test event phenomenology and point out which parameters, other than peak motion values, are required to adequately describe the ground shock environment.

6.0 REFERENCES

1. Glasstone, S., Editor, The Effects of Nuclear Weapons, U.S. Department of Defense and Atomic Energy Commission, Revised Edition. Superintendent of Documents, U.S. Government Printing Office, Washington, D.C., February 1964.

2. Sauer, F. M., G. B. Clark, and D. C. Anderson, "Empirical Analysis of Ground Motion and Cratering, Part IV," Nuclear Geoplosics, DASA-1285 (IV), Defense Atomic Support Agency, Washington, D.C., May 1964.

3. Brode, H. L., A Review of Nuclear Explosion Phenomena Pertinent to Protective Construction, R-425-PR. The Rand Corporation, Santa Monica, Calif., May 1964.

4. Newmark, N. M., and J. D. Haltiwanger, Air Force Design Manual - Principles and Practices for Design of Hardened Structures, AFSWC-TDR-62-138, Air Force Special Weapons Center, Kirtland AFB, N. M., December 1962.

5. Brode, H. L., "Review of Nuclear Weapons Effects": Ann. Rev. Nucl. Sci., Vol. 18, 1968.

6. Brode, H. L., Height of Burst Effects at High Overpressures, RM-6310-DASA. The Rand Corporation, Santa Monica, Calif.; also, DASA 2506, Defense Atomic Support Agency, Washington, D.C., July 1970.

7. Crawford, R. E., C. J. Higgins, and E. H. Bultmann, The Air Force Manual for Design and Analysis of Hardened Structures, AFWL-TR-74-102. Air Force Weapons Laboratory, Kirtland AFB, N.M., October 1974.

8. Rowan, W. H., et al., Failure Analysis by Statistical Techniques (FAST), 24006-601-RU-00, TRW Systems Group, Redondo Beach, Calif.; also, Final Report for period ending 30 April 1974, DNA 3336F-1, Defense Nuclear Agency, Washington, D.C., 31 October 1974.

9. Needham, C. E., et al., Nuclear Blast Standard (1kT), AFWL-TR-73-55. Air Force Weapons Laboratory, Kirtland AFB, N.M., April 1973.

10. Carpenter, H. J., Height of Burst Blast Effects at High Overpressures, DNA 3437F. Defense Nuclear Agency, Washington, D.C., October 1974.

11. Newmark, N. M., Height of Burst Effects on Horizontally Yielding Targets, DNA 3252F. Defense Nuclear Agency, Washington, D.C., 18 March 1974.

12. Korman, H. F., N. Lipner, and J. S. Chiu, "Structural Dynamic to Height-of-Burst Air Blast Loading", Shock and Vibration Bulletin A5, Shock and Vibration Information Center, Research Laboratory, Washington, D.C., June 1975.

13. Carpenter, H. J., and H. L. Brode, Height-of-Burst at High Overpressure. R & D Associates, Santa Monica, Calif., 1975.

14. Seifert, K, and P. Welsh, Mach Reflection Effects at High Overpressure, PIFR-376. Physics International Company, San Leandro, Calif.; also, DNA 3643F. Defense Nuclear Agency, Washington, D.C., 15 June 1975.

15. Cooper, H. F., Jr., "A Review of Ground Motion from Nuclear and High Explosive Experiments", presented at DNA Strategic Structures Review Meeting, Stanford Research Institute, Menlo Park, Calif., February 1975.

16. Swift, L. M., D. C. Sachs, and F. M. Sauer, Operation PLUMBBOB, Project 1.4, Ground Acceleration and Strain at High Incident Overpressures, WT-1404. Defense Atomic Support Agency, Albuquerque, N.M., April 1961.

17. Perret, W. R., Operation PLUMBBOB, Project 1.5, Ground Motion Studies at High Incident Overpressure, WT-1405. Defense Atomic Support Agency, Albuquerque, N.M., June 1960.

18. Salmon, V., and S. R. Hornig, Operation TUMBLER, Project 1.7, Earth Acceleration vs Time and Distance, WT-517. Armed Forces Special Weapons Project, Washington, D. C., February 1953.

19. Sauer, F. M., and C. T. Vincent, FERRIS WHEEL Series, FLAT TOP Event, Project 1.2/1.3a, Earth Motion and Pressure Histories, POR 3002 (WT-3002). Stanford Research Institute, Menlo Park, Calif., April 1967.

20. Murrell, D. W., Operation PRAIRIE FLAT, Project LN 302: Earth Motion and Stress Measurements, TR N-72-2. U.S. Army Engineer Waterways Experiment Station, Vicksburg, Miss., February 1972.

21. Hoffman, H. V., F. M. Sauer, and B. Barclay, Operation PRAIRIE FLAT, Project LN-308, Strong Ground Shock Measurements, POR-2108. Stanford Research Institute, Menlo Park, Calif., 5 April 1971.

22. Jones, G. D., Operation PRAIRIE FLAT, Project LN-317, Ground Displacement Study. The Boeing Company, Seattle, Washington, January 1969.

23. Murrell, D. W., Operation DIAL PACK, Project LN-305, Earth Motion and Stress Measurements in the Outrunning Region, TR-N-73-4. U.S. Army Engineer Waterways Experiment Station, Vicksburg, Miss., May 1973.

24. Murrell, D. W., Operation SNOWBALL, Project 3.6, Earth Motion Measurements, TR-1-759. U.S. Army Engineer Waterways Experiment Station, Vicksburg, Miss., March 1967.

25. Seknicka, J. E., and H. H. Druebert, Operation SNOWBALL Ground Displacement Study, WL-TR-64-175. Air Force Weapons Laboratory, Kirtland AFB, N.M., August 1965.

26. Ingram, J. K., Operation DISTANT PLAIN, Events 1, 2A, 3, 4 and 5, Project 3.02A, Earth Motion and Stress Measurements, TR-N-71-3. U.S. Army Engineer Waterways Experiment Station, Vicksburg, Miss., May 1971.

27. Murrell, D. W., DISTANT PLAIN Events 6 and 1A Project 3.02A Earth Motion and Stress Measurements, TR N-70-14. U.S. Army Engineer Waterways Experiment Station, Vicksburg, Miss., September 1970.

28. Sauer, F. M., Summary Report on DISTANT PLAIN, Events 6 and 1A, Ground Motion Experiments, DASA-2587. Stanford Research Institute, Menlo Park, Calif., October 1970.

29. Jaramillo, E. E., and R. E. Pozega, MIDDLE GUST Free Field Data Analysis, AFWL-TR-73-251. Air Force Weapons Laboratory, Kirtland AFB, N.M., April 1974.

30. Jaramillo, E. E., Data Report MIDDLE GUST I, AL-831. EG&G, Albuquerque, N.M., 26 July 1972.

31. Pozega, R. E., Free Field Data Report MIDDLE GUST II, AL-831-2. EG&G, Albuquerque, N.M., 5 March 1973.

32. Jaramillo, E. E., Free Field Data Report MIDDLE GUST III, AL-831-3. EG&G, Albuquerque, N.M., 2 February 1973.

33. Pozega, R. E., Free Field Data Report MIDDLE GUST IV, AL-831-4. EG&G, Albuquerque, N.M., 1 May 1973.

34. Jaramillo, E. E., Free Field Data Report MIDDLE GUST V, AL-831-5. EG&G, Albuquerque, N.M., 15 March 1973.

35. Murrell, D. W., et al., MIDDLE GUST Calibration Shots Ground Motion Measurements, TR-N-75-1. U.S. Army Engineer Waterways Experiment Station, Vicksburg, Miss., February 1975.

36. DASIAC, Proceedings of the MIXED COMPANY/MIDDLE GUST Results Meeting 13-15 March 1973, Vol. I, DNA 3151-P1. General Electric Co.-Tempo, Santa Barbara, Calif., May 1973.

37. Chisolm, S. P., MIDDLE NORTH Series, MIXED COMPANY Event, Air Blast and Ground Motion Experiments, POR 6630. Air Force Weapons Laboratory, Kirtland AFB, N.M., 16 May 1975.

38. Perret, W. R., Operation IVY, Project 6.5, Ground Motion Produced by MIKE Shot of Operation IVY, SC-RR-68-754. Sandia Laboratories, Albuquerque, N.M., December 1968.

39. Ferrito, J. M., and J. B. Forrest, Ground Motions from Pacific Cratering Experiments 1000 lb. Explosive Shots, NCEL TR-R808. Naval Civil Engineering Laboratory, Port Hueneme, Calif., January 1975.

40. Joachim, C. E., MINE SHAFT Series, Events MINE UNDER and MINE ORE, Subtask SS222, Ground Motion and Stress Measurements, TR N-72-1. U.S. Army Engineer Waterways Experiment Station, Vicksburg, Miss., January 1972.

41. Hoffman, H. V., and C. T. Vincent, Ground Motion and Close-in Stress Measurements on MINE SHAFT, DASA 2320. Stanford Research Institute, Menlo Park, Calif., August 1969.

42. Murrell, D. W., and H. D. Carleton, Operation MINE SHAFT Ground Shock from Underground and Surface Explosions in Granite, MS-2159 and 2160. U.S. Army Engineer Waterways Experiment Station, Vicksburg, Miss., April 1973.

43. Murrell, D. W., Operation MINE SHAFT, MINERAL ROCK Event, Far Out Ground Motions from a 100-Ton Detonation over Granite. TR-N-72-6, U.S. Army Engineer Waterways Experiment Station, Vicksburg, Miss., April 1972.

44. Cooper, H. F., and J. L. Bratton, Calculation of Vertical Airblast Induced Ground Motions from Nuclear Explosions on Frenchman Flat, AFWL-TR-73-111. Air Force Weapons Laboratory, Kirtland, N.M., May 1973.

45. Jackson, J. G., One Dimensional Wave Propagation vs Field Measurements - PRISCILLA. U.S. Army Engineer Waterways Experiment Station, Vicksburg, Miss., March 1973.

46. Hadala, P. F., Effect of Constitutive Properties of Earth Media on Outrunning Ground Shock from Large Explosions, TR-S-73-6, U.S. Army Engineer Waterways Experiment Station, Vicksburg, Miss., August 1973.

47. Maxwell, D., J. Reaugh, and B. Gerber, JOHNIE BOY Crater Calculations, DNA 3048F. Physics International Company, San Leandro, Calif., April 1973.

48. Zelasko, J. S., and G. Y. Balada, Free Field Code Predictions vs Field Measurements, A Comparative Analysis for the PRAIRIE FLAT Event, S-71-6. U.S. Army Engineer Waterways Experiment Station, Vicksburg, Miss., March 1971.

49. Hendron, A. J., Jr., Correlation of Operation SNOWBALL Ground Motions with Dynamic Properties of Test Site Soils, Misc. Paper 1-745. U.S. Army Engineer Waterways Experiment Station, Vicksburg, Miss., October 1965.

50. Phillips, B. R., and G. Y. Baladi, Results of Two Free Field Code Calculations vs Field Measurements for the DISTANT PLAIN 1A Event, S-73-21. U.S. Army Engineer Waterways Experiment Station, Vicksburg, Miss., April 1973.

51. McCormick, J. M., M. L. Baron and I. Nelson, Studies on the DISTANT PLAIN 1A Event, DASA-2213. Defense Atomic Support Agency, Washington, D.C., July 1968.

52. Schuster, S., Preshot Prediction Calculations for MIDDLE GUST 3, ATR-72-26-1. Applied Theory, Inc., Los Angeles, Calif., 26 April 1972.

53. Schuster, S., Preshot Prediction Calculations for MIDDLE GUST 4, ATR-72-36-1. Applied Theory, Inc., Los Angeles, Calif., 20 June 1972.

54. Sandler, I. S., Parameter Studies of MIXED COMPANY, S-72-2. U.S. Army Engineer Waterways Experiment Station, Vicksburg, Miss., June 1975.

55. Sandler, I. S., et al., Ground Motion Calculations for the MIXED COMPANY Event, S-74-4. U.S. Army Engineer Waterways Experiment Station, Vicksburg, Miss., October 1974.

56. Ialongo, G., Prediction Calculations for the MIXED COMPANY Event, DNA 3206F. Shock Hydrodynamics, Sherman Oaks, Calif., November 1973.

57. Buckingham, A. C., et al., Calculations of CACTUS Ground Motion and Design of the MINE THROW II Charge, DNA 3141-3. Physics International Company, San Leandro, Calif., August 1973.

58. Reaugh, J., Computations for MINE ORE/MINERAL ROCK, DNA 2852F. Physics International Company, San Leandro, Calif., April 1972.

59. Sandler, I. S., F. L. DiMaggio, and G. Y. Baladi, Generalized CAP Model For Geological Materials, DNA 3443T. Defense Nuclear Agency, Washington, D.C., November 1974.

60. Palaniswamy, K., and J. L. Merritt, Empirical Scaling Studies of MIDDLE GUST Data, 74-003-T2. Consulting and Special Engineering Services, Inc., Redlands, Calif., August 1975.

61. Lipner, N., Three Dimensional Constitutive Behavior of Ottawa Sand, TRW System Group, Redondo Beach, Calif., February 1971.

62. Johnson, H. S., et al., Anisotropic Mechanical Properties of Kayenta Sandstone (MIXED COMPANY) for Ground Motion Calculations, DNA TR 74-61. Defense Nuclear Agency, Washington, D.C., December 1974.

63. Faust, L. Y., "Seismic Velocity as a Function of Depth and Geologic Time", Geophysics, Vol. XVI, Nos. 1-4, pp. 192-206, 1951.

64. Wilson, S. D., and E. A. Sibley, "Ground Displacements from Air-Blast Loading", Journal of Soil Mechanics and Foundation Division, American Society of Civil Engineers, December 1962.

65. Seamon, L., and R. Whitman, Stress Propagation In Soils, DASA-1266-4. Defense Atomic Support Agency, Washington, D.C., June 1964.

66. Sackman, J. L., "Uniformly Moving Load on a Layered Half Plane". American Society of Civil Engineers, Trans, Vol. 127, Part I, p. 823, 1962.

67. Cooper, H. F., On the Prediction of Crater Volumes and Crater-Induced Ground Motions from Nuclear Explosions, RDA-TR-193-DNA. R & D Associates, Santa Monica, Calif., 23 April 1973.

68. Sauer, F. M., Quarter-Root Scaling of Cratering Induced Ground Motions, PITN-402-1. Physics International Company, San Leandro, Calif., April 1972.

69. Cooper, H. F., A Critical Review of Proposed Quarter-Root Crater Volume Scaling of Crater-Induced Ground Motions, RDA-TR-079-AFWL. R & D Associates, Santa Monica, Calif., June 1972.

70. Perret, W. R., Operation FLINT LOCK, Shot PILEDRIVER, Free Field Ground Motion in Granite, POR-4001. Sandia Laboratories, Albuquerque, N.M., September 1968.

71. Higgins, C. J., and H. L. Schreyer, An Analysis of Outrunning Ground Motions, AFWL-TR-72-220. Air Force Weapons Laboratory, Albuquerque, N.M., July 1974.

72. Palaniswamy, K., and J. L. Merritt, Inferred In-Situ Uniaxial Stress-Strain Curves for MIDDLE GUST, CIST and Related Sites, 74-003-T1. Consulting and Special Engineering Service, Inc., Redlands, Calif., 17 July 1975.

73. Cooper, H. F., Height of Burst Effects on Strong Motion Seismic Ground Motion from Nuclear Explosions, RDA-TR-063-DNA. R & D Associates, Santa Monica, Calif., 29 April 1972.

APPENDIX

ENVIRONMENT RECOMMENDATIONS FOR THE VULNERABILITY-ANALYSIS SYSTEM OF THE DEFENSE INTELLIGENCE AGENCY

This appendix summarizes the ground shock environment scaling recommended for DIA/VAS. The following tables specify the peak surface burst values for horizontal and vertical displacement, velocity, acceleration and stress for the air slap, DI/CI (close in), and ground roll (further-out) components. Within the transition region where the DI/CI and ground roll effects are on the same order, they should be combined in such a manner that the peak displacement or velocity is not greater than that predicted by either effect alone. Scaling of tne peak ground shock parameters with HOB is given in Section 4.3.

Representative motion and stress waveforms are given for near surface response to a 1-MT surface burst detonation for ranges corresponding to 1000, 100 and 10 psi peak overpressure for each generic site in Section 4.2.4 (except for the 10 psi overpressure stress waveforms for the rock sites). The undamped shock spectrum for each ground motion waveform is also presented in that section.

TABLE A-1. SURFACE BURST DRY SOIL PEAK AIR SLAP PARAMETERS

$$\text{Environment Value} = \left(\text{Reference Value}\right)\left(\frac{W}{1\ \text{MT}}\right)^{A}\left(\frac{P}{1000\ \text{psi}}\right)^{B}\exp\left[-\frac{z}{L_0}\right]$$

ENVIRONMENT PARAMETER	REFERENCE VALUE	SCALING FACTORS*			2σ UNCERTAINTY FACTOR
		A	B	L_0 (ft)	
d_V (in)	42	(1)	2/3	150	2.5
d_H (in)	7	(1)	1/3	500	3.0
v_V (ips)	540	0	1	(2)	2.5
v_H (ips)	80	0	0.6	∞	2.5
a_V (g's)	2800	0	1	(3)	3.0
a_H (g's)	400	0	0.6	(3)	3.5
σ_V (psi)	1000	0	1	∞	2.0
σ_H (psi)	350	0	0.8	∞	3.0

*Scaling Range: 20 kT ≤ W ≤ 50 MT
10 psi ≤ P ≤ 5000 psi
z ≤ 50 ft

(1) $A = \frac{1}{6}\left(\frac{P}{1000\ \text{psi}}\right)^{0.23}$

(2) $L_0 = 50\ \text{ft}\left(\frac{P}{1000\ \text{psi}}\right)^{-1/4}\left(\frac{W}{1\ \text{MT}}\right)^{1/12}$

(3) $a_{V,H} = \frac{5v_{V,H}}{\left(1+\frac{z}{4\ \text{ft}}\right)}$ g's/ips, $z > 0$

TABLE A-2. SURFACE BURST WET SOIL PEAK AIR SLAP PARAMETERS

$$\text{Environment Value} = \left(\text{Reference Value}\right) \left(\frac{W}{1\ \text{MT}}\right)^{A} \left(\frac{P}{1000\ \text{psi}}\right)^{B} \exp\left[-\frac{z}{L_0}\right]$$

ENVIRONMENT PARAMETER	REFERENCE VALUE	SCALING FACTORS*			2σ UNCERTAINTY FACTOR**
		A	B	L_0 (ft)	
d_V (in)	12	(1)	2/3	250	2.5
d_H (in)	15	(1)	2/3	∞	3.0
v_V (ips)	160	0	1	250	2.5
v_H (ips)	60	0	0.6	∞	2.5
a_V (g's)	830	0	1	(2)	3.0
a_H (g's)	420	0	0.6	(2)	3.5
σ_V (psi)	1000	0	1	∞	2.0
σ_H (psi)	1000	0	1	∞	2.0

*Scaling Range: 20 kT ≤ W ≤ 50 MT
10 psi ≤ P ≤ 5000 psi
z ≤ 50 ft

(1) $A = \frac{1}{6} \left(\frac{P}{1000\ \text{psi}}\right)^{0.23}$

(2) $a_{V,H} = \frac{5v_{V,H}}{\left(1 + \frac{z}{9\ \text{ft}}\right)}$ g's/ips, $z > 0$

TABLE A-3. SURFACE BURST SOFT ROCK PEAK AIR SLAP PARAMETERS

$$\text{Environment Value} = \left(\text{Reference Value}\right)\left(\frac{W}{1\ \text{MT}}\right)^{A}\left(\frac{P}{1000\ \text{psi}}\right)^{B}\exp\left[-\frac{z}{L_0}\right]$$

ENVIRONMENT PARAMETER	REFERENCE VALUE	SCALING FACTORS*			2σ UNCERTAINTY FACTOR**
		A	B	L_0 (ft)	
d_V (in)	4	1/3	0.4	400	2.5
d_H (in)	4	1/3	0.4	400	3.0
v_V (ips)	65	0	1	600	2.5
v_H (ips)	40	0	0.6[+]	∞	2.5 to 3.5
a_V (g's)	330	0	1	30	3.0
a_H (g's)	330	0	1	30	3.5 to 4.5
σ_V (psi)	1000	0	1	∞	2.0
σ_H (psi)	1000	0	1	∞	3.0 to 4.0

*Scaling Range $20\ \text{kT} \le W \le 50\ \text{MT}$; $10\ \text{psi} \le P \le 5000\ \text{psi}$; $z \le 50\ \text{ft}$

[+] $v_H = v_V$ for $P < 300$ psi

**When ranges of values are given, the uncertainties are largest for the lower overpressure, outrunning region; and smallest for the high overpressure, superseismic region.

TABLE A-4. SURFACE BURST HARD ROCK PEAK AIR SLAP PARAMETERS

$$\text{Environment Value} = \left(\text{Reference Value}\right)\left(\frac{W}{1\ \text{MT}}\right)^{A}\left(\frac{P}{1000\ \text{psi}}\right)^{B}\exp\left[-\frac{z}{L_0}\right]$$

ENVIRONMENT PARAMETER	REFERENCE VALUE	SCALING FACTORS*			2σ UNCERTAINTY FACTOR**
		A	B	L_0 (ft)	
d_V (in)	1.3	1/3	0.4	∞	2.5
d_H (in)	1.3	1/3	0.4	∞	3.0
v_V (ips)	23	0	1	∞	2.5
v_H (ips)	30	0	1	∞	2.5 to 3.5
a_V (g's)	120	0	1	60	3.0
a_H (g's)	120	0	1	60	3.5 to 4.5
σ_V (psi)	1000	0	1	∞	2.0
σ_H (psi)	1000	0	1	∞	3.0 to 4.0

*Scaling Range: 20 kT ≤ W ≤ 50 MT
20 psi ≤ P ≤ 5000 psi
z ≤ 50 ft

**When ranges of values are given, the uncertainties are largest for the lower overpressure, outrunning region; and smallest for the high overpressure, superseismic region.

Table A-5. SURFACE BURST CLOSE-IN PEAK-DI/CI PARAMETERS

$$\text{Environment Value} = \left(\text{Reference Value}\right)\left(\frac{W}{1\ \text{MT}}\right)^{A}\left(\frac{1000\ \text{ft}}{R}\right)^{B}$$

ENVIRONMENT PARAMETER	REFERENCE VALUE				SCALING FACTORS		2σ UNCERTAINTY FACTOR
	Dry Soil	Wet Soil	Soft Rock	Hard Rock	A	B	
Crater Volume (10^6 ft^3)	50	170	40	30	1	0	1.8
Displacement (in)	100	510	75	50	4/3	3	3.5
Velocity (ips)	50	180	110	150	2/3	2	3.5
Acceleration (g's)	5	15	25	140	1	4	5
Stress (psi)	75	750	880	5000	2/3	2	4

TABLE A-6. SURFACE BURST PEAK GROUND ROLL PARAMETERS

$$\text{Environment Value} = \left(\text{Reference Value}\right)\left(\frac{W}{1\ MT}\right)^{A}\left(\frac{10{,}000\ ft}{R}\right)^{B}$$

PREDICTION PARAMETER	ENVIRONMENT PARAMETER	GENERIC SITE				SCALING FACTORS	
		Dry Soil	Wet Soil	Soft Rock	Hard Rock	A	B
REFERENCE VALUE	Displacement (in)	1.5	1.5	0.6	0.6	2/3	1
	Velocity (ips)	6.0	6.0	2.4	2.4	1/2	3/2
2 σ UNCERTAINTY FACTOR	Displacement	3.5	4.0	5.0	5.0	—	—
	Velocity	3.5	3.5	4.0	4.0	—	—

ABBREVIATIONS AND SYMBOLS

Abbreviations

AFDM	Air Force design manual
AFWL	Air Force Weapons Laboratory
AI	air-blast-induced
ATI	Applied Theory, Inc.
BLEST	Berm-Loaded Explosive Simulation Technique
CI	crater-induced
CIST	Cylindrical in Situ Test
DI	direct-induced
DIA	Defense Intelligence Agency
DIHEST	Direct-Induced/High Explosive Simulation Technique
EPG	Eniwetok Proving Ground
FAST	Failure Analysis by Statistical Techniques
HEST	High Explosive Simulation Technique
HOB	height-of-burst
HRSD	Hard Rock Silo Development
NTS	Nevada Test Site
PI	Physics International Company
RDA	R & D Associates
RQD	rock quality designation
SES	Suffield Experimental Station
SRI	Stanford Research Institute
S^3	Systems, Science and Software
VAS	Vulnerability Analysis System
WA	Weidlinger Associates
WES	Waterways Experimental Station

Symbols

a	peak ground particle acceleration
A	ground shock yield scaling parameter
B	ground shock overpressure scaling parameter
C	ground shock wave-speed
C_e	average seismic wave-speed
C_i	seismic wave-speed
C_L	peak stress ground shock wave-speed
C_p	pressure coefficient for bermed surface
d	peak ground particle displacement; also, coefficient in double-exponential dynamic pressure definition
D_u^+	dynamic pressure positive-phase duration
f	coefficient in double-exponential dynamic pressure definition
g	acceleration due to gravitational effects
G	ground medium unloading shear modulus
H	depth to bedrock
I	air blast positive-phase impulse
L_o	air slap ground shock depth-attenuation parameter
M_L	ground medium loading-constrained modulus
M_U	ground medium unloading-constrained modulus
n	ratio of peak acceleration to average acceleration
p	overpressure
P	peak overpressure
P_F	average overpressure on front face of bermed surface
P_L	minimum overpressure between peaks in double-peaked region
P_R	average overpressure on rear face of bermed surface

Symbols

P_1	initial peak overpressure in double-peaked region
P_2	second peak overpressure in double-peaked region
q	dynamic pressure
Q	peak dynamic pressure
R	range from ground zero
t	time
t_d	time to peak ground displacement
t_R	ground particle velocity rise time
t_0	air blast arrival time at ground zero
t_{00}	overpressure initial decay time intercept
t'_{00}	dynamic pressure initial decay time intercept
t_1	air blast arrival time at ground range, R
t_2	time of second peak in double-peaked region
T	time after air blast arrival, normalized to dynamic pressure positive-phase duration; also, ground roll waveform period
u	air blast particle velocity
U	air blast shock speed
v	peak ground particle velocity
V	apparent crater volume
W	weapon yield
z	depth below ground surface
Z	ratio of weapon height-of-burst to ground range
γ	ratio of peak stress impedance to seismic impedance
δ	exponential parameter in double-exponential dynamic pressure definition
σ	standard deviation; also, ground shock stress
ϕ	exponential parameter in double-exponential dynamic pressure definition

Symbols (Subscripts)

BR	bedrock parameter
H	horizontal response parameter
HOB	height-of-burst parameter
SB	surface burst parameter
V	vertical response parameter

DISTRIBUTION LIST

DEPARTMENT OF DEFENSE

Assistant Secretary of Defense Intelligence
ATTN: ODASD IA

Assistant to the Secretary of Defense
ATTN: COL R. N. Brodie
ATTN: Honorable Donald R. Cotter

Director
Defense Advanced Research Project Agency
ATTN: NMRO
ATTN: PMO
ATTN: STO
ATTN: Technical Library

Director
Defense Civil Preparedness Agency
Assistant Director for Research
ATTN: Admin. Officer
ATTN: Staff Dir. Rcsr., George N. Sisson

Director
Defense Communications Agency
ATTN: Code 930
ATTN: Code 930, Franklin D. Moore

Defense Documentation Center
2 cy ATTN: TC

Director
Defense Intelligence Agency
ATTN: DT-1C
ATTN: DT-2, Weapons & Systems Division
ATTN: Technical Library
ATTN: DI-7E
2 cy ATTN: Charles A. Fowler
ATTN: DI-7D, Edward O'Farrell

Director
Defense Nuclear Agency
ATTN: DDST
ATTN: STSI, Archives
2 cy ATTN: SPAS
3 cy ATTN: STTL, Technical Library
2 cy ATTN: SPSS

Director of Defense Research & Engineering
ATTN: DD/TWP
ATTN: Rear Admiral Ross Williams
ATTN: AD/SW
ATTN: DD/I&SS
ATTN: DD/S&SS

Commander
Field Command, Defense Nuclear Agency
ATTN: FCPR
ATTN: FCTMOF

Director
Interservice Nuclear Weapons School
ATTN: Technical Library

Chief
Livermore Division, Field Command, DNA
Lawrence Livermore Laboratory
ATTN: FCPRL

DEPARTMENT OF DEFENSE (Continued)

Director
Joint Strategic Target Planning Staff, JCS
ATTN: XPFS
ATTN: DOXT
ATTN: STINFO Library
ATTN: JLTW-2

DEPARTMENT OF THE ARMY

Director
BMD Advanced Tech. Center
ATTN: 1CRDABH-X
ATTN: CRDABH-S

Program Manager
BMD Program Office
ATTN: John Shea

Commander
BMD System Command
ATTN: BDMSC-TEN, Noah J. Hurst

Dep. Chief of Staff for Rsch. Dev. & Acq.
ATTN: DAMA(CS), MAJ A. Gleim
ATTN: Technical Library

Chief of Engineers
ATTN: DAEN-RDM
ATTN: DAEN-MCE-D

Deputy Chief of Staff for Ops. & Plans
ATTN: Technical Library
ATTN: Dir. of Chem. & Nuc. Ops.

Chief
Engineer Strategic Studies Group
ATTN: DAEN-FES, LTC Hatch

Commander
Harry Diamond Laboratories
ATTN: DRXDO-TI, Technical Library
ATTN: DRXDO-NP

Commander
Picatinny Arsenal
ATTN: B. Shulman
ATTN: Technical Library

Commander
Redstone Scientific Information Center
U.S. Army Missile Command
ATTN: Chief, Documents

Commander
U.S. Army Armament Command
ATTN: Technical Library

Director
U.S. Army Ballistic Research Laboratories
ATTN: A. Ricchiazzi
2 cy ATTN: Technical Library, Edward Baicy
ATTN: W. Taylor
ATTN: DRXBR-X, Julius J. Meszaros
ATTN: AMXBR-TL-IR, J. H. Keefer

DEPARTMENT OF THE ARMY (Continued)

Commander
U.S. Army Comb. Arms Combat Dev. Acty.
ATTN: LTC G. Steger
ATTN: LTC Pullen

Commander
U.S. Army Communications Command
ATTN: Technical Library

Commander
U.S. Army Electronics Command
ATTN: DRSEL-TL-IR, Edwin T. Hunter

Commander
U.S. Army Engineer Center
ATTN: ATSEN-SY-L

Division Engineer
U.S. Army Engineer Division
ATTN: HNDSE-R, Michael M. Dembo

Division Engineer
U.S. Army Engineer Division
ATTN: Technical Library

Commandant
U.S. Army Engineer School
ATTN: ATSE-CTD-CS
ATTN: ATSE-TEA-AD

Director
U.S. Army Engineer Waterways Experiment Station
ATTN: William Flathau
ATTN: Technical Library
ATTN: Leo Ingram
ATTN: Guy Jackson
ATTN: John N. Strange

Commander
U.S. Army Foreign Science & Tech. Center
ATTN: Research & Concepts Branch

Commander
U.S. Army Mat. & Mechanics Research Center
ATTN: Technical Library
ATTN: Richard Shea
ATTN: John Mescall

Commander
U.S. Army Materiel Dev. & Readiness Command
ATTN: W. H. Hubbard
2 cy ATTN: DRCRD-BN
ATTN: DRCDE-D, Lawrence Flynn
ATTN: Technical Library
ATTN: DRCRD-WN

Commander
U.S. Army Missile Command
ATTN: J. Hogan
ATTN: DRSMI-XS, Chief Scientist

Commander
U.S. Army Mobility Equipment R & D Center
ATTN: Technical Library

Commander
U.S. Army Nuclear Agency
ATTN: ATCA-NAW
ATTN: Technical Library

DEPARTMENT OF THE ARMY (Continued)

Commander
U.S. Army Training and Doctrine Command
ATTN: LTC J. Foss
ATTN: LTC Auveduti, COL Enger

Commandant
U.S. Army War College
ATTN: Library

U.S. Army Mat. Cmd. Proj. Mngr. for Nuc. Munitions
ATTN: DRCPM-NUC

DEPARTMENT OF THE NAVY

Chief of Naval Material
ATTN: MAT 0323

Chief of Naval Operations
ATTN: OP 985F
ATTN: Code 604C3, Robert Piacesi
ATTN: OP 982, CAPT Toole/LCDR Smith/LTC Dubac
ATTN: OP 03EG

Chief of Naval Research
ATTN: Code 464, Thomas P. Quinn
ATTN: Code 464, Jacob L. Warner
ATTN: Technical Library
ATTN: Nicolas Perrone

Officer-In-Charge
Civil Engineering Laboratory, NCB Center
ATTN: R. J. Odello
ATTN: Technical Library
ATTN: Stan Takahashi

Commanding General
Development Center
Fire Support Branch
ATTN: LTC Gapenski/CAPT Hartneady

Commandant
Marine Corp
ATTN: POM

Commander
Naval Electronic Systems Command
Naval Electronic Systems Command Headquarters
ATTN: PME-117-21A

Commander
Naval Facilities Engineering Command, Headquarters
ATTN: Code 03A
ATTN: Technical Library
ATTN: Code 04B

Superintendent
Naval Postgraduate School
ATTN: Code 2124, Tech. Rpts. Librarian

Director
Naval Research Laboratory
ATTN: Code 8440, F. Rosenthal
ATTN: Code 2027, Technical Library

Commander
Naval Sea Systems Command
ATTN: ORD-91313, Library
ATTN: Code 03511
ATTN: SEA-9931G
ATTN: ORD-033

DEPARTMENT OF THE NAVY (Continued)

Commander
Naval Ship Engineering Center
ATTN: Technical Library
ATTN: NSEC 6105G

Commander
Naval Ship Research and Development Center
ATTN: Code L42-3, Library

Commander
Naval Ship Research and Development Center
Underwater Explosive Research Division
ATTN: Technical Library

Commander
Naval Surface Weapons Center
ATTN: Code WA501, Navy Nuc. Prgms. Office
ATTN: Code 240, C. J. Aronson
ATTN: G. L. Matteson
ATTN: M. Kleinerman
ATTN: Code WX21, Technical Library

Commander
Naval Surface Weapons Center
ATTN: Technical Library

Commander
Naval Undersea Center
ATTN: Technical Library

President
Naval War College
ATTN: Technical Library

Commander
Naval Weapons Center
ATTN: Code 533, Technical Library

Commanding Officer
Naval Weapons Evaluation Facility
ATTN: R. Hughes
ATTN: Technical Library

Director
Office of Naval Research
ATTN: E. H. Weinburg

Director
Strategic Systems Project Office
ATTN: NSP-272
ATTN: NSP-273
ATTN: NSP-43, Technical Library

DEPARTMENT OF THE AIR FORCE

Commander
ADC/XP
ATTN: XPQDQ
ATTN: XP

AF Geophysics Laboratory, AFSC
ATTN: SUOL AFCRL, Research Library
ATTN: LWW, Ker C. Thompson

AF Institute of Technology, AU
ATTN: Library AFIT Bldg. 640, Area B

Commander
ASD
ATTN: Technical Library

DEPARTMENT OF THE AIR FORCE (Continued)

AF Weapons Laboratory, AFSC
ATTN: DES, M. A. Plamondon
ATTN: DEV, Jimmie L. Bratton
ATTN: DE-I
ATTN: Robert Henny
ATTN: Robert Port
ATTN: SUL
ATTN: DEX

Headquarters
Air Force Systems Command
ATTN: Technical Library
ATTN: DLCAW
ATTN: R. Cross

Commander
Armament Development & Test Center
ATTN: Technical Library
ATTN: ADBRL-2

Assistant Secretary of the Air Force
Research and Development
Headquarters, U.S. Air Force
ATTN: Col R. E. Steere

Deputy Chief of Staff
Research and Development
ATTN: Col J. L. Gilbert

Commander
Foreign Technology Division, AFSC
ATTN: TD-BTA, Library
ATTN: ETET, Capt Richard C. Husemann
ATTN: TDFBD
ATTN: TDPMG

HQ USAF/IN
ATTN: IN

HQ USAF/PR
ATTN: PRE

HQ USAF/RD
ATTN. RDQRM, Maj S. C. Green
ATTN: RDPS, Lt Col A Chiota
ATTN: RDPM
ATTN: RDQPN
ATTN: RDQPN, Maj F. Vajda

Commander
Rome Air Development Center, AFSC
ATTN: EMTLD, Doc. Library
ATTN: EMREC, R. W. Mair

SAMSO/DE
ATTN: DEB

SAMSO/DY
ATTN: DYS

SAMSO/MN
ATTN: MNNH
ATTN: MMH

SAMSO/RS
ATTN: RSS, Col Donald Dowler

SAMSO/XR
ATTN: XRTB

DEPARTMENT OF THE AIR FORCE (Continued)

Commander in Chief
Strategic Air Command
ATTN: NRI-STINFO Library
ATTN: XPFS

ENERGY RESEARCH & DEVELOPMENT ADMINISTRATION

Division of Military Application
ATTN: Doc. Control for Test Office

University of California
Lawrence Livermore Laboratory
ATTN: Ted Butkovich, L-200
ATTN: Tech. Info. Dept., L-3
ATTN: M. Fernandez
ATTN: Richard G. Dong, L-90
ATTN: Robert Schock, L-437
ATTN: Jerry Goudreau
ATTN: Jack Kahn, L-7
ATTN: J. Carothers, L-7
ATTN: J. R. Hearst, L-205
ATTN: Larry W. Woodruff, L-96
ATTN: D. M. Norris, L-90

Los Alamos Scientific Laboratory
ATTN: Doc. Control for Reports Library
ATTN: Doc. Control for Al Davis
ATTN: Doc. Control for G. R. Spillman

Sandia Laboratories
Livermore Laboratory
ATTN: Doc. Control for Technical Library

Sandia Laboratories
ATTN: L. Hill
ATTN: Doc. Control for A. J. Chaban
ATTN: Doc. Control for Luke J. Vortman
ATTN: Doc. Control for W. Roherty
ATTN: Doc. Control for 3141, Sandia Rpt. Coll.
ATTN: Doc. Control for M. L. Merritt

U.S. Energy Research & Development Administration
Albuquerque Operations Office
ATTN: Doc. Control for Technical Library

U.S. Energy Research & Development Administration
Division of Headquarters Services
ATTN: Doc. Control for Class. Tech. Library

U.S. Energy Research & Development Administration
Nevada Operations Office
ATTN: Doc. Control for Technical Library

Union Carbide Corporation
Holifield National Laboratory
ATTN: Civil Def. Res. Project
ATTN: Doc. Control for Tech. Library

OTHER GOVERNMENT AGENCIES

Central Intelligence Agency
ATTN: RD/SI, Rm 5G48 Hq. Bldg. for
NED/OSI-5G48 Hqs.

Department of the Interior
U.S. Geological Survey
ATTN: Cecil B. Raleigh
ATTN: J. H. Healy

OTHER GOVERNMENT AGENCIES (Continued)

Department of the Interior
Bureau of Mines
ATTN: Technical Library

Department of the Interior
Bureau of Mines
ATTN: James J. Scott

NASA
Ames Research Center
ATTN: Robert W. Jackson

Office of Nuclear Reactor Regulation
Nuclear Regulatory Commission
ATTN: Lawrence Shao
ATTN: Robert Heineman

DEPARTMENT OF DEFENSE CONTRACTORS

Aerospace Corporation
ATTN: Prem N. Mathur
2 cy ATTN: Tech. Info. Services

Agbabian Associates
ATTN: M. Agbabian

Analytic Services, Inc.
ATTN: George Hesselbacher

Applied Theory, Inc.
2 cy ATTN: John G. Trulio

Artec Associates, Inc.
ATTN: Steven Gill

Avco Research & Systems Group
ATTN: William Broding
ATTN: Research Library, A830, Rm 7201

Battelle Memorial Institute
ATTN: R. W. Klingesmith
ATTN: Technical Library

The BDM Corporation
ATTN: A. Lavagnino
ATTN: Technical Library

The BDM Corporation
ATTN: Richard Hensley

The Boeing Company
ATTN: Aerospace Library
ATTN: R. H. Carlson

Brown Engineering Company, Inc.
ATTN: Manu Patel

California Institute of Technology
ATTN: Thomas J. Ahrens

California Research & Technology Inc.
ATTN: Technical Library
ATTN: Ken Kreyenhagen
ATTN: Sheldon Shuster

Calspan Corporation
ATTN: Technical Library

Civil/Nuclear Systems Corp.
ATTN: Robert Crawford

DEPARTMENT OF DEFENSE CONTRACTORS (Continued)

Communications Satellite Corporation
ATTN: Jim Petrousky

University of Dayton
Industrial Security Super KL-505
ATTN: Hallock F. Swift

University of Denver
Colorado Seminary
Denver Research Institute
ATTN: Sec. Officer for J. Wisotski
ATTN: Sec. Officer for Tech. Library

EG&G, Inc.
ATTN: Technical Library

Electric Power Research Institute
ATTN: George Sliter

Engrg. Decision Analysis Co., Inc.
ATTN: R. P. Kennedy

The Franklin Institute
ATTN: Zenons Zudans

General American Transportation Corp.
General American Research Division
ATTN: G. L. Neidhardt

General Electric Company
Space Division
ATTN: M. H. Bortner, Space Science Lab.

General Electric Company
Re-entry & Environmental Systems Division
ATTN: L. D. Audrea
ATTN: Arthur L. Ross

General Electric Company
TEMPO-Center for Advanced Studies
ATTN: DASIAC

General Research Corporation
ATTN: Benjamin Alexander

Honeywell Incorporated
Ordnance Division
ATTN: T. N. Helvig

IIT Research Institute
ATTN: Technical Library
ATTN: Milton R. Johnson
ATTN: R. E. Welch

Institute for Defense Analyses
ATTN: IDA Librarian, Ruth S. Smith

J. H. Wiggins, Co., Inc.
ATTN: John Collins

Kaman AviDyne
Division of Kaman Sciences Corp.
ATTN: Norman P. Hobbs
ATTN: E. S. Criscione
ATTN: Technical Library

Kaman Sciences Corporation
ATTN: Paul A. Ellis
ATTN: Library
ATTN: Frank H. Shelton

DEPARTMENT OF DEFENSE CONTRACTORS (Continued)

Lockheed Missiles & Space Co., Inc.
ATTN: Technical Library

Lovelace Foundation for Medical Education & Research
ATTN: Asst. Dir. of Res. Robert K. Jones
ATTN: Technical Library

Martin Marietta Aerospace
ATTN: G. Fotieo

McDonnell Douglas Corporation
ATTN: Robert W. Halprin

Merritt Cases, Incorporated
ATTN: J. L. Merritt
ATTN: Technical Library

Meteorology Research, Inc.
ATTN: William D. Green

The Mitre Corporation
ATTN: Library

Newmark, Nathan M.
Consulting Engineering Services
ATTN: Nathan M. Newmark

Pacifica Technology
ATTN: R. Bjork
ATTN: G. Kent

Physics International Company
ATTN: Doc. Control for Tech. Library
ATTN: Doc. Control for Robert Swift
ATTN: Doc. Control for Coye Vincent
ATTN: Doc. Control for Dennis Orphal
ATTN: Doc. Control for Charles Godfrey
ATTN: Doc. Control for Fred M. Sauer
ATTN: Doc. Control for E. T. Moore
ATTN: Doc. Control for Larry A. Behrmann

R & D Associates
ATTN: Bruce Hartenbaum
ATTN: Henry Cooper
ATTN: Albert L. Latter
ATTN: William B. Wright, Jr.
ATTN: Technical Library
ATTN: J. G. Lewis
ATTN: Arlen Fields
ATTN: Paul Rausea
ATTN: Cyrus P. Knowles
ATTN: Harold L. Brode
ATTN: Jerry Carpenter

The Rand Corporation
ATTN: C. C. Mow
ATTN: Technical Library

Science Applications, Inc.
ATTN: D. E. Maxwell
ATTN: David Bernstein

Science Applications, Inc.
ATTN: Michael McKay
ATTN: Technical Library

Southwest Research Institute
ATTN: A. B. Wenzel
ATTN: Wilfred E. Baker

DEPARTMENT OF DEFENSE CONTRACTORS (Continued)

Science Applications, Inc.
ATTN: R. A. Shunk

Stanford Research Institute
ATTN: George R. Abrahamson
ATTN: Carl Peterson

Systems, Science and Software, Inc.
ATTN: Robert Sedgewick
ATTN: Technical Library
ATTN: Donald R. Grine
ATTN: Ted Cherry
ATTN: Thomas D. Riney

Terra Tek, Inc.
ATTN: Technical Library
ATTN: A. H. Jones
ATTN: Sidney Green

Tetra Tech, Inc.
ATTN: Technical Library
ATTN: Li-san Hwang

TRW Systems Group
ATTN: Gregory D. Hulcher

Universal Analytics, Inc.
ATTN: E. I. Field

Westinghouse Electric Company
ATTN: W. A. Volz

DEPARTMENT OF DEFENSE CONTRACTORS (Continued)

TRW Systems Group
ATTN: Tech. Info. Center, S-1930
ATTN: William Rowan
ATTN: Benjamin Sussholtz
ATTN: Jack Farrell
ATTN: Norm Lipner
ATTN: Paul Lieberman
ATTN: Pravin Bhutta
ATTN: Donald C. Anderson
ATTN: Peter K. Dai

URS Research Company
ATTN: Technical Library
ATTN: Ruth Schneider

Wang, The Eric H.
Civil Engineering Research Facility
ATTN: Neal Baum
ATTN: Larry Bickle

Washington State University
Administrative Office
ATTN: Arthur Miles Hohorf for George Duval

Weidlinger Assoc. Consulting Engineers
ATTN: Melvin L. Baron
ATTN: J. M. McCormick